STUDY OF CONCRETE FILLED UPVC TUBES AS COLUMNS IN SEVERE ENVIRONMENT

Ph.D. THESIS

by

Virendra Kumar Verma

DEPARTMENT OF CIVIL ENGINEERING
INDIAN INSTITUTE OF TECHNOLOGY ROORKEE
ROORKEE – 247 667 (INDIA)
November, 2014

STUDY OF CONCRETE FILLED UPVC TUBES AS COLUMNS IN SEVERE ENVIRONMENT

A THESIS

Submitted in partial fulfilment of the requirements for the award of the degree of

DOCTOR OF PHILOSOPHY

in

CIVIL ENGINEERING

by

Virendra Kumar Verma

DEPARTMENT OF CIVIL ENGINEERING
INDIAN INSTITUTE OF TECHNOLOGY ROORKEE
ROORKEE – 247 667 (INDIA)
November, 2014

INDIAN INSTITUTE OF TECHNOLOGY ROORKEE
ROORKEE

CANDIDATE'S DECLARATON

I hereby certify that the work which is being presented in the thesis entitled **"STUDY OF CONCRETE FILLED UPVC TUBES AS COLUMNS IN SEVERE ENVIRONMENT",** in partial fulfilment of the requirements for the award of the Degree of Doctor of Philosophy and submitted in the Department of Civil Engineering of the Indian Institute of Technology Roorkee is an authentic record of my own work carried out during the period from July, 2011 to November, 2014 under the supervision of **Dr. P. K. Gupta,** Professor, Department of Civil Engineering, Indian Institute of Technology Roorkee.

The matter presented in the thesis has not been submitted by me for the award of any other degree of this or any other Institute.

(VIRENDRA KUMAR VERMA)

This is to certify that the above statement made by the candidate is correct to the best of my knowledge.

(P. K. Gupta)
Supervisor

Date:

ABSTRACT

It is difficult to achieve long term durability of reinforced concrete structure in coastal areas. Sea water deteriorates concrete structures due to combined effect of chemical action of sodium chloride and magnesium sulfate present in it. Concrete structures older than 10-15 years show a considerable amount of deterioration in the form of cracking & spalling of concrete and corrosion of reinforcement. This major problem has led to the development of new construction materials which could protect the structure against the cause of deterioration. Concrete filled plastic tubes (CFPT) can be treated as a new construction material which could safeguard both concrete and reinforcement by providing a skin. Plastics have exceptional properties, such as high resistance to severe environmental attack, low cost, and high strength to weight ratio. Their service life goes beyond fifty years. UPVC is a plastic material which is being used for a wide variety of civil engineering applications. UPVC pipes are generally employed for water supply across the world. These pipes are designed for induced internal pressure of flowing water.

In this thesis an experimental, numerical and analytical study has been carried out. In which UPVC pipes are filled with concrete and tested as compression members for their suitability for coastal area. Tested 114 specimens were categorized into three categories viz plain concrete filled UPVC tube (PCFUT), reinforced concrete filled UPVC tube (RCFUT) and bare reinforced concrete column (RCC). Bare R.C.C specimens were obtained from RCFUT specimens by removing the outer tube. Casting of specimens was carried out in two stages. In first stage, 90 specimens were cast while in second stage 24 specimens were cast. For the first stage of casting, the UPVC tubes of class 3, 4 and 5 (as per IS:4985-2000) with nominal pressure of 0.6, 0.8 and 1.0 MPa having diameters of 160 mm, 200 mm and 225 mm were taken. For second stage of casting, UPVC tubes of 160 mm diameter of class 1 with nominal pressure of 0.25 MPa were taken. The internal hydrostatic pressure tests were conducted to get the confining pressure of UPVC tube.

A numerical simulation study was also carried out using Finite element method by development of three-dimensional Finite element model using 'ANSYS' software. The concrete core, UPVC tube, and reinforcement are modeled and then bond are created between them to simulate the modeling of concrete filled UPVC columns. Suitable material constitutive models for UPVC tube, concrete core and reinforcement are adopted. Numerical results were compared with experimental results in the form of load-displacement curves and associated

modes of failure. Based on the results, it may be concluded that the proposed models can predict the structural behavior and load carrying capacity of such columns with good accuracy.

In the study of PCFUT, a stress-strain model for concrete confined with UPVC tube is proposed. The effect of diameter to thickness ratio (D/t) on the failure stress of confined concrete is obtained and discussed with an empirical relationship. To calculate the load carrying capacity of concrete filled UPVC tubular columns, an equation is proposed. An analysis is done to understand the failure mechanism of confined concrete with the help of Mohr-Coulomb failure criterion. Inclination of failure plane for different confining pressure is calculated. The results are verified with experimental results.

Since the strength increment due to confinement given by UPVC tube is only 5-10 MPa. Therefore it necessary to opt reinforced concrete to fill the UPVC tube to get sufficient strength of column. Since transverse reinforcement in the form of lateral ties may also provide additional confinement to the concrete core in the form of arch action. This action becomes more effective when the spacing between the lateral ties is smaller, therefore lateral ties are provided at higher spacing to avoid the confining effect. RCFUT column specimens were cast by filling the reinforced concrete in UPVC tube. 50% of RCFUT specimens were converted to bare RCC specimens by removing UPVC tube.

A specific study was carried out to understand the confinement through transverse reinforcement in reinforced concrete column under axial compression, a three dimensional Finite element model is developed using ANSYS software and the results are also verified with experimental results. Total eighteen specimens of different diameters and lengths were tested to obtain load-displacement variations. A parameter A_{tie}/S^2 (ratio of cross-sectional area of lateral tie to the square of spacing between lateral ties) was taken to check the effective confinement of concrete core in R.C. column. It was concluded that if A_{tie}/S^2 is greater than 0.02 then confinement model of concrete proposed by Mander et al. (1988-a) may be used and if it is less than 0.02 then concrete should be modeled as unconfined. In present study, the spacing between lateral ties was more, therefore an unconfined stress-strain model of concrete was found suitable for the modeling of reinforced concrete columns. Even there was no strength gain observed due to confinement though lateral ties but there was an enhancement in the ductility.

Some experiments were carried out to study the behaviour of reinforced concrete inside UPVC tube and bare reinforced concrete exposed to artificially made sea water. Compressive strength, ductility, energy absorption capacity and modes of failure of bare RCC and RCFUT column were obtained from experimental data. It was found that concrete showed an increment in

strength, ductility and energy absorption capacity when UPVC tube was used as outer layer for RCC. In composite column like RCFUT, outer tube may work as a wall between concrete and aggressive environment. UPVC tubes used in composite column (like RCFUT column) may protect the column from corrosion of steel and degradation of concrete against the attack of salts presents in sea water. Moreover, UPVC tubes may work as a weather proof jacket to the concrete during the whole year. When RCFUT specimens with class 1 UPVC pipes were submerged in different concentration of artificial sea water for different durations, it was found that degradation in concrete was almost negligible. Therefore it may be concluded that the UPVC pipes with minimum nominal/working pressure (0.25MPa) may also be used as the protective layer for concrete against sea water.

Some token specimens were cast and tested to get the strain maps at different stage of loading with the use of Digital Image Correlation (DIC) system. The digital images, which were recorded during testing of specimen, were processed using Vic-3D commercial code to obtain strain map. These strains are compared with the strains obtained from simulations. The strains obtained from Vic-3D and ANSYS are almost equal at the maximum displacement stage. It was observed that the strains on the surface of specimen along the failure plane were increased while at other locations the strains were nearly equal during compression process between peak load to failure load.

ACKNOWLEDGEMENTS

"GOD, I thank you from the bottom of my heart for all that you have done in my life till date and all that you are going to do in my future.

I express my sincere thanks and heartfelt gratitude to my research guide, **Dr. P. K. Gupta,** Professor in the Department of Civil Engineering, I.I.T. Roorkee, for his constant support, guidance, motivation, attention throughout my research work. I would like to mention here that besides being a good teacher, he is a good human being first. It is my privilege to come across a person like him in my life and I commit to continue this relationship throughout my life. I am grateful for his blessings, concern, patience, and cooperation during my moments of trouble. I express my heartfelt indebtedness to him for his intellectual discussions and for sharing his vast knowledge with me. I thank him for always showing faith in my capability, correcting me when I was wrong and for strengthening my conviction and boost up my moral in righteous path of professional life. He always challenged me to do my best and made sure I did. I could not have imagined having a better guidance for my Ph.D. thesis. I thankfully acknowledge him for his blessings and giving me opportunity to work under his sincere guidance. I am really going to miss working with him.

I express my gratitude to **Dr. Deepak Kashyap**, Professor and Head of Department for his enormous help by providing me good laboratory facilities and healthy research environment in the department. I also thank Chairman, Student Research Committee **Dr. Akhil Upadhyay,** Professor, Department of Civil Engineering and other SRC members – **Dr. A.K. Ahuja**, Professor, Department of Civil Engineering, and **Dr. R.N. Dubey**, Assistant Professor, Department of Earthquake Engineering, for their support valuable suggestions, inputs and guidance during various stages of my work. I would like to express my sincere thanks to other faculty members of Civil Engineering Department, **Sh. V.K. Gupta,** Professor, and **Dr. Anupam Chakravarti,** Associate Professor, for their moral support during my research work. My special thanks to **Dr. A.K. Ahuja** for delivering cooperative and enthusiastic advices during my research work.

I express my deepest gratitude to **Dr. B.S. Bisht**, former Vice Chancellor, G.B.Pant University of Agriculture and Technology, Pantnagar, Uttarakhand, for sponsoring me for Ph.D. under Quality Improvement Programme (QIP). I express my deep appreciation to **Dr.**

M.P. Singh, former Dean, College of Technology, Pantnagar and **Dr. P.S. Mahar,** Head, Department of Civil Engineering, College of Technology, Pantnagar for their kind support and help to pursue research at IIT Roorkee. My sincere thanks to my colleague friends, **Dr. Sanjeev Suman, Mr. Sandeep Gupta** and **Mr. Dheeraj Kumar** for their motivational spirit and encouragement.

I highly appreciate the financial support from **Ministry of Shipping, Government of India,** to carry out experimental work through project awarded to IIT Roorkee. I am thankful to **Dean Academics, Dean Students Welfare;** and **Assistant Registrar** (Academic) for their cooperation. My special thanks to **Dr. Rama Bhargava**, Professor and Coordinator of QIP centre at IIT Roorkee for allowing me to pursue my research at IIT Roorkee. I am also thankful to staff members of QIP centre **Mr. Anil** and **Mr. Rajeev** and staff members of Academic and Accounts section, IIT Roorkee for their help and support during my research work.

I would like to express deep appreciation to my friends and colleague research scholars – **Manish, Heaven, R.R. Sahu, Ashish, Gaurav, S.K. Katariya, Banti, Sunil Rajput,** and **Pankaj** for their assistance and valuable guidance. I am especially thankful to **Ziad kubba and Ravi Khandelwal**, Research Scholars for their help in ANSYS software during my computational work.

I would like to express my thanks to **Dr. Bhupendra Singh**, Associate Professor, & Officer in-charge, Concrete laboratory and **Dr. Umesh Sharma**, Associate Professor & Officer in-charge, test hall of Structural Engineering laboratory for their help and support for my research work. I am also thankful to technical staff, **Sh. Surendra, Sh. Anil** and **Sh. Chetan** and other staff members of structural Engineering laboratory for their cooperation and overwhelming support during my experimental work.

I am also thankful to the staff members of Civil Engineering Department **Mr. J.N. Gupta**, **Mrs. Chitra** and others for their help. My sincere thanks to the staff members of Central Facilities especially to **Shri J. P. Dhiman, Shri Rajeev Grover** and **Shri Shyam Sunder** for their help and support during my research.

I am grateful to my father **Shri M.C.Verma** and mother **Late Smt Krishna Devi** for being pillars of my strength, motivation and inspiration. I have no words to express my heartfelt

gratitude for their unwavering faith in me, for their words of wisdom, unconditional love and countless blessing they have always showered on me. I also express my gratitude to my brother **Shri N.K. Verma** and sister in-law Smt. **Ranjana** for their immense love and encouragement. I wish to express my indebted love and gratitude to my wife, **Richa**, who supported me through her enlightened heart during our stay at IIT Roorkee. I have no words to express my deep love and feelings to my sweet little princess, my daughter **Bhavya,** her innocent face and charming smile also gave me constant inspiration to make this research work possible.

At last but not the least, I would like to express my deepest gratitude to all those who have contributed directly or indirectly in the course of my research work and throughout my passage of life. I am thankful to them for inspiring me through their enlightened hearts, for touching me through their acts of kindness and honesty, and illuminating me through their wisdom and knowledge. I may not be able to recall all their names (please forgive me), but I am grateful to them in helping me to learn, to rise and to achieve in life.

"Thank You" Almighty for blessing me with this wonderful life, amazing family, loving friends, countless well-wishers and ample opportunities, without which this work would not have been possible.

Roorkee, November 2014 **(VIRENDRA KUMAR VERMA)**

TABLE OF CONTENTS

LIST OF FIGURES

LIST OF TABLES

LIST OF SYMBOLS

D	External diameter of UPVC tube
t	Thickness of tube
f_{ck}	Characteristic strength of concrete
f_y	Yield strength of steel
ϕ	Diameter of steel bar
E_c	Young's modulus of concrete
E_s	Young's modulus of steel
f_l	Confining pressure
f_c	Unconfined Compressive strength of concrete cylinder
f_{cc}	Confined compressive strength of concrete
ε_c	Axial compressive strain at peak stress of unconfined concrete
ε_{cc}	Axial compressive strain at peak stress of confined concrete
k_1	Triaxial factor
A_c	Cross-sectional area of concrete core
A_p	Cross-sectional area of UPVC tube
f_u	Ultimate tensile strength of UPVC tube
k_3	Material degradation parameter depending upon D/t ratio
α	Constraining factor
β	Confinement ratio
μ	Ductility ratio
ξ	Energy ratio
Δ	Axial displacement

E	Absorbed energy
Δ_y	Displacement at yield
E_y	E_y is the absorbed energy at yielding
Δ_{80}	Displacement at 80% of peak load
E_{80}	E_{80} is the absorbed energy at the load drops 80% of peak load
θ	Angle of failure plane

CHAPTER-1

INTRODUCTION

1.1 GENERAL

To achieve the long term durability of reinforced concrete structure in coastal areas is a difficult task. Concrete exposed to sea water get deteriorated due to combined effect of chemical action of sodium chloride and magnesium sulphate present in sea water. Concrete structures older than 10-15 years show a considerable amount of deterioration in the form of cracking & spalling of concrete and corrosion of reinforcement. This major problem has led to the development of new construction materials which could protect the structure against the cause of deterioration. A as Concrete filled plastic tubes (CFPT) can be considered as a new construction material which provides non-corrosive characteristics to infill concrete. Plastics have exceptional properties, such as high resistance to severe environmental attack, low cost, and high strength to weight ratio. Their service life goes beyond fifty years. UPVC is a polymer which is being used for a wide variety of civil engineering applications. Relatively low cost, biological and chemical resistance and workability made it useful in construction of the structures exposed to corrosive environments. . UPVC pipes are generally employed for water supply across the world. These pipes are designed for induced internal pressure of flowing water. On the basis of resistance against the water pressure, these pipes are categorized into different classes (IS: 4985-2000) on the basis of nominal pressure exerted by flowing water.

1.2 AXIAL LOAD CARRYING MECHANISM OF CONCRETE FILLED TUBES

When axial load is applied on concrete section/entire section of concrete filled tube (CFT), the structural behaviour of CFT is considerably affected by the difference between the Poisson‘s ratios of the tube and concrete core. In the initial stage of loading, the Poisson‘s ratio of the concrete is lower than that of tube. Thus, the tube has no confining effect on the concrete core. As longitudinal strain increases, the lateral expansion of concrete gradually becomes greater than expansion of tube. At this stage, the concrete core and tube experience tri-axial and bi-axial stresses and consequently the compressive strength of core concrete increases which as a result increases the load carrying capacity and enhances the ductility of columns. Fig.1.1 shows

the load carrying mechanism of concrete filled tubular (CFT) column and Fig.1.2 shows stress-strain curve of the confined and unconfined concrete.

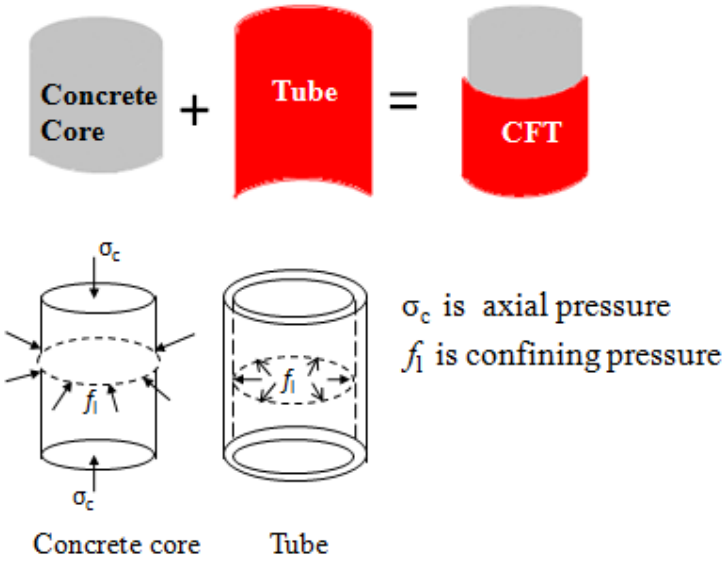

Fig. 1.1 Load Carrying Mechanism of CFT Column

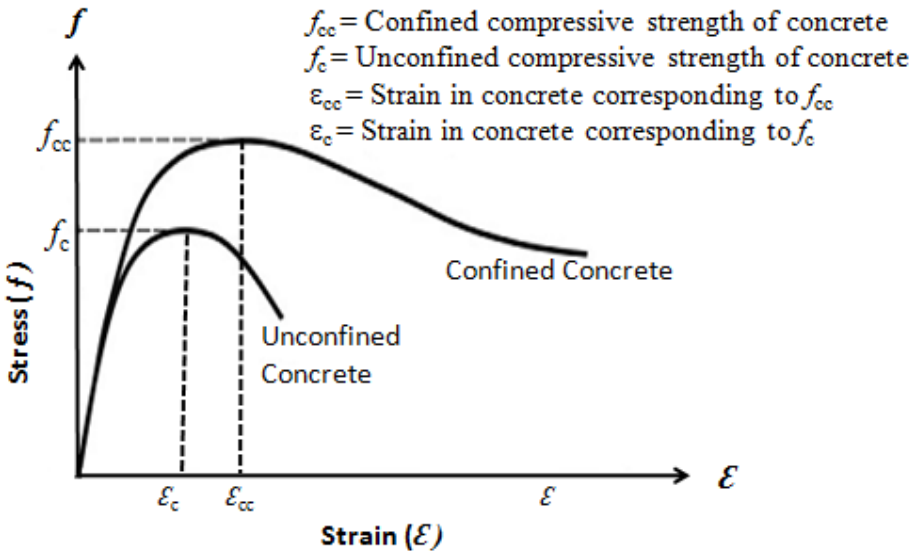

Fig. 1.2 Stress-strain curve for unconfined and confined concrete

1.3 REASONS FOR USING UPVC TUBES FOR CFT

In reinforced cement concrete (R.C.C.) structures, concrete exposed to marine environment get deteriorated due to the combined effects of chemical action of sea water constituents on cement hydration products, alkali aggregate expansion (when reactive aggregates are present),

crystallization pressure of salts within concrete if one face of the structure is subject to wetting and others to drying conditions, frost action in cold climates, corrosion of embedded steel in reinforced or prestressed members, and physical erosion due to wave action on floating objects. Concrete filled steel tubes (CFST) are used as structural members in multistorey buildings. Corrosion of steel is the main disadvantage of CFST. In addition to the corrosion problems, steel tubes would be lesser efficient in development of confinement at low load levels due to its higher Poisson's ratio, compared to that of concrete.

In recent years, Fibre Reinforced polymer (FRP) tubes have been frequently proposed to replace CFST due to their high strength to weight ratio, fatigue resistance, corrosion resistance. But these tubes may buckle under the weight of wet concrete during construction because of their low elastic modulus to strength ratio. These tubes are having a much lower breaking elongation (only 2 to 6%) and break suddenly when the radial deformation of the concrete core is unable to be restricted. FRP tubes are equally suitable for marine environment as UPVC tubes but they have some disadvantage. These include their relatively high cost, linear-elastic-brittle stress-strain behavior, low elastic modulus to strength ratio. UPVC tubes are having low cost, good ductility, excellent durability characteristics. Concrete filled UPVC tubes (CFUT) may be used for variety of application such as bridge piers, columns, piles or other structural members in marine and saline environment. It may also be used for overhead sign structures and light poles.

1.4 APPLICATIONS OF CFT

1.4.1 Concrete filled steel tubes (CFST)

Concrete filled steel tubes are being used as structural elements in constructions of different structures in Australia, Japan, Europe, United States of America, China, UK and Singapore. Structures constructed in different countries are shown in Fig.1.3. The Hearst Tower in New York, U.S. with the height of 182 m was completed in the year 2006. The concrete filled steel tubular columns used in this building act as lateral load resisting systems (Fig 1.3(a)). The latitude building 222 m high, in Sydney, Australia was completed in the year 2005. The CFST columns of 508 m in diameter with 80 MPa concrete were used on perimeter frame (Fig 1.3(b)). SEG plaza, in Shenzhen, China constructed in the year 2000 with the use of CFST columns was the first tallest building in the world at the time of construction. Its height is 291.6 m (Fig 1.3(c)). The Shimizu super high rise with a height of 550 m (Fig 1.3(d)) is one of the super tall skyscrapers in which circular CFST was used.

(a) Hearst Tower, New York , U.S.

(b) Latitude building, Australia

(c) SEG Plaza in Shenzhen, China

(d) Shimizu super high rise, Japan

Fig. 1.3 Structures constructed using CFST columns across the world.

1.4.2 Concrete filled fiber reinforced polymer tubes (CFFT)

CFFT tubes may be suitable for the use in piles, overhead sign structure, poles, column and pier and bridge piers. One of the example of CFFT in field application is port Hadlock, Indian Island, Washington (Fig.1.4(a)). Total 138 CFFT composite piles of 418 mm diameter and 25.9

m length were used in the project. A highway bridge made up with concrete filled FRP tubes is shown in Fig.1.4(b). It consists of 23 CFFT tubes of diameter 12 inches. CFFT were bent to the proper shape, and infused with resin.

(a) **Port Hadlock project-Washington State**

(b) Highway Bridge

Fig. 1.4 Structures constructed using CFFT columns across the world.

1.4.3 Concrete filled plastic tubes (CFPT)

Very few researchers have studied the behavior of concrete filled plastic tubes. They have investigated the influence of plastic pipes on the behavior of concrete filled inside it. The concrete filled plastic tubular column may be used in the structure constructed near the coastal areas, poles, overhead sign structure. A reinforced concrete filled PVC pipe shelter constructed in Hawaii is shown in Fig. 1.5 (Kratky and Roan, 1986).

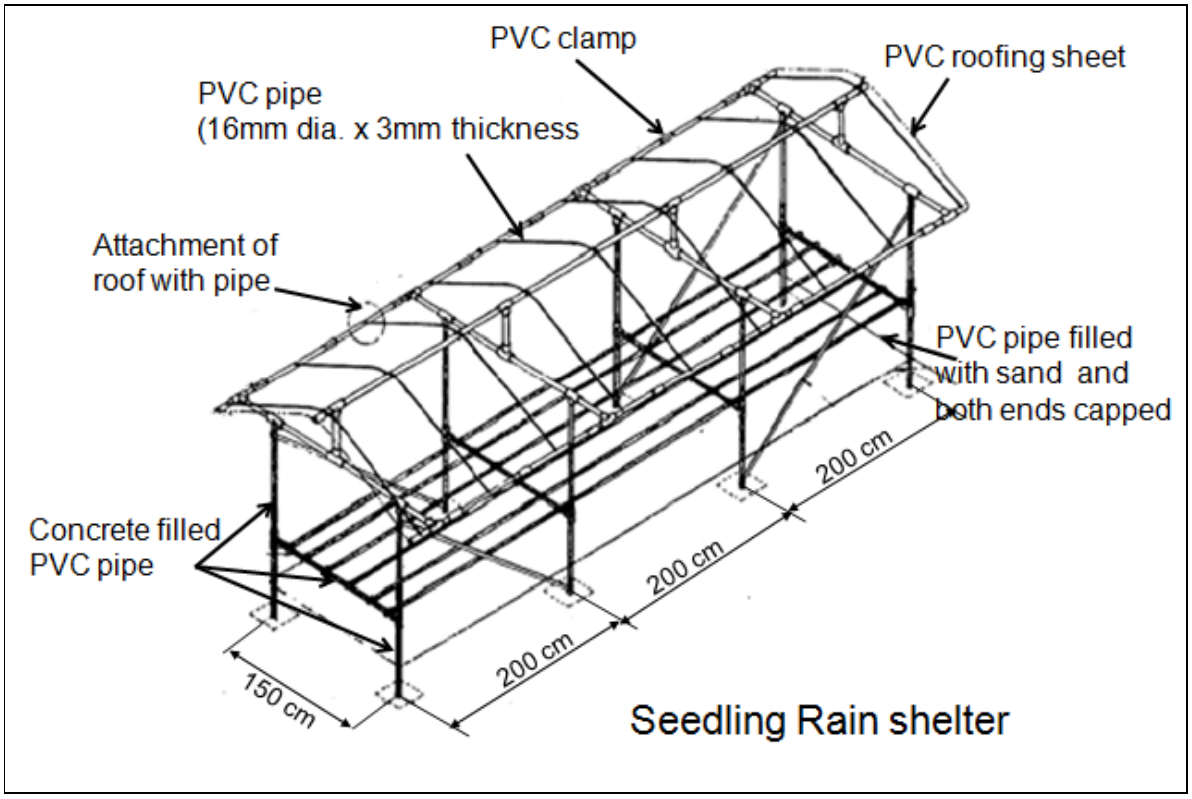

Fig. 1.5 Concrete filled PVC shelter constructed in Hawaii

1.5 DEVELOPMENT OF CONCRETE FILLED TUBES

Concrete filled steel tubes were first used as columns for the construction of road bridges in the late 1870's in Great Britain. Japan was among the few early nations who had worked on CFST because of its improved of earth quake resistant properties. First design recommendations for CFST column were established in 1967 by the Architectural Institute of Japan (AIJ). Then it was revised in 1981. In these recommendations CFST columns were considered a kind of Steel Reinforced Concrete (SRC) column because of their similarity in usage and mechanical characteristics. The recommendations made it possible to utilize CFST columns for the construction of buildings of more than 6 storeys.

Over the period of time, various countries have developed and designed their codes for the design of CFST as columns. Some of the standard codes of practice are given below:-

(a) Euro code 4 - European Code

(b) BS 5400 - British Code

(c) AIJ Code - Japanese code

(d) AISC- LRFD - American Code

(e) ACI 318 -American Code

(f) NBR 8800:2008(21) - Brazilian Code

(g) CAN/CSA S16-01:2001(24) -Canadian Code

(h) ANSI/AISC 360:2005(23) -American Code

1.6 OBJECTIVES OF THE PRESENT STUDY

At present, research work available in literature regarding the behavior of concrete filled plastic tubular column is too limited. Stress-strain model for the concrete confined with UPVC tubes is not developed till now. Furthermore, effect of sea water on behavior of concrete filled UPVC tubular column is still a subject of research. Therefore, present study covers experimental, analytical and numerical investigations on the behavior of Concrete filled UPVC tubular (CFUT) columns.

1.7 METHODOLOGY OF PRESENT STUDY

In the present research work, experimental, analytical and numerical studies are carried out to understand the behavior of concrete filled UPVC tubular (CFUT) column. In these columns, UPVC pipes of class 1, 3, 4 and 5 (as per IS: 4985-2000) used for water supply with nominal pressure of 0.25, 0.6, 0.8 and 1.0 MPa and the diameters of 160 mm, 200 mm and 225 mm are used. The different investigations are carried out in the following sequence.

1) Internal hydrostatic pressure tests on various UPVC pipes of different diameter to thickness ratio are conducted to ascertain the confining pressure.

2) Scanning electron microscopy (SEM) test was also performed to examine microstructure of UPVC specimen before and after immersion in sea water.

3) Plain concrete filled UPVC tubular (PCFUT) columns are prepared for the study of confinement effect and to develop the stress-strain model for concrete confined with UPVC tubes. An analysis is done to understand the failure mechanism of confined concrete. Inclination of failure plane for different confining pressure is calculated with the help of Mohr-Coulomb failure criterion. The results are verified with experimental results.

4) Reinforced concrete filled UPVC tubular (RCFUT) columns are prepared to study the behaviour of RCFUT with their submergence in artificial sea water.

5) Bare R.C. columns obtained by removing the outer tube of RCFUT columns are considered to see the effect of sea water on their behaviour and load carrying capacity.

6) RCFUT with class 1 pipes are prepared exclusively to see the effect of sea water on the concrete confined with minimum thickness of UPVC tubes.

7) A three dimensional Finite Element model is developed using ANSYS software to simulate the concrete filled UPVC tube (CUFT) subjected to axial compression. Suitable material constitutive models for UPVC tube, concrete core and reinforcement are adopted.

All the specimens are tested for axial compression by applying load on concrete core only. The setup for loading is given in Fig. 1.6. The value of D/t and grade of concrete are varied. Axial compression test are conducted in INSTRON load testing machine of 2500 kN capacity. The results obtained from testing are used to find out the confinement ratio, ductility ratio and energy absorption capacity of CFUT column specimens.

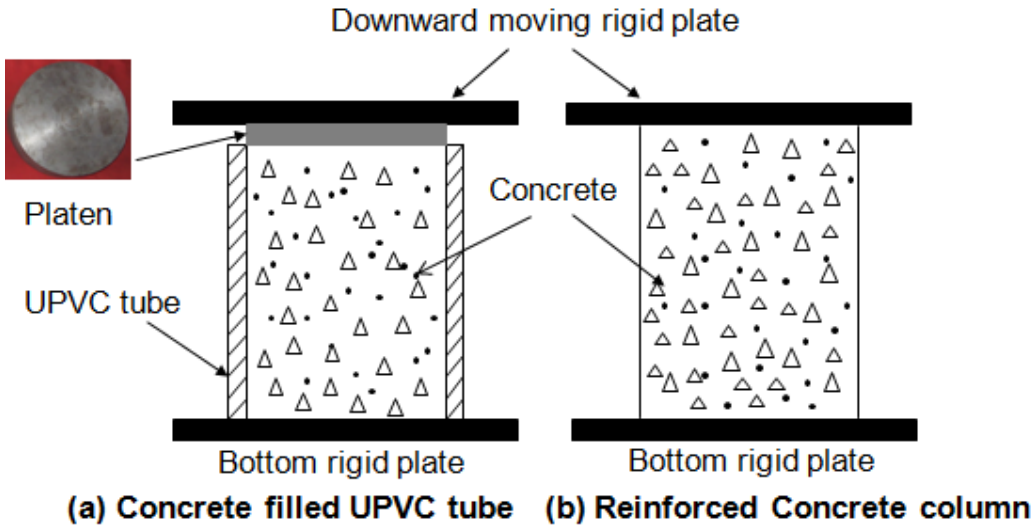

Fig. 1.6 Setup for loading: (a) concrete filled UPVC tube (b) RCC column

1.8 OUTLINE OF THE THESIS REPORT

The thesis is presented in systematic manner to understand in better way. All the topics are covered in ten chapters.

Chapter One presents the brief introduction about the different types of concrete filled tubes and their field applications, problems related with reinforced concrete in marine environment. This chapter also presents the reason of using CFUT columns.

Chapter Two covers the review of available literature regarding active and passive confinement of concrete, Stress-strain model of unconfined and confined concrete, performance of concrete in sea water, numerical modeling of Concrete filled tubes.

Chapter Three describes the experimental programs in details, material properties, Composition of artificial sea water, casting and testing procedure.

Chapter Four covers the details of proposed Finite element model for simulating the PCFUT columns, RCFUT columns and bare R.C. columns. Experimental results are verified with numerical results.

Chapter Five describes the results of experimental and numerical investigations on PCFUT specimens. Stress-strain model of concrete confined with UPVC tube is discussed. Mohr-coulomb failure theory is used to calculate the angle of failure plane and load capacity of specimens.

Chapter Six covers the study of confinement in reinforced concrete column and the suitability of stress-strain model for R.C. column is discussed.

Chapter Seven presents the results of experimental and numerical investigations on RCFUT and bare R.C. column specimens. Effect of sea water is also discussed on bare R.C.C and RCFUT specimens.

Chapter Eight presents the results of experimental and numerical investigations on RCFUT made with UPVC pipes of class 1. This study was conducted exclusively to see the effect of sea water on reinforced concrete having protection of UPVC pipe with minimum thickness.

Chapter Nine presents the strain measurement using Digital Image Correlation (DIC) System with software Vic-3D. Strain obtained with DIC is compared with strain obtained from Simulation.

Chapter Ten covers the conclusions obtained from all the chapters included in the thesis.

CHAPTER 2

LITERATURE REVIEW

2.1 GENERAL

The research investigations on the use of composite material for the columns and beams are available since long (sofi et al., 2007; Wu et al., 2010; Raman et al., 2011; Alhozaimy et al., 2012-a; Alhozaimy et al., 2012-b; Baidya et al., 2013). Some of the researchers studied the behavior of structural elements of composite materials (Menon, 2001; Thanoon et al., 2004-a; Thanoon et al., 2004-b; Borsaikia et al., 2006; Laskar et al., 2008-a; Laskar et al., 2008-b; Laskar et al., 2008-c; Chakrabarti et al., 2012-a; Chakrabarti et al., 2012-b; Chakrabarti et al., 2012-c; Chakrabarti et al., 2013). Few researchers carried out numerical modeling of structural elements (Balendra, 1983; Sridevi and Agrawal, 1991; Umar et al., 1994; Umar et al, 1996; Menon and Reddy, 1998; Revathi and Menon, 2005; Choubey et al. 2006; Partheepan et al., 2008). For the safety of structure, the parameters like strength, ductility, durability were taken as important parameters by the researchers in their research (Agrawal and Chourasia, 2003; Gupta et al., 2003; Agrawal and Chourasia, 2005; Rai and Prasad, 2005-a; Rai and Prasad, 2005-b; Rai et al., 2006).

The research works which are directly related to the present work have been described in this chapter. This chapter starts with the literature review of use of composite material in general construction followed by the views of different researchers on active and passive confinement of concrete. In connection with active and passive confinement, triaxial compression tests on concrete cylinder and study of concrete filled tubular columns are also included. Reviews on stress-strain model for unconfined and confined concrete given by researchers are also covered and presented. The review of load carrying capacity, ductility and energy absorption of different structural elements are discussed especially in context with concrete and reinforced filled tubular columns exposed to marine environment. Based on the literature review, objectives of the research work are formulated.

2.2 CONFINEMENT

2.2.1 Active confinement

Richart et al. (1928) studied the failure behavior of concrete under biaxial and triaxial compression. They took cylinder specimens having 100 mm diameter and 200 mm length of three different concrete strengths (17.75 MPa, 25.24 MPa and 7.24 MPa) for triaxial compression test. They applied different confining pressure and axial load on the specimens to get different failure modes. They found that at low confining pressure, most of the specimens failed by development of inclined cracks while at large confining pressure, a pronounced bulging was noticed. They showed that the strength of specimen increased by 4.1 times the lateral confining pressure. They proposed empirical relationships for strength and strain of confined concrete.

$$f_{cc} = f_c + k_1 f_l \tag{2.1}$$

$$\varepsilon_{cc} = \varepsilon_c \left(1 + k_2 \frac{f_l}{f_c}\right) \tag{2.2}$$

Where,

f_{cc} => Axial compressive strength of confined concrete.

f_c => Uniaxial compressive strength of the concrete.

ε_{cc} => Strain in concrete corresponding to f_{cc}.

ε_c => Strain in concrete corresponding to f_c.

k_1 => Constant and equal to 4.1.

k_2 => Constant and equal to 20.5

f_l => Lateral confining pressure.

Palaniswamy and Shah (1974) conducted experiments on the specimens of cement paste, mortar and concrete of size 76 mm x 230 mm to see the mechanics of failure of concrete under triaxial stresses. They applied a constant hydrostatic pressure first and then increasing axial stress till the specimen failed. They used four values hydrostatic pressure i.e. 14 N/mm^2, 28 N/mm^2, 41 N/mm^2, 55 N/mm^2. They observed the two types of failure, a splitting failure at low confining pressure (14 N/mm^2 & 28 N/mm^2) and a crushing failure at large confining pressure (41 N/mm^2 & 55 N/mm^2). They proposed a stress-strain relationship for the concrete under triaxial compression.

Ahmad and shah (1982) proposed the equations for the ascending and descending branch of stress-strain curve of concrete subjected to triaxial compressive stress. The stress-strain relation was dependent on three principal stresses and strain. To verify proposed analytical stress-strain relationship, they conducted some experiments on concrete filled steel tubes by taking three different compressive strength of concrete and two different thicknesses of tube. They observed a larger slope of the post peak branch of the stress-strain curve for higher compressive strength of concrete.

Imran and Pantazopoulou (1996) conducted experiments to study the behavior of concrete under different combinations of triaxial stresses. Cylindrical specimens of size 54 mm diameter and 115 mm length were taken. Confining pressures in terms of fraction of uniaxial compressive strength equal to 0, 0.05, 0.1, 0.2, 0.4, 0.7 and 1.0 were applied. Four types of load combinations were applied on the specimens. In first load combination, axial compressive load was applied gradually with constant confining pressure. In second load combition, the confining pressure and axial stress both were increased simultaneously. In third load combination, the confining pressure was reduced with increase in axial stress. In fourth combination, axial stress was applied in cyclic manner with constant confining pressure. They noticed macrocracks on the surface of specimens subjected to low level of confinement (i.e. 5 to 20 % of uniaxial compressive strength) and bulging in specimens was observed at high level of confinement (greater than 40 % of uniaxial compressive strength). They observed that concrete subjected to cyclic loading experienced large volumetric expension compared to concrete subjected to monotonic loading i.e. cyclic loading damages the concrete at faster rate.

Attard and Setunge (1996) developed active confinement model for the stress-strain relationship for confined and unconfined concrete. Confinement pressure for the active confinement was taken from 1 to 20 MPa. The uniaxial compressive strength was taken from 60 to 130 MPa. They found that effect of confining pressure is similar whether it is active or passive. They concluded that their stress-strain model may be used for the analysis of reinforced concrete columns and concrete filled steel tube columns to get deformation and ductility response.

Rutland and Wang (1997) performed triaxial tests on cement mortar cylinders (50 mm x 100 mm) to study the failure mechanism. Different angles of failure plane were obtained at different

confining pressure ranging from 0 to 56 MPa. They concluded that angle of failure plane relative to the direction of maximum compressive stress increased with increasing confining pressure.

Ansari and Li (1998) conducted experimental study on normal and high strength concrete subjected to triaxial compression. The tests were performed on 100 mm x 200 mm concrete cylindrical specimens of strengths 42, 69 and 103 MPa. The confining pressures were applied from 8.3 to 83 MPa. It was observed that effect of confining pressure on the failure strength of high strength concrete was not as pronounced as on normal strength concrete. Further it was observed that at high confining pressure failure strain increases by many fold. Shear failure was observed in most of the specimens.

Nielsen (1998) performed triaxial compression tests on high strength and normal strength concrete. He applied the Coulomb failure criteria to analyze the data. He found that at small confining pressure, triaxial strength was governed by cohesion and at for higher confining pressure, it was governed by internal coefficient of friction. The angle of friction was found approximately 51^0 for small confinement, reflecting the brittle failure and it was 30^0 at higher confinement, reflecting ductile sliding failure.

Sfer et al. (2002) performed experiments on 150 mm x 300 mm cylindrical specimens to study the behavior under triaxial compression. A confining pressure of 0 to 60 MPa was used to obtain the brittle-ductile transition behavior of the material. They found that load carrying capacity under axial compression increases significantly with an increase in the confining pressure. There was distributed microcracking and several macrocracks at zero or lower confinement while at higher confinement failure was by development of fine microcracks and a few macrocracks that seperated the specimens into two or three blocks.

2.2.2 Passive confinement

2.2.2.1 Concrete filled steel tubes (CFST)

Gardner and Jacobson (1967) studied the behavior of concrete filled steel tubes subjected to axial compression. They found that the structural behavior of CFST elements are considerably affected by the difference between the Poisson‘s ratios of the steel tube and concrete core. They noticed that steel tube had no confining effect on the concrete core at initial stage of loading due to lower Poisson‘s ratio of the concrete compared to steel. At the stage, when lateral expansion of

concrete became greater than expansion of steel tube, concrete core became tri-axially and steel tube bi-axially stressed and consequently load carrying capacity and ductility of column increased (Fig 2.1).

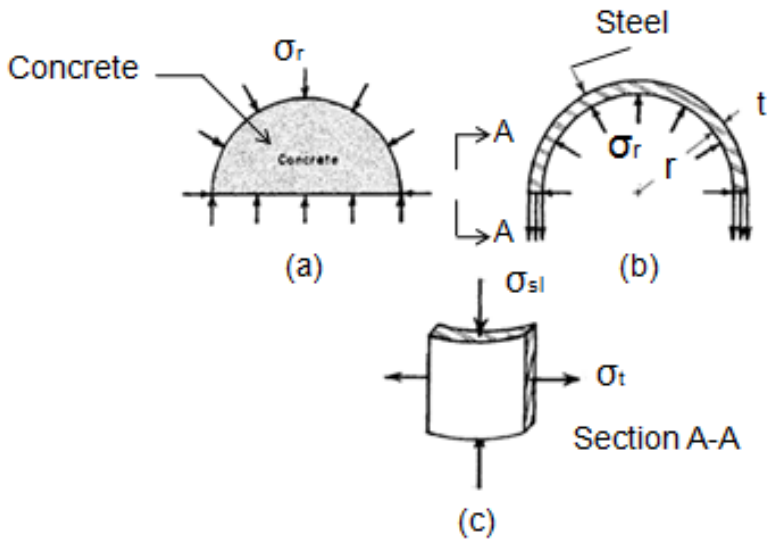

Fig. 2.1 Free body diagram showing the forces on concrete core and steel tube Gardner and Jacobson (1967)

$$\sigma_t = (r/t) \times \sigma_r \quad (2.3)$$

$$\sigma_c = f_c + K\,\sigma_r \quad (2.4)$$

Where,

σ_r = Internal radial pressure.

σ_t = Hoop tensile stress.

t = Thickness of tube.

r = Radius of tube

σ_c = Stress in concrete

f_c = Unconfined crushing strength of concrete

σ_{sl} = Longitudinal stress in steel tube

K = Empirical factor (experimentally determined equals to 4)

Schneider (1998) tested fourteen specimens of concrete filled steel tube columns having only three of circular shape to investigate the effect of steel tube shape and wall thickness on ultimate strength of concrete column. He reported that for small dimensional CFST columns, smaller D/t ratio provides a significant increase in yield load. He also concluded that the specimen having small D/t ratio exhibited more favorable post-yield behavior.

Gupta et al. (2007) tested eighty one specimens of CFST columns to investigate the effect of length to diameter (L/D) and D/t of a steel tube on the load carrying capacity of concrete filled tubular columns. The study reported that for smaller D/t values, steel tube provides good confinement effect to the concrete. It was also reported that the load carrying capacity of the steel tube per unit volume decreases as the D/t value increases and hence it was suggested to fix a correct D/t value in order to make optimum usage of the materials. This was also found that for higher value of L/D, specimens which deform in Euler buckling, the confinement was of lower magnitude.

Liu et al. (2009) carried out experiments on circular tube confined reinforced-concrete (CTRC) columns and circular reinforced concrete (CRC) under cyclic and monotonic axial compression. They proposed an equation to calculate the axial load strength of CTRC. They found that CTRC columns showed higher flexural strength and ductility compared to CRC with the same column size and longitudinal reinforcing bars. They suggested modified ACI code method to calculate moment strength of cross section of CTRC columns.

Liang et al. (2009) carried out parametric studies to investigate the effect of D/t value, concrete compressive strength and yield strength of steel on strength and ductility of CFST columns. They reported reduction in axial ductility performance of CFST columns with increase in D/t value. They also found that circular CFST columns with D/t values ranging from 60-100 exhibit strain softening behavior.

2.2.2.2 Concrete filled fiber reinforced polymer tubes (CFFT)

El-Kareim and Soliman (2011) tested long columns having slenderness ratio between 10.0 and 17.5. Failure mechanism and failure mode with theoretical model for calculation of column capacity was investigated. They found that column of slenderness ratio 10, 12 & 12.5 were failed due to the failure of plastic tube while the column with slenderness ratio 14, 15, & 17.5 were failed due to excessive increase of the horizontal displacements.

Hamdy and Radhouane (2010) tested 23 concrete filled FRP tube (CFFT) columns under axial & eccentric load. They compared the experimental results and theoretical predicted values by American codes and guidelines. They concluded that the failure of the CFFT specimens with length to diameter ratio ranged from 2 to 7 was mainly due to the rupture of FRP tubes.

Fam and Rizkalla (2001) presented experimental study and compared the behaviour of concrete filled GFRP tube to concrete filled steel tube. They concluded that GFRP tube provides similar confined concrete strength to that provided by steel tubes while using 37% less wall thickness than steel tube. They also concluded that interface condition between the tube and concrete has an insignificant effect on the behaviour when both the concrete core and tube are axially loaded.

Teng et al. (2007) performed flexural test on Hybrid FRP-concrete-steel double skin tubular columns. They found that such beams have a very ductile response and GFRP tube in such beams enhances the structural behaviour by providing confinement to the concrete and additional shear resistance.

2.2.2.3 Concrete filled plastic tubes (CFPT)

Kurt (1978) studied behavior of concrete filled plastic columns with the help of experiments and theoretical analysis. He observed that when the concrete core of concrete filled plastic column is loaded axially, an effective compressive pressure is generated on the boundary between the core and pipe due to Poisson effect. He conducted some experiments to see the influence of slenderness ratio on the behavior of concrete filled plastic columns. He observed that approximately 62% of ultimate load is carried by shorter column at an 8% strain level and total collapse occurred after this strain level while total collapse of long column occurred at the strain level of 2% only. He found that slenderness effect was more important when the slenderness ratio was greater than 20.

Marzouck et al. (2002) conducted experimental study on concrete filled PVC tubes with 100 mm internal diameter and 3 mm thickness of tube. Different lengths of tubes were taken such as 758, 562, 416 and 270 mm. They concluded that the PVC tube provides considerable lateral confinement to the concrete core. They also reported that as the slenderness ratio increases, the compressive strength of concrete filled PVC tube decreases. They found that tube exhibits large lateral deformation before failure.

Wang and Yang (2010) presented an experimental study on concrete filled high density polyethylene pipe (HDPE). They reported that both thickness and unconfined compressive strength

of concrete affects the ultimate strength and post-peak behavior of PPC. They observed that at lower confinement, the mode of failure was shear while at higher confinement it was drum type.

Gupta (2013) carried out experimental study to investigate the effectiveness of UPVC tube for the confinement of concrete columns. In his study he employed UPVC tubes of 140 mm, 160 mm and 200 mm diameters filled with concrete of compressive strength of 20 MPa, 25 MPa and 40 MPa. He reported that confinement of concrete columns with UPVC tubes enhances their load carrying capacity and ductility. He observed shear type failure of all the tested specimens.

Tan et al. (2013) carried out some experiments on capsule shaped plain concrete columns with different aspect ratio and confined with fiber reinforced polymer (FRP) sheets. They tested the columns for monotonically increasing axial load. They found an increase in the strength of columns by 143%, 72%, 22% and 28% for column section aspect ratio of 1, 2, 3 and 4 respectively. They proposed a confinement model for circular, rectangular and capsule shaped columns confined with FRP using a modified effective confinement coefficient.

Kratky and Roan (1986) designed a seedling shelter of size 6 m x 1.5 m. Reinforced concrete filled PVC pipes were used for the design of basic framework. PVC pipes of 5 cm diameter and 110 cm length were taken. Along with concrete a 13 mm diameter steel rod was placed inside the pipe as reinforcement. For the protection of PVC pipes it was suggested that PVC pipes should be ultraviolet treated or painted dark to protect against ultraviolet rays of Sun and then painted with white paint again to provide maximum reflectance of rays.

2.3 STRESS-STRAIN MODEL FOR MATERIALS

2.3.1 Concrete

Saenz (1964) proposed a stress-strain (f-ε) curve for concrete under uniaxial compression. Stress-strain relation was given in the following form:

$$f = \frac{E\varepsilon}{1+(R+R_E-2)\left(\frac{\varepsilon}{\varepsilon_0}\right)-(2R-1)\left(\frac{\varepsilon}{\varepsilon_0}\right)^2+R\left(\frac{\varepsilon}{\varepsilon_0}\right)^3} \tag{2.5}$$

where $R_E = \frac{E}{E_s}$ is the modular ratio, $R = \frac{R_E(R_f-1)}{(R_\varepsilon-1)^2}-\frac{1}{R_\varepsilon}$ is the ratio relation

$R_f = \frac{f_0}{f_f}$ is the stress ratio, and $R_\varepsilon = \frac{\varepsilon_f}{\varepsilon_c}$ is the strain ratio

E_s = Secant modulus, f_0 = Maximum stress , ε_0 = strain at maximum stress,

f_f =stress at failure, ε_f = strain at failure

Popovics (1973) proposed an equation to describe the stress-strain behavior of unconfined concrete. Stress-strain formula was given as:

$$\frac{f}{f_0} = \frac{n\frac{\varepsilon}{\varepsilon_0}}{(n-1)+\left(\frac{\varepsilon}{\varepsilon_0}\right)^n} \tag{2.6}$$

Where the power 'n' can be expressed as an approximate function of compressive strength of normal-weight concrete as follows:

$$n = 0.4 \times 10^{-3} f_0(\text{psi}) + 1.0 \tag{2.7}$$

f_0 = Maximum stress, ε_0 = strain at maximum stress.

Desayi et al. (1978) conducted tests on circular columns with spiral transverse reinforcement and proposed an equation to describe the pre and post peak behavior of confined concrete.

$$f = \frac{A}{1+B\varepsilon+C\varepsilon^2+D\varepsilon^3} \tag{2.8}$$

where, parameters A, B, C and D were obtained from boundary conditions and test results.

$$A = E_c \tag{2.9}$$

$$B = \left[\frac{1-2k\beta+k\beta^2}{k(\beta-1)^2}\frac{E_c}{E_{c'}} - \frac{2\beta+1}{\beta}\right]\frac{1}{\bar{\varepsilon}_c} \tag{2.10}$$

$$C = \left[\frac{\beta+2}{\beta} - \frac{2(1-k)}{k(\beta-1)^2}\frac{E_c}{E_c^{'}}\right]\frac{1}{\bar{\varepsilon}_c^2} \tag{2.11}$$

$$D = \left[\frac{(1-k)}{k(\beta-1)^2}\frac{E_c}{E_c^{'}} - \frac{1}{\beta}\right]\frac{1}{\bar{\varepsilon}_c^3} \tag{2.12}$$

$$E_c^{'} = \frac{\bar{f}_c}{\bar{\varepsilon}_c} \tag{2.13}$$

$$\beta = \frac{\bar{\varepsilon}_{0.85}}{\bar{\varepsilon}_c} = \frac{1.8 + 46.5C_i}{1.0 + 23.0C_i} \tag{2.14}$$

where 'k' and 'β' are constant and C_i is the coefficient index and equals to

$$C_i = (p_b - \bar{p}_b)\frac{f_y}{f_c^{'}} \tag{2.15}$$

Where p_b is the ratio of volume of spiral reinforcement to the volume of confined concrete, $\bar{p}_b$ is the value of p_b when the pitch of spiral is equal to the least lateral dimension of the specimens.

Mander et al. (1988-a) tested circular, rectangular and square R.C. columns to investigate the influence of different transverse reinforcement (spiral or lateral ties) on the effectiveness of confinement. They observed that stress-strain behavior was similar regardless the arrangement of transverse reinforcement. They presented a stress-strain model for concrete confined by transverse reinforcement. The model was based on the equation given by popovics (1973). The equation for monotonic compression loading was given as:

$$\frac{f_c}{f_{cc}} = \frac{r\frac{\varepsilon_c}{\varepsilon_{cc}}}{(r-1) + \left(\frac{\varepsilon_c}{\varepsilon_{cc}}\right)^r} \tag{2.16}$$

Where f_{cc} is the compressive strength of confined concrete.

$$r = \frac{E_c}{E_c - E_{\sec}} \tag{2.17}$$

$$E_c = 5000\sqrt{f_{co}}\,MPa \tag{2.18}$$

$$E_{\sec} = \frac{f_{cc}}{\varepsilon_{cc}} \tag{2.19}$$

$$\varepsilon_{cc} = \varepsilon_{co}\left[1+5\left(\frac{f_{cc}}{f_{co}}-1\right)\right] \tag{2.20}$$

$$f_{cc} = f_{co}\left(-1.254+2.254\sqrt{1+\frac{7.94 f_l}{f_{co}}-2\frac{f_l}{f_{co}}}\right) \tag{2.21}$$

Where f_{co} is the unconfined compressive strength of concrete and f_l is the confining pressure.

$$f_l = \frac{1}{2}k_e \rho_s f_{yh} \tag{2.22}$$

where ρ_s is the ratio of the volume of transverse confining steel to volume of confined concrete core, f_{yh} is the yield strength of transverse reinforcement and k_e is confinement coefficient.

For circular hoops- $k_e = \dfrac{\left(1-\dfrac{s'}{2d_s}\right)^2}{1-\rho_{cc}}$ (2.23)

For circular spirals- $k_e = \dfrac{\left(1-\dfrac{s'}{2d_s}\right)}{1-\rho_{cc}}$ (2.24)

Where ρ_{cc} is the ratio of longitudinal reinforcement to area of core of the section, s' is the spiral or hoop bars, d_s is the diameter of the spiral.

Mirmiran and shahawy (1996) developed a stress-strain model for varying lateral confining pressure of concrete filled FRP tube. They compared their model with the model of Mander et al. (1988) for constant confining pressure and concluded that Mander's model overestimates the intermediate stresses by 17%.

Fam and Rizkalla (2001) introduced an analytical model to study the behavior of axially loaded circular concrete columns confined by fiber reinforced polymer (FRP) tubes. They modified the confinement model of concrete confined by steel reinforcement given by Mander et al. (Mander et al. 1988). They observed that Mander's model is suitable for constant confining pressure while in case of FRP tube the confining pressure increases continuously during the loading history. They proposed an incremental passive confinement model using Mander's model.

Hu et al. (2003) simulated the post peak behavior of concrete confined with steel tube by a linear variation and gave a parameter k_3 to obtain a stress-strain model. They proposed empirical relationships between confining pressure and k_3 as a function of diameter/wall thickness (D/t) for the two ranges of D/t values (21.7 to 47 and 47 to 150). They reported that circular tubes having smaller D/t values (say D/t < 40) provide a greater confinement. The proposed stress-strain curve is shown in Fig. 2.2. The first part of the curve (AB) defines the linear property of confined concrete with the proportional limit stress of $0.5f_{cc}$. The second part of the stress-strain curve (BC) is nonlinear curve, started from the proportional limit stress $0.5f_{cc}$, ends at the confined strength f_{cc}. This part was obtained from Eq. 2.1 given by Saenz (1964). The third part of the curve (CD) starts from f_{cc} and ends at k_3f_{cc} with the corresponding strain $11\varepsilon_{cc}$. The reduction factor k_3 depends upon (D/t) values of tube.

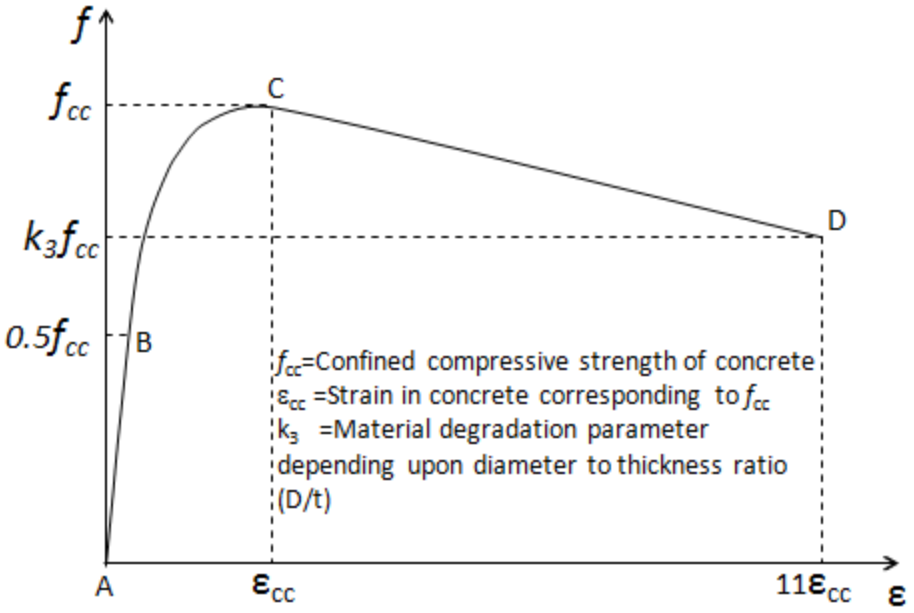

Fig.2.2 Stress-strain curves for concrete confined by Steel tube

2.3.2 Polymers

Ward (1971) reviewed the yield behavior of polymers. He discussed the effect of hydrostatic stress component and viscoelastic nature on yield behavior of polymers. He also studied the behavior of oriented polymers. He found that effect of orientation was much larger than that of the hydrostatic component of stress.

Raghava et al. (1973) conducted experiments on polyvinyl chloride and polycarbonate polymers to investigate their yield behavior. They proposed a new relation for the yield behavior of polymers, which was a new version of von Mises criteria. This relation accommodates the difference in tensile and compressive yield strength.

Caddell et al. (1974) considered two forms of modified von-Mises criterion with the effect of hydrostatic pressure on yield behavior of polymers. They compared their analytical results with experimental information available in literature. They concluded that for more pronounced pressure conditions, criterion suggested by Raghava et al. (1973) provided a better correlation with experimental results.

Ragab et al. (2000) tested rigid PVC pipes in biaxial stress system covering the four quadrants of the plane-stress space. The loading was considered as tension, compression, torque and internal & external pressurization. They tested specimens at different strain rates and temperatures. In their experiments, they took rigid PVC pipes with 60 mm diameter and 5.3 mm thickness having 1 MPa working pressure. They plotted the yield loci at various strain rates and temperatures. They observed that yielding of rigid PVC pipes follows the von-Mises yield criterion.

Neelam et al. (2002) determined the elastic material properties of Polyvinyl Chloride (PVC) with the help of experiments. They conducted tension tests to obtain stress-strain relationship and ring bending tests to get pipe flexural stiffness. They also tested short pipes under axial compression to evaluate the buckling load. They observed that initial modulus from tension test was 3500 MPa and Poisson's ratio was 0.31. Elastic modulus of PVC in compression was found 15 to 31% less than the tensile modulus. They found pipe stiffness between 1.0 and 3.2 N/mm.

Clausen et al. (2011) suggested a constitutive model for thermoplastic materials. They divided the model into two parts: A hyperelastic-viscoplastic response due to intermolecular resistance and an entropic hyperelastic response due to re-orientation of molecular chains. They performed uniaxial tension and compression tests on HDPE and PVC material to obtain 11 non-zero coefficients for the model. They also performed numerical simulations of three-point bending tests on the same materials for the verification of constitutive model.

2.4 LOAD CARRYING CAPACITY

Gardner and Jacobson (1967) showed that load carrying capacity of CFST columns was higher than the nominal load carrying capacity calculated based on strength of steel and concrete acting alone. They proposed a formula for calculating the load carrying capacity of short and long CFST columns. The proposed formula for short CFST column was given as:

$$P = A_c f_c^{'} + \frac{K}{2} A_s \sigma_t A_s \sigma_{sl} \tag{2.25}$$

Where, P is ultimate load carrying capacity, A_c and A_s are the areas of concrete core and steel tube respectively. f_c' is compressive strength of unconfined concrete and σ_{sl} is longitudinal stress in steel tube. σ_t is the yield stress of steel tube. K is confinement parameter and equals to 4. The buckling load for long CFST column was proposed as:

$$P_{cr} = \pi^2 \left(\frac{E_s I_s + E_c I_c}{L^2} \right) \tag{2.26}$$

Where, E_s and E_c are tangent modulus of elasticity of steel and concrete, respectively. I_s and I_c are moment of inertia of steel and concrete, respectively. L is the effective length of column.

Giakoumelis and Lam (2004) investigated load carrying capacity of short CFST column by varying the diameter to thickness ratio of tube and grade of concrete. D/t ratios were taken from 22.9 to 30.5 and concrete strengths were 30, 60 and 100 MPa. They compared the experimental results with the values obtained by Euro code 4, Australian standards and American codes. The reported that Euro code 4 provides a good prediction for the axial strength of concrete filled steel tube columns. They observed that the axial strengths of columns predicted using Australian standards and American codes were 35% lower than experimental values.

Gupta et al. (2007) studied, effect of D/t ratio on the load carrying capacity of CFST columns filled with fly ash based concrete. Fly ash was added in the mix with different percentage as 15%, 20% and 25%. They reported that as D/t ratio increases, load carrying capacity decreases and an increase in the length decreases the load carrying capacity.

Ahmad et al. (2012) studied effect of lateral confinement on the load carrying capacity of reinforced concrete columns. They prepared circular and rectangular specimens with seismic hooks

(135^0) and non-seismic hooks (90^0). They found that load carrying capacities of columns were increased with increase in ratio of volume of hooks to the volume of concrete core. They observed that column with seismic hooks had higher peak strength compared to columns with non-seismic hooks. They also found that circular hoops are more effective than rectangular hoops.

2.5 NUMERICAL SIMULATION

Schneider (1998) developed a three dimensional Finite element model using ABAQUS software to study the behavior of axially loaded concrete filled steel tubular columns. The concrete core was modeled using 20 node brick elements and steel tube was modeled with eight node shell element. The contact area between concrete and steel was modeled with the interface element. He conducted experiments to verify analytical results. He observed that the variation in the strength of concrete filled tubes obtained from experiments and analysis was within 5% and mode of failure was similar.

Shams and Saadeghvaziri (1999) performed a parametric study, using three dimensional Finite element model to identify the effect of D/t ratio and concrete uniaxial compressive stress on the behavior of CFST columns under axial loading. They found that as D/t value increases the yield stress of steel tube decreases. The decrease in yield stress of steel tube compared to normal yield stress is more significant in columns with higher D/t and could be as low as 85 percent of the normal yield stress. They proposed a relationship between maximum stress and D/t for both circular and square columns.

Hu et al. (2003) carried out a nonlinear Finite element analysis (FEA) of concrete filled steel tubular (CFT) columns with circular section, square section and square section stiffened by reinforcing ties to study the behavior of CFT columns. They simulated the post peak behavior of concrete confined with steel tube and reported that circular tubes having smaller D/t values (say $D/t < 40$) provide a greater confinement compared to tubes having higher D/t values.

Ellobody et al. (2006) carried out Finite element analysis using ABAQUS software to study the behavior of axially loaded CFST columns. The specimens were having D/t values ranging from 15 to 70. The stress-strain curve of confined concrete proposed by Hu et al. (2003) was used. They conducted experiments to verify numerical results. The results obtained from experiments and

analyses were quite similar. They observed that column strength increased due to the decrease of the D/t ratio up to 55 and strength slightly increased for D/t ratio from 55 to 70.

Son and Fam (2008) developed a Finite element model to study the flexural behaviour of hollow and concrete filled FRP tubes (CFFTs). The Tsai-Wu failure criterion for the failure of FRP material was used and model was verified by comparing findings with experimental results. They concluded that model was capable to capture the local buckling failure mode of thin walled hollow tubes.

El-Heweity (2012) conducted a parametric study using Finite element analysis to investigate the influence of diameter of concrete filled tubular column and yield stress of steel. The diameters of tubes were 100 mm, 140 mm and 200 mm and yield strength of these steel tubes were 240 MPa, 360 MPa and 520 MPa. He reported that failure axial strain for smaller diameter specimen was higher as compared to larger diameter specimen. The values of the strains were 0.032 for columns having large diameter and 0.046 for small diameter columns.

Gao et al. (2013) developed a numerical model to predict the axial load capacity of circular tubular steel braces strengthened by carbon fiber reinforced polymer (CFRP) sheets. They found that enhancement in the strength and stiffness of long braces was dependent on the number of CFRP layers used. They developed a linear relationship between axial load and number of CFRP layers.

2.6 DUCTILITY AND DURABILITY

Rao et al. (2011) studied the influence of properties of interface between cement paste and aggregate on the ductility and stiffness of concrete. They found that ductility of concrete decreases with increases in the surface area of interface. They observed that the fracture toughness of interface was very low compared to cement paste, mortar and concrete.

Mather (1964) studied, effect of sea water on concrete. He found that the deterioration of concrete in warm water was mainly due to the chemical action of chloride and sulphates present in water and in colder water, the main damage was done by temperature change. He suggested that a suitable type of cement and good sound aggregates might be a better option for protection of concrete.

Idorn (1967) did a survey of 431 marine structures, which were 20 to 50 years old. He found that 40% of structurs were completely deteriorated while 35% were suffered with severe surface damage to slight deteriotation. In the examination of deteriorated structures, it was found that concrete below the low water level lost its strength due to suphate attack, while concrete above high water level cracked due to freezing and thawing action.

Kamal and Salama (1990) carried out tests on reinforced concrete beams to determine the bond behavior and bond strength between concrete and steel after exposure of ammonium nitrate solution with different concentrations. The specimens were divided into two groups 'A' and 'B'. The group A specimens were exposed to aggressive medium without protection while the surface of group B specimens were coated with epoxy resin before exposure to aggressive medium. They concluded that solvent free epoxy resin coating on concrete surface provided protection against ammonium nitrate solution.

Oshiro and Tanikawa (1990) get constructed a reinforced concrete building in 1984 and exposed it for 5 years and 3 months to marine environment under sub-tropical weather of Okinawa, Japan. Half of the buildig on sea side was coated with acrylic rubber type coating and another half was left as uncoated. They performed field tests to this building to determine concentration and amount of chloride ions in concrete, corroded area on steel reinforcement and bond strength of coating. On the basis of results, they concluded that epoxy concrete were quite capable of resisting acid/alkali attack to a satisfactory extent except for concentrated nitric acid. They suggested that the mix design for epoxy concrete should be done carefully, since epoxy resin alone accounted to more than 80 to 90 % of the cost of overlay.

Iskander et al. (1998) discussed the FRP composite material for piling in corrosion soil and marine environment. They reported that FRP offered better performance compared to steel, concrete and timber piles. They reviewed the American research, testing, design and practice of composite piles. They concluded that FRP piles had better durability and resistance against environmental attacks but at the same time they had some disadvanges like higher cost, less efficient drivability and high compressibility.

Jaafar et al. (2002) tested 108 concrete cubes of size 150x150x150 mm using ultrasonic pulse velocity (UPV) to get strength of concrete. They took four different grades of concrete (i.e.Grade 10, 20, 30 and 400. They conducted experiments in different environments, namely oven-dry, air

dry and saturated conditions. They found the strength of concrete varying from 10 to 40 MPa. They observed that UPV test was not suitable to get accurate results in a saturated environment. They developed a relation between UPV values and cube strength of concrete. He also observed that UPV values were affected by the presence of moisture in the structure.

Bharatkumar et al. (2005) studied, effect of fly ash and slag as cement replacement materials on the fracture characteristics of high performance concrete (HPC). They conducted experiments on beam specimens with 25% fly ash and 50% slag as cement cement replacement. They concluded that fracture energy decreases due to addition of fly ash or slag. They also concluded that the post peak behavior is steeper for the fly ash or slag based HPC mixes compared to normal concrete mixes.

Islam et al. (2012) studied the effect of sea water on the compressive strength of concrete. They cast the specimens with mixing of sea water and cured the specimens under sea water for 7, 28, 90 and 180 days. They took four concrete mix proportions (i.e. 1:1.5:3 with w/c ratio of 0.4, 1:1.5:3 with w/c ratio of 0.45, 1:2:4 with w/c ratio of 0.4 and 1:2:4 with w/c ratio of 0.45). They observed that specimens exposed to sea water showed dark grey to whitish gray colour while specimens kept in normal water showed no colour change. They found that the specimens made and cured with sea water experienced the strength loss of 10% compared with plain water mixed and cured concrete.

Emmanuel et al. (2012) investigated the effect of salinity on the compressive strength of reinforced concrete. They cast the specimens with mix of 1:3:6 using the lagoon and ocean water. They found reduction in compressive strength of specimens over the period of 150 days. They recommended a rich mix for the protection of concrete under saline attack and a higher value of concrete cover for the safety of reinforcement against corrosion.

2.7 CONCLUSION

It is clear from the literature that there have been a lot of research conducted on the investigation of behavior and performance of concrete under triaxial stresses with active and passive confinement. To study the behavior of concrete filled tubes (CFT) subjected to axial loading and combined axial and bending, several experiments were conducted, softwares were used and analysis were done by many researchers. Most of the studies on CFT were carried out using steel tubes and fiber reinforced ploymer (FRP) tubes while little work has been done on concrete filled plastic tubes.

Stress-strain model for concrete confined with steel tube and FRP tube were given by few researchers. But no body reported the stress-strain behavior of concrete confined with UPVC tube. Researchers in past have shown that concrete in marine environment get degraded due to effect of salts present in sea water. To reduce the effect of sea water on concrete, some of them suggested to add specific materials in cement concrete and a few suggested FRP covering to concrete. But these measures are either costly or difficult to apply. To cover-up the research gap a new type of composite column i.e. concrete filled unplasticised poly-vinyl chloride tubular (CFUT) column was introduced to protect the concrete against the attack of salts present in sea water with additional benefit of strength and ductility. Experimental, Numerical and analytical work was done in this process.

CHAPTER-3

EXPERIMENTAL PROGRAM

3.1 GENERAL

This chapter covers the details of experiments and their test procedure. The flow chart of experimental details is given in Fig. 3.1. Total 114 specimens were planned, cast and tested to study the use of UPVC pipes in preparation of columns having improved resistance against marine environment. The prepared column specimens are categorized into three types. These are plain concrete filled UPVC tube (PCFUT), reinforced concrete filled UPVC tube (RCFUT) and bare reinforced concrete column (RCC), which was obtained by removing the outer tube of RCFUT. Casting of specimens was carried out in two stages. In first stage, 90 specimens were cast while in second stage 24 specimens were cast. For the first stage of casting, the UPVC tubes of class 3, 4 and 5 (as per IS:4985-2000) with nominal pressure of 0.6, 0.8 and 1.0 MPa having diameters of 160 mm, 200 mm and 225 mm were taken. 18 RCFUT and 18 bare RCC specimens were kept completely submerged in artificial sea water of salt concentration of 20N over the period of six months. For second stage of casting, UPVC tubes of class 1 having 160 mm diameter with nominal pressure of 0.25 MPa were taken. These specimens were submerged in different concentration of sea water (i.e. 0N, 10N, 15N and 20N) for the period of 3 months, 6 months and 9 months. Tensile test and Scanning electron microscopy (SEM) test were performed on UPVC specimen (before and after submergence in sea water) to obtain physical properties and microstructure of UPVC.

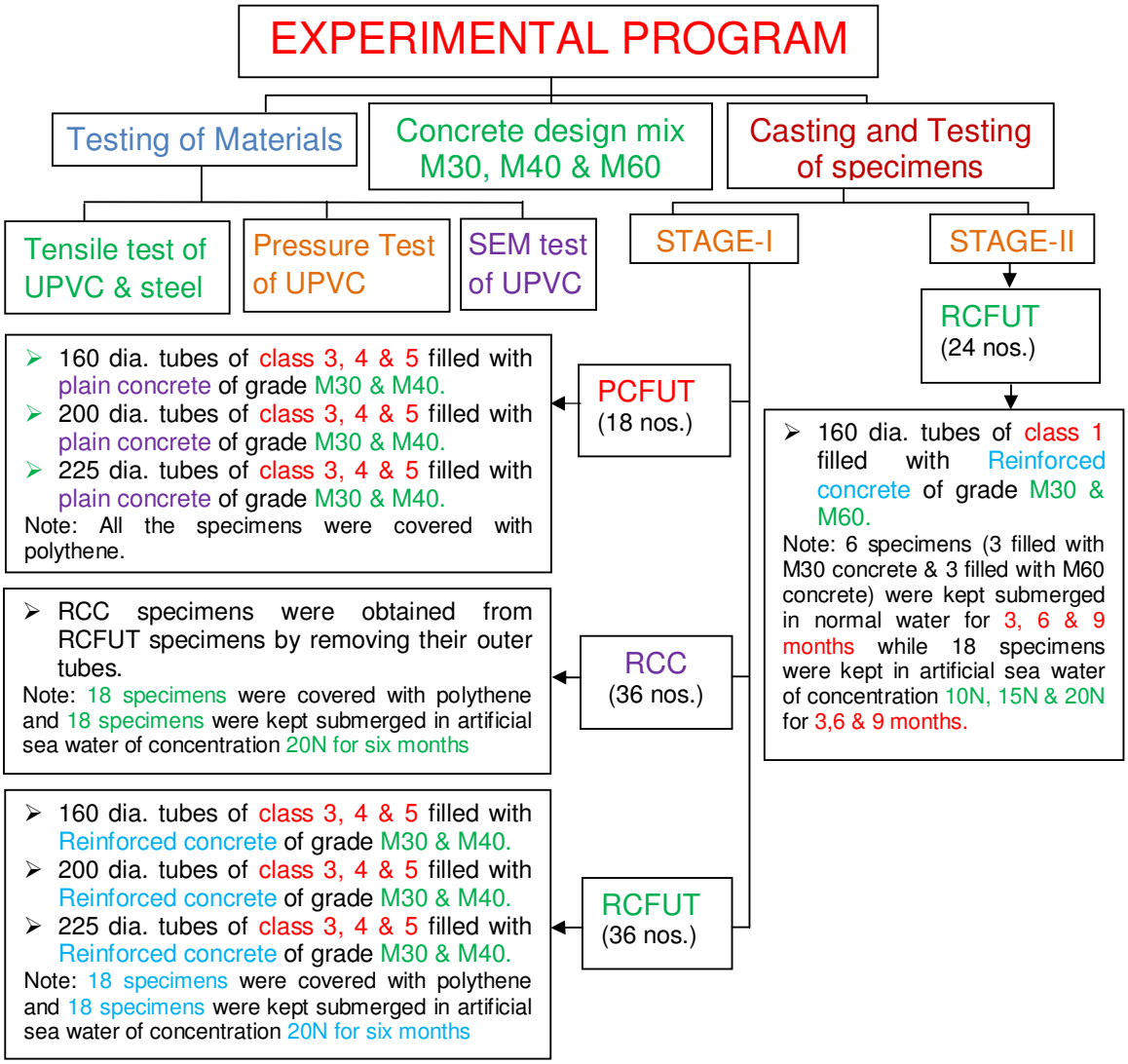

Fig. 3.1 Flow chart of experimental program

3.2 MATERIALS

3.2.1 UPVC tubes

UPVC pipes generally employed for water supply are categorized into six categories (category 1 to 6 as per IS: 4985-2000) on the basis of water pressure. UPVC pipes of class 3, 4 and 5 designed for nominal pressure of 0.6, 0.8 and 1.0 MPa and having the diameters of 160 mm, 200 mm and 225 mm were used for the casting of PCFUT specimens and RCFUT specimens in first stage of casting. For the casting of RCFUT specimens in second stage, UPVC pipes of class 1 having 160 mm diameter with nominal pressure of 0.25MPa were used. The pipes were cut and levelled to obtain the tubes of length 800 mm (Fig. 3.2). The tensile test (as per ASTM-D638-10) of UPVC pipes before and after immersion in sea water conducted in the laboratory to get stress-strain curve as well as ultimate tensile strength (Fig. 3.3). The internal hydrostatic pressure test (as per IS: 12235 (part 8)-1986) was conducted to get an idea of confining pressure (Fig. 3.4). Scanning electron microscopy (SEM) test was also performed to examine microstructure of UPVC (Fig. 3.5). The specimens were prepared as per ASTM standard-E2015-04(2009). The top surface of specimens was examined with machine "FEI Quanta 200F". The physical properties of UPVC are given in Table 3.1. The geometrical dimensions and their hydrostatic pressures obtained after testing are given in Table 3.2.

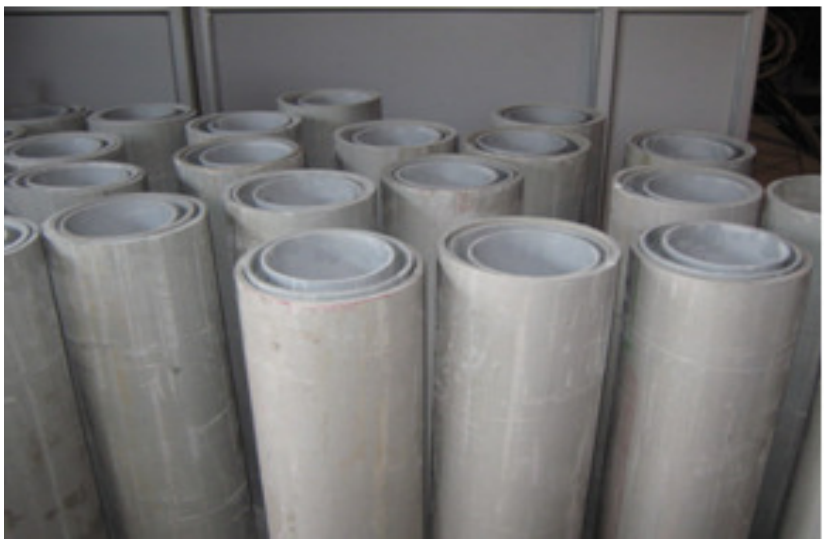

Fig. 3.2 UPVC tubes of different diameters and thicknesses after Cutting and levelling

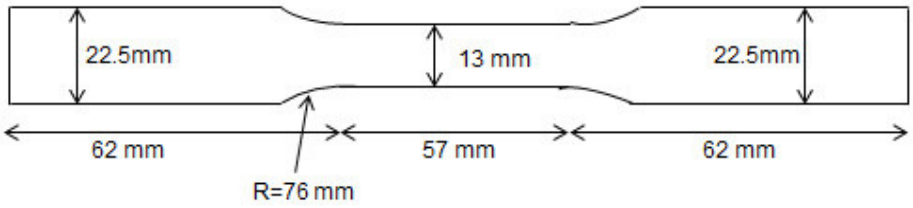

(a)

(b)

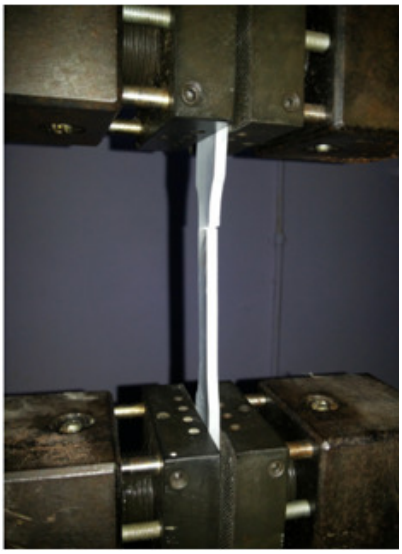

(c)

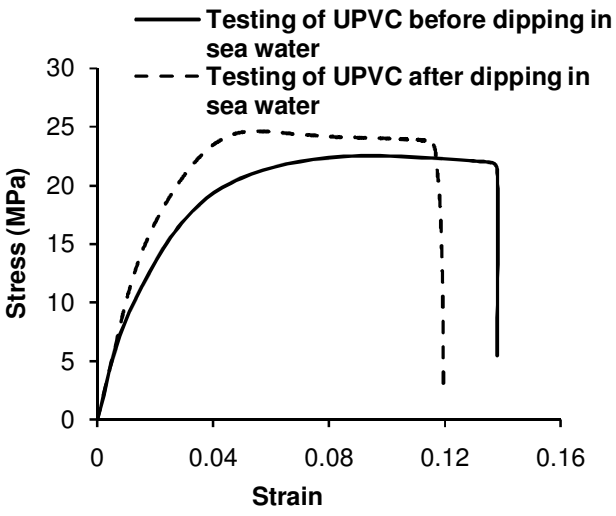

(d)

Fig. 3.3 Tension test of UPVC (a) Line diagram of test specimen (b) Photograph of specimen (c) Testing of specimen (d) Stress-strain curve of UPVC

Fig. 3.4 Typical arrangement of internal hydrostatic pressure test to find confining pressure

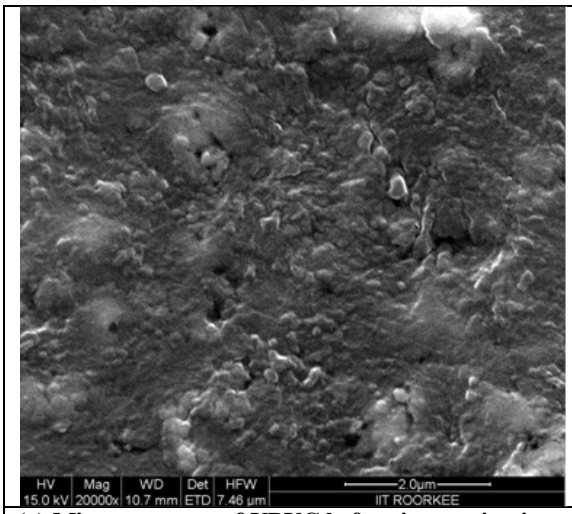

(a) Microstructure of UPVC before immersion in sea water

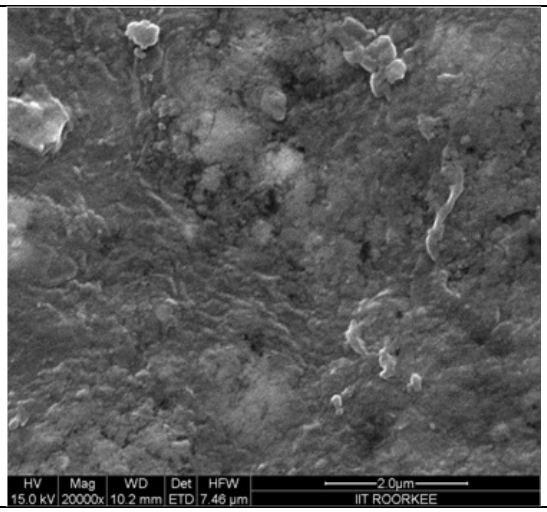

(b) Microstructure of UPVC after immersion in sea water

Fig. 3.5 Microstructure of UPVC with SEM

Table 3.1 Physical properties of UPVC

Characteristics	Value in normal condition	Value after submerging in sea water for six months
Density	1.3 gm/cm^3	1.3 gm/cm^3
Elastic modulus	880 MPa	1016 MPa
Ultimate tensile strength	22.5 MPa	24.64 MPa
Percentage elongation	11.80	11.95
Poisson's ratio	0.35	0.35
Service life	>50 years	>50 years

Table 3.2 Geometrical dimensions of UPVC tubes

Class of pipes	Nominal outer diameter (mm)	Length (mm)	Average outer diameter (mm)	Average thickness (mm)	L/D ratio	D/t ratio	Designed nominal pressure (MPa)	Hydrostatic pressure (MPa)
1.	160	800	159.75	2.30	5.0	69.45	0.25	0.64
3.		800	160.15	3.99	5.0	40.14	0.6	1.15
4.		800	159.88	5.22	5.0	30.63	0.8	1.52
5.		800	160.19	7.02	5.0	22.82	1.0	2.15
3.	200	800	199.85	5.94	4.0	33.64	0.6	1.35
4.		800	199.56	8.11	4.0	24.61	0.8	1.99
5.		800	199.22	8.89	4.0	22.41	1.0	2.25
3.	225	800	224.78	8.65	3.56	25.99	0.6	1.72
4.		800	224.58	9.58	3.56	23.44	0.8	2.00
5.		800	224.13	9.97	3.56	22.48	1.0	2.17

3.2.2 Cement

OPC 43 grade cement was used. Cement for entire requirement was calculated and procured from a single lot so that the same physical properties could be maintained. The cement used was stored in a silo in controlled conditions in the concrete laboratory. Conducting laboratory experiment, the Specific gravity of cement through testing was found 3.15.

3.2.3 Coarse aggregate (CA)

Coarse aggregate of 12.5 mm nominal size was used for the concrete mix. All the coarse aggregates were procured in one lot for the entire experimental requirements so that same properties of concrete could be maintained. These were periodically washed to remove any impurities, sun dried and suitably

stored as per the requirements of relevant codes (Fig. 3.6(a)). The physical properties of C.A. are given in Table 3.3.

3.2.4 Fine aggregate (FA)

Fine aggregate conforming to ZONE-III was selected (Fig. 3.6(b)). Fine aggregate was procured in one lot for the entire experimental requirements so that same properties of concrete could be maintained. This is then suitably stored as per the relevant code requirements. The physical properties of F.A. are given in Table 3.3.

Table 3.3 Physical properties of the fine and coarse aggregates

Characteristics	Fine Aggregate	Coarse Aggregate
Fineness Modulus	2.47	6.92
Specific gravity	2.55	2.53
Water absorption (%)	0.6	0.7

Fig. 3.6 (a) Washing of coarse aggregate

Fig. 3.6 (b) Drying of fine aggregate

3.2.5 Reinforcement

TMT steel bars of Tata TISCON were used for the main reinforcement and lateral ties. Steel cages with lateral ties of different diameter were prepared for reinforced concrete of specimens (Fig. 3.7). The details of cages as given below:

1. Longitudinal bars : 12mm dia.
2. Lateral ties : 8mm dia.
3. No. of lateral ties : Five
4. No. of longitudinal bars : Six
5. Spacing of stirrups : 150mm c/c
6. Yield stress (f_y) : 500MPa

Steel bars were tested on the Universal testing machine and stress-strain curves were obtained and drawn (Fig. 3.8). The yield stress and ultimate stress were found as 500 MPa and 618 MPa respectively.

Fig. 3.7 Reinforcement cages

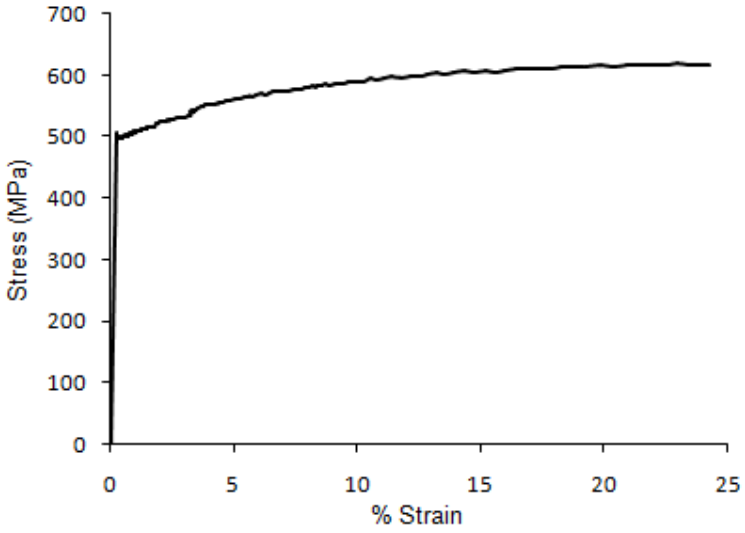

Fig. 3.8 Typical stress-strain curve of steel bar of diameter 12 mm

3.3 MIX DESIGN

The Mix was design as per "IS: 10262-2009". The design Mixes were obtained for M30, M40 and M60 grade of concrete. The concrete Mix proportion and compressive strengths of cylinder are given in Tables 3.4 and 3.5 respectively.

3.3.1 Mix design for M30 grade concrete

TEST DATA FOR MATERIAL

a. Cement used = OPC 43

b. Specific gravity of cement = 3.15

c. Specific gravity of CA = 2.53

d. Specific gravity of FA = 2.55

PROPORTIONING

Characteristic Compressive Strength at 28 days = 30

Standard deviation - IS: 10262 Table 1 = 5

Target strength of concrete *f*ck = 38.25

Water cement ratio- IS: 456 Table 4/5 = 0.45

Cement content -IS :456 Table 4/5 = 340

Adjustment to Min. Cement Content- IS: 456 Table 6 = 40

Super plasticizer to reduce water (%) = 0.25

Water contain IS 10262 Table 2/IS: 456 Table 5 = 171

Volume of CA/Unit vol. of total Aggregates = 0.62

Slump target- IS: 456 Clause No. 7.1 = 75-100

Entrained air –IS: 456 Clause No.8.2.2.3 = 2

MIX CALCULATION

Volume of concrete = 0.98

Volume of cement = 0.12

Volume of water = 0.17

Volume of all aggregate = 0.69

Mass of CA = 1088.9

Mass of FA = 672.68

Table 3.4 Concrete mix proportions

Grade	w/c ratio	Water (kg/m^3)	Cement (kg/m^3)	Fine Aggregate (kg/m^3)	Coarse Aggregate (kg/m^3)	Admixture (%)	Silica fume (%)	Cube strength f_{ck} (MPa)
M30	0.45	171	380	673	1089	0.25	-	42.22
M40	0.40	160	400	675	1093	0.35	-	48.88
M60	0.28	134	445	693	1130	1.0	7.0	65.47

Table 3.5 Compressive strength (f_c) of concrete cylinder (150 mm x 300 mm) in MPa

Grade	28 days	3 months	6 months	9 months
M30	35.08	36.03	37.54	38.10
M40	39.05	-	41.69	-
M60	52.38	53.95	55.65	56.96

3.4 SPECIMENS

3.4.1 Casting of specimens

Table 3.6 shows the geometrical and material properties of concrete filled UPVC tubular (CFUT) column specimens. A total of 114 specimens were cast. Before casting of specimens; moulds were prepared to fix the UPVC pipes so that the concrete may fill properly (Fig. 3.9 and 3.10). The prepared column specimens are kept into three categories. These are plain concrete filled UPVC tubular (PCFUT) column specimens, reinforced concrete filled UPVC tube (RCFUT) column specimens and bare reinforced concrete (RCC) specimens, which were obtained by removing the outer tube of RCFUT specimens. Castings of specimens were carried out in two stages. In first stage, 90 specimens were cast while in second stage 24 specimens were cast. (Fig. 3.11). 18 RCFUT and 18 bare RCC specimens were kept completely submerged in artificial sea water (Table 3.7.) of salt concentration of 20N over the period of six months while remaining 18 specimens of each RCFUT and bare RCC were tightly covered with thick polyethylene sheet to avoid the evaporation of water for 28 days testing (Fig. 3.12). It replicates the true condition in the practice field. Before dipping the specimens in sea water, the plastic sheets were fixed on top and bottom side of specimens with the help of adhesive to avoid the direct contact of sea water with concrete (Fig. 3.13 and 3.14). It is generally adopted that 20N concentration of sea water has the same effect on concrete in one year as the sea water of 1N concentration in 20 years. Therefore, to see the effect of sea water (1N) in 10 years, specimens in the present study were submerged in sea water of 20N concentration for six months. The concentration of sea water was measured after six months. Due to the evaporation of water it was increased marginally and found 21.17 N.

For the first stage of casting, UPVC pipes of class 3, 4 and 5 (as per IS:4985-2000) with nominal pressure of 0.6, 0.8 and 1.0 MPa having diameters of 160 mm, 200 mm and 225 mm were taken. The pipes were cut and levelled to get the specimens of length 800 mm and filled with concrete having M30 and M40 grades. The main reinforcement was taken 2.0 to 4.05% of gross cross-sectional area. 6-12ϕ bars were used as main reinforcement and 8ϕ lateral ties

@150c/c were used for transverse reinforcement. All the specimens were tested for axial loading by loading concrete core only.

For the second stage of casting, UPVC pipes of class 1 (as per IS: 4985-2000) with nominal pressure of 0.25 MPa having diameters of 160 mm were taken. In this stage, total 24 specimens were cast and submerged them in different concentration of sea water (i.e. 0N, 10N, 15N and 20N) for the period of 3 months, 6 months and 9 months. Here the UPVC pipes of lowest class (class 1) were exclusively taken to see the effect of different concentration of sea water at various time spans on strength of concrete and ductility of concrete inside the tube. M30 and M60 grade of concrete were used to fill the tubes. The length of specimens and reinforcement were kept same as taken in RCFUT specimens in first stage of casting.

3.4.2 Nomenclature of specimens

Typical nomenclatures are used to designate the specimens. For example specimen 160P3PC30: 160-stands for the outer diameter of tube, P3 stands for pipe of class 3 (nominal pressure of 0.6 MPa), PC30 stands for plain concrete of grade M30. Therefore, 200P5PC40 indicates the specimen made with tube of class 5 having nominal diameter 200 mm, filled with plain concrete of grade M40. 160P3RC30 represents the specimen made of 160 diameter tube of class 3, filled with reinforced concrete of grade M30. Specimen 160P3BRC30 is a bare reinforced concrete column specimen which was obtained by removing the tube of 160P3RC30.

The specimens which were submerged in artificial sea water are designated as follows:

160P3RC30-20N6 indicates the specimen 160P3RC30 which is submerged in the sea water of 20N concentration for 6 months.

160P1RC30-0N3 represents the specimen made of 160 diameter tube of class 1, filled with reinforced concrete of grade M30 and submerged in normal water for 3 months. Other specimens are designated in the same manner.

Table 3.6 Geometrical and material properties of CFUT specimens

S.N.	Specimen	Dimensions (mm)			Ratios		Material Properties (MPa)	
		Nominal outer diameter (D)	Thick-ness (t)	Length (L)	D/t	L/D	f_c	f_u
1.	160P3PC30	160	3.99	800	40.13	5	35.08	22.5
2.	160P4PC30	160	5.22	800	30.63	5	35.08	22.5
3.	160P5PC30	160	7.02	800	22.82	5	35.08	22.5
4.	200P3PC30	200	5.94	800	33.64	4	35.08	22.5
5.	200P4PC30	200	8.11	800	24.61	4	35.08	22.5
6.	200P5PC30	200	8.89	800	22.41	4	35.08	22.5
7.	225P3PC30	225	8.65	800	25.99	3.56	35.08	22.5
8.	225P4PC30	225	9.58	800	23.44	3.56	35.08	22.5
9.	225P5PC30	225	9.97	800	22.48	3.56	35.08	22.5
10.	160P3PC40	160	3.99	800	40.13	5	39.05	22.5
11.	160P4PC40	160	5.22	800	30.63	5	39.05	22.5
12.	160P5PC40	160	7.02	800	22.82	5	39.05	22.5
13.	200P3PC40	200	5.94	800	33.64	4	39.05	22.5
14.	200P4PC40	200	8.11	800	24.61	4	39.05	22.5
15.	200P5PC40	200	8.89	800	22.41	4	39.05	22.5
16.	225P3PC40	225	8.65	800	25.99	3.56	39.05	22.5
17.	225P4PC40	225	9.58	800	23.44	3.56	39.05	22.5
18.	225P5PC40	225	9.97	800	22.48	3.56	39.05	22.5
19.	160P3RC30	160	3.99	800	40.13	5	35.08	22.5
20.	160P4RC30	160	5.22	800	30.63	5	35.08	22.5
21.	160P5RC30	160	7.02	800	22.82	5	35.08	22.5
22.	200P3RC30	200	5.94	800	33.64	4	35.08	22.5
23.	200P4RC30	200	8.11	800	24.61	4	35.08	22.5
24.	200P5RC30	200	8.89	800	22.41	4	35.08	22.5
25.	225P3RC30	225	8.65	800	25.99	3.56	35.08	22.5
26.	225P4RC30	225	9.58	800	23.44	3.56	35.08	22.5
27.	225P5RC30	225	9.97	800	22.48	3.56	35.08	22.5
28.	160P3RC40	160	3.99	800	40.13	5	39.05	22.5
29.	160P4RC40	160	5.22	800	30.63	5	39.05	22.5
30.	160P5RC40	160	7.02	800	22.82	5	39.05	22.5
31.	200P3RC40	200	5.94	800	33.64	4	39.05	22.5
32.	200P4RC40	200	8.11	800	24.61	4	39.05	22.5
33.	200P5RC40	200	8.89	800	22.41	4	39.05	22.5
34.	225P3RC40	225	8.65	800	25.99	3.56	39.05	22.5
35.	225P4RC40	225	9.58	800	23.44	3.56	39.05	22.5
36.	225P5RC40	225	9.97	800	22.48	3.56	39.05	22.5
37.	160P3BRC30	160	3.99	800	40.13	5	35.08	22.5
38.	160P4BRC30	160	5.22	800	30.63	5	35.08	22.5
39.	160P5BRC30	160	7.02	800	22.82	5	35.08	22.5
40.	200P3BRC30	200	5.94	800	33.64	4	35.08	22.5
41.	200P4BRC30	200	8.11	800	24.61	4	35.08	22.5
42.	200P5BRC30	200	8.89	800	22.41	4	35.08	22.5
43.	225P3BRC30	225	8.65	800	25.99	3.56	35.08	22.5
44.	225P4BRC30	225	9.58	800	23.44	3.56	35.08	22.5
45.	225P5BRC30	225	9.97	800	22.48	3.56	35.08	22.5

46.	160P3BRC40	160	3.99	800	40.13	5	39.05	22.5
47.	160P4BRC40	160	5.22	800	30.63	5	39.05	22.5
48.	160P5BRC40	160	7.02	800	22.82	5	39.05	22.5
49.	200P3BRC40	200	5.94	800	33.64	4	39.05	22.5
50.	200P4BRC40	200	8.11	800	24.61	4	39.05	22.5
51.	200P5BRC40	200	8.89	800	22.41	4	39.05	22.5
52.	225P3BRC40	225	8.65	800	25.99	3.56	39.05	22.5
53.	225P4BRC40	225	9.58	800	23.44	3.56	39.05	22.5
54.	225P5BRC40	225	9.97	800	22.48	3.56	39.05	22.5
55.	160P3RC30-20N6	160	3.99	800	40.13	5	35.08	22.5
56.	160P4RC30-20N6	160	5.22	800	30.63	5	35.08	22.5
57.	160P5RC30-20N6	160	7.02	800	22.82	5	35.08	22.5
58.	200P3RC30-20N6	200	5.94	800	33.64	4	35.08	22.5
59.	200P4RC30-20N6	200	8.11	800	24.61	4	35.08	22.5
60.	200P5RC30-20N6	200	8.89	800	22.41	4	35.08	22.5
61.	225P3RC30-20N6	225	8.65	800	25.99	3.56	35.08	22.5
62.	225P4RC30-20N6	225	9.58	800	23.44	3.56	35.08	22.5
63.	225P5RC30-20N6	225	9.97	800	22.48	3.56	35.08	22.5
64.	160P3RC40-20N6	160	3.99	800	40.13	5	39.05	22.5
65.	160P4RC40-20N6	160	5.22	800	30.63	5	39.05	22.5
66.	160P5RC40-20N6	160	7.02	800	22.82	5	39.05	22.5
67.	200P3RC40-20N6	200	5.94	800	33.64	4	39.05	22.5
68.	200P4RC40-20N6	200	8.11	800	24.61	4	39.05	22.5
69.	200P5RC40-20N6	200	8.89	800	22.41	4	39.05	22.5
70.	225P3RC40-20N6	225	8.65	800	25.99	3.56	39.05	22.5
71.	225P4RC40-20N6	225	9.58	800	23.44	3.56	39.05	22.5
72.	225P5RC40-20N6	225	9.97	800	22.48	3.56	39.05	22.5
73.	160P3BRC30-20N6	160	3.99	800	40.13	5	35.08	22.5
74.	160P4BRC30-20N6	160	5.22	800	30.63	5	35.08	22.5
75.	160P5BRC30-20N6	160	7.02	800	22.82	5	35.08	22.5
76.	200P3BRC30-20N6	200	5.94	800	33.64	4	35.08	22.5
77.	200P4BRC30-20N6	200	8.11	800	24.61	4	35.08	22.5
78.	200P5BRC30-20N6	200	8.89	800	22.41	4	35.08	22.5
79.	225P3BRC30-20N6	225	8.65	800	25.99	3.56	35.08	22.5
80.	225P4BRC30-20N6	225	9.58	800	23.44	3.56	35.08	22.5
81.	225P5BRC30-20N6	225	9.97	800	22.48	3.56	35.08	22.5
82.	160P3BRC40-20N6	160	3.99	800	40.13	5	39.05	22.5
83.	160P4BRC40-20N6	160	5.22	800	30.63	5	39.05	22.5
84.	160P5BRC40-20N6	160	7.02	800	22.82	5	39.05	22.5
85.	200P3BRC40-20N6	200	5.94	800	33.64	4	39.05	22.5
86.	200P4BRC40-20N6	200	8.11	800	24.61	4	39.05	22.5
87.	200P5BRC40-20N6	200	8.89	800	22.41	4	39.05	22.5
88.	225P3BRC40-20N6	225	8.65	800	25.99	3.56	39.05	22.5
89.	225P4BRC40-20N6	225	9.58	800	23.44	3.56	39.05	22.5
90.	225P5BRC40-20N6	225	9.97	800	22.48	3.56	39.05	22.5
91.	160P1RC30-0N3	160	2.3	800	69.45	5	35.08	22.5
92.	160P1RC30-10N3	160	2.3	800	69.45	5	35.08	22.5
93.	160P1RC30-15N3	160	2.3	800	69.45	5	35.08	22.5
94.	160P1RC30-20N3	160	2.3	800	69.45	5	35.08	22.5
95.	160P1RC30-0N6	160	2.3	800	69.45	5	35.08	22.5
96.	160P1RC30-10N6	160	2.3	800	69.45	5	35.08	22.5
97.	160P1RC30-15N6	160	2.3	800	69.45	5	35.08	22.5
98.	160P1RC30-20N6	160	2.3	800	69.45	5	35.08	22.5

99.	160P1RC30-0N9	160	2.3	800	69.45	5	35.08	22.5
100.	160P1RC30-10N9	160	2.3	800	69.45	5	35.08	22.5
101.	160P1RC30-15N9	160	2.3	800	69.45	5	35.08	22.5
102.	160P1RC30-20N9	160	2.3	800	69.45	5	35.08	22.5
103.	160P1RC60-0N3	160	2.3	800	69.45	5	52.38	22.5
104.	160P1RC60-10N3	160	2.3	800	69.45	5	52.38	22.5
105.	160P1RC60-15N3	160	2.3	800	69.45	5	52.38	22.5
106.	160P1RC60-20N3	160	2.3	800	69.45	5	52.38	22.5
107.	160P1RC60-0N6	160	2.3	800	69.45	5	52.38	22.5
108.	160P1RC60-10N6	160	2.3	800	69.45	5	52.38	22.5
109.	160P1RC60-15N6	160	2.3	800	69.45	5	52.38	22.5
110.	160P1RC60-20N6	160	2.3	800	69.45	5	52.38	22.5
111.	160P1RC60-0N9	160	2.3	800	69.45	5	52.38	22.5
112.	160P1RC60-10N9	160	2.3	800	69.45	5	52.38	22.5
113.	160P1RC60-15N9	160	2.3	800	69.45	5	52.38	22.5
114.	160P1RC60-20N9	160	2.3	800	69.45	5	52.38	22.5

Table 3.7 Composition of artificial sea water (Jain, 2007)

Name of chemical	**Chemical formula**	**Amount (gm/litre)**	**Total chemical (%)**	**Remarks**
Sodium chloride	NaCl	29.0	78.21	These amounts of chemicals were dissolved in plain water to prepare 1.0 litre of sea water of 1N concentration. To prepare sea water of 20N concentration, chemical were taken 20 times as used for 1N concentration
Magnesium chloride	$MgCl_2$	3.93	10.60	
Magnesium sulphate	$MgSO_4$	1.87	5.04	
Calcium sulphate	$CaSO_4$	1.17	3.15	
Potassium sulphate	K_2SO_4	0.9	2.43	
Calcium carbonate	$CaCO_3$	0.11	0.30	
Magnesium bromide	$MgBr_2$	0.10	0.27	
Total		37.08	100.00	

Fig. 3.9 Moulds for specimens

Fig. 3.10 Specimens fixed in moulds

Fig. 3.11 Casting of specimens

Fig. 3.12 Specimens covered with polyethylene

Fig. 3.13 Plastic sheet fixed on top and bottom of specimens

Fig. 3.14 Specimens submerged in sea water

3.5 TESTING OF SPECIMENS

CFUT specimens were tested on Universal testing machine of INSTRON make having capacity of 250 tonnes. During the testing, specimens were kept on bottom platen of the machine. The gauge length of the specimen was the entire length of the specimen. The test was conducted with the strain control method and ramp rate of 0.4 mm/minute. The plumb-bob and Tri square were used to place the specimen at right angle to the bottom plate. The concentric loading was the main concern for the test to be exact and reliable. Hence, proper levelling of the specimen surface for placing steel plate and placing specimen at right angle for the concentric loading was given the utmost importance. The load-displacement curves were recorded by the machine automatically. The compression process of CFUT specimen was continued till the specimen failed. Since the tensile strength of UPVC tube material (f_u) is smaller and approximately 22.5 MPa, tubes were used only for confinement purpose. All the specimens were tested by applying the axial load on concrete core only. Repeatability of the testing was assured by testing three samples of each type. The typical arrangement of loading and testing is depicted in Fig. 3.15. Before testing the specimens, steel platens of desired diameters were prepared on lathe machine to transfer the load from machine to concrete core (Fig. 3.16). Specimens were leveled before testing (Fig. 3.17). Typical photographs for the testing of specimens are given in Fig. 3.18.

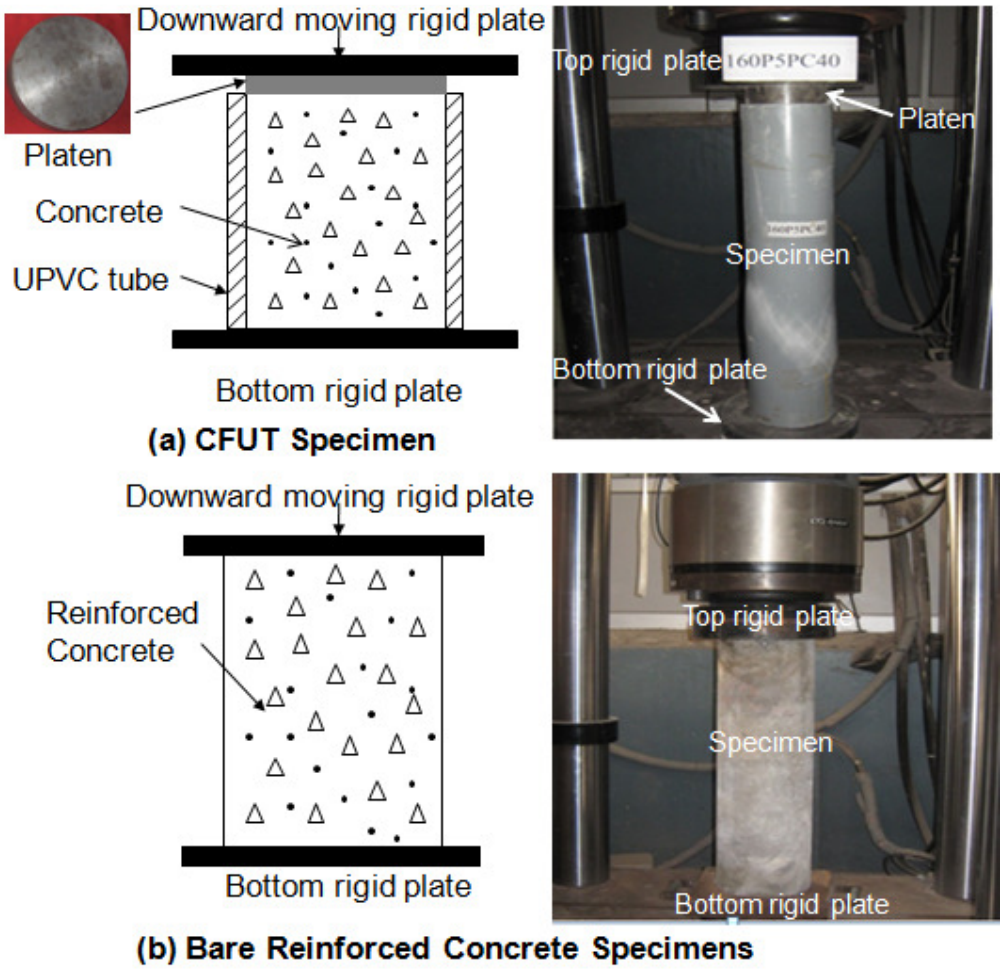

Fig. 3.15 (a) Loading and (b) testing arrangements

Fig. 3.16 Platens of different diameters

Fig. 3.17 Levelling of specimen before testing

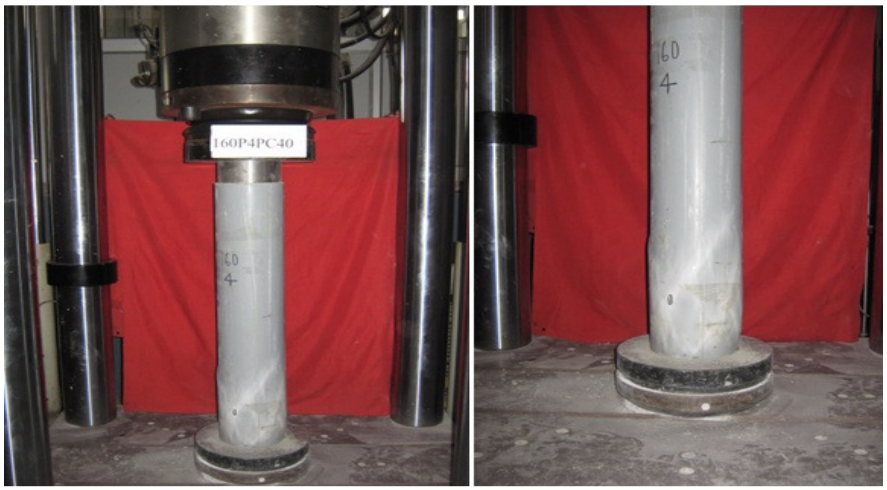

(a) PCFUT specimen

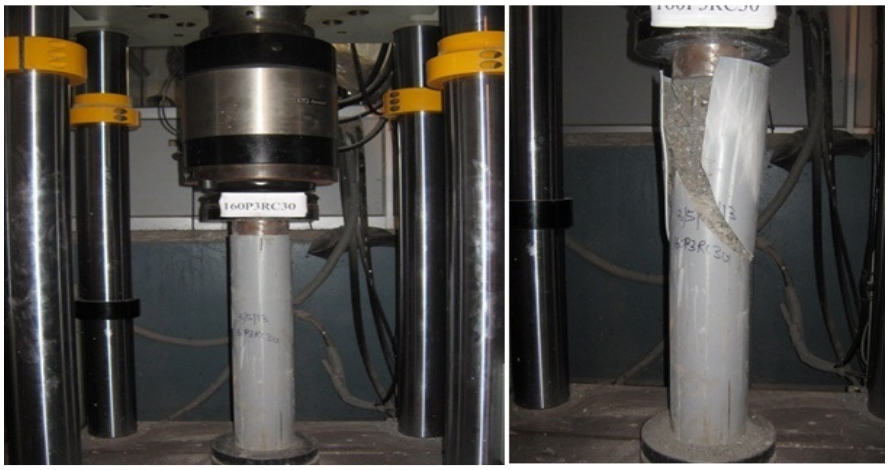

(b) RCFUT specimen

(c) Bare RCC specimen

Fig. 3.18 Typical photographs of testing of specimens

CHAPTER-4

MODELING AND SIMULATION

4.1 GENERAL

Sometime it is difficult, costly and time consuming to perform experiments on full scale real structural member. Moreover, due to the limitation in the geometrical configuration of the engineering material, it may be difficult to prepare the specimens with desired material configuration. Therefore, modeling and simulation may be a better alternative. In this chapter, details of numerical simulation through the Finite element modeling are covered. Modeling of axially loaded concrete filled UPVC tubular columns having different geometrical and material properties is explained by development of three-dimensional Finite element model using commercial code ANSYS. Validation of developed model with the help of experimental results is also covered. The concrete core, UPVC tube, and reinforcement are modeled and then bond are created between them to simulate the modeling of concrete filled UPVC columns. Suitable material constitutive models for UPVC tube, concrete core and reinforcement are adopted and explained in this chapter.

4.2 MODELING OF UPVC TUBE

4.2.1 Element

To simulate the behavior of thin UPVC tube, there are two elements available in ANSYS library: shell element and solid element. If the shell elements are used then elements needed through thickness of tube are lesser in numbers and affect the accuracy of analysis. The shell element of larger size also reduces the total number of elements to discretize the hollow UPVC tube, which significantly limits the accuracy.

Therefore, a three-dimensional solid element (SOLID 45) (ANSYS, 2009-b) is adopted for modeling of UPVC tube. Element (SOLID 45) is defined by eight nodes having three degree of freedom at each nodes: translations in the nodal x, y, and z directions as shown in Fig. 4.1. The element is capable of plastic deformation, creep, swelling, stress-stiffening, large deflection and large strain.

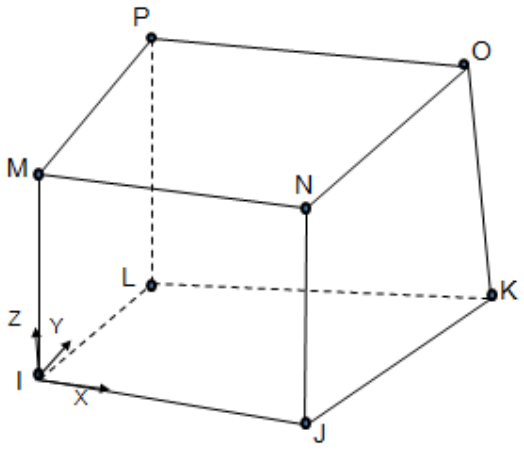

Fig. 4.1 Geometry of Element- SOLID 45

4.2.2 Material Model

Elastic behavior of UPVC tube is modeled using isotropic linear elastic model with initial modulus of elasticity of 880 MPa and Poisson's ratio 0.35. Modulus of elasticity is measured in between 0.05 % and 0.25 % strain (BS EN ISO 527-1:2012), to avoid zero offset and clamp slippage effects.

Plastic behavior of UPVC tube is simulated using rate-independent plasticity theory which is characterized by the irreversible straining that occurs in a material once a certain level of stress is reached (ANSYS, 2009-d). There are three aspects in the rate-independent theory: yield function, flow rule and the hardening rule. Stress level at initial yielding and subsequent yield surface can be obtained with the help of yield function. von Mises yield criterion is used to define the elastic limit of UPVC material (Ragab et al. 2000). The direction of plastic straining is obtained from flow rule. It relates the plastic strain increments to stress increments. Flow rule may be defined as associated flow rule when the direction of plastic strains occurs in a direction normal to the yield surface at the time of yielding (ANSYS, 2009-d). Associated flow rule is used to model the direction of plastic strains in UPVC tube. The flow rule delineates the change of the yield surface with progressive yielding (i.e. defines the motion of the subsequent yield surface during plastic loading stage) so that the state of stress for subsequent yielding can be established (ANSYS, 2009-d). There are two hardening rules available: isotropic (or work) hardening and kinematic hardening. In the case of isotropic hardening, the centre of the yield surface remains fixed but the size of the surface increases as the plastic strains develop, assuming that the yield surface expands uniformly (Fig. 4.2 (a)). While in case of kinematic hardening, the center of the yield surface moves but the size of the surface remains constant

(Fig. 4.2 (b)). (ANSYS, 2009-d). However it is also possible to model the yield surface as perfectly plastic or elastoplastic. Elastic perfectly plastic model refers that Yield surface does not change with plastic strains.

When UPVC tube is subjected to triaxial stresses, a von Mises yield surface as shown in Fig. 4.3 and criterion F is used to define the elastic limit (Ragab et al. 2000) , which is written as:

$$F = \sqrt{3J_2} = \frac{1}{\sqrt{2}}\sqrt{(\sigma_1-\sigma_2)^2 + (\sigma_2-\sigma_3)^2 + (\sigma_3-\sigma_1)^2} = \sigma_y$$

Where J_2 = Second stress invariant of the stress deviator tensor.

σ_1, σ_2, & σ_3 are the Principal stresses.

σ_y = yield stress of material under uniaxial tension.

Plastic behavior of UPVC tube is modeled using a plastic based model available in ANSYS that is multilinear isotropic hardening material model (MISO). The required input for this model is stress-strain curve of UPVC material given in Fig. 4.4.

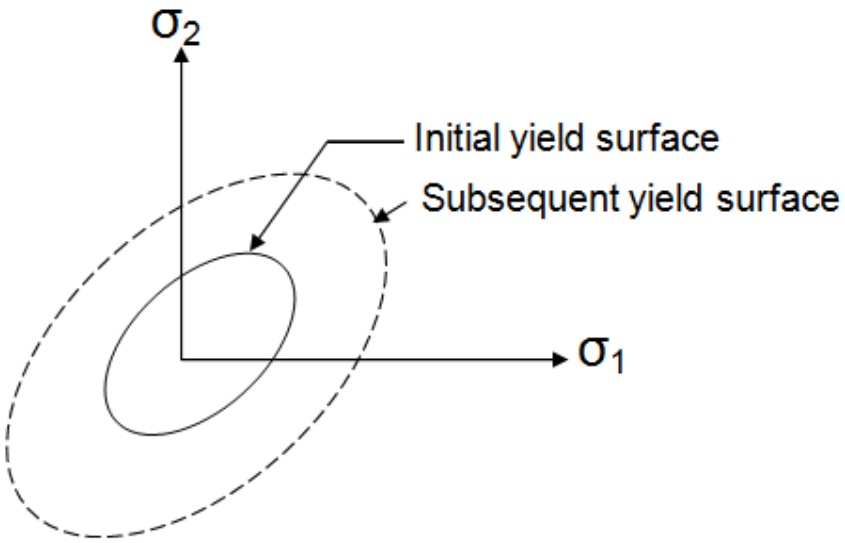

(a) Isometric hardening

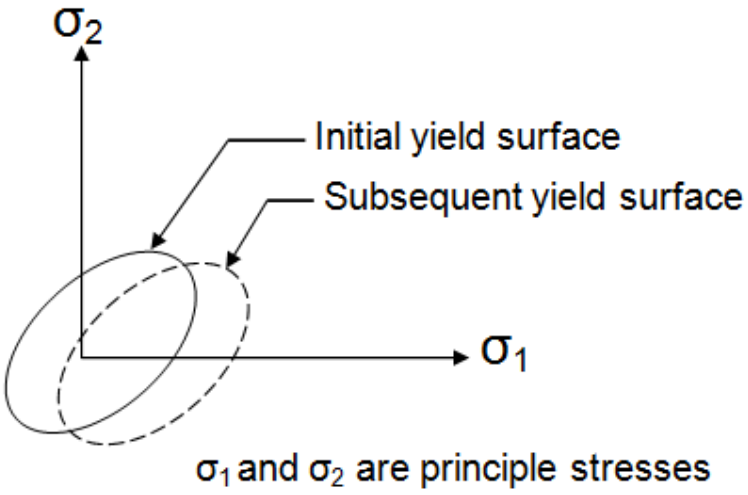

(b) Kinematic hardening

Fig. 4.2 Hardening Rules (ANSYS, 2009-d)

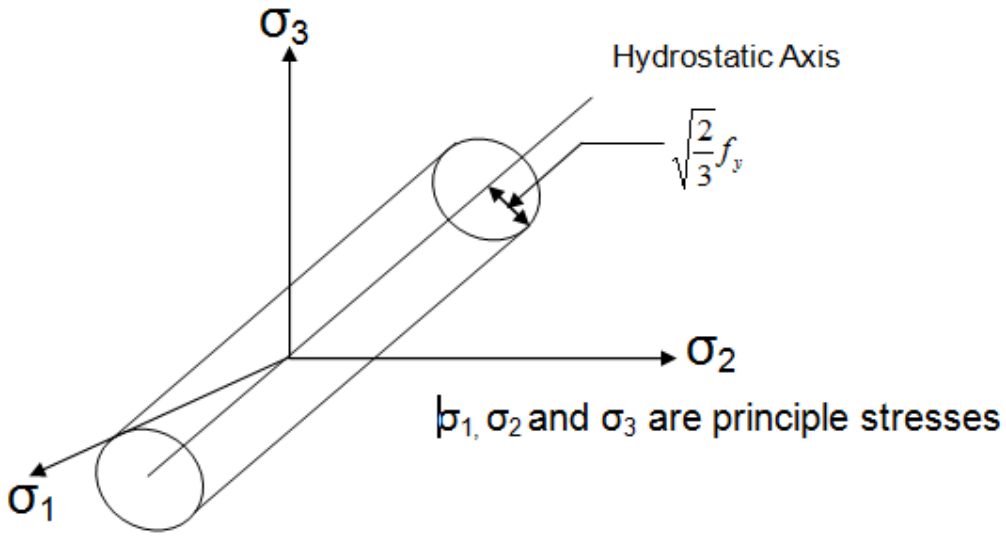

Fig. 4.3 von Mises yield surface with three principles stresses (ANSYS, 2009-d)

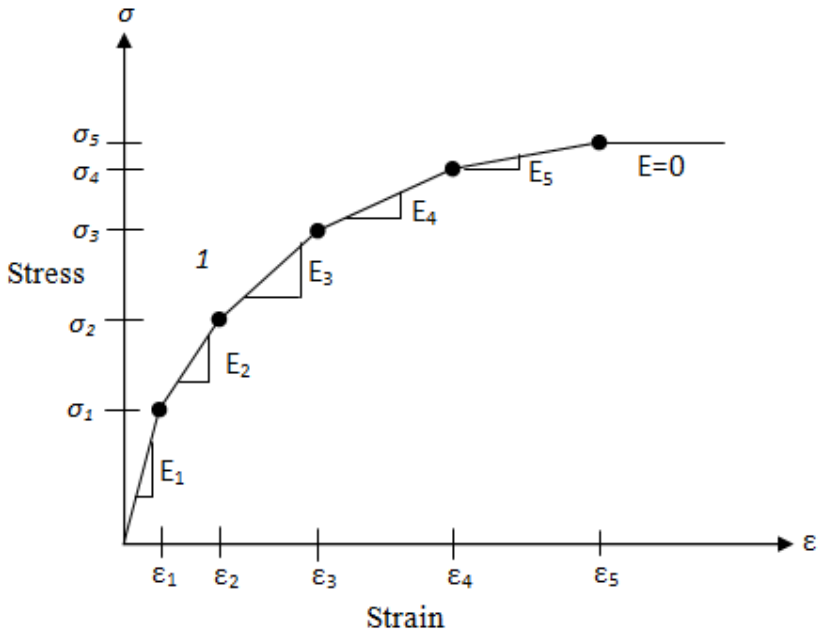

Fig. 4.4 Multilinear Isotropic Hardening (ANSYS, 2009-d)

4.3 MODELLING OF CONCRETE CORE

4.3.1 Element

3-D reinforced concrete solid element (SOLID 65) is used for modeling of plain concrete as well as concrete with reinforcing bars (rebar). This element is capable of cracking in tension and crushing in compression (ANSYS, 2009-b). In concrete applications, solid capability of element is used to model the concrete while the rebar capability is used for modeling the reinforcement behavior using smeared theory of modeling. This element may also be used for reinforced composites such as fiberglass and geological materials (such as rock). This element is defined by eight nodes having three degree of freedom at each node: translations in the nodal x, y, and z directions (Fig. 4.5).

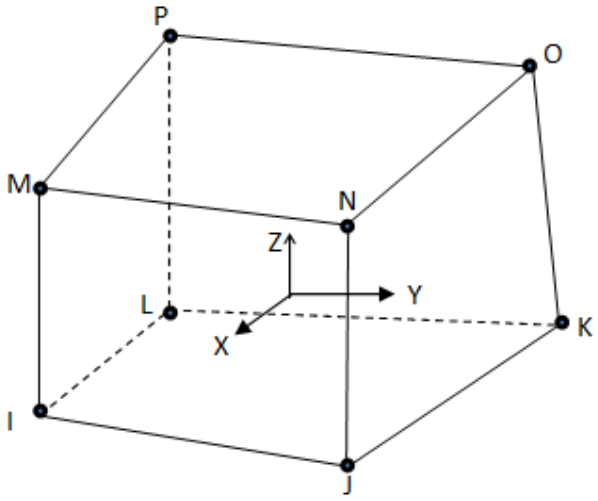

Fig. 4.5 Geometry of Element-SOLID 65

4.3.2 Material Model

To obtain stress-strain curve for concrete under triaxial stress, the required parameters are peak stress, elastic modulus, strain at peak stress and stress as well as strain at failure. The peak stress of concrete f_{cc} confined by tube and corresponding strain ε_{cc} are calculated by the following equations (Richart et al., 1928).

$$f_{cc} = f_c + k_1 f_l \qquad (2.1)$$

$$\varepsilon_{cc} = \varepsilon_c(1 + k_2 \frac{f_l}{f_c}) \quad (2.2)$$

where, f_c is the unconfined compressive cylinder strength of concrete, k_1 and k_2 are constant, generally taken as 4.1 and 20.5, The value of ε_c is usually between 0.002 to 0.003. For confined concrete it may be taken as 0.003 (ACI-318, 2008). Poisson's ratio of concrete was assumed '0.2' as recommended by Bangash (2001). f_l is the lateral confining stress induced due to confinement provided by tube and depends upon D/t & ultimate tensile strength of UPVC tube (f_u).

The response of concrete is modelled by an elastic-plastic theory with associated flow and kinematic hardening rule. During plastic deformation, the expansion of yield surface can be guided by the uniaxial stress-strain curve.

The stress-strain curve for concrete confined with UPVC tube as shown in Fig. 4.6 is obtained by the modification of stress-strain curve for concrete confined with steel tube given by Hu et al, 2003. The stress-strain curve of concrete confined by steel tube proposed by Hu et al. (2003) contains three parts as shown in Fig. 2.2. Stress-strain curve of concrete confined by UPVC tube is discussed in details in chapter 5.

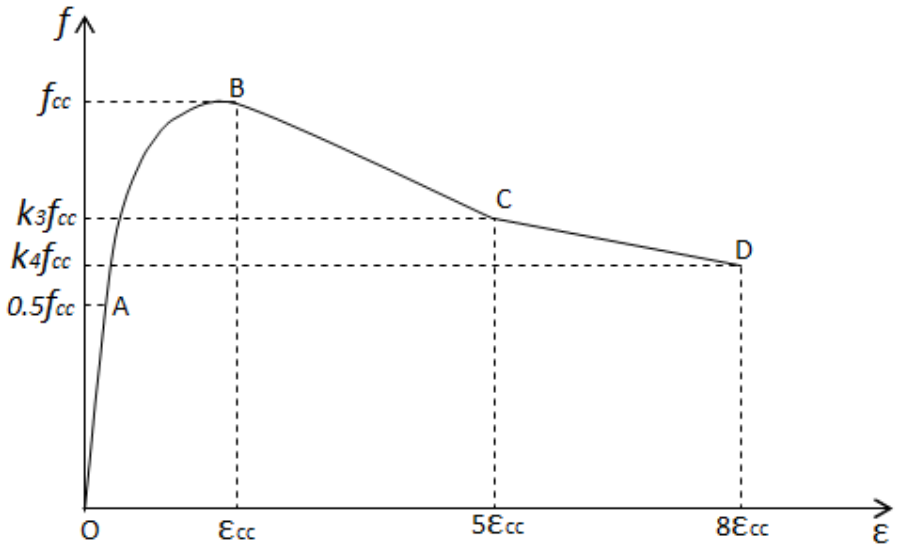

Fig. 4.6 Stress-strain curve for concrete confined by UPVC tube

4.4 MODELLING OF REINFORCEMENT

Three techniques are available to model the steel reinforcement for reinforced concrete structures (ANSYS, 2009-d)

- Discrete model
- Embedded model
- Smeared model

These models are discussed in the following sections:

4.4.1 Discrete model

In the discrete model (Fig. 4.7(a)), the link, truss or beam element is used as a reinforcement and connected to concrete mesh nodes using node sharing (node merging) technique (ANSYS, 2009-c). Therefore, the concrete and reinforcement mesh share the same nodes and concrete occupies the same regions occupied by the reinforcement. In this technique, it is assumed that full bond exists between concrete and reinforcement. A drawback of this approach is that the concrete meshing is restricted by the location of the reinforcement and the volume of rebar is not deducted from the concrete volume. That is why the meshing of big structure is very difficult.

4.4.2 Embedded model

In the embedded model (Fig. 4.7(b)), concrete core and steel reinforcement are mesh separately (ANSYS, 2009-c). This model overcomes the concrete mesh restriction. In this model, steel rebars are modeled in such a way that the rebar displacement is compatible with the surround concrete element. This model is advantageous for complex structures. With this modeling, number of nodes and degree of freedom increases, therefore run time for program increases.

4.4.3 Smeared model

In this model (Fig. 4.7(c)), reinforcement is assumed to be uniformly distributed throughout the concrete element in a selected region of finite element mesh. The concrete element can be selected on the basis of location of reinforcement. Element ‘SOLID 65’ in ANSYS supports this approach. On the basis of volume ratio between total volume of rebars and volume of concrete elements, numbers of concrete elements to be reinforced can be calculated. Orientation angle as a real constant may be the input for rebars. In this approach, since there is no need to create a separate geometry to model the rebar hence this reduces the time of preprocessing and post processing. This approach is suitable for large scale models where

reinforcement does not contribute significantly to the overall response of the structure. A drawback of this approach is that the study of response of rebar is not possible.

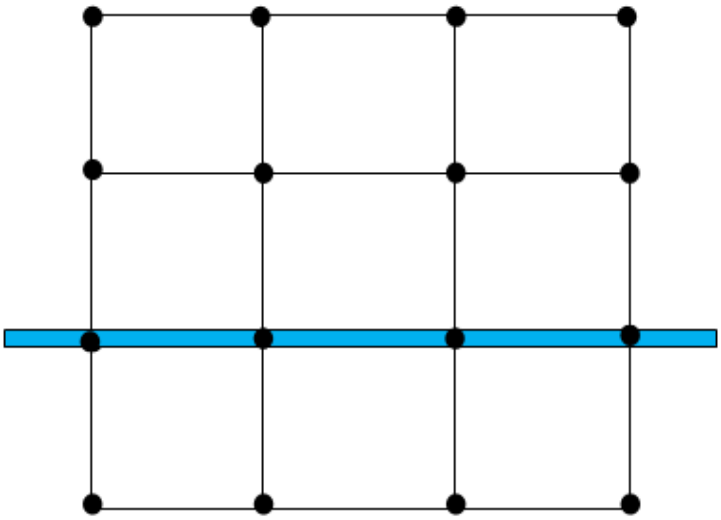

(a) Discrete model

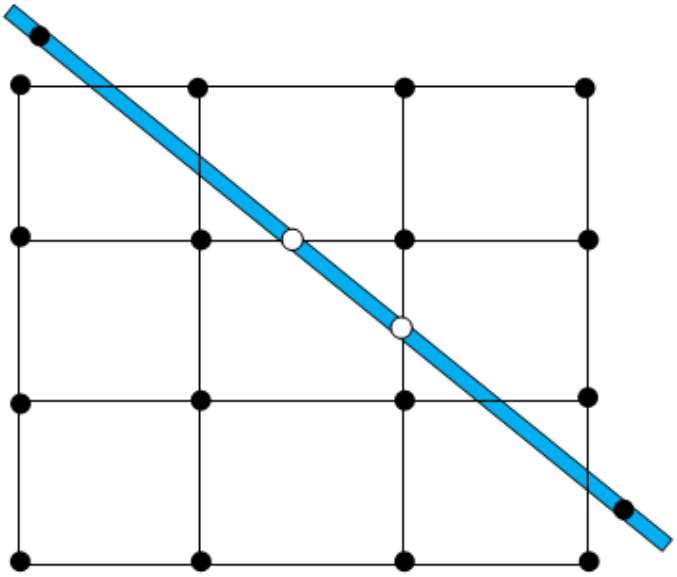

(b) Embedded model

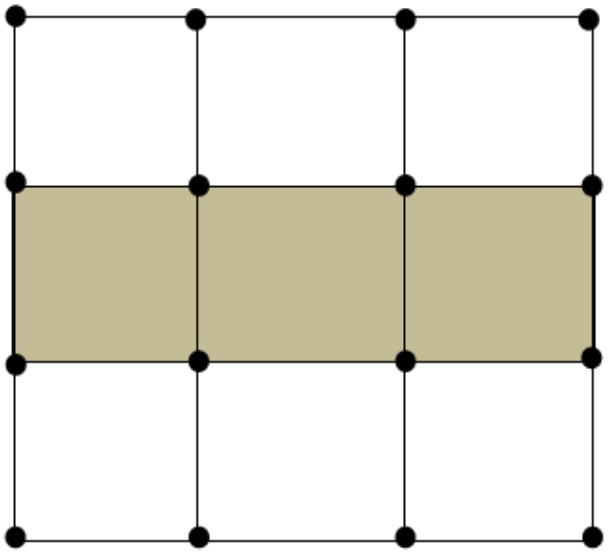

(c) Smeared model

Fig. 4.7 (a-c) Techniques for modeling of reinforcement

4.5 INTERFACE MODELING

To create the Contact between the concrete core and UPVC tube, surface to surface contact element was adopted to simulate the interface between the concrete core and tube (ANSYS,2009-a). The inner surface of tube was selected as target and outer surface of concrete core was selected as contact, as shown in Fig. 4.8. Contact element (CONTA174) (ANSYS, 2009-a) was used to model the contact elements. Element 'CONTA174' is used to represent contact and sliding between 3-D target surface and a deformable surface. This element is applicable to 3-D structural contact analysis. This element is located on the surface of three dimensional solid or shell elements without mid side nodes (SOLID 65 and SOLID 45 etc.). TRAGE 170 was defined as target element as per the recommendation of ANSYS (2009-a).

The composite action between concrete and UPVC was simulated by modeling the behavior of contact surface in normal direction and tangential direction. In normal direction contact pressure model was used (normal pressure turns to zero if separation between two surfaces occurs). In tangential direction, isotropic, Coulomb's friction model was used to define the friction condition between the contact surface and target surface.

Different coefficients of friction (0.05 to 0.4) were tried and it was observed that coefficient of friction has negligible effect on the numerical results. It was found that friction factor of 0.2 was suitable to achieve a quick convergence.

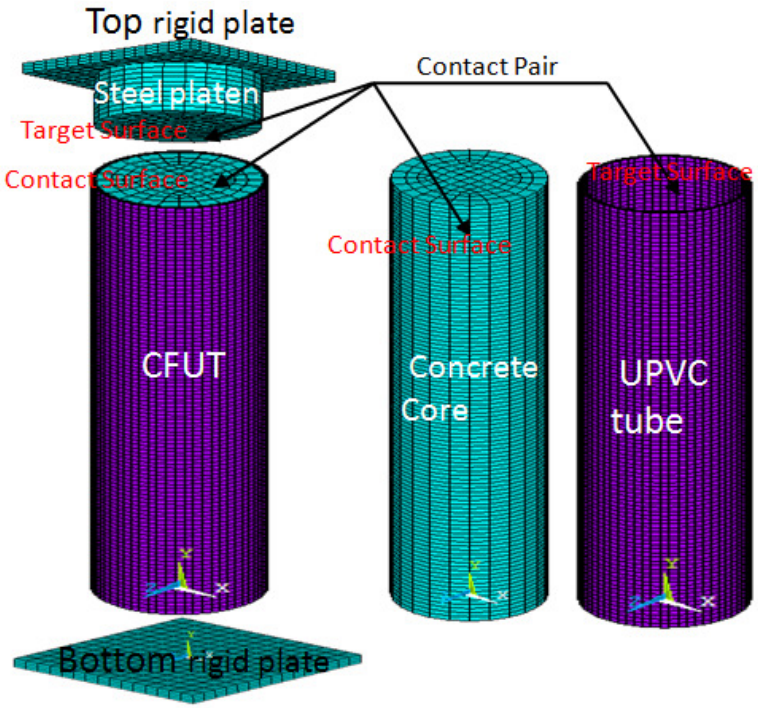

Fig. 4.8 Contact pair for concrete with UPVC tube and steel platen

4.6 MODELING OF STEEL PLATEN AND RIGID PLATES

The steel platen for the loading of concrete core of specimen was also modeled by 'SOLID 45' element. The yield stress of steel platen was taken 1000MPa and stress-strain variation was modeled using elastic-perfectively plastic material option. The platen was behaved as almost rigid. Two rigid plates were modeled to simulate rigid cross heads of machine. Such rigid plates were necessary to avoid stress concentration to lead initiating premature failure.

Load was applied to the column through the top loading plate. In the compression test, direct contact exist between the bottom end plate and bottom surface of column while at top surface, contact was exist between steel platen and top surface of concrete core of the column. Therefore surface to surface contact (CONTA 174) was used to simulate the interaction between rigid plate, platen and column surface. Different coefficients of friction (0.05 to 0.4) were taken and it was found that coefficient of friction between 0.2 and 0.3 provide the best results when compared with experimental results and thus it was adopted as 0.2 (Fig. 4.9). In this model, the lower rigid plate contacting the bottom of column was fixed in all six directions by reference node. The upper rigid plate at the top of the column was modeled fixed in five directions and only allowed movement in column axis at reference node.

4.7 GENERAL INVESTIGATIONS OF MODELING

For the nonlinear analysis, Newton-Raphson approach available in ANSYS software was used. In this approach, the total displacement is subdivided into a series of load increments. To investigate the effect of step length, different values of steps (steps shows the displacement in one increment) were tried. Auto stepping, 0.15 mm, 0.30 mm, 0.5 mm and 1.0 mm step size were tried. ANSYS defines the automatic stepping size for faster convergence, if convergence is not achieved with a certain step size; ANSYS breaks the steps into an appropriate size. Numerical results in the form of load-displacement curve and deformed shape for different step sizes are shown in Fig. 4.10 (a & b) to achieve 15 mm as target compression. The effect of mesh size on the simulated results was studied by performing the analysis with different mesh densities (Fig. 4.11). In case of coarse meshing, no deformed shape was obtained. Maximum aspect ratio of 4 for concrete core elements and around 8 for UPVC tube elements provided the best results compared to experimental results. Therefore, these aspect ratios were adopted to generate the mesh.

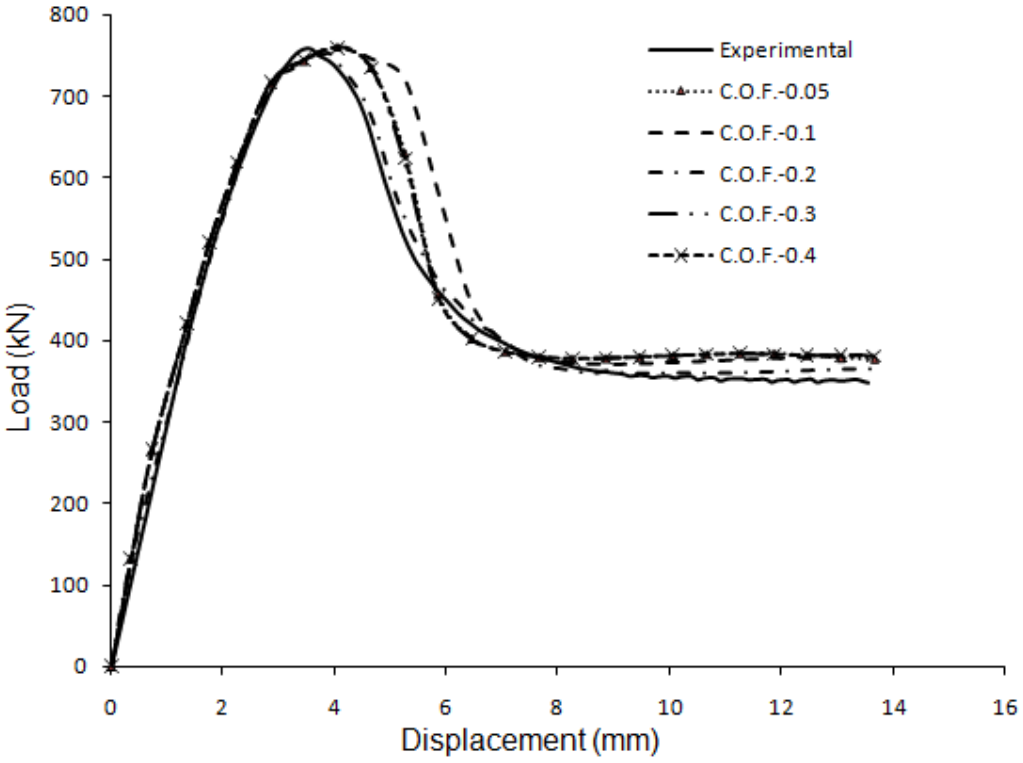

Fig. 4.9 (a) Effect of coefficient of friction on load-displacement curve

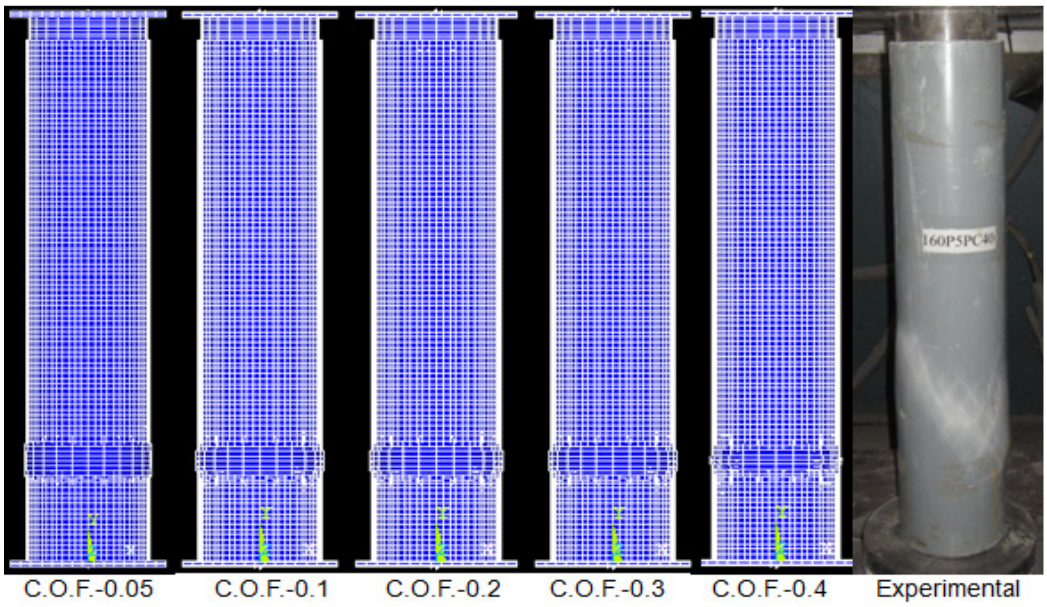

Fig. 4.9 (b) Effect of coefficient of friction on mode of deformation

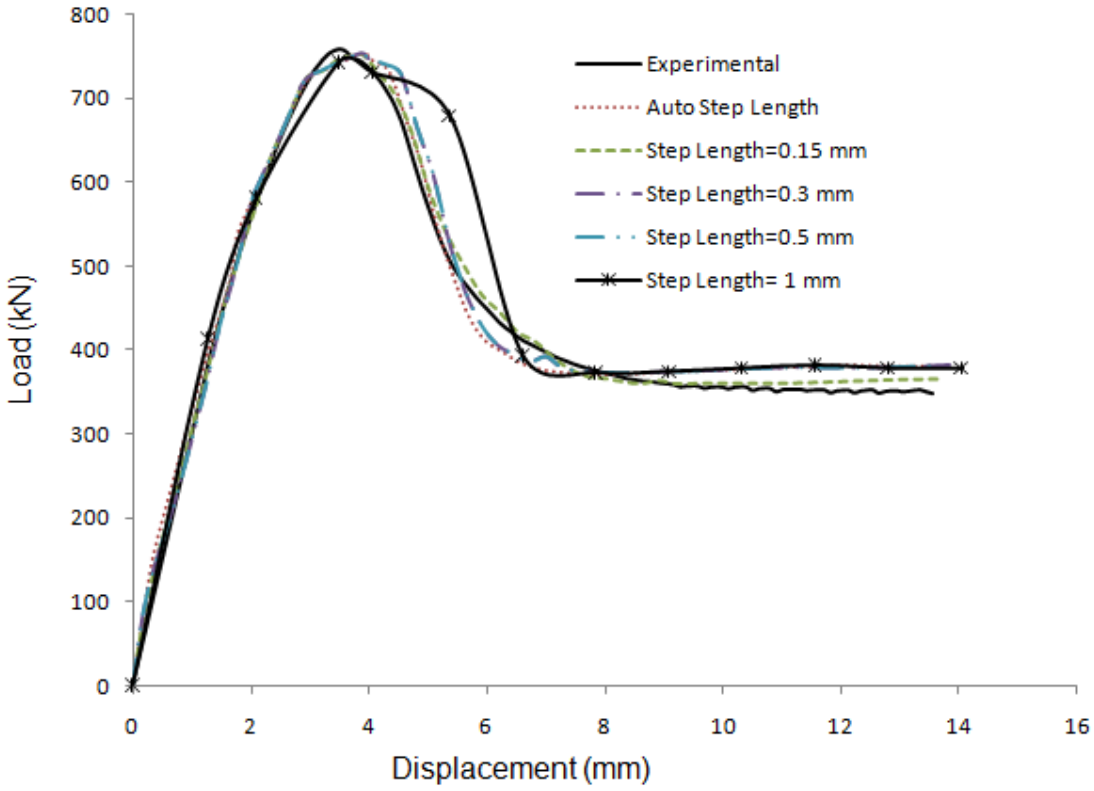

Fig. 4.10 (a) Effect of step length on load-displacement curve

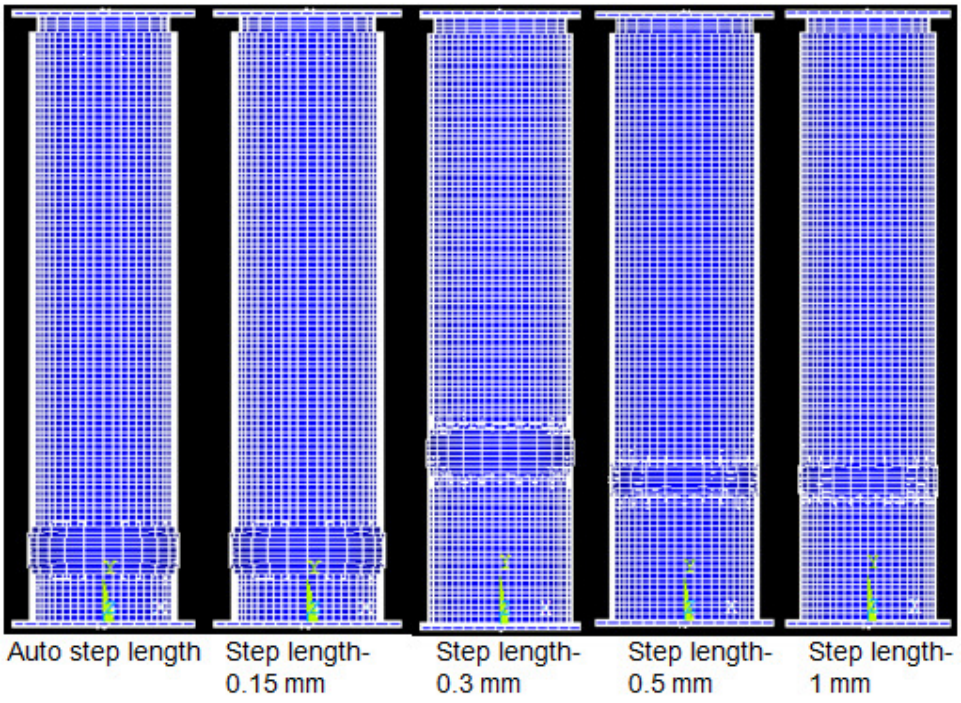

Fig. 4.10 (b) Effect of step length on mode of deformation

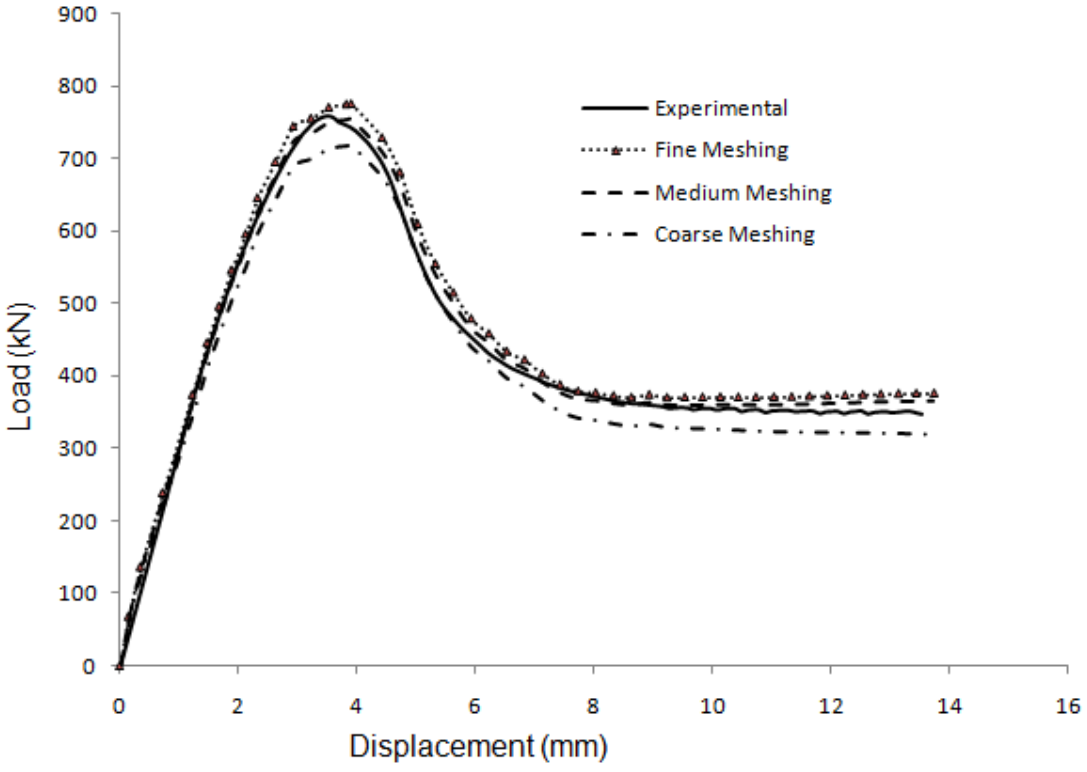

Fig. 4.11 (a) Effect of mesh density on load-displacement curve

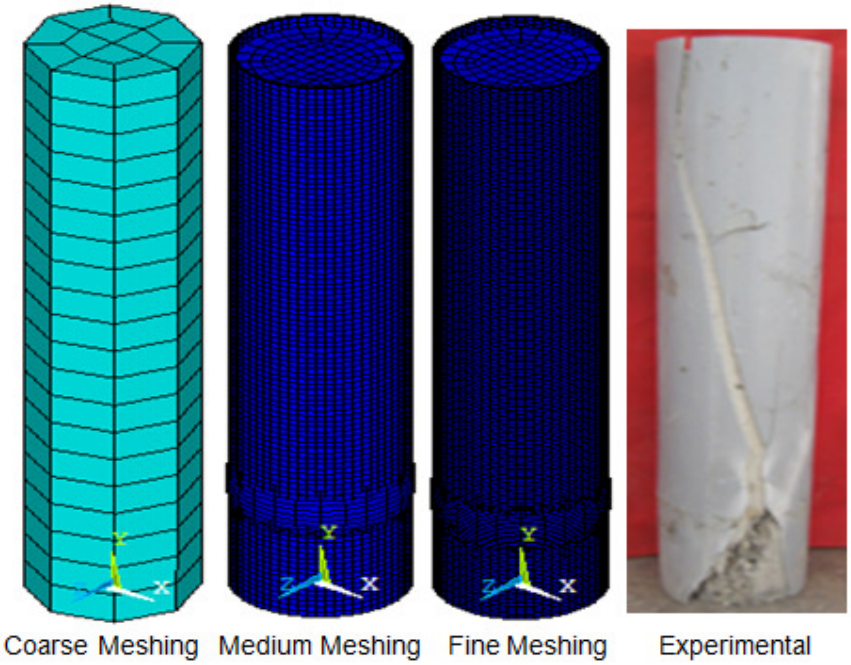

Fig. 4.11 (b) Effect of mesh density on mode of deformation

4.8 MODEL VERIFICATIONS

Results obtained from numerical analysis were verified with the experimental results. PCFUT, RCFUT and bre RCC specimens having different geometrical and material properties were simulated to verify the proposed model. Numerical results were compared with experimental results in the form of load-displacement curves and ultimate load carrying capacity. The results of simulations are given in subsequent chapters. The proposed model for simulating composite columns is shown in Fig. 4.12. Based on the results, it may be concluded that the proposed model can predict the structural behavior and load carrying capacity of such columns with good accuracy.

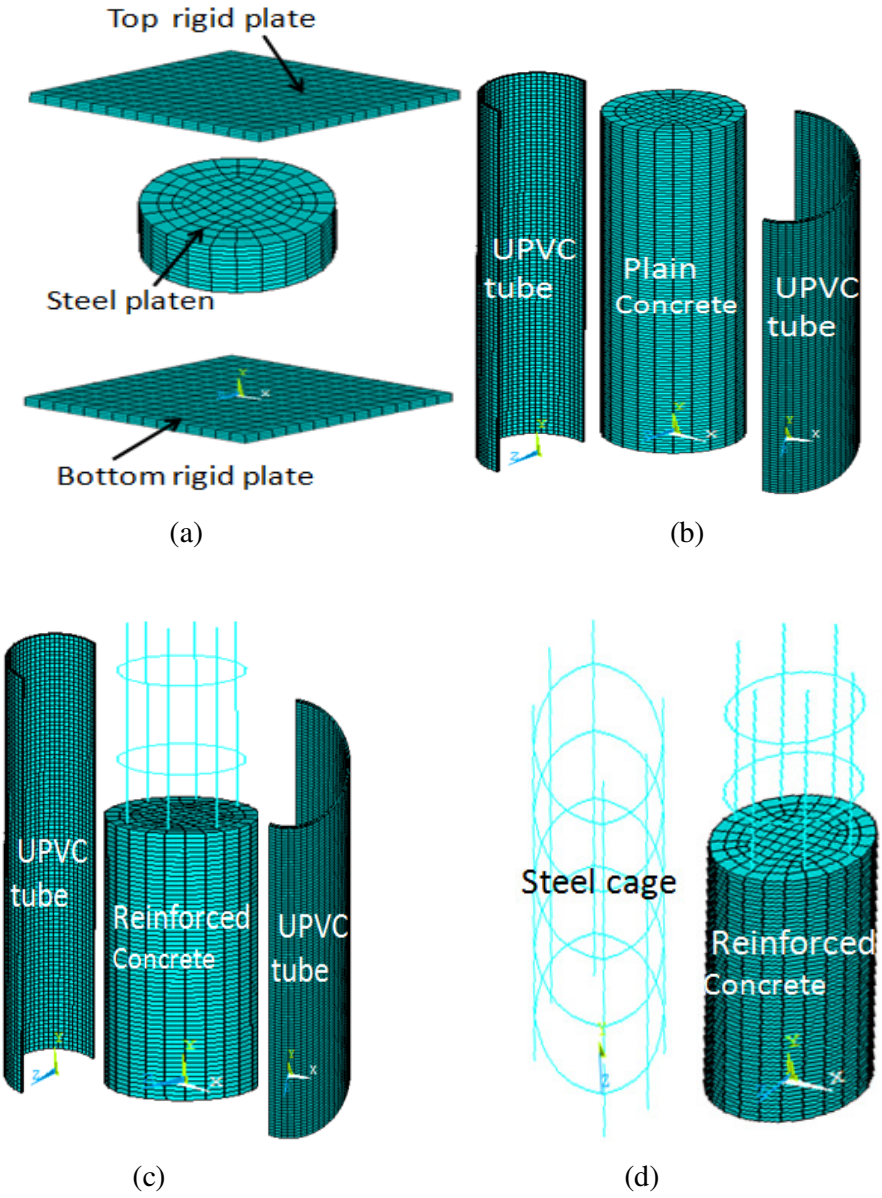

Fig. 4.12 Proposed models for simulation (a) Rigid plates and steel platens (b) PCFUT specimen (c) RCFUT specimen (d) RCC specimen

CHAPTER-5

PLAIN CONCRETE FILLED UPVC TUBULAR (PCFUT) COLUMNN

5.1 GENERAL

This chapter covers study of plain concrete filled UPVC tubes (PCFUT) subjected to axial compression. The study is carried out by performing experiments, analysis and Finite element modeling. Confinement is the main governing factor which influences the behavior of plain concrete filled UPVC tubes (PCFUT) subjected to axial compression. Stress-strain curve of confined concrete, modes of failure, load carrying capacity & ductility, all are dependent on confining pressure exerted by the tube on concrete core. Experiments are carried out to obtain the behavior of concrete core under axial compression confined with UPVC tube and to develop a three dimensional Finite element model using ANSYS software. Mohr-Coulomb failure criterion is used to obtain the angle of failure plane and also to verify the load capacity of tested PCFUT specimens. Fig. 5.1 shows the details of study program.

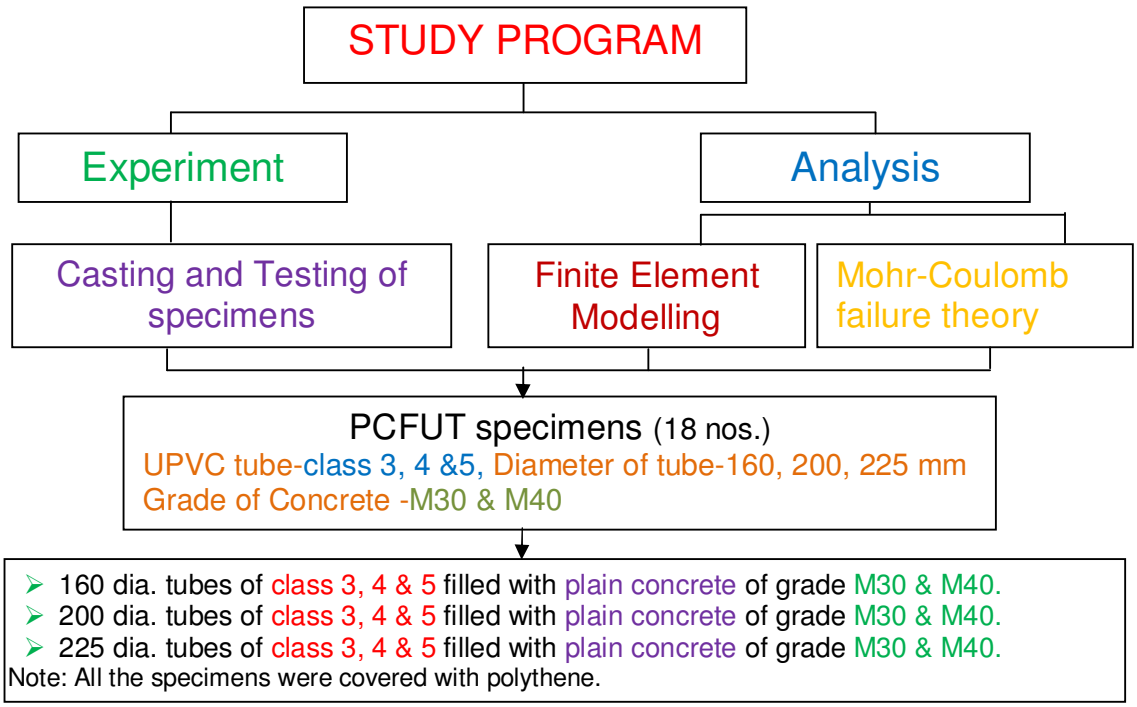

Fig. 5.1 Details of study program of plain concrete filled UPVC tubes

5.2 CASTING AND TESTING OF SPECIMENS

Total 18 specimens are cast and tested by applying axial loading on concrete core only (see Fig. 5.2). For casting of specimens, the UPVC pipes of class 3, 4 and 5 having diameters of 160 mm, 200 mm and 225 mm were taken. Length to diameter ratio and Diameter to thickness ratio varies from 3.56 to 5.0 and 22.48 to 40.13 respectively. Length of specimens was kept as 800 mm. M30 and M40 grades of concrete were prepared to fill the tubes. Table 5.1 shows the geometrical and material properties of PCFUT specimens. The internal hydrostatic pressure tests were conducted to get the confining pressure (discussed in chapter 3). The confining pressures of UPVC tubes obtained from pressure test and from mechanics are quite similar (Table 5.2).

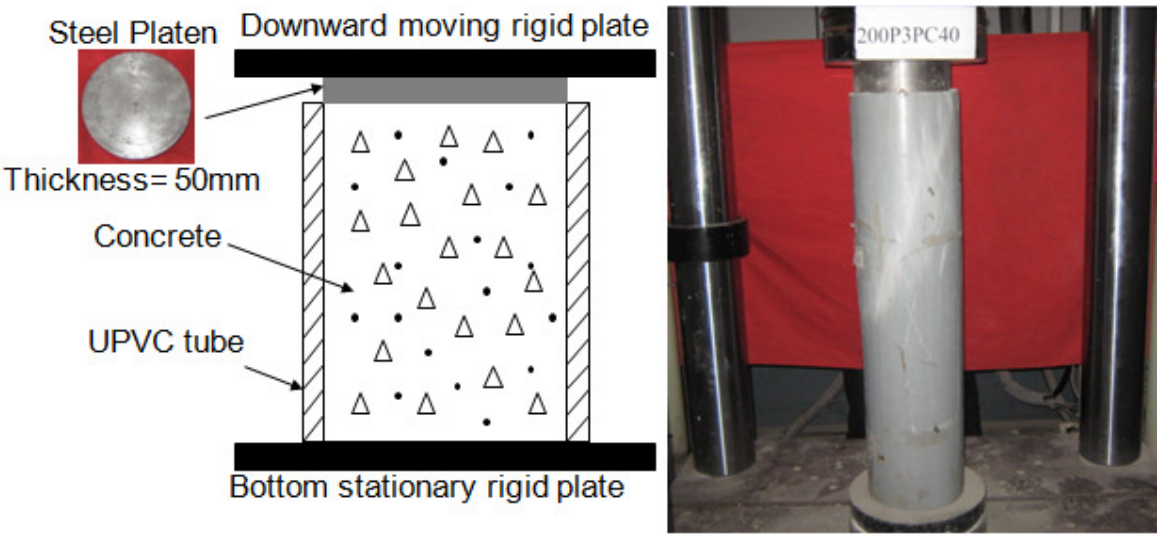

Fig. 5.2 Loading and testing arrangements for PCFUT specimen

Table 5.1 Geometrical and material properties of PCFUT specimens

Specimen	Dimensions (mm)			Ratios		Material Properties (MPa)	
	Mean Outer diameter (D)	Thic-kness (t)	Length (L)	D/t	L/D	Unconfined compressive strength of concrete (f_c)	Ultimate tensile strength of UPVC tube (f_u)
160P3PC30	160.15	3.99	800	40.10	5	35.08	22.5
160P4PC30	159.88	5.22	800	30.65	5	35.08	22.5
160P5PC30	160.19	7.02	800	22.79	5	35.08	22.5
200P3PC30	199.85	5.94	800	33.67	4	35.08	22.5
200P4PC30	199.56	8.11	800	24.66	4	35.08	22.5
200P5PC30	199.22	8.89	800	22.50	4	35.08	22.5
225P3PC30	224.78	8.65	800	26.01	3.56	35.08	22.5
225P4PC30	224.58	9.58	800	23.49	3.56	35.08	22.5
225P5PC30	224.53	9.97	800	22.57	3.56	35.08	22.5
160P3PC40	160.15	3.99	800	40.10	5	39.05	22.5
160P4PC40	159.88	5.22	800	30.65	5	39.05	22.5
160P5PC40	160.19	7.02	800	22.79	5	39.05	22.5
200P3PC40	199.85	5.94	800	33.67	4	39.05	22.5
200P4PC40	199.56	8.11	800	24.66	4	39.05	22.5
200P5PC40	199.22	8.89	800	22.50	4	39.05	22.5
225P3PC40	224.78	8.65	800	26.01	3.56	39.05	22.5
225P4PC40	224.58	9.58	800	23.49	3.56	39.05	22.5
225P5PC40	224.53	9.97	800	22.57	3.56	39.05	22.5

Table 5.2 Confining pressure of UPVC tubes

Class of pipe (Nominal pressure)	Dimensions (mm)			Confining pressure (f_l) (MPa)	
	Mean Outer diameter (D)	Internal diameter (d)	Thickness (t)	Experimental	Calculated $f_l = f_u(2t/d)$
Three (0.6 MPa)	160.15	152.17	3.99	1.15	1.18
	199.85	187.97	5.94	1.35	1.42
	224.78	207.48	8.65	1.72	1.87
Four (0.8 MPa)	159.88	149.44	5.22	1.52	1.57
	199.56	183.34	8.11	1.99	1.99
	224.58	205.42	9.58	2.00	2.09
Five (1.0 MPa)	160.19	146.15	7.02	2.15	2.16
	199.22	181.44	8.89	2.25	2.20
	224.53	204.59	9.97	2.17	2.19

f_l =Confining pressure, f_u= Ultimate tensile strength of UPVC tube, t = thickness of tube, d = internal diameter of tube

5.3 NUMERICAL MODELING AND SIMULATION

5.3.1 Finite element model

A three dimensional Finite element model shown in Fig. 5.3 was developed using ANSYS software to simulate the concrete filled UPVC tube (CUFT) subjected to axial compression. Mesh size was chosen from 5 mm to 10 mm for tube, concrete core and steel platen. Two rigid plates were modelled to simulate rigid cross heads of machine. Load was applied to the column through the top loading plate. In the compression test, direct contact exist between the bottom end plate and bottom surface of column while at top surface, contact was exist between steel platen and top surface of concrete core of the column; therefore a contact available in ANSYS was used to simulate the interaction between rigid plate, platen and column surface. The contact was defined as a surface to surface contact.

To activate the confinement of concrete core in Finite element model, a contact surface pair comprised of the inner surface of the tube and the outer surface of concrete core was adopted. Flexible behavior in the normal direction was assumed with no penetration allowed between the surfaces. Different friction factors (0.1 to 0.4) were taken for the contact surface and it was found that friction factor of 0.2 was suitable to achieve a quick convergence. In Finite element model, the lower rigid plate contacting the bottom of column was fixed in all six directions by

reference node. The upper rigid plate at the top of the column was modelled fixed in five directions and only allowed movement in column axis at reference node. The load was applied as static uniform displacement at upper rigid plate through the reference node at the centre of rigid plate.

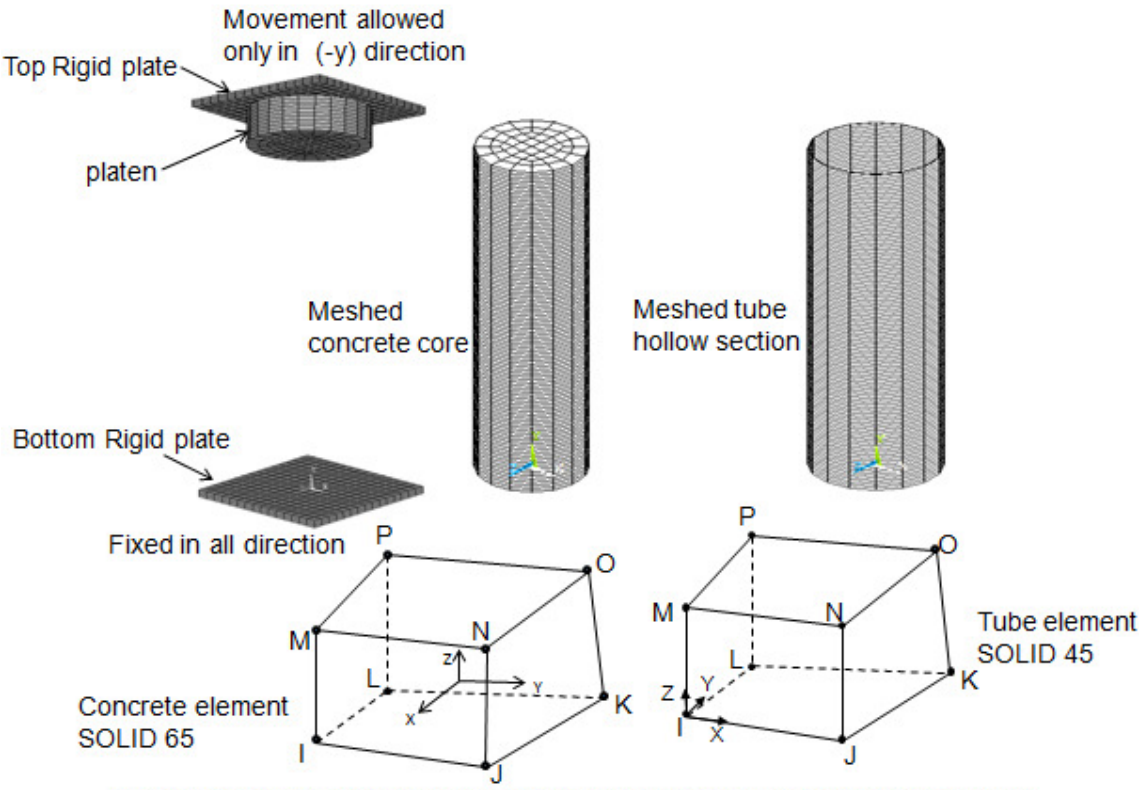

Fig. 5.3 Typical details of Finite element model for Concrete filled tube

5.3.2 Material model of UPVC

Multilinear elastic-plastic material behavior of the UPVC tube is taken (ANSYS, 2009-d) to model it. Elastic modulus of equal to 880 MPa of UPVC was obtained from stress-strain curve (discussed in chapter 3) and Poisson's ratio is taken as 0.35. When tube is subjected to several stresses, a von Mises criterion F is used to define the elastic limit (Ragab et al. 2000) , which is written as

$$F = \sqrt{3J_2} = \frac{1}{\sqrt{2}}\sqrt{(\sigma_1-\sigma_2)^2+(\sigma_2-\sigma_3)^2+(\sigma_3-\sigma_1)^2} = \sigma_y$$

Where J_2 = Second stress invariant of the stress deviator tensor.

σ_1, σ_2, & σ_3 are the Principal stresses.

σ_y = yield stress of material under uniaxial tension.

5.3.3 Material model of confined concrete

The concrete inside the tube is usually subjected to tri-axial compression stresses and the failure of concrete is dominated by compression failure. The maximum stress of confined concrete (f_{cc}) and corresponding strain ε_{cc} are calculated by the following equations (Richart et al., 1928).

$$f_{cc} = f_c + k_1 f_l \tag{2.1}$$

$$\varepsilon_{cc} = \varepsilon_c \left(1 + k_2 \frac{f_l}{f_c}\right) \tag{2.2}$$

where f_c = unconfined compressive cylinder strength of concrete;

k_1, k_2 are constant, generally taken as 4.1 and 20.5, (Richart et al., 1928).

The value of ε_c is usually between 0.002 to 0.003. For confined concrete it may be taken as 0.003 (ACI-318, 2008)

f_l = lateral confining stress induced due to confinement provided by tube and depends upon D/t & tensile strength of UPVC tube (f_u).

The confining pressure is the main governing factor for the post peak behavior of concrete under triaxial stress. At low confinement, concrete exhibits a well defined peak with strain softening behavior while at higher confinement; it shows strain hardening behavior (Sfer et al., 2002). Selecting a stress-strain model for confined concrete is a difficult task. Therefore proper stress-strain model is necessary for better Finite element modeling.

The confining pressure may be obtained with the help of internal hydrostatic pressure test of pipes (as per IS: 12235 part 8 -1986) or may be calculated using formula as:

$$f_l = f_u \left(\frac{2t}{d}\right)$$

where, f_l is the confining pressure, f_u is the ultimate tensile strength of UPVC tube, t is the thickness of tube and d is the internal diameter of tube.

The response of concrete is modelled by an elastic-plastic theory with associated flow and kinematic hardening rule. During plastic deformation, the expansion of yield surface can be guided by the uniaxial stress-strain curve. Confined concrete is subjected to triaxial compressive stresses; the effective stress and effective strain values may be represented by the

uniaxial stress and strain values obtained from the stress-strain equation proposed by (Saenz, 1964). It is given as:

$$f = \frac{E_{cc}\varepsilon}{1+(R+R_E-2)\left(\frac{\varepsilon}{\varepsilon_{cc}}\right)-(2R-1)\left(\frac{\varepsilon}{\varepsilon_{cc}}\right)^2+R\left(\frac{\varepsilon}{\varepsilon_{cc}}\right)^3} \quad (2.5)$$

$$\text{where } R_E = \frac{E_{cc}\varepsilon_{cc}}{f_{cc}},\ R = \frac{R_E(R_\sigma - 1)}{(R_\varepsilon - 1)^2} - \frac{1}{R_\varepsilon}$$

values of R_σ & $R_\varepsilon = 4$ (Elwi and Murray, 1979)

E_{cc} is the initial modulus of elasticity of concrete and calculated from the equation $E_{cc} = 4700\sqrt{f_{cc}}$ (ACI-318, 2008)

The Stress-strain curve for concrete confined with UPVC tube is obtained by the modification of stress-strain curve for concrete confined with steel tube (Hu et al, 2003). The stress-strain curve of concrete confined by steel tube was proposed by Hu et al. (2003) contains three parts as shown in Fig. 2.2. In this curve first two parts are independent of the material used for confinement and can be obtained using equations (2.1), (2.2), (2.5). The third part starts from point (f_{cc}, ε_{cc}) and ends at the point ($k_3 f_{cc}$, $11\varepsilon_{cc}$) is used for post peak part of the curve. This third part is developed for continuous confinement provided by steel tube.

Keeping the stress-strain variation of concrete confined by steel tube in consideration, a stress-strain variation of concrete confined by UPVC tube is developed. The stress-strain variation is developed with having four parts (see Fig. 5.4). The first two parts 'OA' and 'AB' are represented by equations (2.1), (2.2), (2.5). In these equations k_1 and k_2 are taken as 4.1 and 20.5 as suggested by Richart et al. (1928). The first part of stress-strain variation defines the linear property of confined concrete and the proportional limit stress can be assumed $0.5f_{cc}$. The corresponding strain can be obtained using Young's Modulus, $E_{cc} = 4700\sqrt{f_{cc}}$ MPa (ACI-318, 2008). The value of f_l has been obtained by performing water pressure test on the pipes (Fig. 3.4). Generally percentage elongation in steel varies between 22 and 24. On the other hand percentage elongation in UPVC varies between 13 and 16. The last fracture point in stress-strain curve for steel was at $11\varepsilon_{cc}$ strain. This point for UPVC confined concrete may be obtained as ($11\varepsilon_{cc}$ x 16)/24 $=7.33\varepsilon_{cc} \approx 8.0\varepsilon_{cc}$. The parts of the curve 'BC' and 'CD' are dependent on values of k_3 and ε_{cc} were obtained using numerical and experimental curve matching. The 'CD' part of the curve was obtained by taking $k_4 = 0.8k_3$. As a result the coordinates of points 'C' and 'D' are ($k_3 f_{cc}$, $5\varepsilon_{cc}$) and ($k_4 f_{cc}$, $8\varepsilon_{cc}$). Fig. 5.4 shows the stress-

strain variation of concrete having 35.08 MPa compressive strength and confined with UPVC tube of class 3 and having nominal diameter 160 mm.

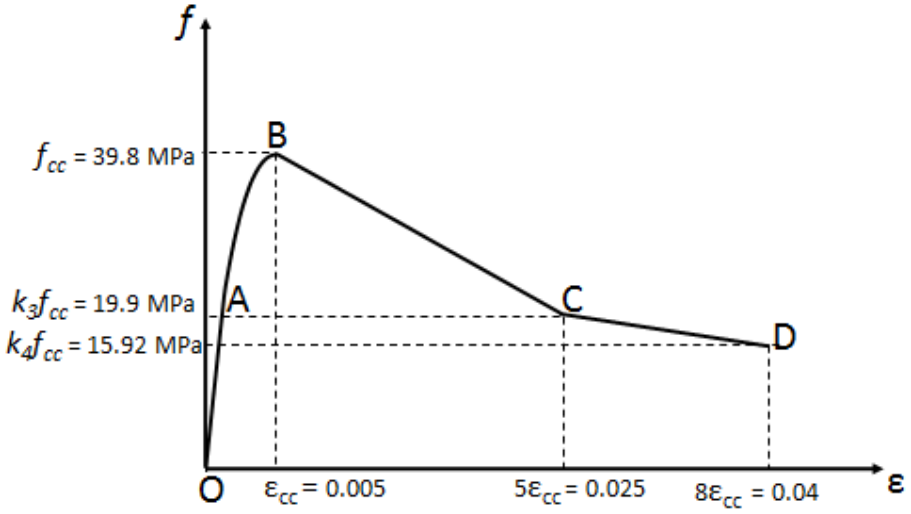

Fig. 5.4 Stress-strain variation of concrete having 35.08 MPa compressive strength and confined with UPVC tube of class 3 and having nominal diameter 160 mm

5.4 ANALYSIS USING MOHR-COULOMB FAILURE THEORY

The failure pattern of confined concrete depends on confinement ratio 'β' (Ansari and Li,1998). The confinement ratio is defined as $\beta = (f_l / f_c)$. They observed that when the value of β was less than 0.1, shear failure was occurred. In the present study the value of β is less than 0.1 for all specimens. The value of β is given in Table 5.3. All tested column specimens were failed by development of shear crack.

Mohr-Coulomb failure theory is the most commonly used hypothesis to describe the failure condition of concrete. The Mohr-Coulomb failure criterion may be understood by Fig. 5.5. In the present study, angle of failure plane and load capacity of CFUT column is calculated with the help of Mohr-Coulomb failure criterion. When column specimen is acted upon by external stress (σ_c) and confining pressure (f_l) resulted to shear failure, the angle of failure is obtained by equating the shear strength of concrete and shear stress developed in concrete. According to Mohr-Coulomb failure criterion, the relationship between shear strength of concrete (τ_c) and normal stress (σ_n) on failure plane can be expressed as following:

$$\tau_c = c + \sigma_n \tan\phi \tag{5.1}$$

c is the cohesion of material and computed as: (Montaya et al., 2001)

$$c = f_c \frac{1-\sin\phi}{2\cos\phi} \tag{5.2}$$

ϕ is the angle of internal friction and equals to 37^0 for concrete (Montaya et al., 2001).

Where

$$\sigma_n = \left(\frac{\sigma_c + f_l}{2}\right) + \left(\frac{\sigma_c - f_l}{2}\right)\cos 2\theta \tag{5.3}$$

$$\sigma_c = f_l\left(\frac{1+\sin\phi}{1-\sin\phi}\right) + 2c\left(\frac{\cos\phi}{1-\sin\phi}\right) \tag{5.4}$$

$$\tau_c^{'} = \left(\frac{\sigma_c - f_l}{2}\right)\sin 2\theta \tag{5.5}$$

Where σ_c is the axial stress applied on specimen, f_l is confining pressure and τ'_c is the shear stress developed at failure plane.

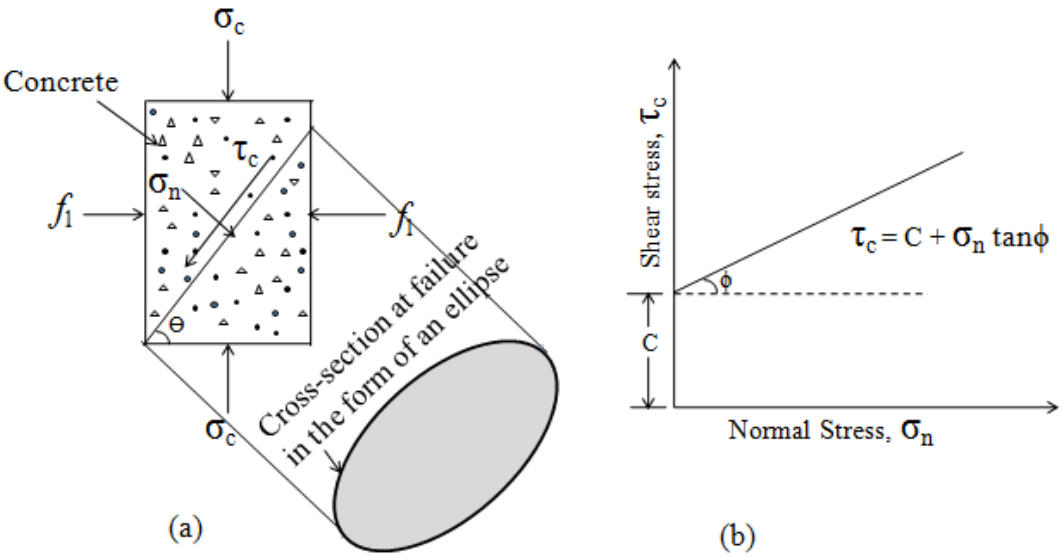

Fig. 5.5 Mohr-Coulomb failure criterion

5.5 RESULTS AND DISCUSSIONS

5.5.1 Stress-strain model

To get the stress-strain model of confined concrete, first of all, confined compressive strength of concrete (f_{cc}) and ε_{cc} is calculated using equation no. 2.1 & 2.2 respectively. By having the

value of f_{cc} and ε_{cc}, it is possible to draw stress-strain curve upto the peak. Now to obtain the post peak behavior of curve, the experimental results are matched with the numerical results by taking the various trial values of k_3 and k_4 with corresponding strains. After getting the appropriate values of k_3 and k_4, an empirical relation between k_3 and D/t is obtained through regression analysis. A stress-strain model for concrete confined with UPVC tube is obtained by using the values of f_{cc}, ε_{cc}, k_3 and k_4.

For the parameter k_3, following empirical relation is proposed.

$$k_3 = 0.0001\left(\frac{D}{t}\right)^2 - 0.011\left(\frac{D}{t}\right) + 0.7635 \quad \left(20 \le {}^{D}\!/_{t} \le 40\right) \tag{5.6}$$

It was observed that the values of f_l and k_3 decrease with the increase in diameter to thickness ratio. Confining pressure depends on the tensile strength of tube and the value of D/t. As a result the value of f_l varies from 1.15 to 2.25 when UPVC pipes with nominal pressure 0.6 MPa, 0.8 MPa and 1.0 MPa were used. In the case of CFUT specimens, the degradation parameter (k_3) varies from 0.5 to 0.58 and k_4 is taken as $0.8k_3$. Fig. 5.6 shows the variation of k_3 with D/t ratio for UPVC tube confined concrete.

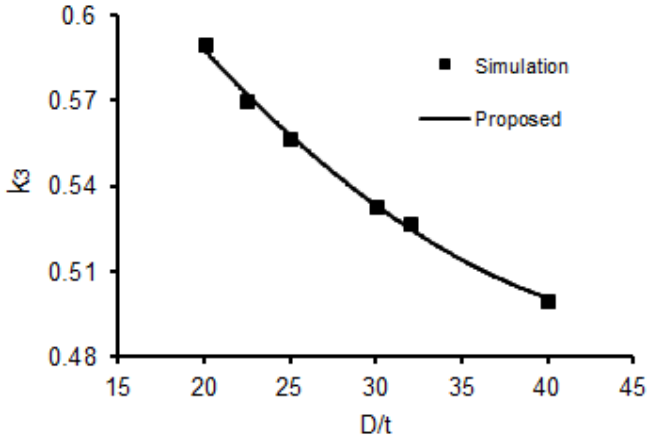

Fig. 5.6 Variation of k_3 with diameter/wall thickness (D/t)

5.5.2 Load carrying capacity and Load–displacement curves

Load carrying capacity obtained from experiments and numerical simulations of PCFUT are given in Table 5.3. They are in good agreement and it can be seen that error in the results obtained from simulation is within 1%. The load-displacement curves of specimens are plotted in Fig. 5.7(a-r). The maximum displacement at failure was observed between 10 and 14 mm. Strain at maximum load ε_{cc} was found to be 0.0043 to 0.0068. The post peak displacement is important regarding ductile behavior of material. From the load-displacement curve, it was found that the displacement after the peak load was about 5 to 10 mm. (Fig. 5.8(a-f)) represents

typical variation of load-displacement curves for the specimens made with tubes of same class and different diameters. It can be seen form Fig. 5.8(a-f) that the initial slope of curves increases as the diameter of tubes increases and the post peak slope are nearly same. Fig. 5.9(a-f) represents typical variation of load-displacement curves for the specimens made with tubes of different class and same diameter. From Fig. 5.9(a-f), it may be observed that the initial slope is nearly equal and the post peak slope is decreasing with the higher class of tube due to enhancement of confinement.

For the design of concrete filled UPVC tubular column, load carrying capacity is required. An equation is proposed to get the load capacity of CFUT. Proposed equation is as follow:

$$P_u = f_c A_c + 2 f_u A_p \tag{5.7}$$

The ultimate load capacities of all the specimens are calculated using the above equation and presented in Table 5.3. The load calculated using above equation are within 0.35 to 7.5 % higher and lower of from experimental load. To verify the above proposed equation, the ultimate load capacities of specimens from literature are calculated using equation no.5.11 and presented in Table 5.4. The calculated load capacities are within ±8.5% of experimental capacities. Experimental load capacities (from literature) versus load capacities computed from equation no. 5.7 are graphically presented in Fig. 5.10. It can be concluded that proposed equation may be used for assessing the load capacity of concrete filled UPVC tubular columns.

Table 5.3 Experimental and numerical results of PCFUT specimens

Specimen	Ultimate Load (kN)			Constraining parameter $\alpha=A_p f_u/A_c f_c$	Confinement ratio $\beta=(f_l/f_c)$	Mode of failure	Failure load	Max. strain at failure
	Experiment	Simulation	From Eq. $P_u=f_c A_c+2f_u A_p$					
160P3PC30	759	753	724	0.067	0.034	Shear cracks with slight bulge	348.28	0.0169
160P4PC30	769	763	726	0.089	0.045		350.70	0.0150
160P5PC30	793	788	734	0.123	0.062		372.08	0.0149
200P3PC30	1123	1127	1131	0.081	0.041		509.40	0.0151
200P4PC30	1142	1135	1136	0.114	0.057		656.69	0.0149
200P5PC30	1182	1176	1135	0.125	0.063		614.16	0.0140
225P3PC30	1352	1354	1439	0.107	0.053		607.22	0.0150
225P4PC30	1420	1411	1440	0.119	0.059		695.44	0.0146
225P5PC30	1491	1482	1441	0.125	0.062		772.05	0.0138
160P3PC40	816	811	796	0.060	0.030		324.59	0.0155
160P4PC40	839	832	795	0.080	0.040		383.80	0.0142
160P5PC40	850	845	800	0.111	0.055		456.14	0.0132
200P3PC40	1231	1223	1241	0.073	0.036		564.15	0.0138
200P4PC40	1245	1239	1241	0.102	0.051		598.87	0.0138
200P5PC40	1280	1273	1237	0.113	0.056		650.86	0.0130
225P3PC40	1486	1471	1573	0.096	0.048		693.89	0.0143
225P4PC40	1550	1538	1572	0.107	0.054		759.42	0.0134
225P5PC40	1610	1597	1571	0.112	0.056		806.35	0.0128
75P3PC30-concrete loaded (Long column)		147	-	0.162	0.032	Buckling	69	0.536
75P3PC30-both loaded (long Column)		153	-	0.162	0.032	Buckling	72	0.567
75P3PC30-concrete loaded (Short Column)		161	164	0.162	0.032	Buckling	76	4.7

Note: 160P3PC30 represents the specimen composed of 160 mm diameter UPVC tube of class 3 (nominal pressure of 0.6 MPa) filled with plain concrete of grade M30. Other CFUT specimens are represented in the same manner. Similarly '75P3PC30' represents the specimens of 75 mm diameter tube with different lengths having same properties as the specimen '160P3PC30'.

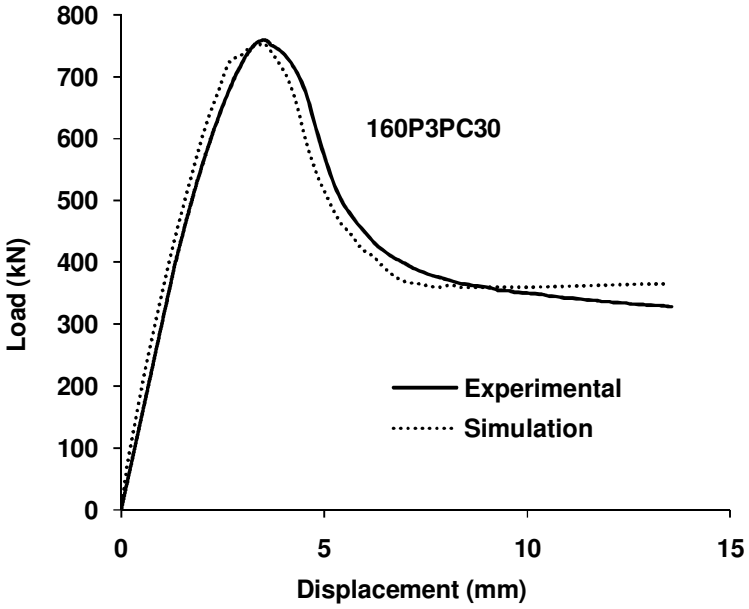

(a)

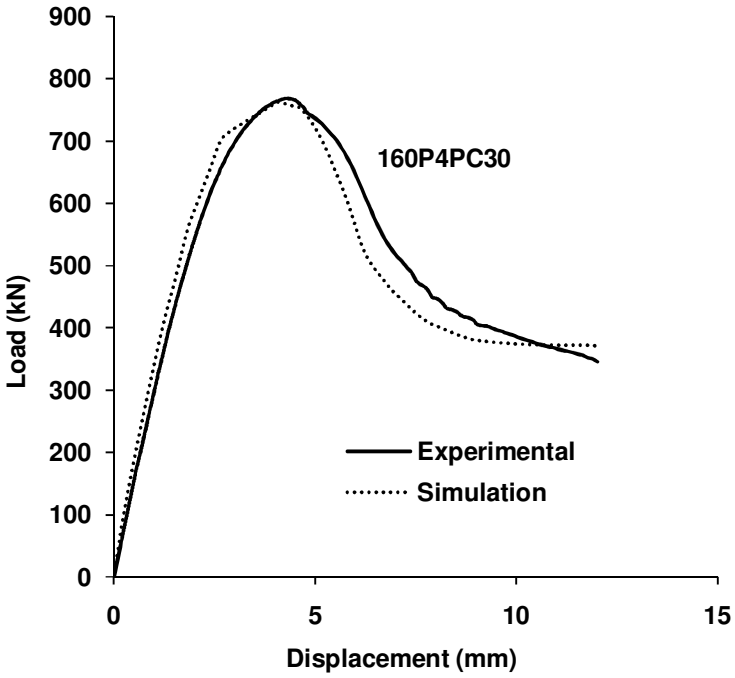

(b)

Fig. 5.7 (a-r) Load-Displacement curves of PCFUT specimens obtained from experiment and simulation

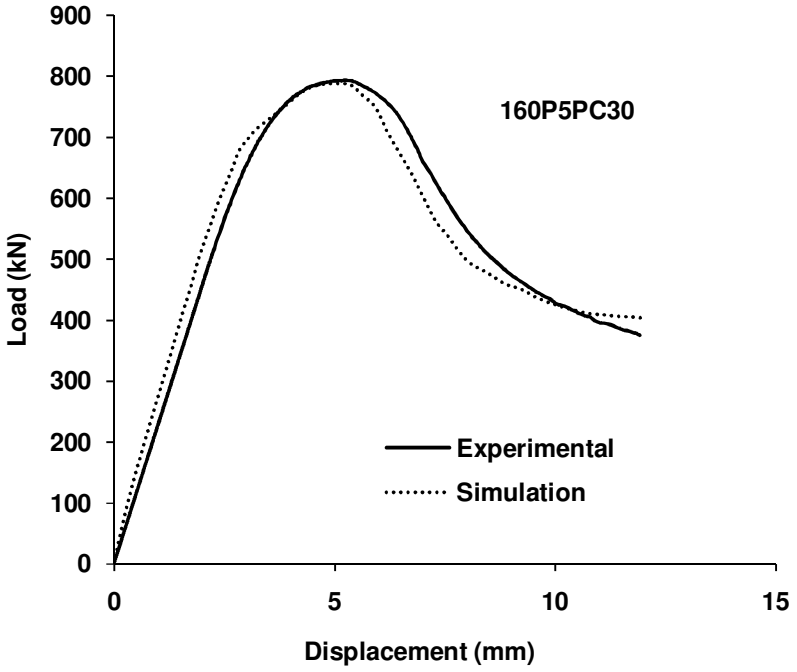

(c)

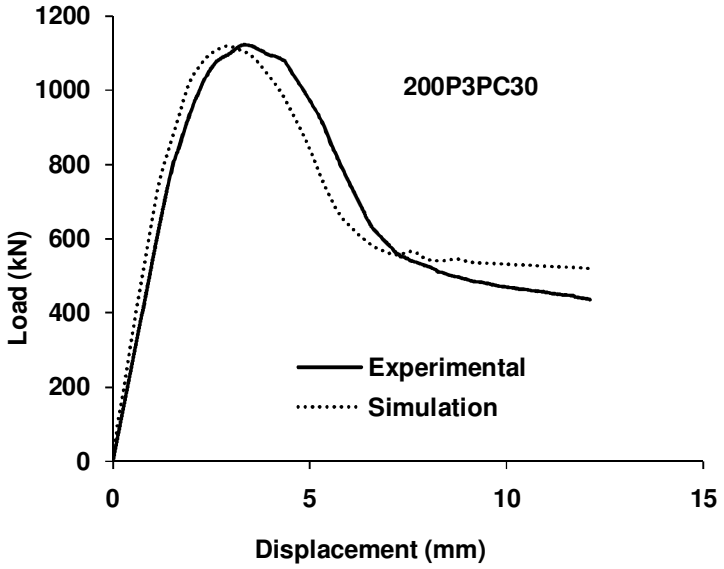

(d)

Fig. 5.7 (a-r) Load-Displacement curves of PCFUT specimens obtained from experiment and simulation

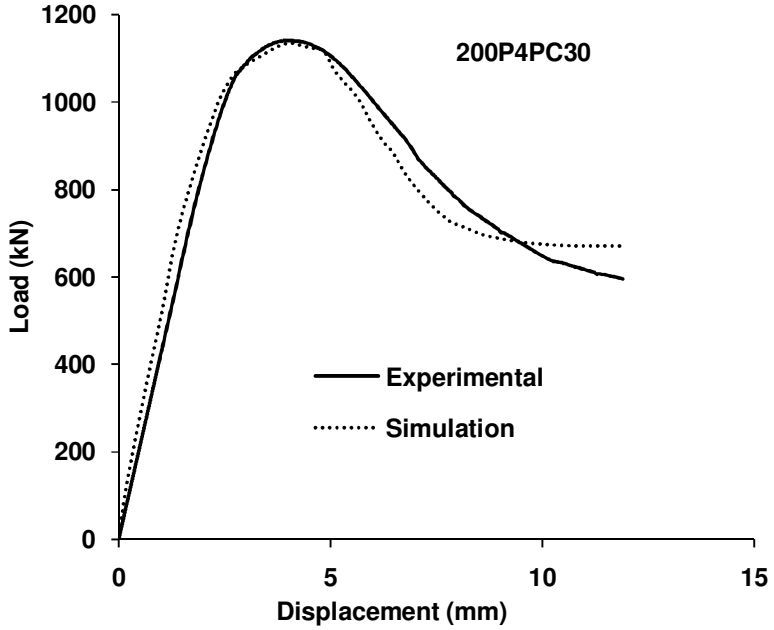

(e)

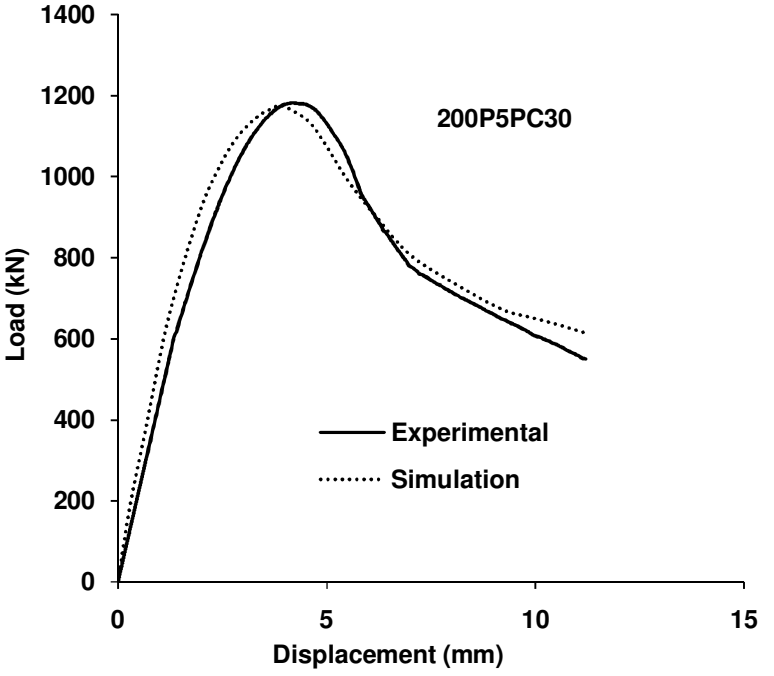

(f)

Fig. 5.7 (a-r) Load-Displacement curves of PCFUT specimens obtained from experiment and simulation

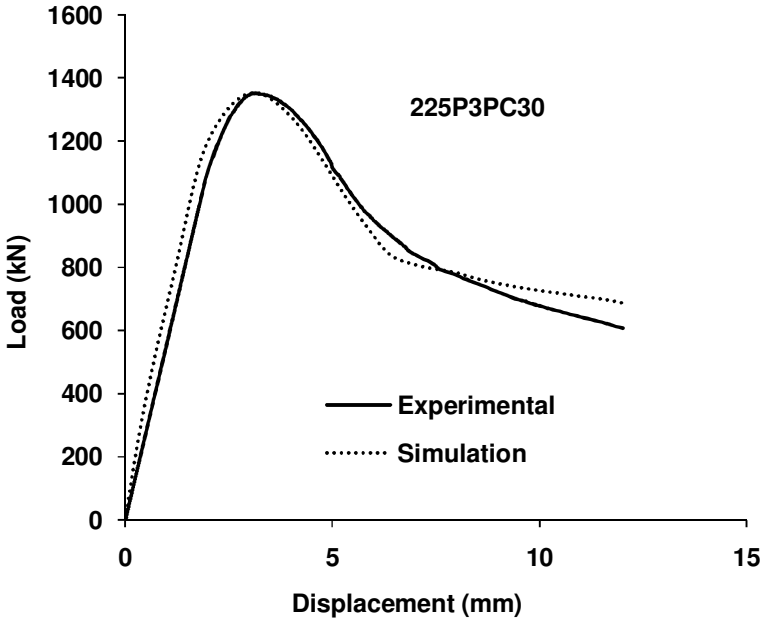

(g)

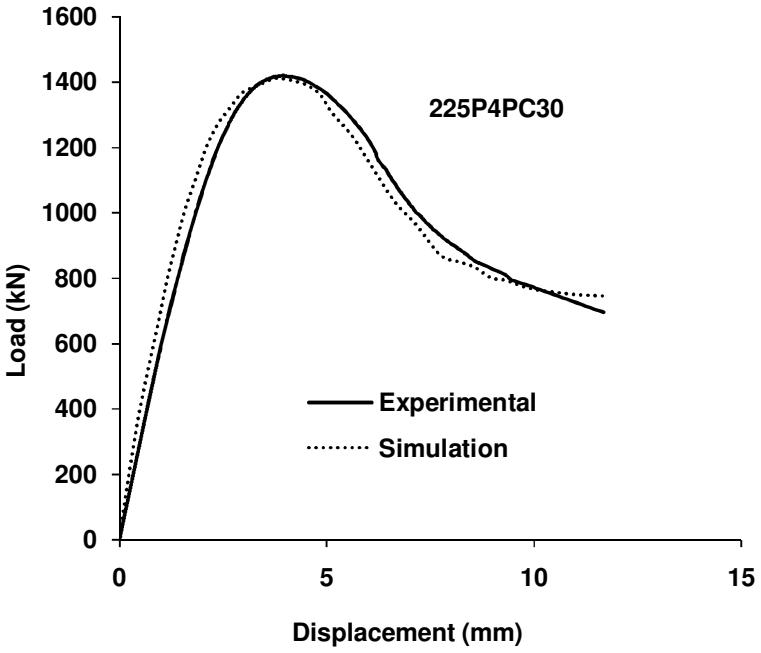

(h)

Fig. 5.7 (a-r) Load-Displacement curves of PCFUT specimens obtained from experiment and simulation

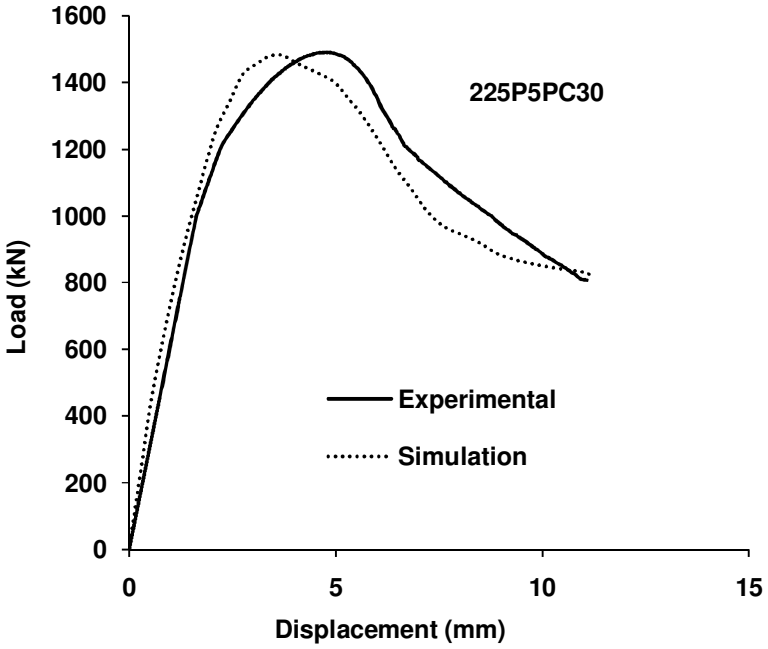

(i)

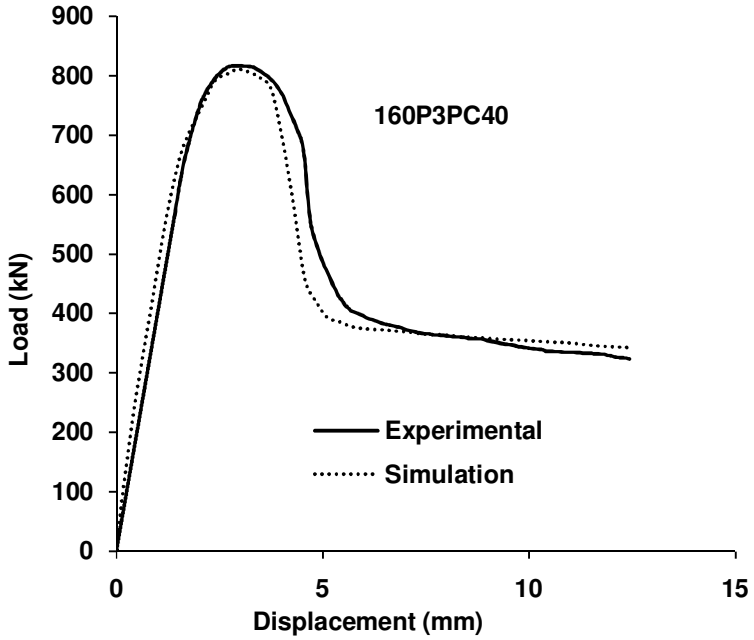

(j)

Fig. 5.7 (a-r) Load-Displacement curves of PCFUT specimens obtained from experiment and simulation

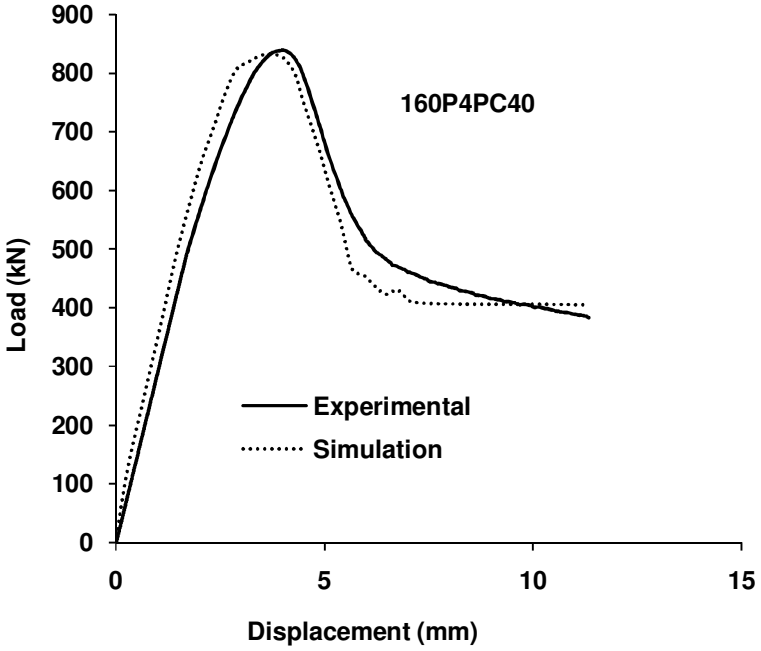

(k)

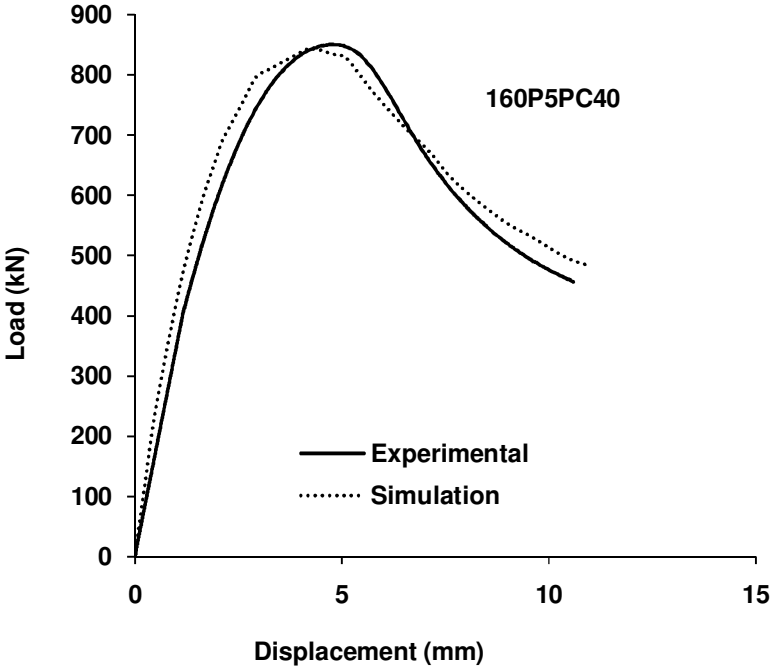

(l)

Fig. 5.7 (a-r) Load-Displacement curves of PCFUT specimens obtained from experiment and simulation

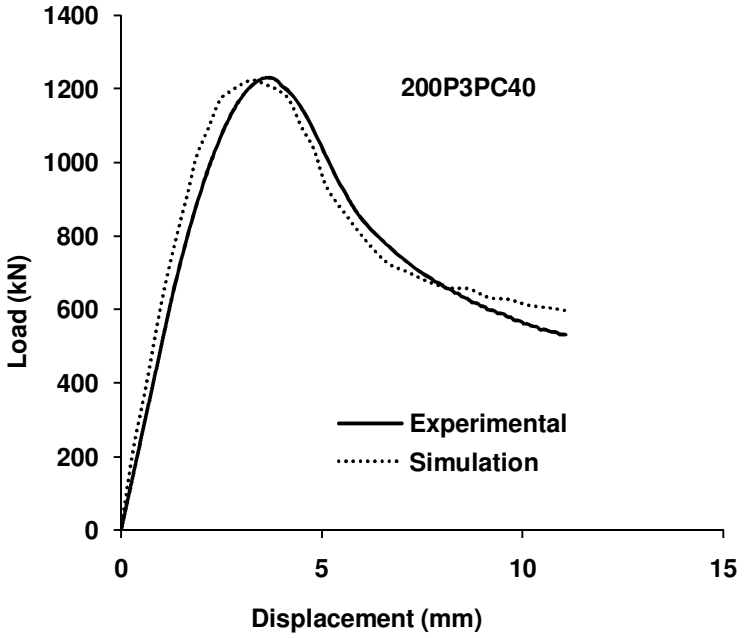

(m)

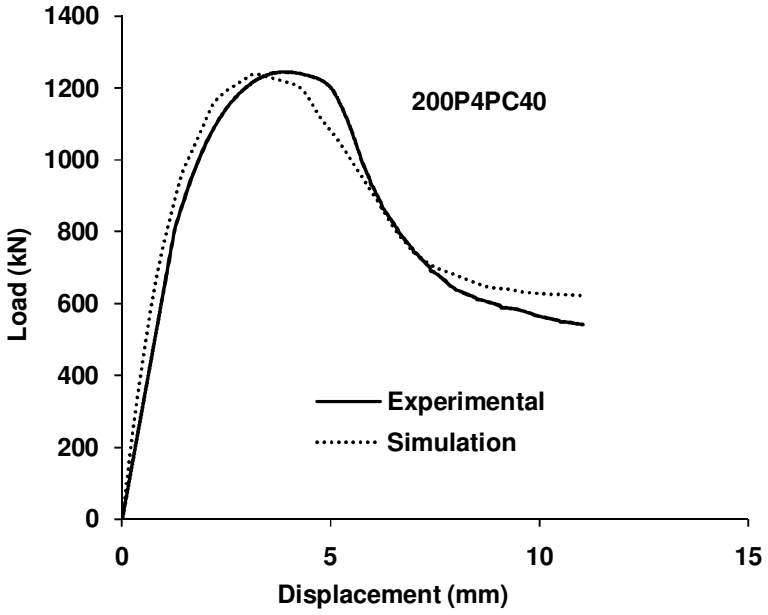

(n)

Fig. 5.7 (a-r) Load-Displacement curves of PCFUT specimens obtained from experiment and simulation

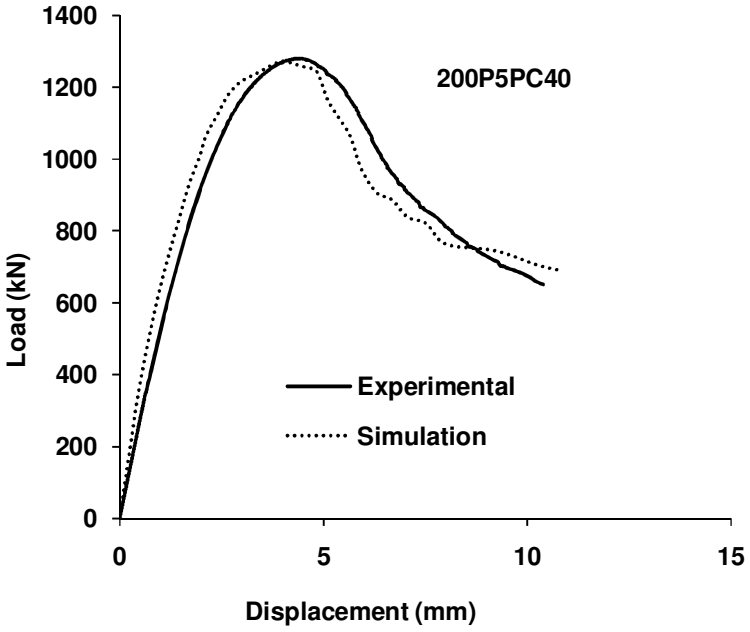

(o)

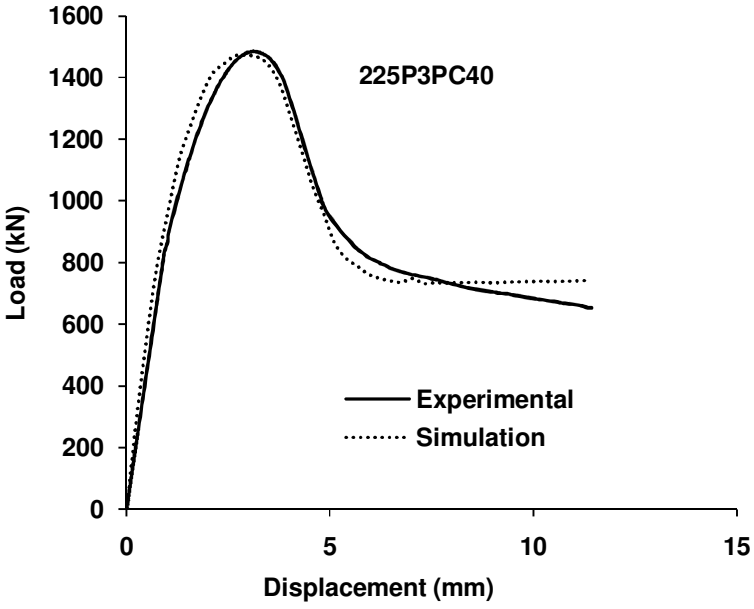

(p)

Fig. 5.7 (a-r) Load-Displacement curves of PCFUT specimens obtained from experiment and simulation

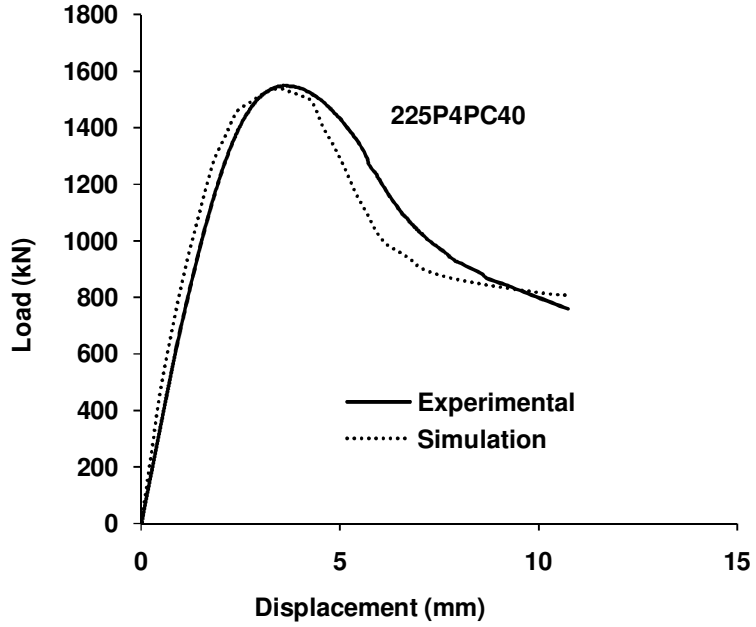

(q)

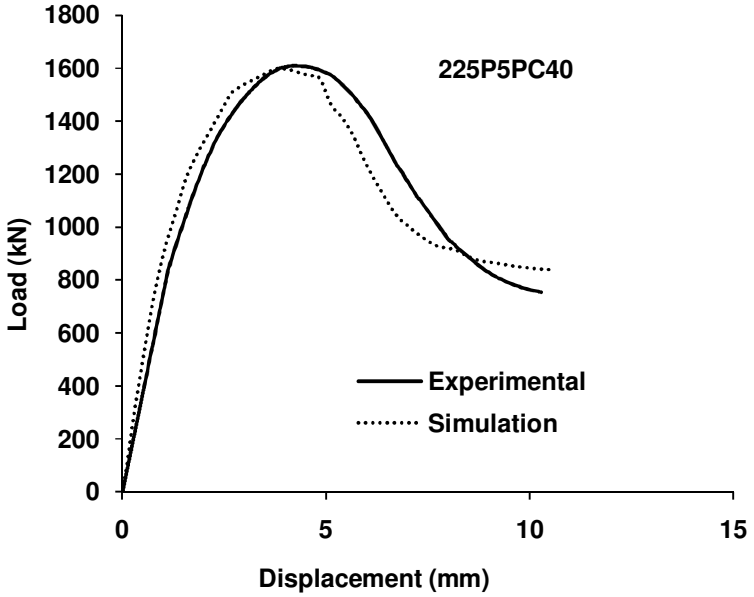

(r)

Fig. 5.7 (a-r) Load-Displacement curves of PCFUT specimens obtained from experiment and simulation

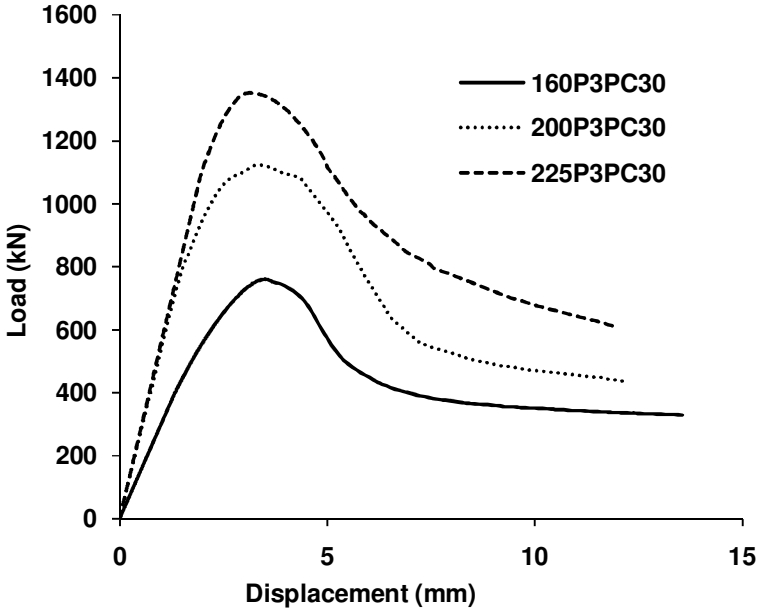

(a)

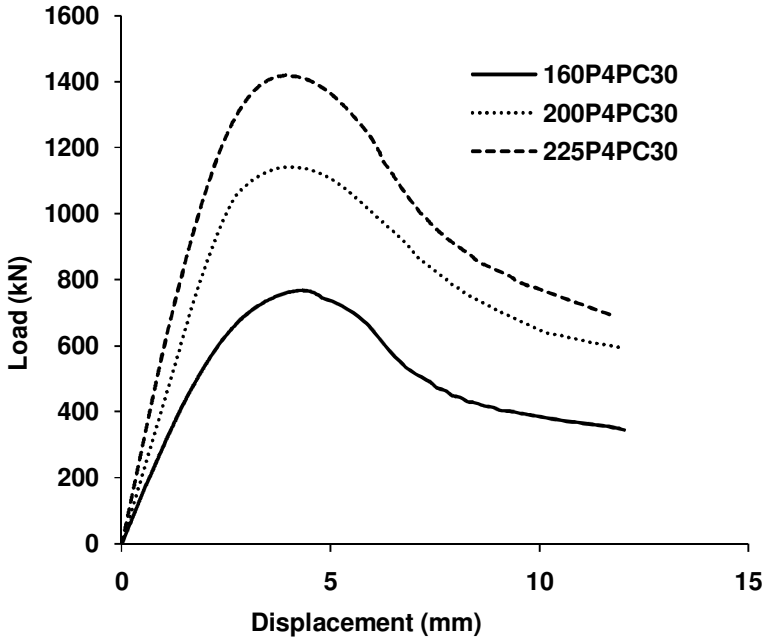

(b)

Fig. 5.8 (a-f) Load-Displacement curves of PCFUT specimens made with tubes of same class and different diameters

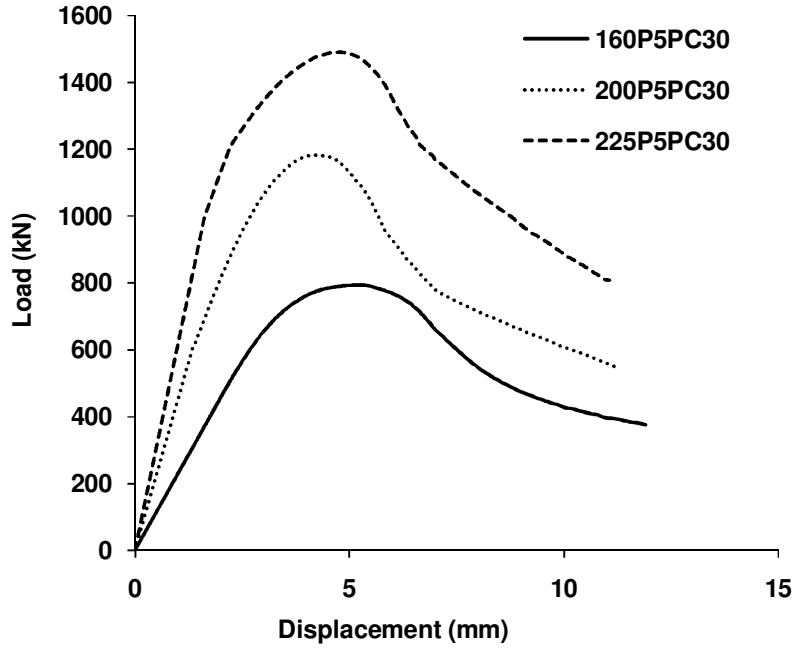

(c)

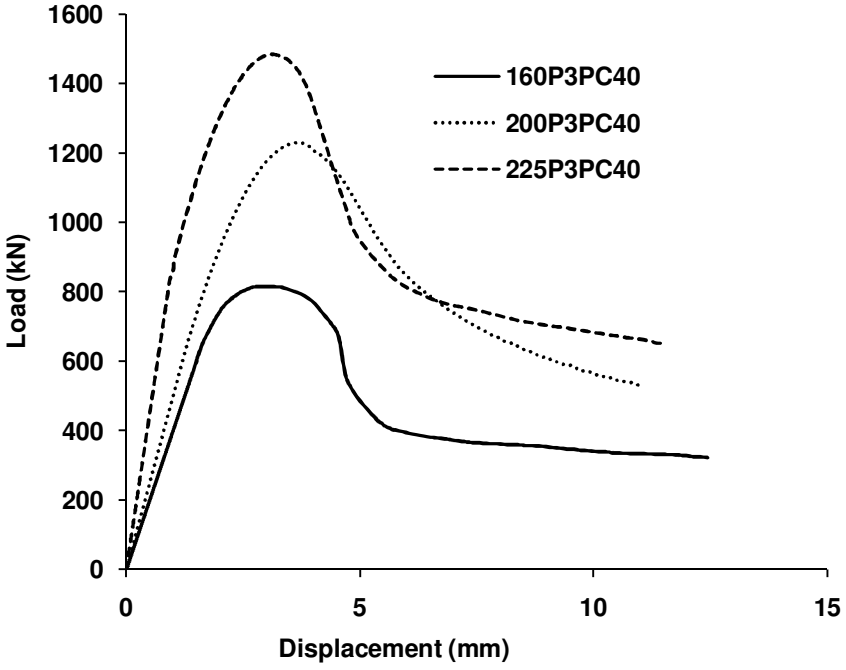

(d)

Fig. 5.8 (a-f) Load-Displacement curves of PCFUT specimens made with tubes of same class and different diameters

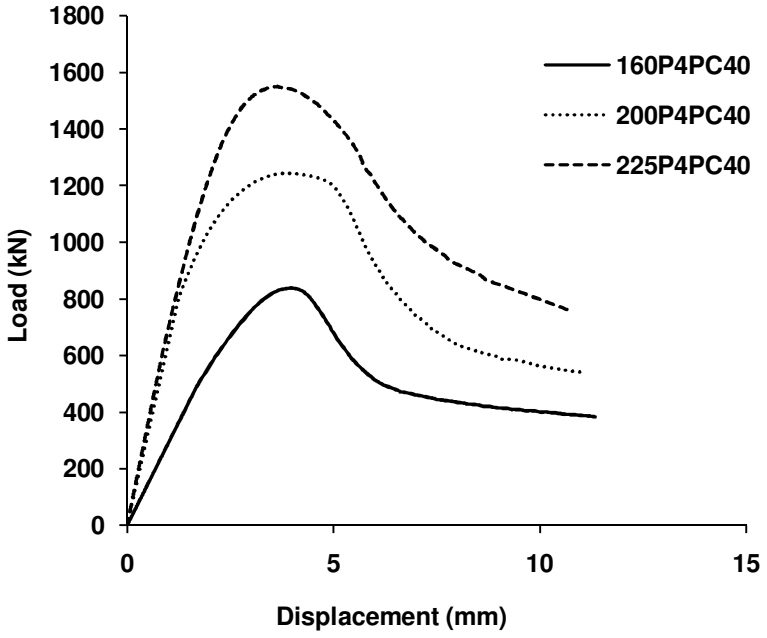

(e)

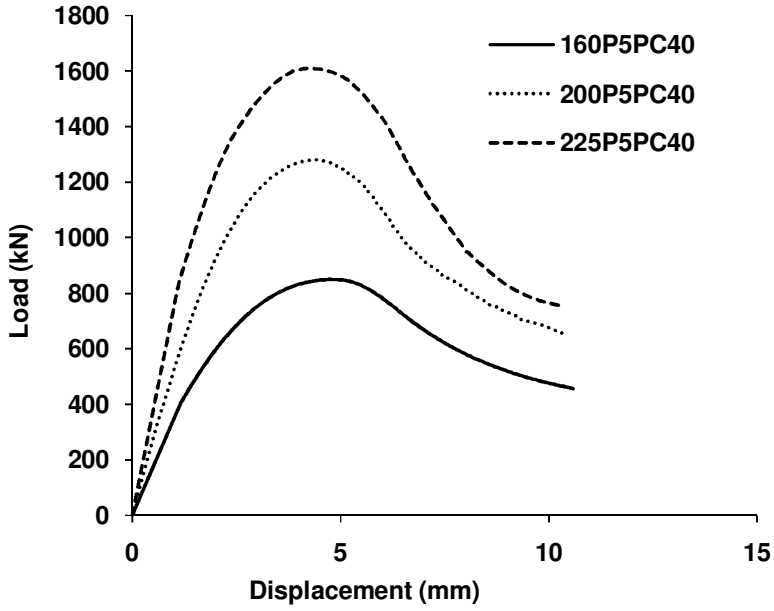

(f)

Fig. 5.8 (a-f) Load-Displacement curves of PCFUT specimens made with tubes of same class and different diameters

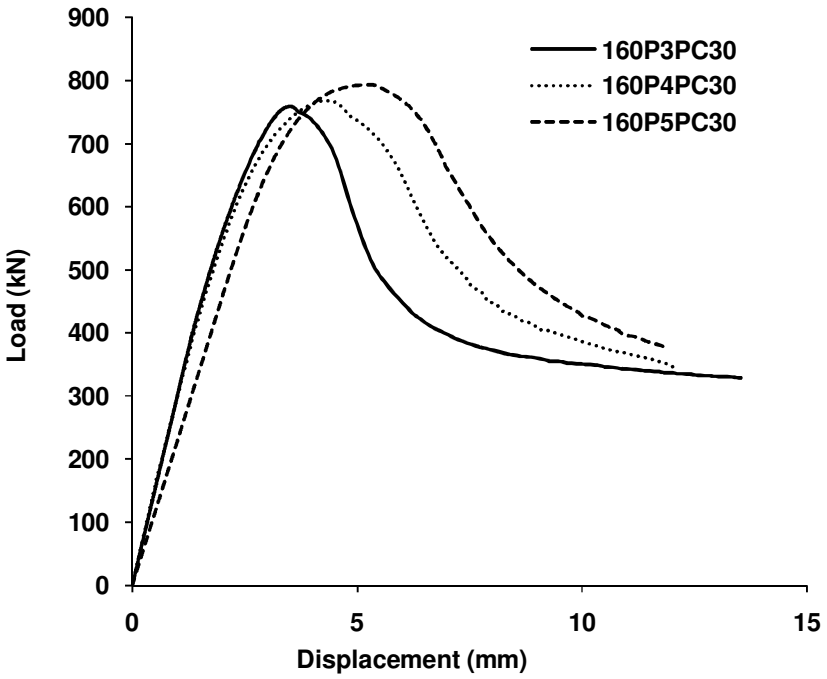

(a)

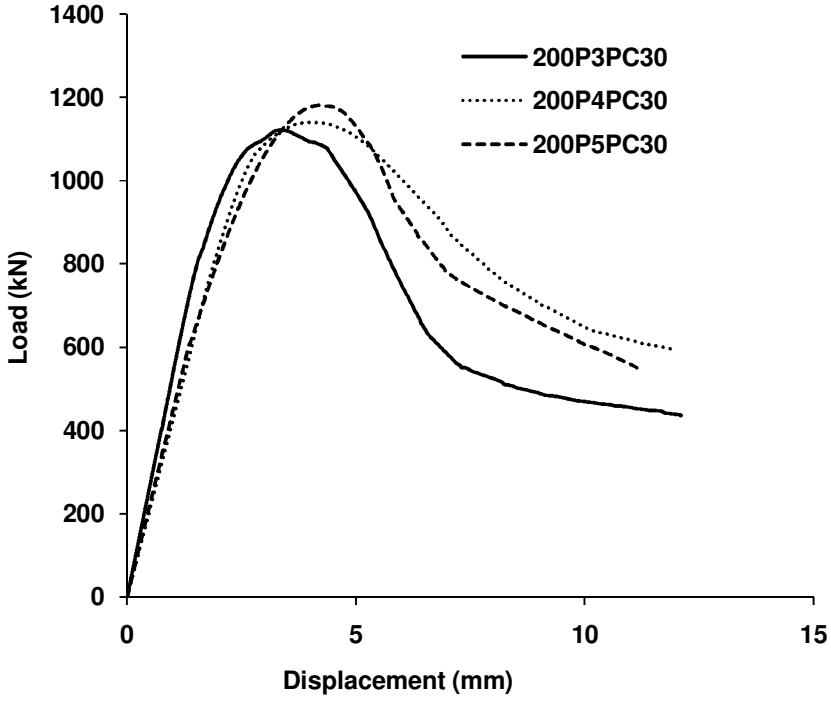

(b)

Fig. 5.9 (a-f) Load-Displacement curves of PCFUT specimens made with tubes of different class and same diameters

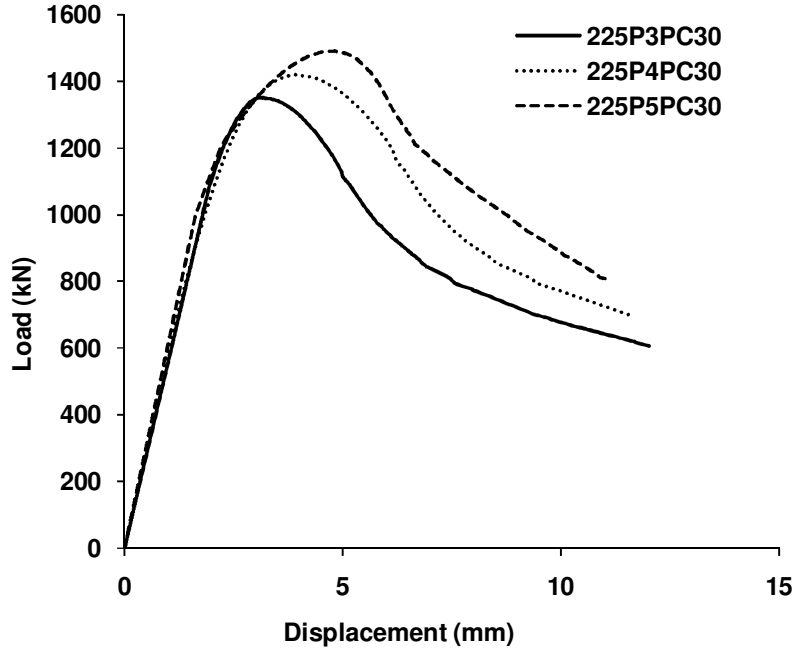

(c)

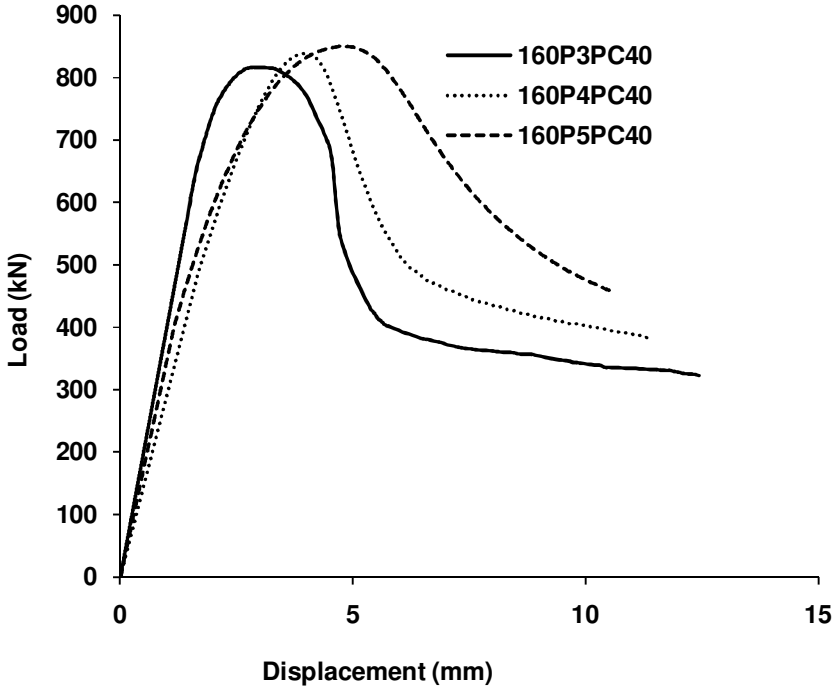

(d)

Fig. 5.9 (a-f) Load-Displacement curves of PCFUT specimens made with tubes of different class and same diameters

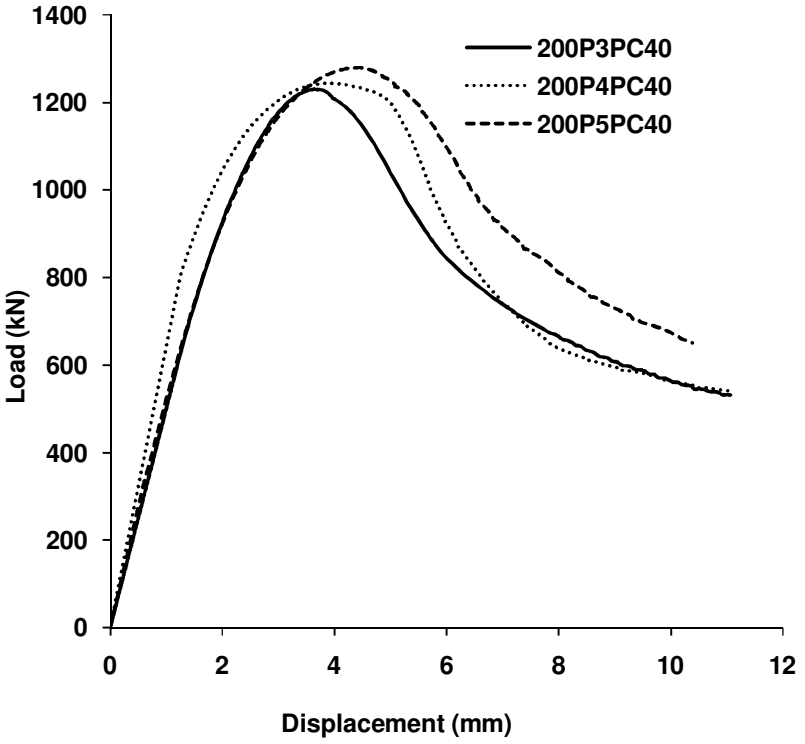

(e)

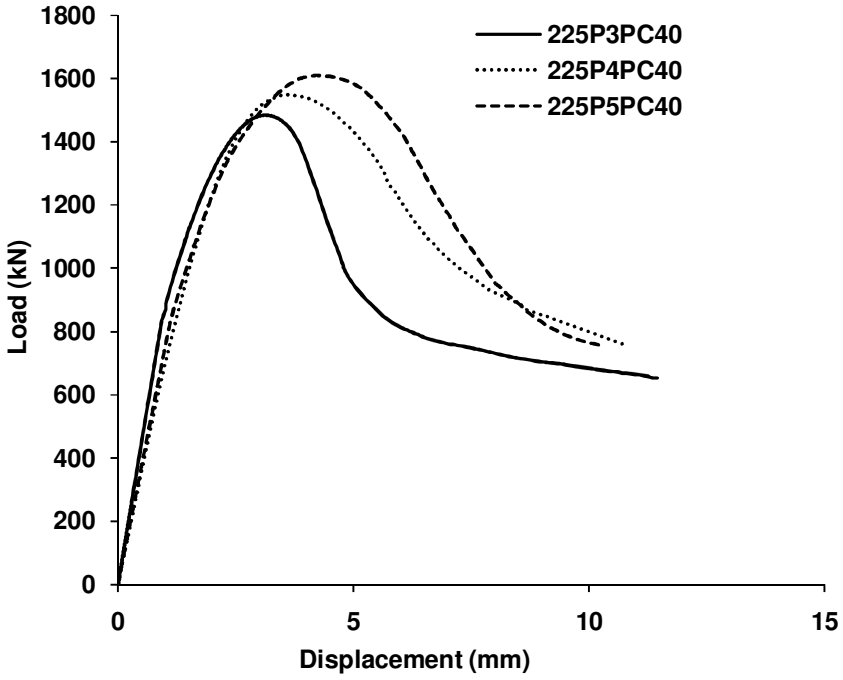

(f)

Fig. 5.9 (a-f) Load-Displacement curves of PCFUT specimens made with tubes of different class and same diameters

Table 5.4 Verification of proposed equation for load capacity of PCFUT

Reference	Specimen	Ultimate Load (kN)		
		Experiment	From Equation $P_u = f_c A_c + 2 f_u A_p$	% variation
(Kurt, 1978)	2(B)	171	160	6.43
	7(C)	309	283	8.41
	9(B)	149	143	4.03
	14(C)	41	39	4.88
	18(C)	251	240	4.38
(Gupta, 2013)	T160M20PC-1	639	601	5.95
	T200M20PC-1	1026	958	6.63
	T140M25PC-1	530	533	0.57
	T140M40PC-1	714	738	3.36

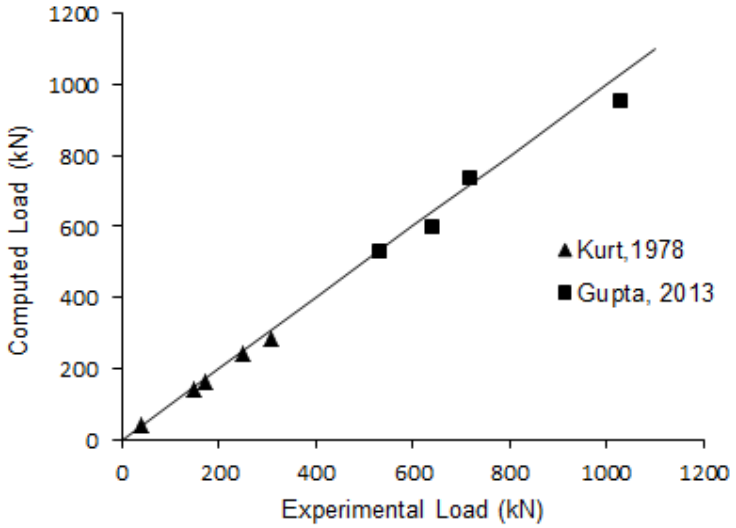

Fig. 5.10 Graphical representation of load capacities to verify proposed equation no. 5.7

5.5.3 Comparison of load carrying capacity obtained from experiments and calculated using different models

In past, few researchers developed confinement model to quantify the effect of confinement on load capacity of concrete. In the beginning of 20th century, Richart et al. (1928) suggested the following relationships between confining strength and unconfined strength of concrete.

$$f_{cc} = f_c + k_1 f_l \tag{2.1}$$

Where k_1 is a constant and equals to 4.1.

Kurt (1978) suggested the value of $k_1 = 3.29$ for PVC pipes.

Saatcioglu & Razvi (1992) gave a relation between k_1 and f_l based on test data of Richart et al. (1928):

$$k_1 = 6.7(f_l)^{-0.17} \tag{5.8}$$

Mander et al. (1988-a) proposed a confinement model for reinforced concrete column. It is most widely used. The relation between confined and unconfined strength of concrete is as given below:

$$f_{cc} = f_c\left(2.254\sqrt{\left(1+7.94\frac{f_l}{f_c}\right)}-2\left(\frac{f_l}{f_c}\right)-1.254\right) \tag{5.8}$$

Table 5.5 presents the comparison of load carrying capacity of specimens obtained from experiments and calculated using different models. It can be seen from Table 5.5 that models proposed by Richart et al. (1928) and Kurt (1978) predict the capacities on conservative side. On the other hand the capacities calculated by Mander et al. (1988-a) and Saatcioglu & Razvi (1992) are on higher side. The graphical representation of load capacities obtained from experiments and calculated by predicted models are depicted in Fig. 5.11.

Table 5.5 Comparison of experimental capacity of PCFUT with capacity calculated using different models

Specimens	Experiment	Richart et al. (1928)	Mander et al. (1988)	Kurt (1978)	Saatcioglu & Razvi (1992)
160P3PC30	759	726	776	709	778
160P4PC30	769	717	773	697	773
160P5PC30	793	717	782	692	777
200P3PC30	1123	1152	1246	1116	1243
200P4PC30	1142	1141	1247	1098	1239
200P5PC30	1182	1128	1235	1084	1226
225P3PC30	1352	1485	1628	1426	1614
225P4PC30	1420	1461	1603	1402	1589
225P5PC30	1491	1448	1588	1389	1575
160P3PC40	816	798	849	781	850
160P4PC40	839	787	844	767	842
160P5PC40	850	784	851	758	844
200P3PC40	1231	1262	1359	1226	1353
200P4PC40	1245	1246	1355	1203	1343
200P5PC40	1280	1231	1342	1187	1328
225P3PC40	1486	1619	1767	1560	1749
225P4PC40	1550	1592	1740	1533	1721
225P5PC40	1610	1578	1724	1520	1705
Mean	-	0.989	1.074	0.955	1.067
Standard Deviation	-	0.054	0.062	0.050	0.060
Coefficient of Variance	-	5.43%	5.80%	5.24%	5.62%

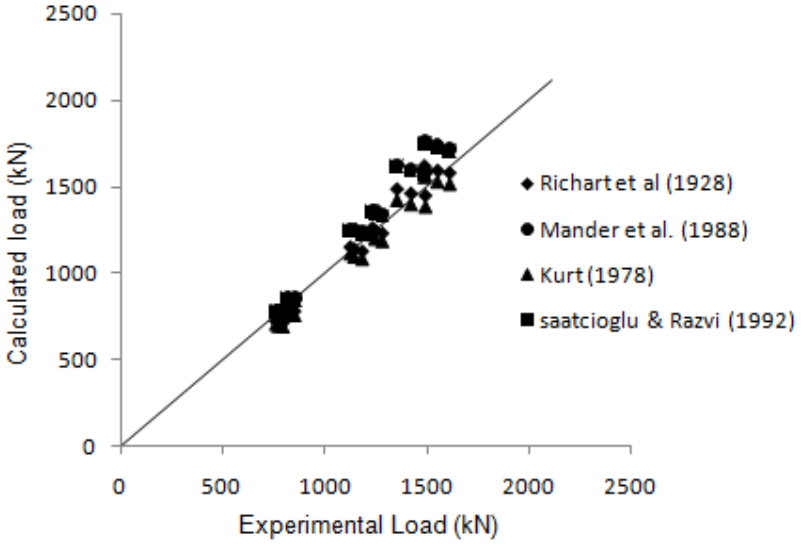

Fig. 5.11 Graphical representation of load capacities of PCFUT specimens obtained from experiments and models

5.5.4 Slenderness effect

To see the slenderness effect on the capacity of CFUT; Finite element analysis was carried out for long and short column, designated as "75P3PC30" with diameter 75 mm. Lengths were kept as 1875 mm for long column and 300 mm for short column by keeping properties of tube and concrete same as in 160P3PC30. For long column, load was applied in two ways; only on concrete core and on concrete and tube both. For short column only concrete core was loaded. Buckling was occurred in long column in both the cases. The values of strains corresponding to failure stress ($k_4 f_{cc}$) were 0.536 % (concrete loaded) and 0.567 % (both loaded) for long column and 4.7 % for short column (Table 5.3). The deformed shape of and load-displacement curves for the specimen "75P3PC30" are shown in Fig. 5.12(a) and 5.12(b).

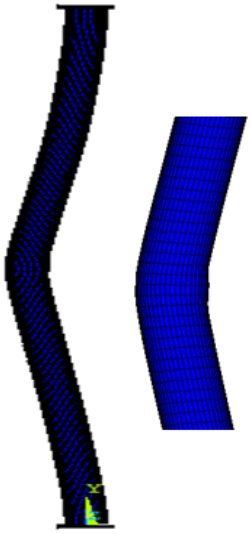

Fig. 5.12(a) Deformed shapes of long PCFUT column

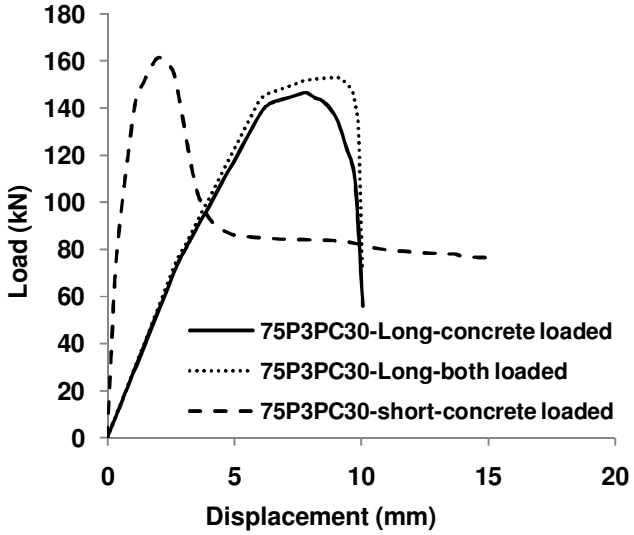

Fig. 5.12(b) Load-displacement curves for long and short PCFUT columns

5.5.5 Mode of failure

The failure patterns of confined concrete specimens depend on the constraining factor (α) given by Wang and Yang (2010), Gupta (2013) and confinement ratio (β) given by Ansari & Li (1998). The constraining factor is defined as:

$$\alpha = A_p f_u / A_c f_c$$

Where A_p and f_u are the cross-sectional area and tensile strength of UPVC tube respectively; A_c and f_{ck} are the cross-sectional area and compressive strength of concrete cylinder respectively. The confinement ratio is defined as:

$$\beta = (f_l / f_c)$$

Both the parameters are calculated and given in Table 5.3. It was found that the value of β is twice the value of α. In the present case the value of α is less than 0.2 and β is less than 0.1 for all specimens. The failure pattern was observed as shear failure with slight bulging of tube. Wang and Yang (2010) and Gupta (2013) also found that specimens failed due to shear when the value of α was less than 0.204 and bulging when value of α was more than 0.204. The specimen no. 114 (Richart el al., 1928) having the value of β equals to 0.07 showed the shear failure. Sfer et al. (2002) observed the failure due to several vertical and inclined cracks when confining pressure was less than 4.5 MPa (or $\beta < 0.15$). The deformed shapes obtained from experiments and simulations are shown in Fig. 5.13. The typical deformed shape obtained from experiment is verified by the typical deformed shapes picked up from literature (Fig. 5.14).

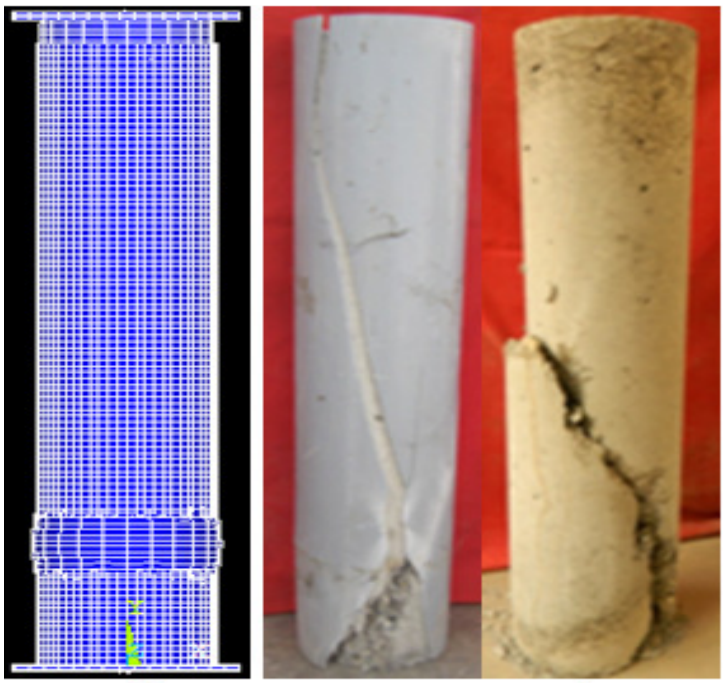

160P3PC40

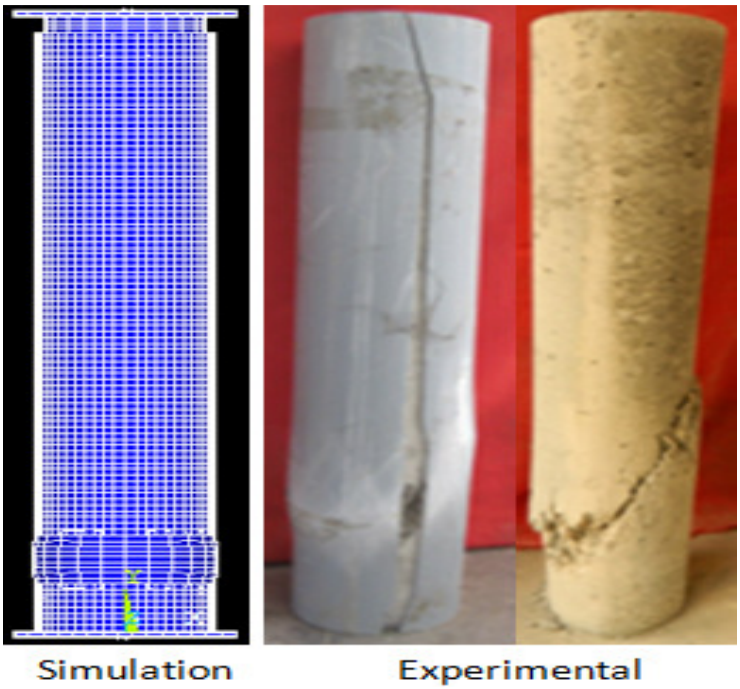

160P5PC40

Fig. 5.13 Deformed shapes of PCFUT specimens

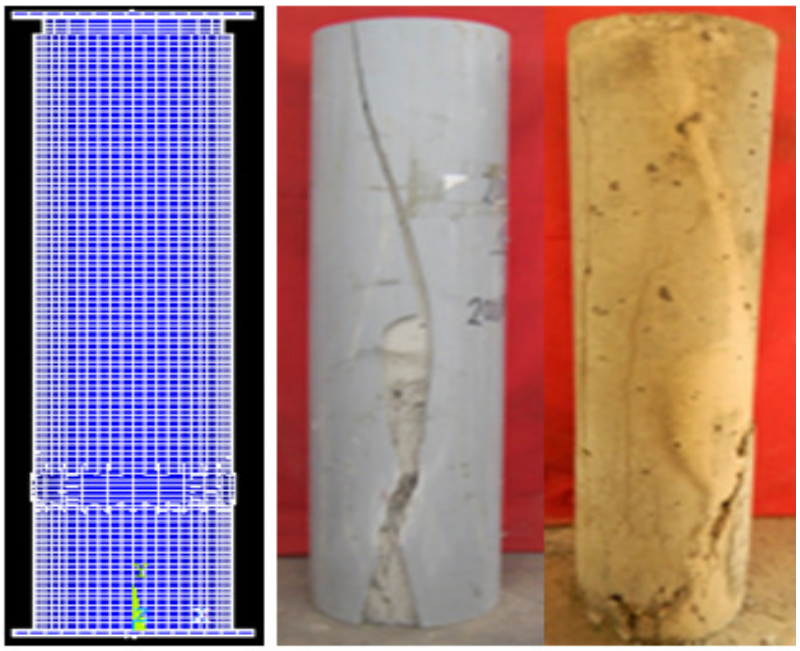

200P4PC30

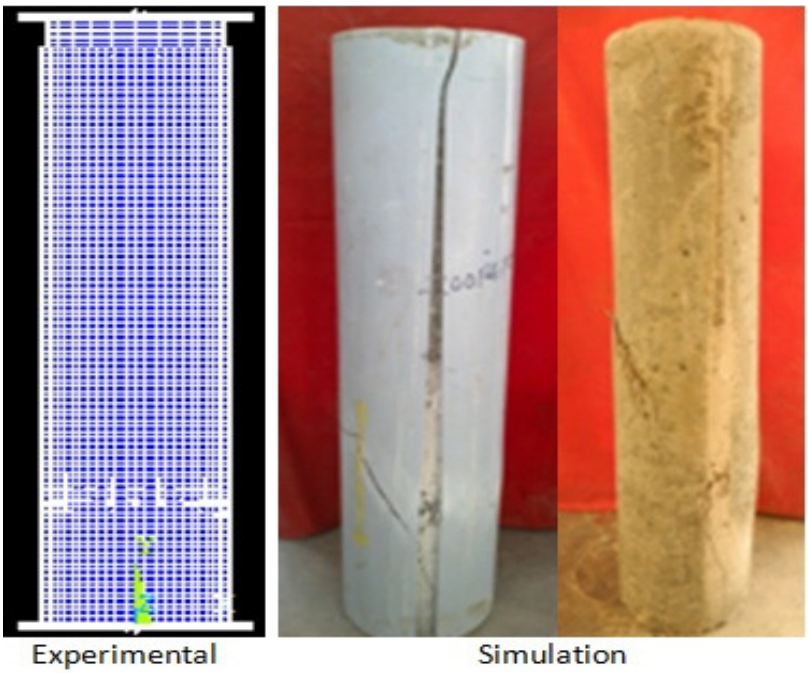

200P4PC40

Fig. 5.13 Deformed shapes of specimens

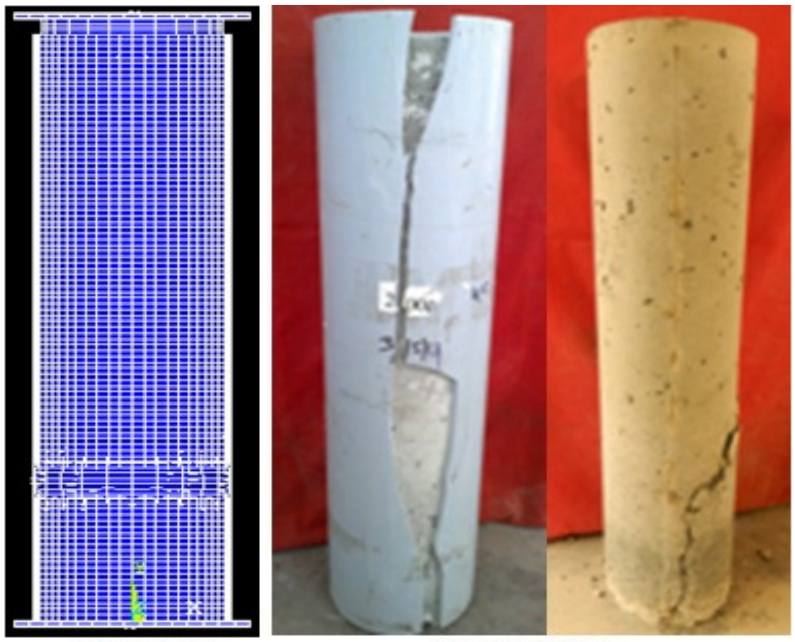

Simulation Experimental

200P5PC40

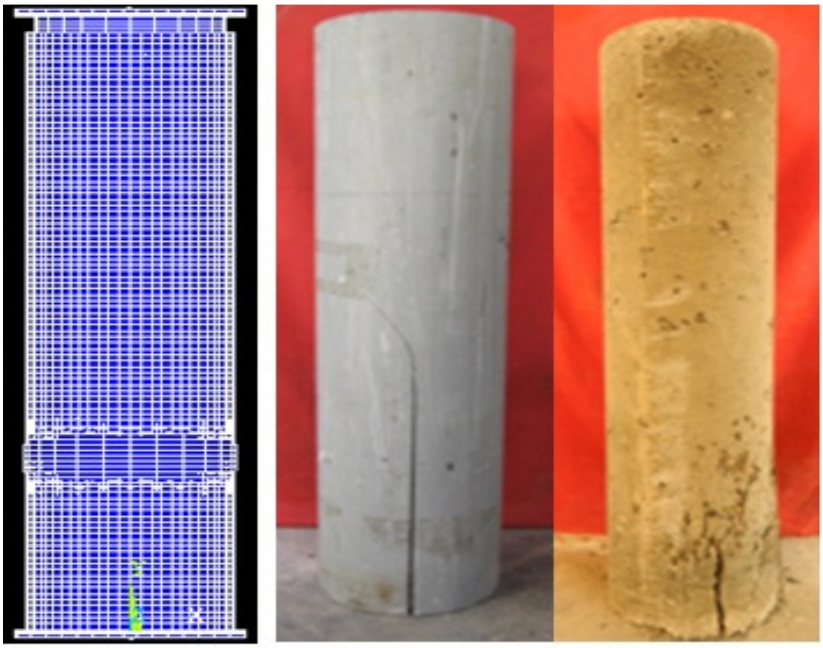

Simulation Experimental

225P3PC30

Fig. 5.13 Deformed shapes of specimens

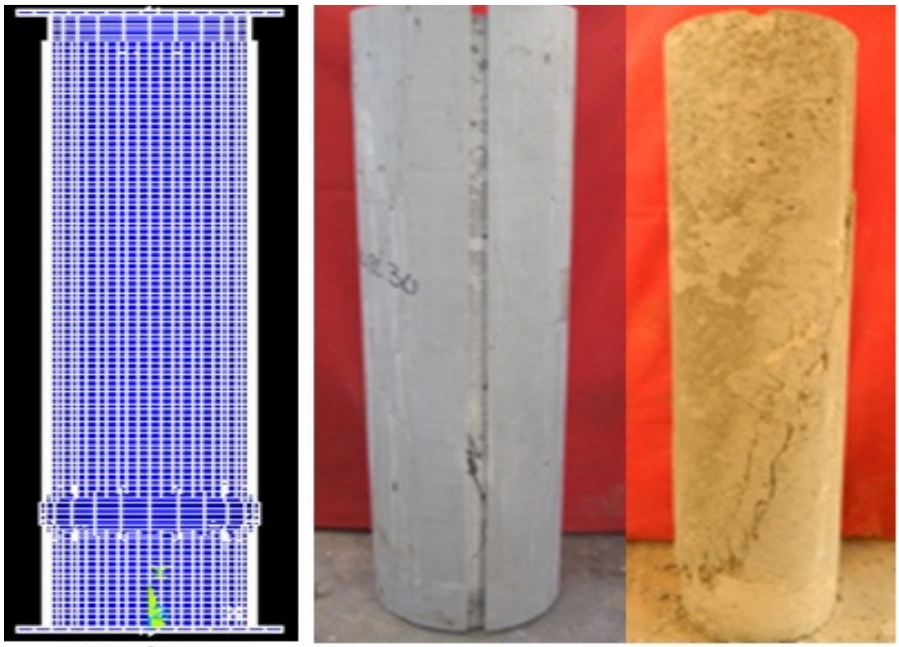

225P4PC30

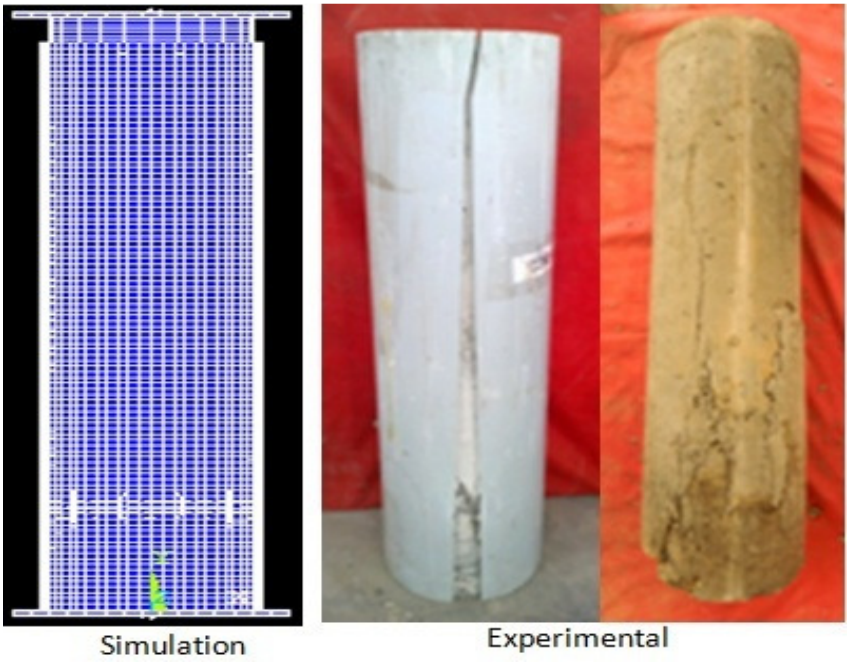

225P5PC40

Fig. 5.13 Deformed shapes of specimens

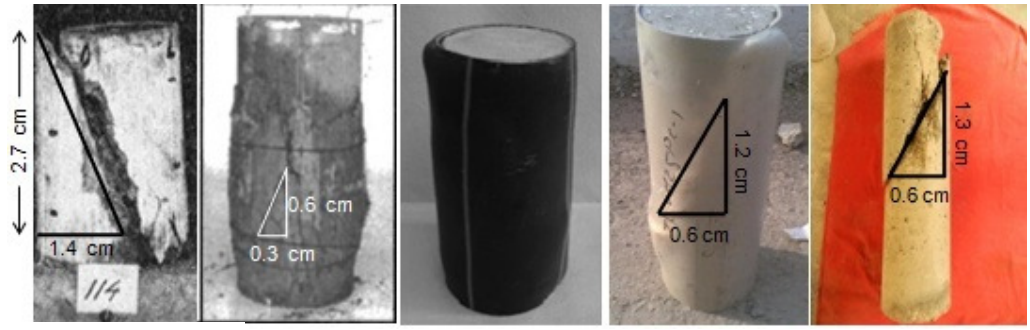

114
(β = 0.07)
($\theta_{exp} = 62.5^0$)
($\theta_{cal} = 63.2^0$)
(Richart et al.,1928)

Specimen 1
(β = 0.05)
($\theta_{exp} = 63.4^0$)
($\theta_{cal} = 64^0$)
(Sfer et al., 2002)

(β< 0.1
(Wang and Yang, 2010)

T140M25
(β = 0.085)
($\theta_{exp} = 63.4^0$)
($\theta_{cal} = 64.3^0$)
(Gupta, 2013)

225P5PC30
(β = 0.062)
($\theta_{exp} = 65^0$)
($\theta_{cal} = 64.2^0$)

Fig. 5.14 Verification of mode of failure and angle of failure plane

5.5.6 Angle of failure plane

The angle of failure plane and load capacity and of CFUT specimens are obtained from Mohr-Coulomb Theory. The angle of failure plane is calculated at shear failure by equating the shear strength of concrete and shear stress develop in concrete due to external load. Load capacity was calculated by axial stress develop at failure. The results obtained from analysis and experiments are given in the Table 5.6. The angle of failure plane for tested specimen and specimens taken from literature is shown in Fig. 5.14. The angle of failure plane for tested specimens measured with horizontal axis was found between 63^0 and 65^0 (Fig. 5.15). The variation in the angle of failure plane calculated from Mohr-Coulomb criterion and experiments is observed from 0 to 2%. The load capacities calculated using Mohr-Coulomb theory (P_{cal}) and experiments (P_{exp}) vary from 0 to 8 %. The angles of failure plane and load capacities of specimens taken from literature are calculated using Mohr-Coulomb theory (Table 5.6). It may be seen from Table 5.6 that the angle of failure plane varies with confining pressure. Its value increases with increase in confinement. It may be concluded that by increasing the confining pressure, angle of failure may be increased to avoid the shear failure. A graph between shear strength/applied shear stress and angle of failure plane is plotted to see the influence of confining pressure on the shear strength of concrete and angle of failure plane (Fig. 5.16). It can be seen from Fig. 5.16 that as the applied axial stress increases, shear stress in the concrete increases while shear strength of concrete decreases. At a particular angle of failure plane shear strength of concrete and shear stress developed becomes equals and cracks initiates. To get understand the effect of confining pressure on angle of failure through graphical representation, Mohr circles have been drawn (Fig. 5.17 and Fig. 5.18). It can be seen from Fig. 5.17(a-c) that

angle of failure plane is varying from 63^0 to 64.5^0 depending upon confining pressure. Mohr circles (as shown in Fig. 5.18) are drawn by taking the hypothetical value of confining pressure from 1MPa to 6MPa to get better understanding of the effect of confining pressure on angle of failure plane. The angle of failure plane varies from 62.8^0 to 66.9^0 when confining pressure varies from 1MPa to 6MPa (Table 5.7).

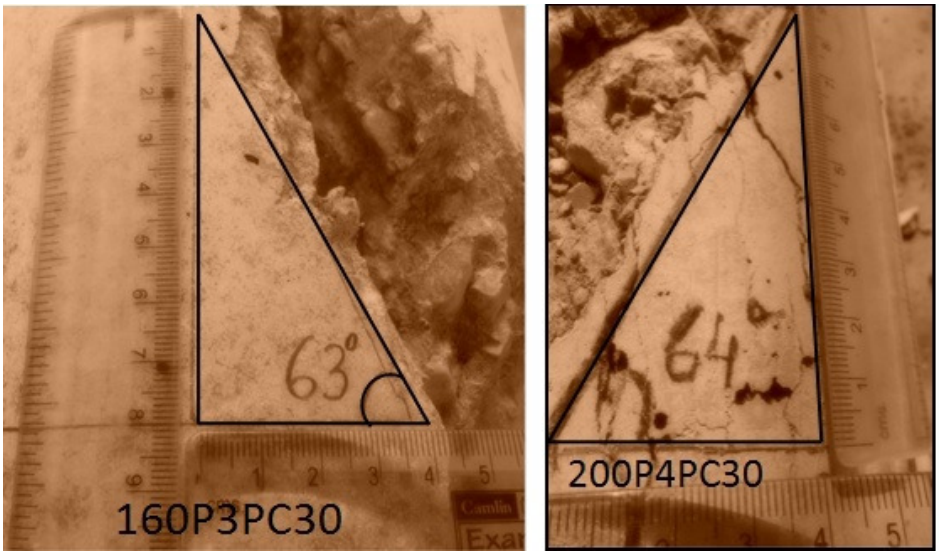

Fig. 5.15 Measurement of angle of failure plane for typical PCFUT specimens

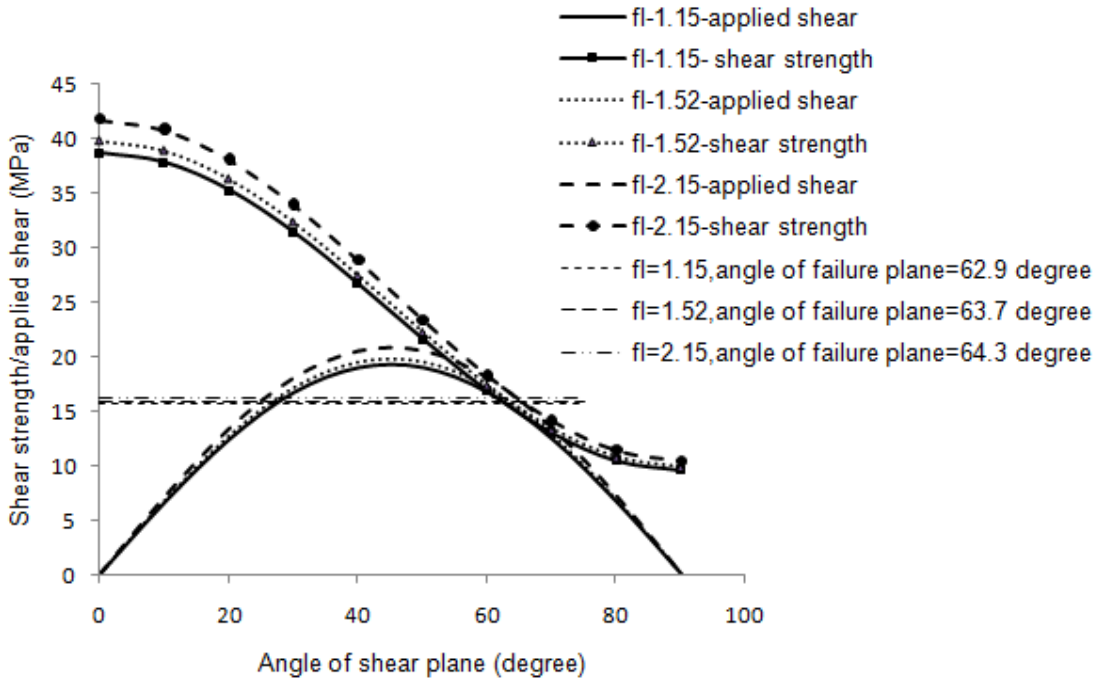

Fig. 5.16 Graph between shear strength/applied shear stress and angle of failure plane

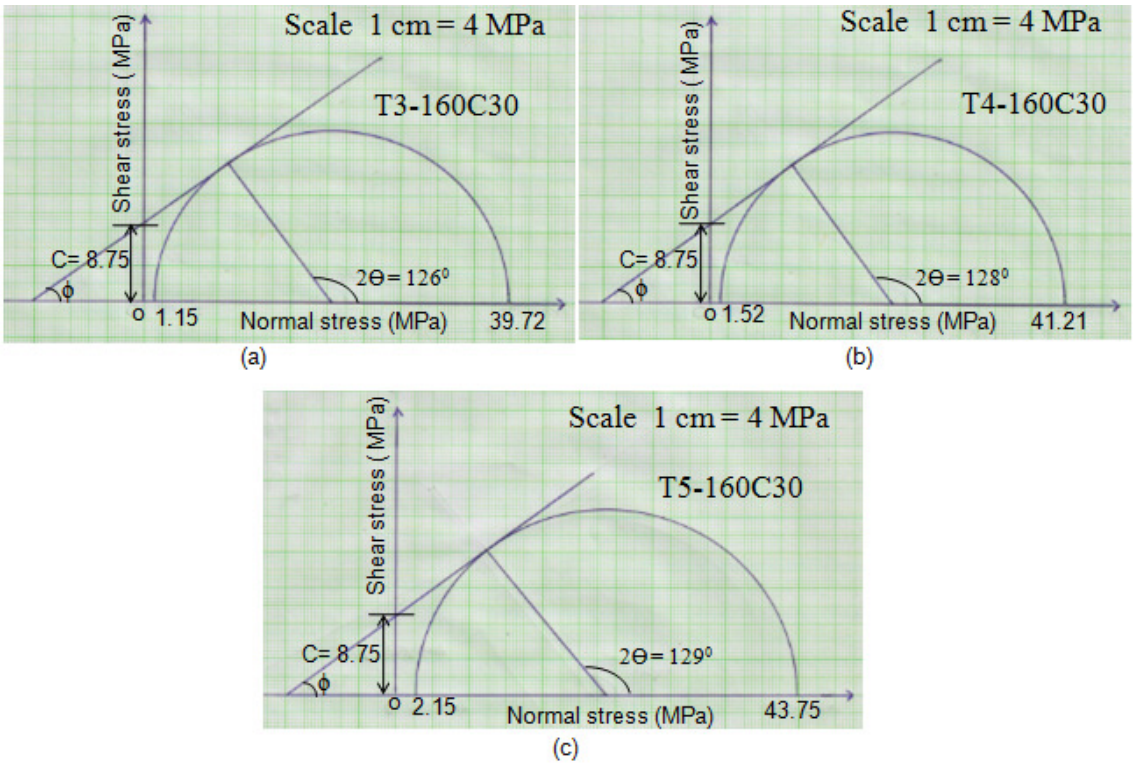

Fig. 5.17 Mohr circle to calculate angle of failure plane

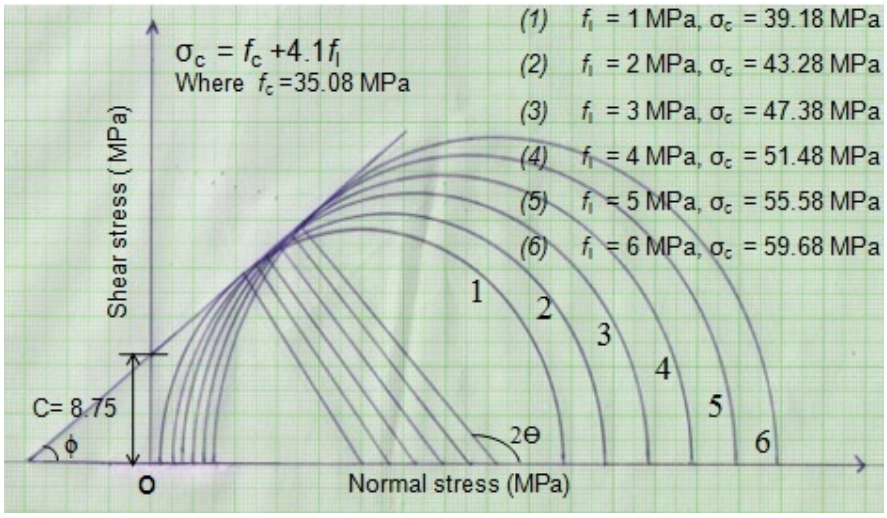

Fig. 5.18 Mohr circles to understand variation of angle of failure plane with confining pressure

Table 5.6 Calculation of angle of failure and load capacity by Mohr-Coulomb theory

Specimen	f_l (MPa)	f_c (MPa)	β	c (MPa)	Angle of failure plane (θ) in degree			τ_c (MPa)	Load capacity		
					θ_{cal}	θ_{exp}	% Vari-ation		P_{cal} (kN)	P_{exp} (kN)	% Vari-ation
160P3PC30	1.15	35.08	0.033	8.75	62.9	63	0.16	15.66	722	759	4.82
160P4PC30	1.52	35.08	0.043	8.75	63.7	64	0.47	15.78	723	769	6.00
160P5PC30	2.15	35.08	0.061	8.75	64.3	65	1.08	16.27	734	793	7.45
200P3PC30	1.35	35.08	0.038	8.75	62.9	63	0.16	15.90	1124	1123	0.10
200P4PC30	1.99	35.08	0.057	8.75	63.7	64	0.47	16.34	1137	1142	0.41
200P5PC30	2.25	35.08	0.064	8.75	64.3	65	1.08	16.39	1141	1182	3.47
225P3PC30	1.72	35.08	0.049	8.75	62.8	63	0.32	16.40	1420	1352	5.02
225P4PC30	2.0	35.08	0.057	8.75	63.7	64	0.47	16.35	1429	1420	0.64
225P5PC30	2.17	35.08	0.062	8.75	64.2	65	1.23	16.34	1440	1491	3.41
160P3PC40	1.15	39.05	0.029	9.72	62.8	63	0.32	17.28	793	816	2.80
160P4PC40	1.52	39.05	0.039	9.72	63.6	64	0.62	17.37	791	839	5.71
160P5PC40	2.15	39.05	0.055	9.72	64.2	65	1.23	17.84	799	850	5.98
200P3PC40	1.35	39.05	0.035	9.72	62.9	63	0.16	17.48	1232	1231	0.08
200P4PC40	1.99	39.05	0.051	9.72	63.7	64	0.47	17.89	1240	1245	0.40
200P5PC40	2.25	39.05	0.058	9.72	64.3	65	1.08	17.91	1242	1280	3.01
225P3PC40	1.72	39.05	0.044	9.72	62.8	63	0.32	17.98	1551	1486	4.40
225P4PC40	2.0	39.05	0.051	9.72	63.7	64	0.47	17.90	1558	1550	0.51
225P5PC40	2.17	39.05	0.056	9.72	64.4	65	0.92	17.77	1696	1610	5.34
114 Richart et al. (1928)	1.24	17.76	0.07	4.42	63.2	62.5	1.12	8.65	178	154	15.58
Specimen 1 Sfer et al. (2002)	1.5	32.6	0.046	8.12	64.0	63.4	0.95	14.63	682	804	15.17
T140M25 Gupta (2013)	2.43	28.6	0.085	7.12	64.3	65	1.08	14.12	593	530	11.89

Table 5.7 Angle of failure plane corresponding to confining pressure using Mohr circle

f_l (MPa)	f_c (MPa)	σ_c	f_l/f_c	c	θ_{cal}
1	35.08	39.18	0.029	8.75	62.8
2	35.08	43.28	0.057	8.75	63.9
3	35.08	47.38	0.086	8.75	65
4	35.08	51.48	0.114	8.75	65.5
5	35.08	55.58	0.143	8.75	66.2
6	35.08	59.68	0.171	8.75	66.9
Note: $(\sigma_c = f_c + 4.1 f_l)$					

5.6 CONCLUSIONS

The present study provides a new type of composite column, which can be obtained by filling concrete in unplasticised poly vinyl chloride (UPVC) tube. On the basis of results obtained, the following points can be concluded.

1. A stress-strain model for concrete confined with UPVC tube is proposed. This model is obtained by modifying the stress-strain model of concrete confined with steel tube. The post peak curve of concrete confined with steel tube is modified by introducing the parameters k_3 and k_4. The Material degradation parameter (k_3) depends on the value of D/t and decreases with the increase of D/t. The parameter meter k_4 depends upon value of k_3 and equals to 0.8 k_3. An empirical relation is proposed to calculate the value of k_3.

2. The failure pattern of short specimens depends upon the constraining parameter (α) and confinement ratio (β). Failure of all specimens leads by development of shear crack and macro cracks with slight bulging.

3. An equation to calculate the load carrying capacity of concrete filled UPVC tubular columns is proposed. So this type of composite column may be easily designed using developed equation.

4. Mohr-Coulomb failure criterion is used to understand the failure mechanism of confined concrete. Inclination of failure plane for different confining pressure is

calculated. Angle of failure plane with horizontal axis varies from 63^0 to 65^0 for all CFUT specimens. Inclination of failure plane increases with increasing confining pressure. Mohr circles are also drawn to get understand the variation of angle of failure plane with confining pressure. Angles of failure plane measured from Mohr circles are nearly equal as calculated using equation.

5. The post peak behavior of load-compression curve depends upon the confining pressure of tube and compressive strength of concrete. The absolute value of slope of curve increases with increase in concrete strength and decreases with increase in confining pressure.

6. The strain at failure for tested short specimens varies from 1.28 % to 1.69 %. It decreases with increases of compressive strength of concrete for the same class of tubes.

CHAPTER-6

CONFINEMENT IN REINFORCED CONCRETE COLUMNS

6.1 GENERAL

UPVC tube filled with plain concrete is not enough to provide sufficient strength to the column, since the strength increment due to confinement offered by UPVC tube is only 5-10 MPa. Therefore it necessary to opt reinforced concrete filled UPVC tubular column to get higher required strength. Reinforcement is also required to provide connection between RCC beam and concrete filled UPVC tubular column. Reinforcement in column enhances the toughness also. In this chapter Finite element modelling for RCC was carried out and obtained the condition for the contribution of confinement through transverse reinforcement. All the RCC specimens are obtained from reinforced concrete filled UPVC tubular specimens by removing their tubes. Fig. 6.1 shows the tree for study program of reinforced concrete column.

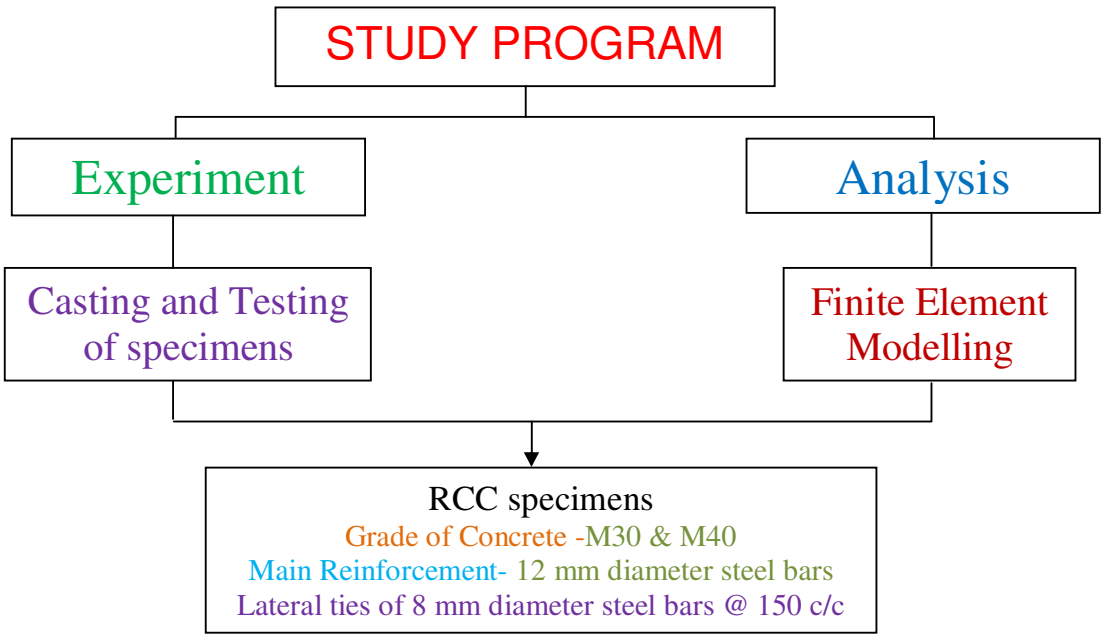

Fig. 6.1 Tree for study program of reinforced concrete column

6.2 CASTING AND TESTING OF SPECIMENS

For this study, a total 18 bare RCC column specimens were obtained from RCFUT specimens by removing their UPVC tube. For the casting of RCFUT specimens, the UPVC pipes of class 3, 4 and 5 with nominal pressure of 0.6, 0.8 and 1.0 MPa having diameters of 160 mm, 200 mm and 225 mm were taken. The pipes were cut and levelled to get the tube of length 800 mm. M30 and M40 grades of concrete were designed as per IS: 10262-2009 to fill the tubes. 6 bars of 12 mm diameter were used as main reinforcement and bars of 8 mm diameter were used for lateral ties spaced @ 150 mm c/c for transverse reinforcement. 12 mm clear cover was provided to the lateral ties. All the specimens were tested for axial loading. Table 6.1 shows the geometrical and material properties of RCFUT and bare RCCC specimens.

Table 6.1 Geometrical and material properties of bare RCC specimens

Specimen	(D) mm	f_c (MPa)	f_y (MPa)	Longitudinal steel (%)	Ratio of area of longitudinal steel to area of confined concrete core (ρ_{cc})
160P3BRC30	152	35.08	500	3.74	0.0600
160P4BRC30	149	35.08	500	3.89	0.0630
160P5BRC30	146	35.08	500	4.05	0.0660
200P3BRC30	188	35.08	500	2.44	0.0355
200P4BRC30	184	35.08	500	2.55	0.0373
200P5BRC30	182	35.08	500	2.61	0.0384
225P3BRC30	208	35.08	500	2.00	0.0279
225P4BRC30	206	35.08	500	2.04	0.0285
225P5BRC30	204	35.08	500	2.08	0.0292
160P3BRC40	152	39.05	500	3.74	0.0600
160P4BRC40	149	39.05	500	3.89	0.0630
160P5BRC40	146	39.05	500	4.05	0.0660
200P3BRC40	188	39.05	500	2.44	0.0355
200P4BRC40	184	39.05	500	2.55	0.0373
200P5BRC40	182	39.05	500	2.61	0.0384
225P3BRC40	208	39.05	500	2.00	0.0279
225P4BRC40	206	39.05	500	2.04	0.0285
225P5BRC40	204	39.05	500	2.08	0.0292

6.3 NUMERICAL MODELING AND SIMULATION

6.3.1 Finite element model

A three dimensional Finite element model was developed using ANSYS software to simulate the reinforced concrete column subjected to axial compression. Fig. 6.2 shows a typical Finite element model adopted for modeling of reinforced concrete column. To model the concrete core, a three dimensional eight node solid element 'SOLID 65' was used. This element has three degree of freedom at each node. Mesh size for concrete core was chosen from 5 mm to 10 mm. Two rigid plates were modeled to simulate rigid cross heads of machine. The main reinforcement and lateral ties were modeled by the link element 'LINK8'. It is a uniaxial tension-compression element with three degree of freedom at each node. It is capable of plastic deformation. Three techniques are available to model the steel reinforcement for reinforced concrete (Wolanski, 2004): the discrete model, the embedded model, and smeared model (Fig. 6.3). In the discrete model, the bar element or beam element used as a reinforcement is connected to concrete mesh nodes. Therefore, the concrete and reinforcement mesh share the same nodes and concrete occupies the same regions occupied by the reinforcement. The embedded model overcomes the concrete mesh restriction because the stiffness of reinforcing steel is evaluated separately from concrete element. This model keeps the reinforcing steel displacements compatible with the surrounding concrete elements. This model is useful when reinforcement is complex. However, due to increase in number of node, the run time increases. In the smeared model, reinforcement is assumed to be spread uniformly throughout the concrete element in a definite region of Finite element mesh. This model is useful for the large structures where reinforcement does not significantly contribute to the overall response of structure. In the present case, the discrete model was used.

Load was applied to the column through the top loading plate. In the compression test, direct contact was exist between the bottom end plate and bottom surface of column; therefore a contact available in ANSYS was used to simulate the interaction between rigid plate and column end surface. The contact was defined as a surface to surface contact. Different friction factors (0.1 to 0.4) were taken for the contact surface and it was found that friction factor of 0.2 was suitable to achieve a quick convergence. In Finite element model, the lower rigid plate contacting the bottom of column was fixed in all six directions by reference node. The upper rigid plate at the top of the column was modeled fixed in five directions and only allowed movement in column axis at reference node. The load was applied as static uniform displacement at upper rigid plate through the reference node at the center of rigid plate

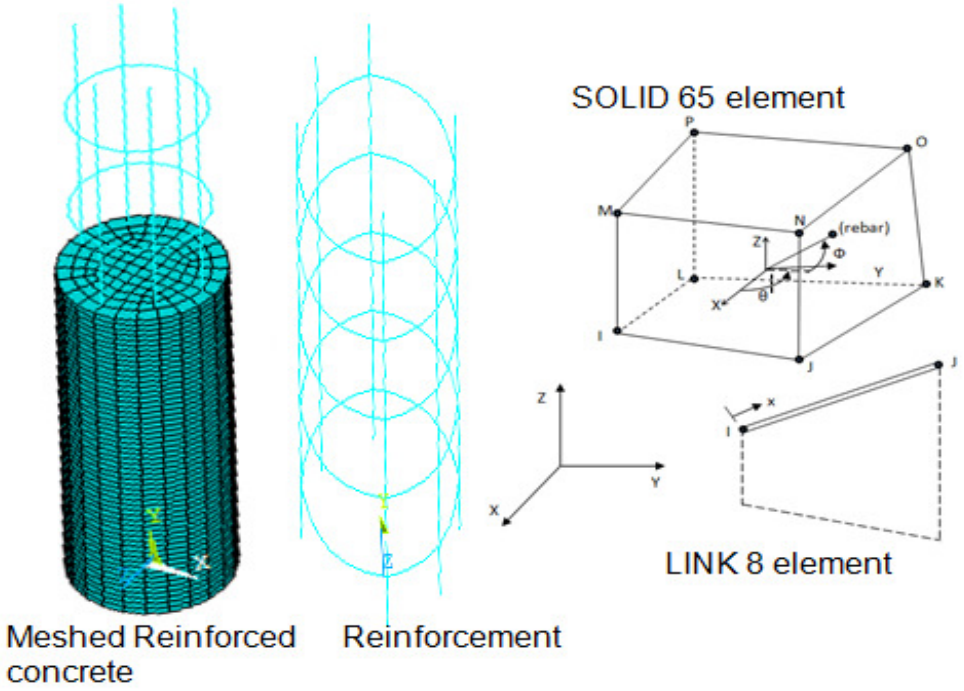

Fig. 6.2 Typical details of Finite element model for reinforced concrete column

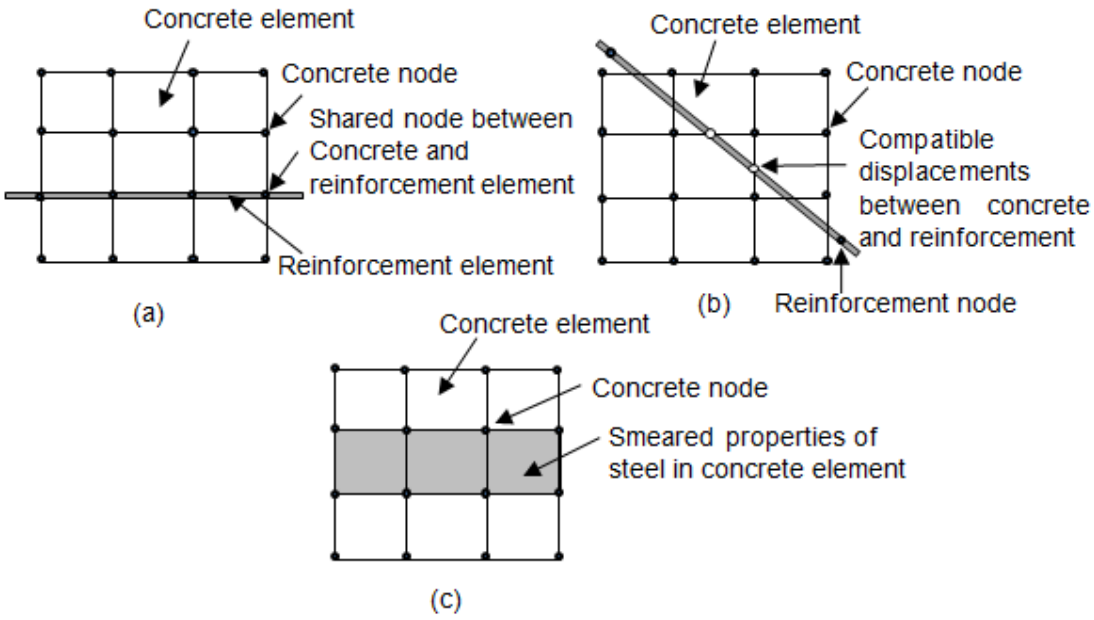

Fig. 6.3 Models for steel bar in reinforced concrete

6.3.2 Material model of reinforcement

Elastic perfectively plastic material behavior of the steel bars is taken to model it. Poisson's ratio and elastic modulus of steel are taken equal to 0.3 and 200 GPa respectively. The yield stress (f_y) is obtained from tensile test of material. Fig. 6.4 shows the stress-strain variation for steel bar.

6.3.3 Material model of concrete

In case of RCC, the effectiveness of confining pressure depends upon the spiral or lateral ties used. The confining pressure will be lesser (or not effective) if the spacing of lateral ties is more. There may be a slight increase in concrete strength and ductility due to confinement with lateral ties (Roy and Sozen, 1964). In the present case the spacing between the lateral ties is higher and equal to 150 mm. Therefore an unconfined stress-strain model given by Saenz (1964) (see Fig 6.5) was tried to model reinforced concrete. The stress-strain equation for unconfined concrete given by Saenz (1964) can be seen in chapter 2 (Eq. 2.1).

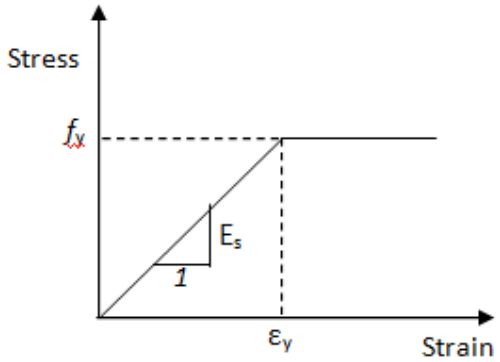

Fig. 6.4 Stress-strain relationship for Steel

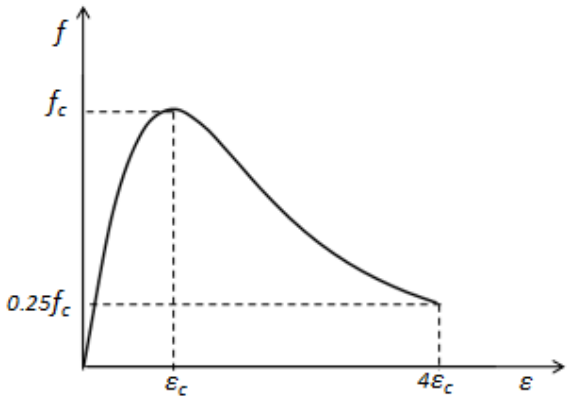

Fig. 6.5 Stress-strain curves for unconfined concrete

6.4 RESULTS AND DISCUSSIONS

In the present study, some experiments were conducted and Finite element model was developed to get the idea about the stress-strain model of concrete in connection with the spacing of lateral ties used for reinforced concrete column. In this process total eighteen specimens were prepared and tested for axial compression. A three dimensional Finite element modeling was carried out with the help of ANSYS software. In case of reinforced concrete column that contains the transverse reinforcement in the form of either spiral or lateral ties;

confinement mainly depends upon the vertical spacing between spiral or lateral ties (S) and on the ratio of the volume of transverse steel to the volume of confined concrete core (ρ_s). For the present study, the confining pressure was computed with the help of equation ($f_l=0.5k_e\ \rho_s f_y$) given by Mander et al. (Mander et al., 1988-a) and it was found between 0.446 MPa to 0.996 MPa.

In the beginning, Stress-strain model for reinforced concrete given by Mander et al. (1988-a) was tried for modeling the axial compression process of specimens. It was found that load-displacement curves obtained from the simulation were not in good agreement with experimental curves in post peak part. Thereafter an unconfined concrete model given by Saenz (1964) was used and the results obtained from simulation were found compatible with the experimental results. The results of experiments and numerical simulations of RCC specimens are given in Table 6.2. It can be seen that error in the results obtained from simulation is within 4%. The load-displacement curves of all specimens obtained from experiments and simulations are shown in Fig. 6.6. The strain at failure was observed between 0.0075 and 0.009. Strain at maximum load ε_{cc} was found to be 0.00285 to 0.003. The post peak part of the load-displacement curve shows ductile behavior of composite material. From the load-displacement curve, it was found that about 0.6% strain develops in the post peak region. From the experiments, it was also observed that higher load capacity can be achieved with lower value of L/D and lower percentage of longitudinal reinforcement while keeping the same length and same concrete compressive strength. A typical deformed shape is plotted in Fig. 6.7. It was found that they were in good match. Fig. 6.8 shows bulging of steel bar in a deformed specimen. The bulging of steel bar in experimental and simulated specimen is in good agreement. Comparison of load-displacement curves of a typical specimen obtained from experiments, simulation using concrete model given by Saenz and Mander (Fig. 6.9).

Now to get the answer of the question that in what condition, the confinement model of concrete would be suitable for reinforced concrete column, an idea was taken from the research conducted by Roy and Sozen (1964). They showed that the confining pressure would be lesser (or not effective) if the spacing of lateral ties was more. They concluded that the strain in the post peak region is governed by the ratio A_{tie}/S^2. To obtain the minimum value of A_{tie}/S^2 for effective confinement, four specimens "C1, C2, C3 and C4" from the experimental data of Mander et al. (1988-b) were simulated and results were obtained. These specimens were having confining pressures from 0.85 MPa to 4.18 MPa. It was found that experimental and analytical results obtained by Mander et al. (1988-b) of specimen C1 and C2 were compatible with the results obtained from the Finite element simulation (Fig 6.10). On the other hand post peak

stress-strain curves of C3 and C4 columns obtained using Finite element simulation were quite different. Moreover the post peak slope of stress-strain curve of specimens C3 and C4 obtained from simulation was quite lower compared to the slope of stress-strain curve obtained from experimental results. It may be concluded that an effective confinement may be obtained when the value of A_{tie}/S^2 is greater than 0.02 (obtained from C2 specimen) and as a result confinement model of concrete should be used for modeling of reinforced concrete columns. Table 6.3 shows the results obtained from simulation of specimens taken from Mander et al. (1988-b).

Table 6.2 Results of bare RCC specimens from experiments and simulation

Specimen	**Ultimate Load (kN)**			**Strain at failure**	**Confining pressure computed from Mander's model (Mander et al., 1988-a)**		
	Experiment	**Analysis**	**% Error**		**ρ_s#**	**(k_e)***	***$f_l=0.5k_e\ \rho_s f_y$***
160P3BRC30	992	1014	2.22	0.0084	0.0111	0.1774	0.495
160P4BRC30	970	990	2.06	0.0081	0.0114	0.1650	0.470
160P5BRC30	941	964	2.44	0.0075	0.0117	0.1524	0.446
200P3BRC30	1331	1376	3.38	0.0088	0.0086	0.3078	0.662
200P4BRC30	1284	1326	3.27	0.0086	0.0088	0.2950	0.649
200P5BRC30	1265	1306	3.24	0.0085	0.0089	0.2885	0.642
225P3BRC30	1549	1610	3.94	0.0090	0.0076	0.3661	0.696
225P4BRC30	1526	1585	3.87	0.0089	0.0077	0.3607	0.694
225P5BRC30	1516	1576	3.96	0.0088	0.0078	0.3551	0.692
160P3BRC40	1064	1088	2.26	0.0081	0.0111	0.1774	0.495
160P3BRC40	1038	1062	2.31	0.0078	0.0114	0.1650	0.470
160P4BRC40	1007	1031	2.38	0.0074	0.0117	0.1524	0.446
200P3BRC40	1443	1489	3.19	0.0085	0.0086	0.3078	0.662
200P4BRC40	1390	1433	3.09	0.0083	0.0088	0.2950	0.649
200P5BRC40	1367	1411	3.22	0.0082	0.0089	0.2885	0.642
225P3BRC40	1684	1749	3.86	0.0088	0.0076	0.3661	0.696
225P4BRC40	1666	1722	3.36	0.0086	0.0077	0.3607	0.694
225P5BRC40	1647	1711	3.89	0.0084	0.0078	0.3551	0.692

ρ_s= Ratio of volume of transverse reinforcement to the volume of confined concrete core; * k_e = confinement coefficient.

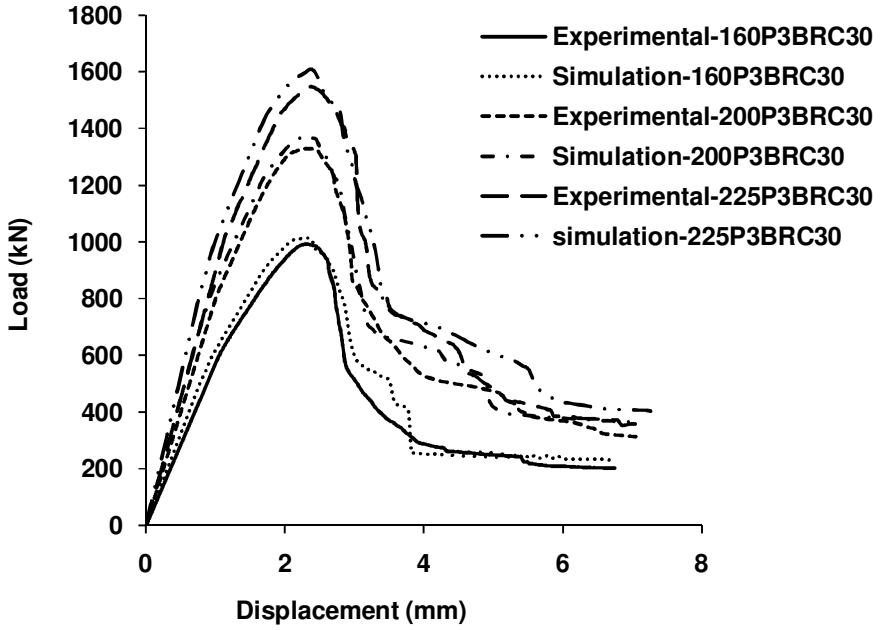

(a)

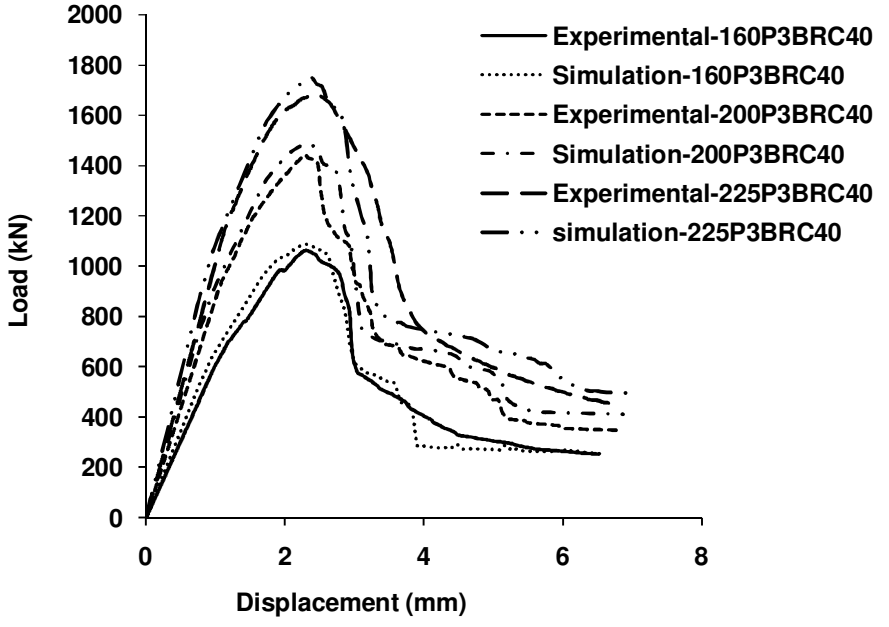

(b)

Fig. 6.6 (a-f) Comparison of load-displacement curves of bare RCC specimens

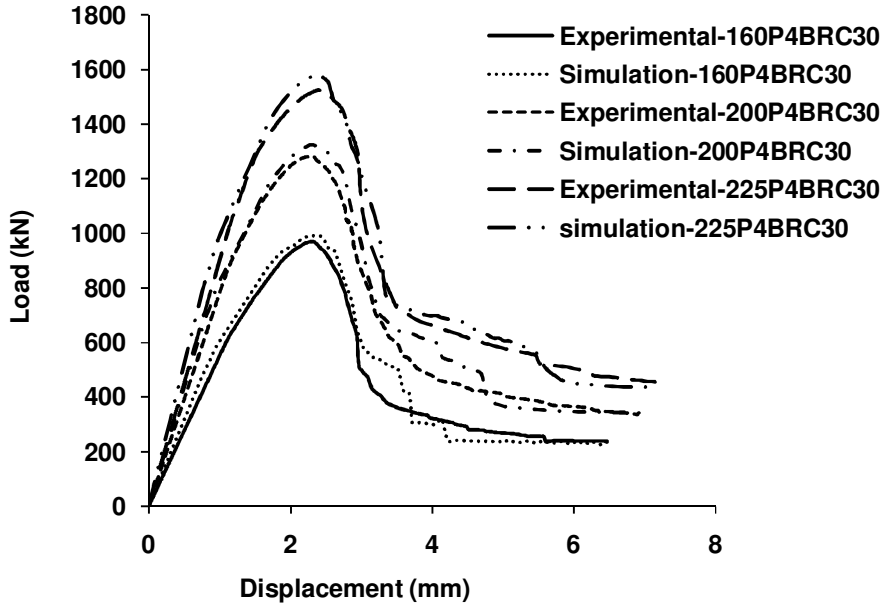

(c)

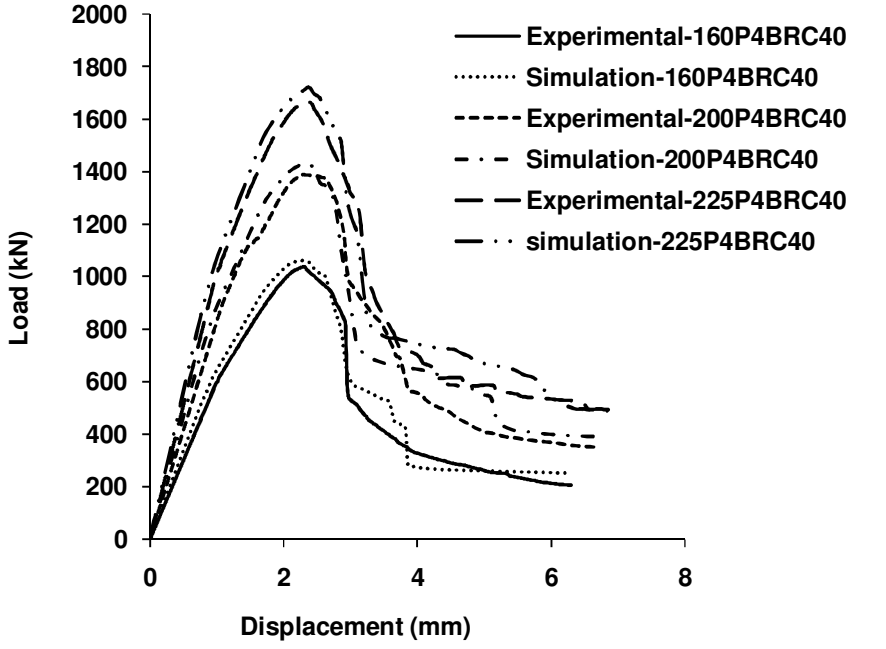

(d)

Fig. 6.6 (a-f) Comparison of load-displacement curves of bare RCC specimens

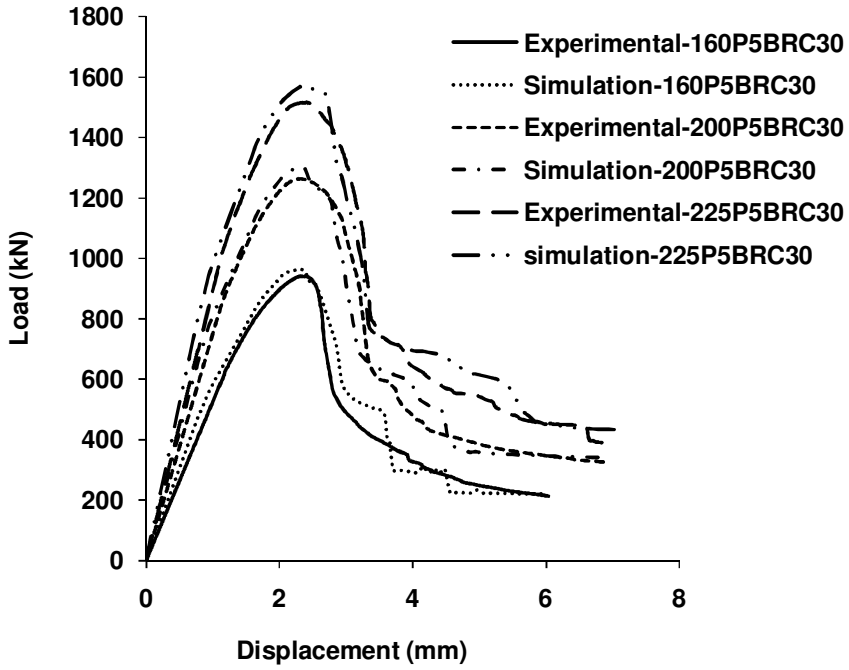

(e)

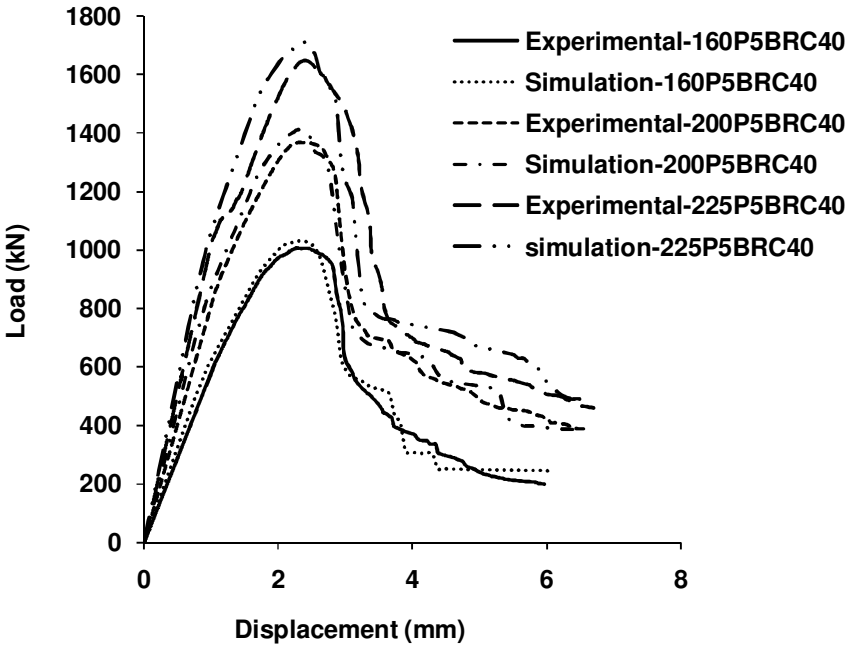

(f)

Fig. 6.6 (a-f) Comparison of load-displacement curves of bare RCC specimens

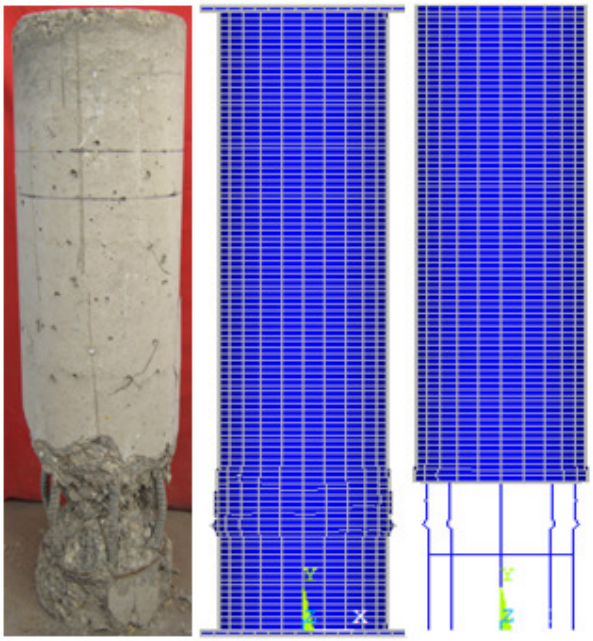

Fig. 6.7 Typical deformed shape of RCC specimen obtained from experiment and simulation

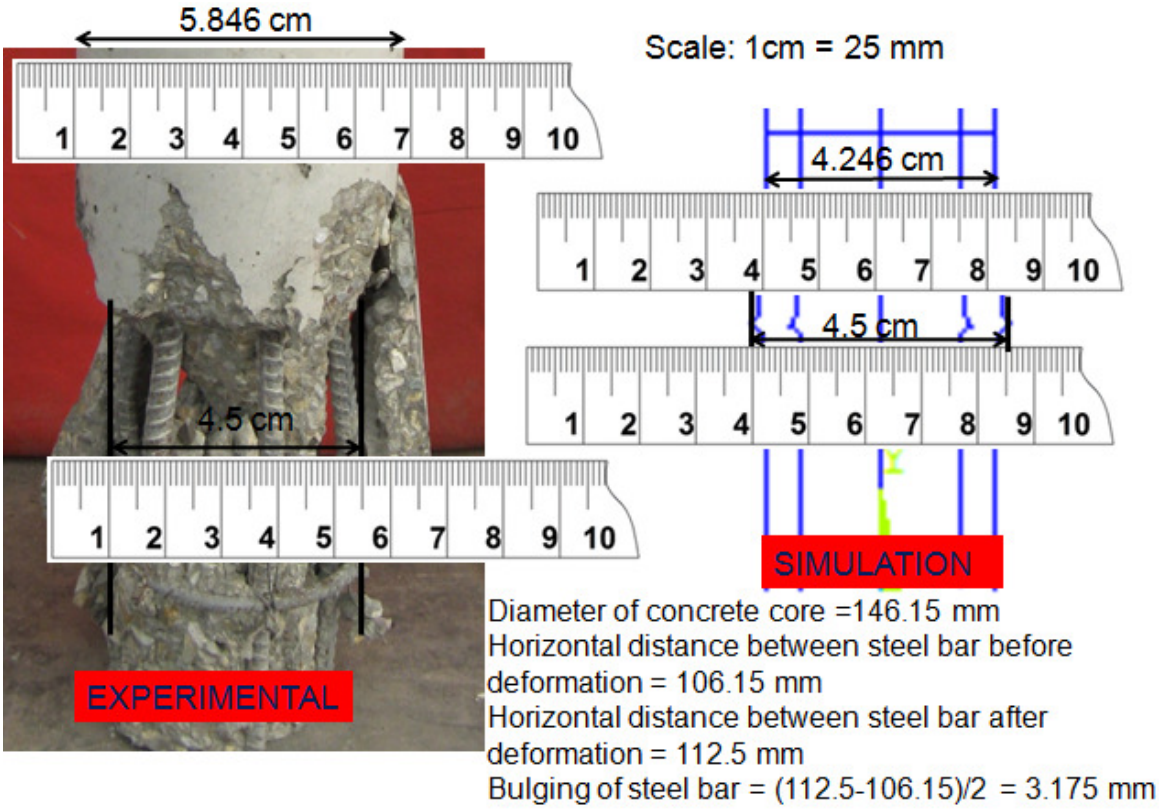

Fig. 6.8 Measurement of bulging of steel bar of deformed RCC specimen "160P5BRC30"

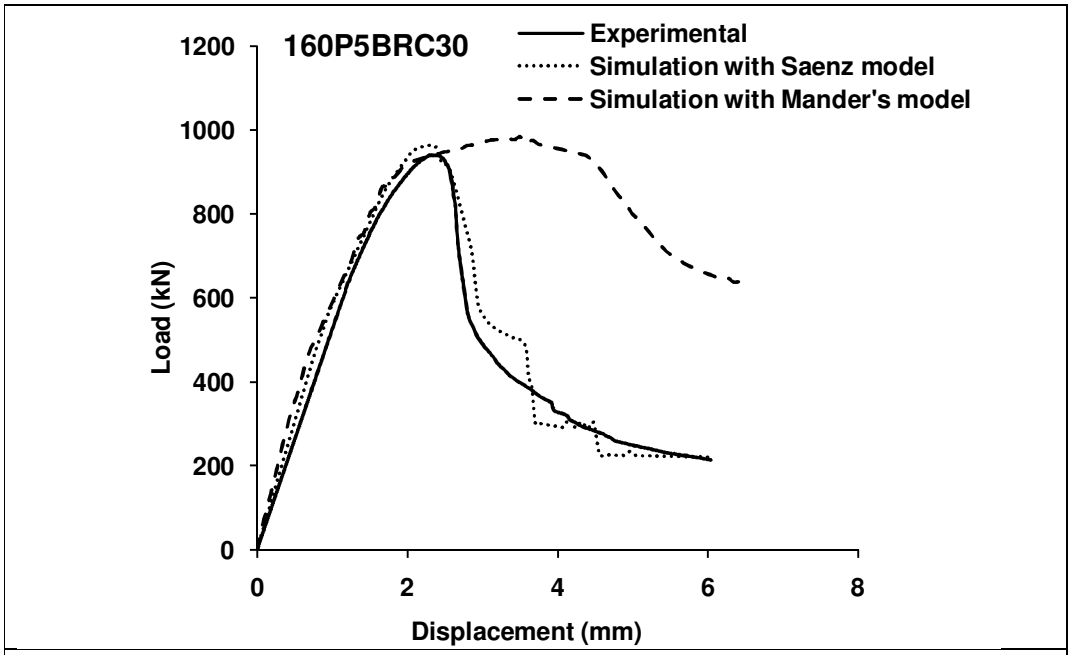

Fig. 6.9 Comparison of load-displacement curves of a typical specimen obtained from experiment, simulation using concrete model given by Saenz and Mander

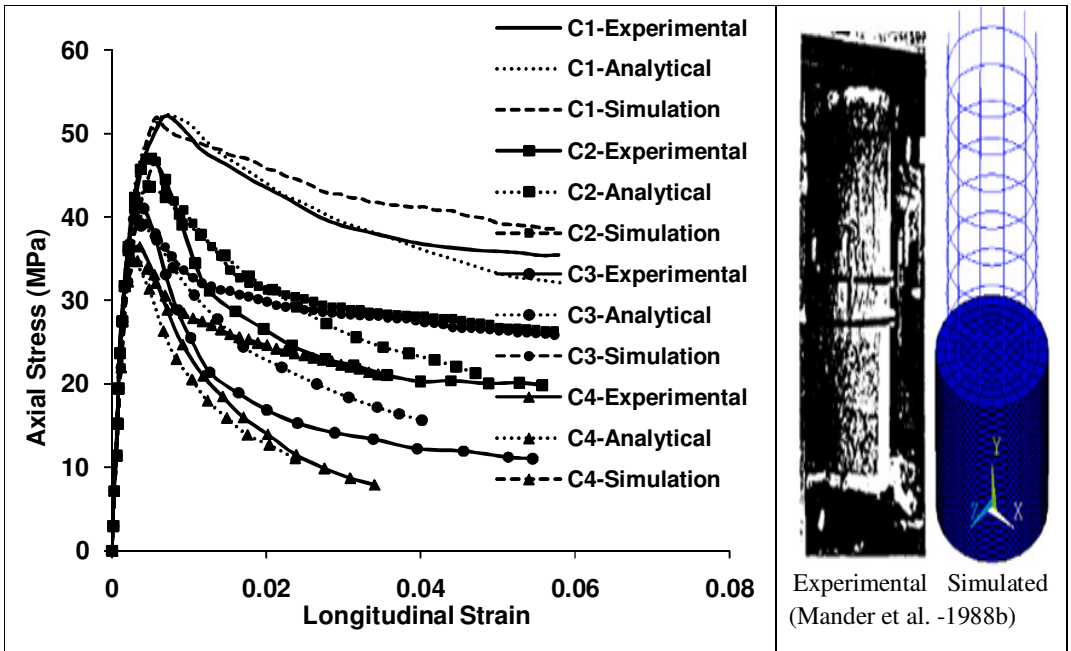

Fig. 6.10 Comparison of stress-strain curves and deformed shapes obtained from literature and simulation

Table 6.3 Comparison of simulated and experimental results for specimens taken from literature

Specimen (Mander et al., 1988-b)	Strength (MPa)			Strain at failure	ρ_s	(k_e)	f_l
	Experiment	Simulation	% Error				
C1	51	51.86	1.69	0.058	0.025	0.983	4.18
C2	46	46.67	1.46	0.056	0.015	0.950	2.42
C3	38.5	39.73	3.20	0.055	0.010	0.911	1.55
C4	34.5	34.66	0.46	0.035	0.006	0.89	0.85

6.5 Conclusions

On the basis of results obtained from experiments and nonlinear Finite element analysis of reinforced concrete columns, the following points can be concluded.

1. The confining pressure of tested specimens was found between 0.446 and 0.696. Since the confining pressure was very small, no strength gain was observed due to confinement but an enhancement in the ductility was noticed. The strain at failure was obtained between 0.0075 and 0.009.
2. Unconfined concrete model is found suitable for modeling of reinforced concrete columns with low value of confining pressure (f_l less than 1.0 MPa).
3. Cross-sectional area and spacing of lateral ties are the governing factors to ascertain the effective confinement in reinforced concrete column. The confinement model of concrete may be used for modeling when the value of A_{tie}/S^2 is greater than 0.02 and f_l greater than 1.0MPa.
4. Unconfined/confined stress strain model may be used for modeling of concrete in reinforced concrete column depending upon the value of A_{tie}/S^2.

CHAPTER-7

REINFORCED CONCRETE FILLED UPVC TUBES (RCFUT) EXPOSED TO SEA WATER

7.1 GENERAL

In this chapter, behavior of axially loaded reinforced concrete column confined with UPVC tubes and bare reinforced concrete columns, exposed to artificially made sea water is studied by performing experiments. For preparing specimens, UPVC pipes of class 3, 4 and 5 (nominal pressure of 0.6, 0.8 and 1.0 MPa) having diameters of 160 mm, 200 mm and 225 mm were filled with the concrete of grade M30 and M40. Compressive strength, ductility, energy absorption capacity and modes of failure of reinforced concrete column (RCC) and reinforced concrete filled UPVC tubes (RCFUT) are obtained from experimental data. Tensile test was performed to see the effect of seawater on the mechanical properties of the UPVC tubes. Moreover scanning electron microscopy (SEM) test was also performed to examine microstructure of UPVC tube before and after immersion in sea water. The tree for study program covered in this chapter is shown in Fig. 7.1.

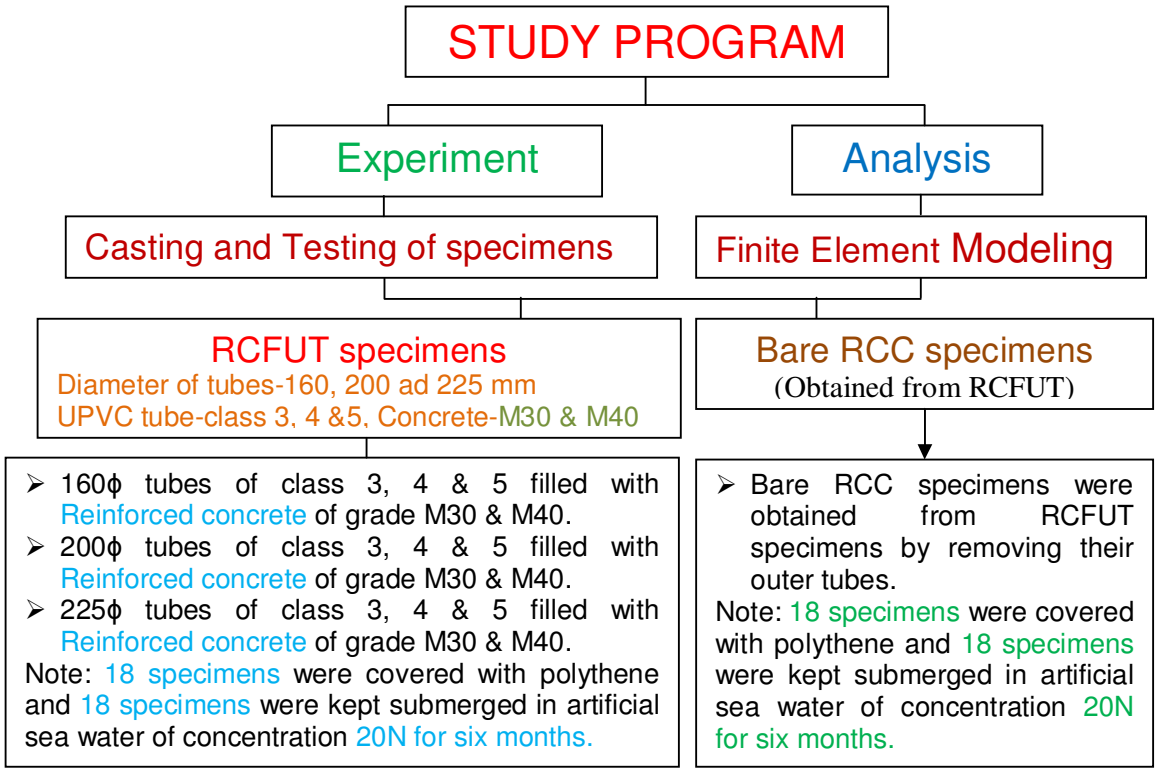

Fig. 7.1 Tree for study program of RCFUT and RCC specimens

7.2 CASTING AND TESTING OF SPECIMENS

Total seventy two RCFUT column specimens were cast by filling the reinforced concrete in UPVC tube. Out of which thirty six specimens were converted to bare RCC specimens by removing UPVC tube. For casting of specimens, the UPVC pipes of class 3, 4 and 5 having diameters of 160 mm, 200 mm and 225 mm were taken. The length of specimens was kept 800 mm. M30 and M40 grades of concrete were used for casting of specimens. 6-12ϕ bars were used as main reinforcement and 8ϕ bars were used for lateral ties spaced @150c/c as transverse reinforcement. The main reinforcement was taken 2.0 to 4.05% of gross cross-sectional area of concrete core. 18 RCFUT and 18 bare RCC specimens were kept completely submerged in artificial sea water of salt concentration 20N over the period of six months while 36 specimens of RCFUT were tightly covered with thick polyethylene sheet to avoid the evaporation of water and kept for 28 days. After 28 days, out of these 36 RCFUT specimens, 18 specimens were tested as bare RCC specimens and 18 as RCFUT specimens. All the specimens were tested for axial loading by applying the load on concrete core only. Top and bottom surface of all the specimens were levelled using hand grinder. Table 7.1 shows the geometrical and material properties of RCFUT and bare RCC specimens.

Typical nomenclatures are used to designate the specimens like 160P3RC30 represents the specimen made of 160 diameter tube of class 3, filled with reinforced concrete of grade M30. Specimen 160P3BRC30 is a bare reinforced concrete column specimen which was obtained by removing the tube of 160P3RC30. The specimens which were submerged in artificial sea water are designated as 160P3RC30-20N6 indicates the specimen 160P3RC30 which is submerged in the sea water of 20N concentration for 6 months.

Table 7.1 Geometrical and material properties of RCFUT and bare RCC specimens

Specimen	Dimensions (mm)			Ratios		Material Properties (MPa)	
	Mean Outer diameter (D)	Thic-kness (t)	Length (L)	D/t	L/D	Unconfined compressive strength of concrete (f_c)	Confining pressure (f_l)
160P3RC30	160.15	3.99	800	40.10	5	35.08	1.15
160P4RC30	159.88	5.22	800	30.65	5	35.08	1.52
160P5RC30	160.19	7.02	800	22.79	5	35.08	2.15
200P3RC30	199.85	5.94	800	33.67	4	35.08	1.35
200P4RC30	199.56	8.11	800	24.66	4	35.08	1.99
200P5RC30	199.22	8.89	800	22.50	4	35.08	2.25
225P3RC30	224.78	8.65	800	26.01	3.56	35.08	1.72
225P4RC30	224.58	9.58	800	23.49	3.56	35.08	2.00
225P5RC30	224.53	9.97	800	22.57	3.56	35.08	2.17
160P3RC40	160.15	3.99	800	40.10	5	39.05	1.15
160P4RC40	159.88	5.22	800	30.65	5	39.05	1.52
160P5RC40	160.19	7.02	800	22.79	5	39.05	2.15
200P3RC40	199.85	5.94	800	33.67	4	39.05	1.35
200P4RC40	199.56	8.11	800	24.66	4	39.05	1.99
200P5RC40	199.22	8.89	800	22.50	4	39.05	2.25
225P3RC40	224.78	8.65	800	26.01	3.56	39.05	1.72
225P4RC40	224.58	9.58	800	23.49	3.56	39.05	2.00
225P5RC40	224.53	9.97	800	22.57	3.56	39.05	2.17
160P3BRC30	160.15	3.99	800	40.10	5	35.08	1.15
160P4BRC30	159.88	5.22	800	30.65	5	35.08	1.52
160P5BRC30	160.19	7.02	800	22.79	5	35.08	2.15
200P3BRC30	199.85	5.94	800	33.67	4	35.08	1.35
200P4BRC30	199.56	8.11	800	24.66	4	35.08	1.99
200P5BRC30	199.22	8.89	800	22.50	4	35.08	2.25
225P3BRC30	224.78	8.65	800	26.01	3.56	35.08	1.72
225P4BRC30	224.58	9.58	800	23.49	3.56	35.08	2.00
225P5BRC30	224.53	9.97	800	22.57	3.56	35.08	2.17
160P3BRC40	160.15	3.99	800	40.10	5	39.05	1.15
160P4BRC40	159.88	5.22	800	30.65	5	39.05	1.52
160P5BRC40	160.19	7.02	800	22.79	5	39.05	2.15

200P3BRC40	199.85	5.94	800	33.67	4	39.05	1.35
200P4BRC40	199.56	8.11	800	24.66	4	39.05	1.99
200P5BRC40	199.22	8.89	800	22.50	4	39.05	2.25
225P3BRC40	224.78	8.65	800	26.01	3.56	39.05	1.72
225P4BRC40	224.58	9.58	800	23.49	3.56	39.05	2.00
225P5BRC40	224.53	9.97	800	22.57	3.56	39.05	2.17
160P3RC30-20N6	160.15	3.99	800	40.10	5	35.08	1.15
160P4RC30-20N6	159.88	5.22	800	30.65	5	35.08	1.52
160P5RC30-20N6	160.19	7.02	800	22.79	5	35.08	2.15
200P3RC30-20N6	199.85	5.94	800	33.67	4	35.08	1.35
200P4RC30-20N6	199.56	8.11	800	24.66	4	35.08	1.99
200P5RC30-20N6	199.22	8.89	800	22.50	4	35.08	2.25
225P3RC30-20N6	224.78	8.65	800	26.01	3.56	35.08	1.72
225P4RC30-20N6	224.58	9.58	800	23.49	3.56	35.08	2.00
225P5RC30-20N6	224.53	9.97	800	22.57	3.56	35.08	2.17
160P3RC40-20N6	160.15	3.99	800	40.10	5	39.05	1.15
160P4RC40-20N6	159.88	5.22	800	30.65	5	39.05	1.52
160P5RC40-20N6	160.19	7.02	800	22.79	5	39.05	2.15
200P3RC40-20N6	199.85	5.94	800	33.67	4	39.05	1.35
200P4RC40-20N6	199.56	8.11	800	24.66	4	39.05	1.99
200P5RC40-20N6	199.22	8.89	800	22.50	4	39.05	2.25
225P3RC40-20N6	224.78	8.65	800	26.01	3.56	39.05	1.72
225P4RC40-20N6	224.58	9.58	800	23.49	3.56	39.05	2.00
225P5RC40-20N6	224.53	9.97	800	22.57	3.56	39.05	2.17
160P3BRC30-20N6	160.15	3.99	800	40.10	5	35.08	1.15
160P4BRC30-20N6	159.88	5.22	800	30.65	5	35.08	1.52
160P5BRC30-20N6	160.19	7.02	800	22.79	5	35.08	2.15
200P3BRC30-20N6	199.85	5.94	800	33.67	4	35.08	1.35
200P4BRC30-20N6	199.56	8.11	800	24.66	4	35.08	1.99
200P5BRC30-20N6	199.22	8.89	800	22.50	4	35.08	2.25
225P3BRC30-20N6	224.78	8.65	800	26.01	3.56	35.08	1.72
225P4BRC30-20N6	224.58	9.58	800	23.49	3.56	35.08	2.00
225P5BRC30-20N6	224.53	9.97	800	22.57	3.56	35.08	2.17
160P3BRC40-20N6	160.15	3.99	800	40.10	5	39.05	1.15
160P4BRC40-20N6	159.88	5.22	800	30.65	5	39.05	1.52
160P5BRC40-20N6	160.19	7.02	800	22.79	5	39.05	2.15

200P3BRC40-20N6	199.85	5.94	800	33.67	4	39.05	1.35
200P4BRC40-20N6	199.56	8.11	800	24.66	4	39.05	1.99
200P5BRC40-20N6	199.22	8.89	800	22.50	4	39.05	2.25
225P3BRC40-20N6	224.78	8.65	800	26.01	3.56	39.05	1.72
225P4BRC40-20N6	224.58	9.58	800	23.49	3.56	39.05	2.00
225P5BRC40-20N6	224.53	9.97	800	22.57	3.56	39.05	2.17

Note: 160P3RC30 represents the specimen composed of 160 mm diameter UPVC tube of class 3 (nominal pressure of 0.6 MPa) filled with reinforced concrete of grade M30. 160P3BRC30 is a bare reinforced concrete column specimen which is obtained by removing the tube of 160P3RC30. 160P3RC30-20N6 indicates the specimen 160P3RC30 which is submerged in the sea water of 20N concentration for 6 months. Other specimens are represented in the same manner.

7.3 NUMERICAL MODELING AND SIMULATION

A three dimensional Finite element model was developed using ANSYS software to simulate the axial compression of reinforced concrete filled UPVC tube (RCUFT). In the same manner, Finite element modeling was done for bare reinforced concrete column subjected to axial compression (Modeling of RCC has been already discussed in chapter 6). To model the concrete core, a three dimensional eight node solid element 'SOLID 65' was used. To model the tube, eight node solid element SOLID 45 was used. The main reinforcement and lateral ties were modeled by the link element 'LINK8'. Discrete model was used to model the longitudinal steel. The contact was defined as a surface to surface contact. Friction factor of 0.2 was taken. Fig.7.2 shows a typical Finite element model adopted for modeling of RCFUT. Material behavior of steel bars is taken as elastic perfectively plastic. Poisson's ratio and elastic modulus of steel are taken as 0.3 and 200 GPa respectively. Material model for confined concrete (Fig. 4.6) is used for the modelling of concrete in RCFUT and unconfined concrete model (shown in Fig. 6.5) proposed by Saenz, (1964) was found suitable for modeling of concrete in RCC

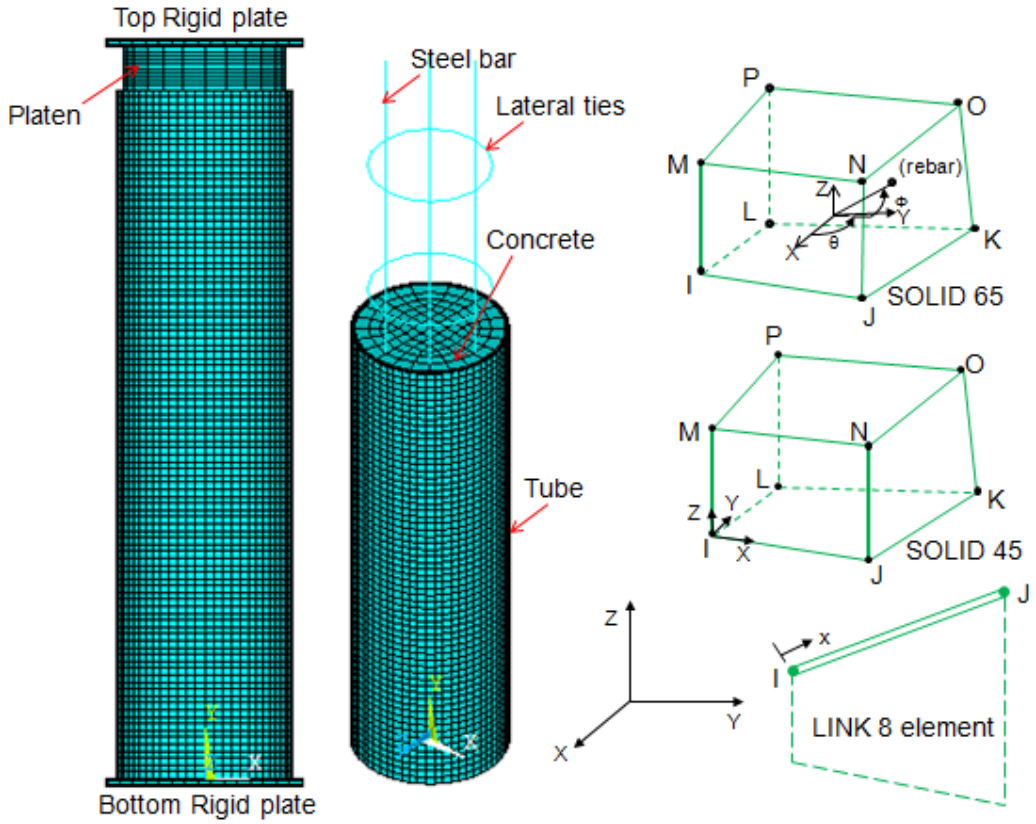

Fig. 7.2 Typical details of Finite element Model for RCFUT

7.4 RESULTS AND DISCUSSIONS

Two types of specimens (RCFUT and bare RCC) were tested. 18 specimens of each RCFUT and bare RCC were tested after 28 days of casting and remaining specimens were tested after six months which were kept submerged in sea water. These specimens were tested to investigate the effect of sea water on their load carrying capacity, ductility, and modes of failure. The results of the load carrying capacity of the different specimens were obtained from their corresponding load-displacement curves obtained during testing. The obtained load-displacement variations are used to calculate the ductility, energy absorption capacity and strength of the specimens. Ductility has been determined by finding the displacement at yield and at 80% of peak load after the peak. Yield load and ultimate loads are determined according to Wu (2004). Ductility ratio has been given by $\mu = \Delta_{80}/\Delta y$, where Δ_{80} is the displacement at 80% of peak load and Δy is the displacement at yield which is defined by an equivalent bilinear response curve that provides an equal area to that of the envelope curve, as shown in Fig. 7.3. The energy ratio has been given by $\xi = E_{80}/E_y$, where E_{80} is the absorbed energy till the load drops 80% of peak load and E_y is the absorbed energy till yield load. Fig.7.4 and 7.5 present the load-displacement curves and modes of failure of RCFUT specimens respectively. It may be seen that load-displacement curves obtained from experiments and simulations of RCFUT are quite compatible. It is clear from Fig. 7.5 that RCFUT specimens were failed with bulging at about 1/4 distance from the top of specimen. Bulging may be due to the confinement offered to concrete by the tube. Load-displacement curves and modes of failure of bare RCC specimens are shown in Fig. 7.6 and Fig 7.7 respectively. Load-displacement curves obtained from experiments and simulations of bare RCC specimens are in good match. Bare reinforced concrete columns were failed due to development of the vertical multiple cracks either from top or bottom side. Energy absorption and ductility of all types of specimens are also studied with the help of load-compression variations. Table 7.2 presents the ultimate load capacity, ductility ratio and energy absorption ratio for different specimens. The ductility ratios μ for bare R.C. columns varies between 1.41 and 1.80 and energy ratio ξ varies between1.79 and 2.49. On the other hand the ductility ratio μ for RCFUT specimens varies between 1.51 and 2.76 and corresponding energy absorption ratio ξ varies between 2.0 and 4.19. It can be seen from Table 7.2 that generally ductility ratio decreases with increase in grade of concrete due to brittleness of concrete. It is also clear from Table 7.2 that as D/t ratio of the UPVC tube decreases, Δ_{80} and E_{80} increases. The energy absorbed (E_{80}) for bare RCC column filled with M30 grade of concrete varies from 1610 Joule to 3293 Joule while for bare RCC column submerged in sea

water varies from 1597 Joule to 2937 Joule. On the other hand, the energy absorbed (E_{80}) for RCFUT specimens filled with M30 grade of concrete varies from 3078 Joule to 11091 Joule while for RCFUT specimens submerged in sea water varies from 3294 Joule to 11859 Joule. The energy absorbed by RCFUT is about 1.91 to 3.37 times that of bare RCC. Fig. 7.8 shows the comparison of load-compression curves of RCFUT and bare RCC specimens submerged in sea water. It can be seen from Fig. 7.8, that the ultimate load capacity and displacement of RCFUT specimens are high compared to bare RCC specimens. It is clear from curves that slope of post peak curve of RCFUT specimens is lesser in comparison of bare RCC specimens. Fig. 7.9 shows the comparison of load-compression curves of all types of specimens obtained from experiments. Fig. 7.10 shows the energy-displacement curves of RCFUT specimens with different diameter of same class of tubes. It can be seen form Fig. 7.10 that energy increases with the increase of diameter of tube. The energy-displacement curves for typical RCFUT and bare RCC specimens are shown in Fig. 7.11. It is clear from Fig. 7.11, that there is large energy absorbed by RCFUT compared to bare RCC specimens.

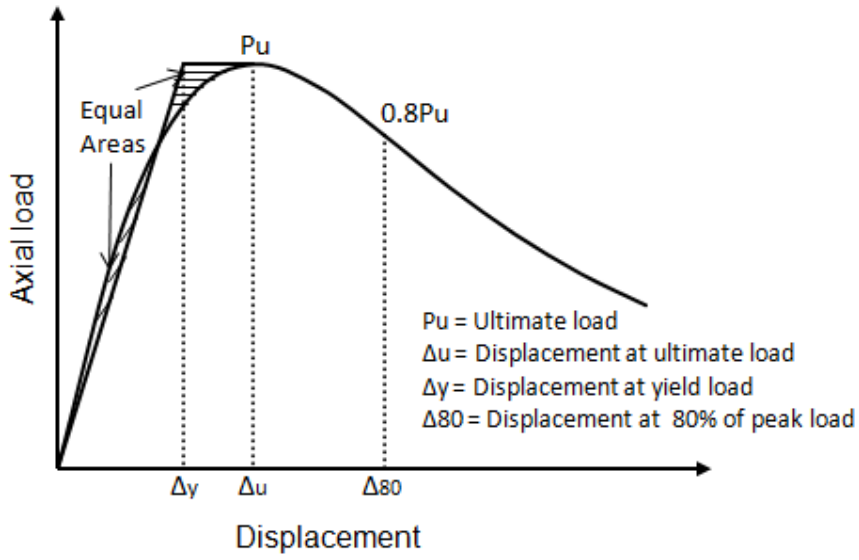

Fig. 7.3 Definition of ductility

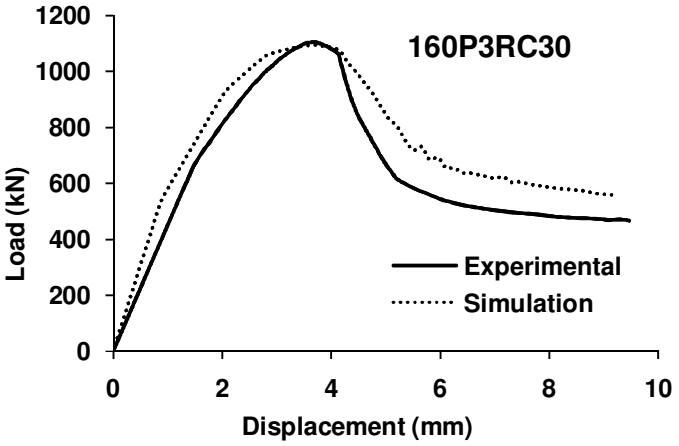

(a)

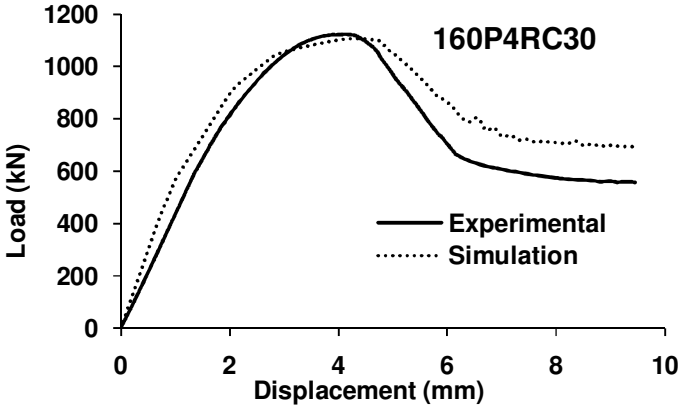

(b)

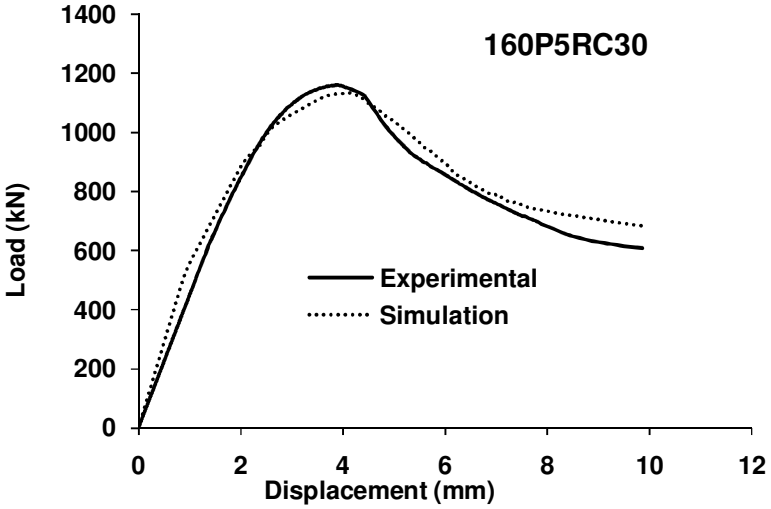

(c)

Fig.7.4(a-r) Load-Displacement curves of RCFUT specimens obtained from experiment and simulation

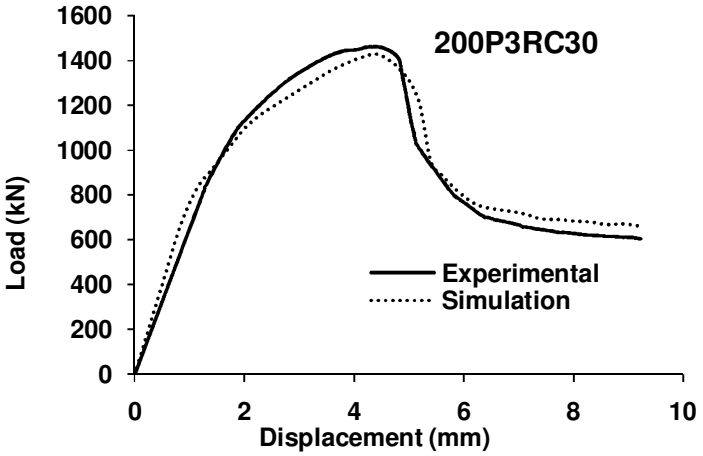

(d)

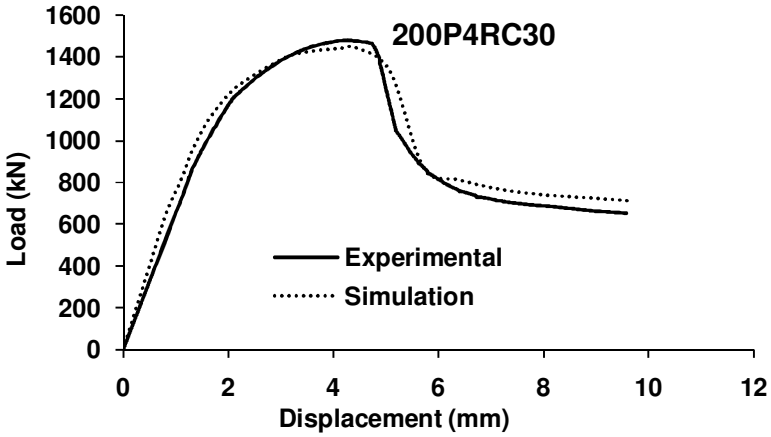

(e)

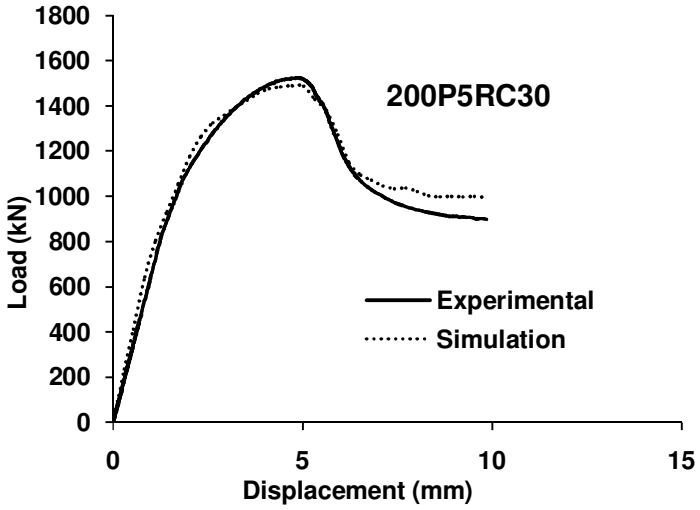

(f)

Fig.7.4(a-r) Load-Displacement curves of RCFUT specimens obtained from experiment and simulation

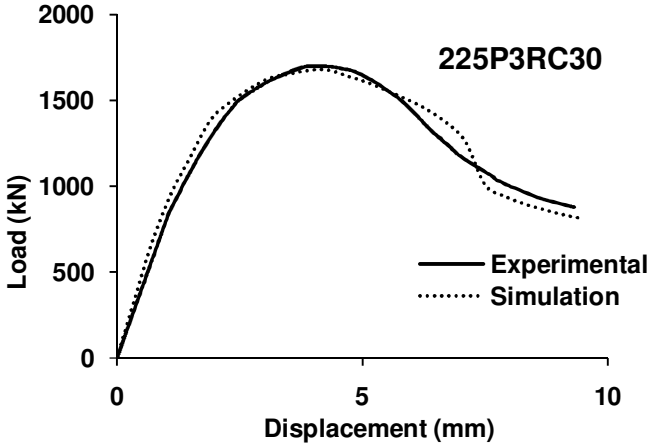

(g)

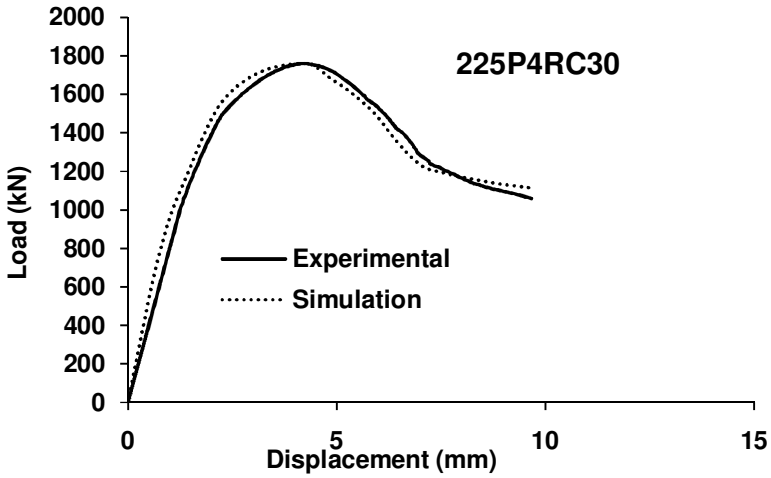

(h)

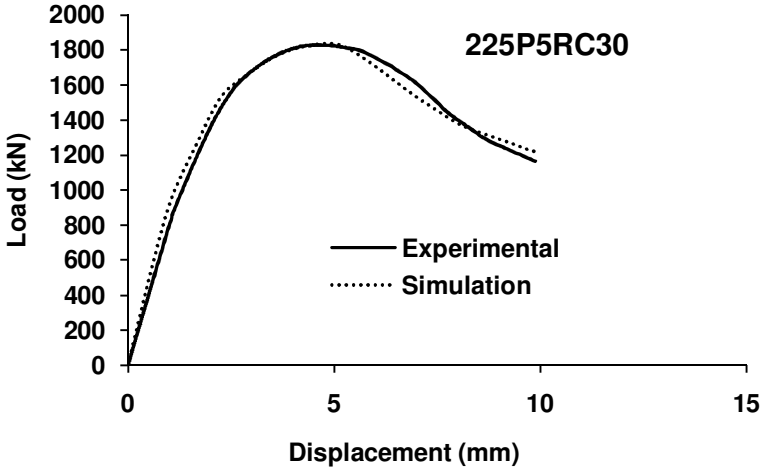

(i)

Fig.7.4(a-r) Load-Displacement curves of RCFUT specimens obtained from experiment and simulation

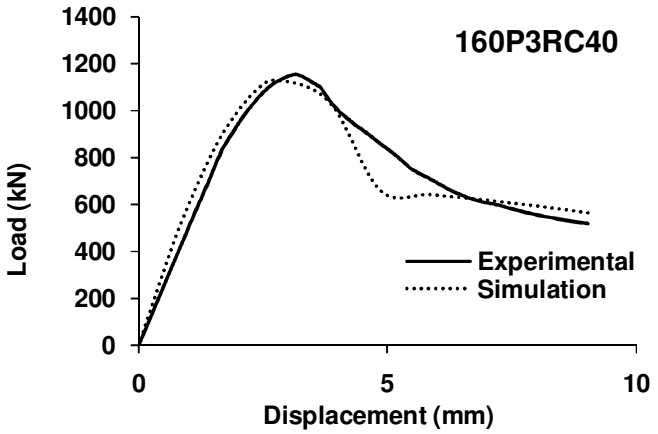

(j)

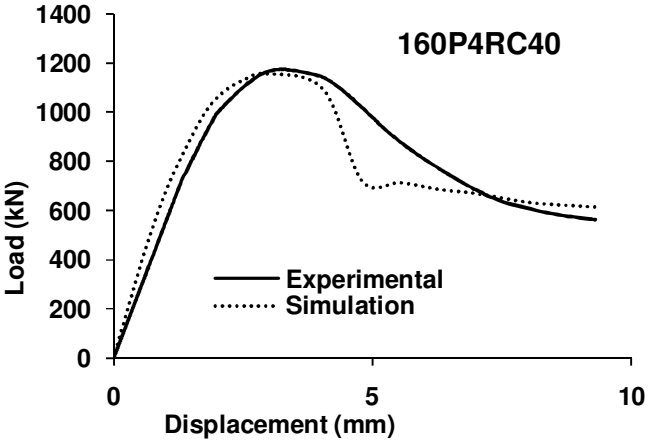

(k)

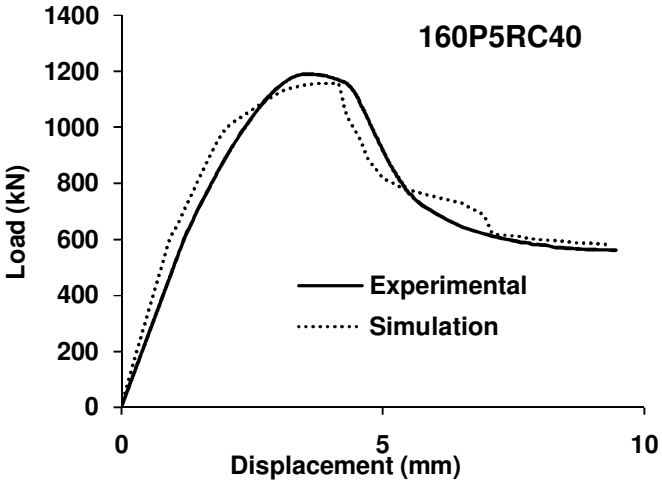

(l)

Fig.7.4(a-r) Load-Displacement curves of RCFUT specimens obtained from experiment and simulation

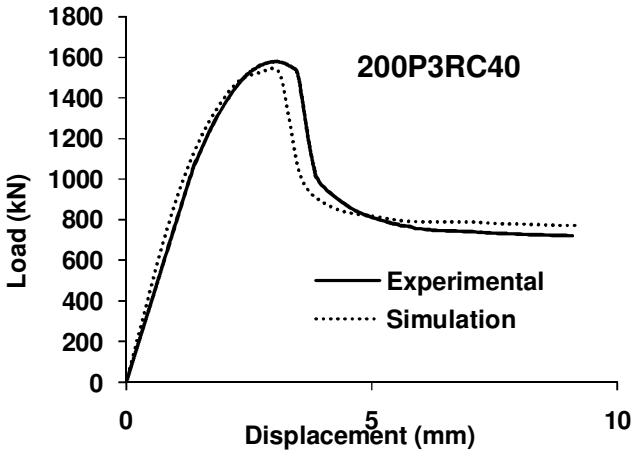

(m)

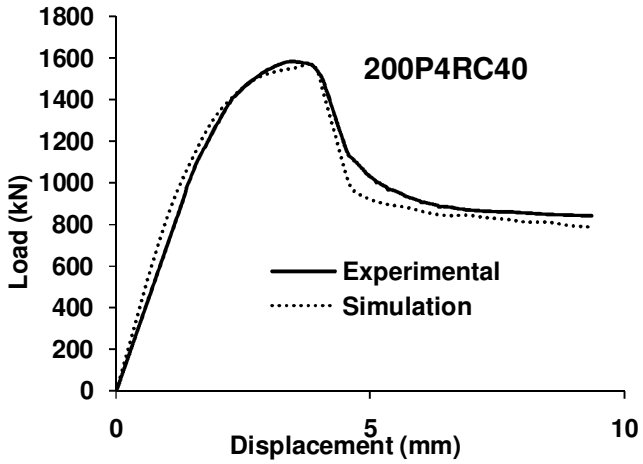

(n)

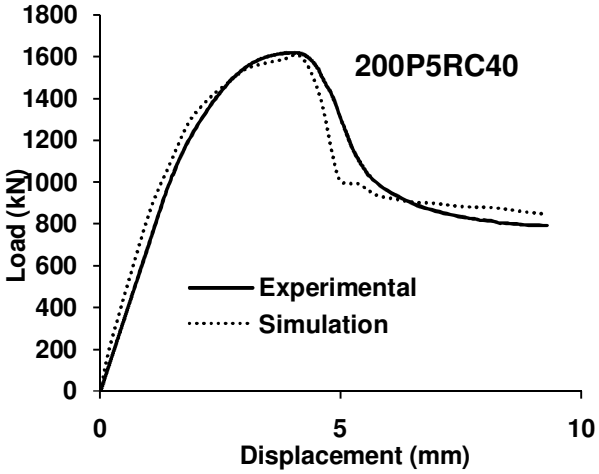

(o)

Fig.7.4(a-r) Load-Displacement curves of RCFUT specimens obtained from experiment and simulation

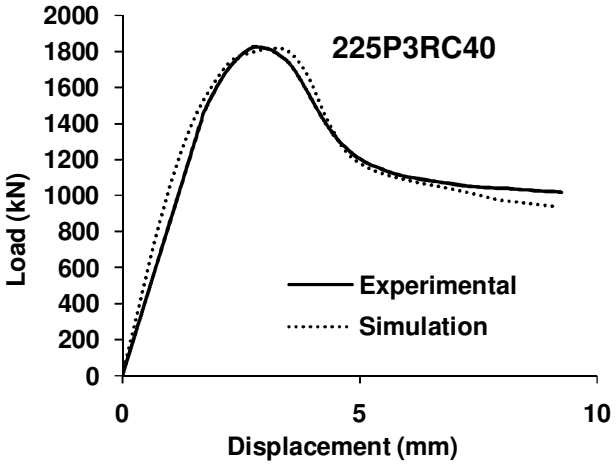

(p)

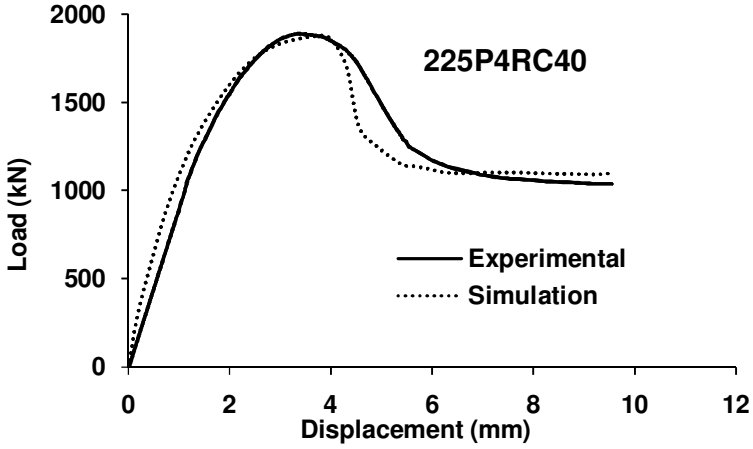

(q)

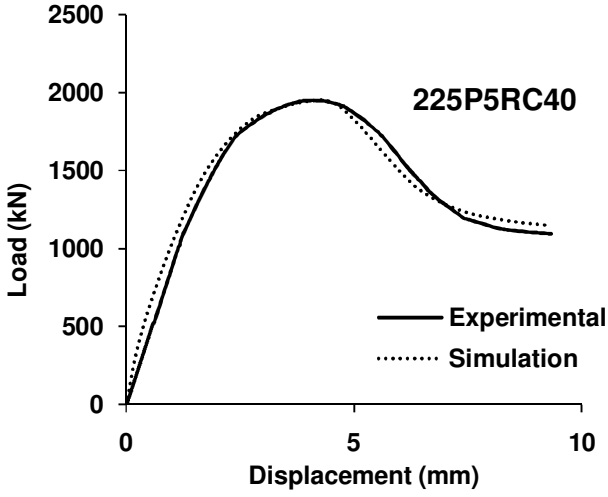

(r)

Fig.7.4(a-r) Load-Displacement curves of RCFUT specimens obtained from experiment and simulation

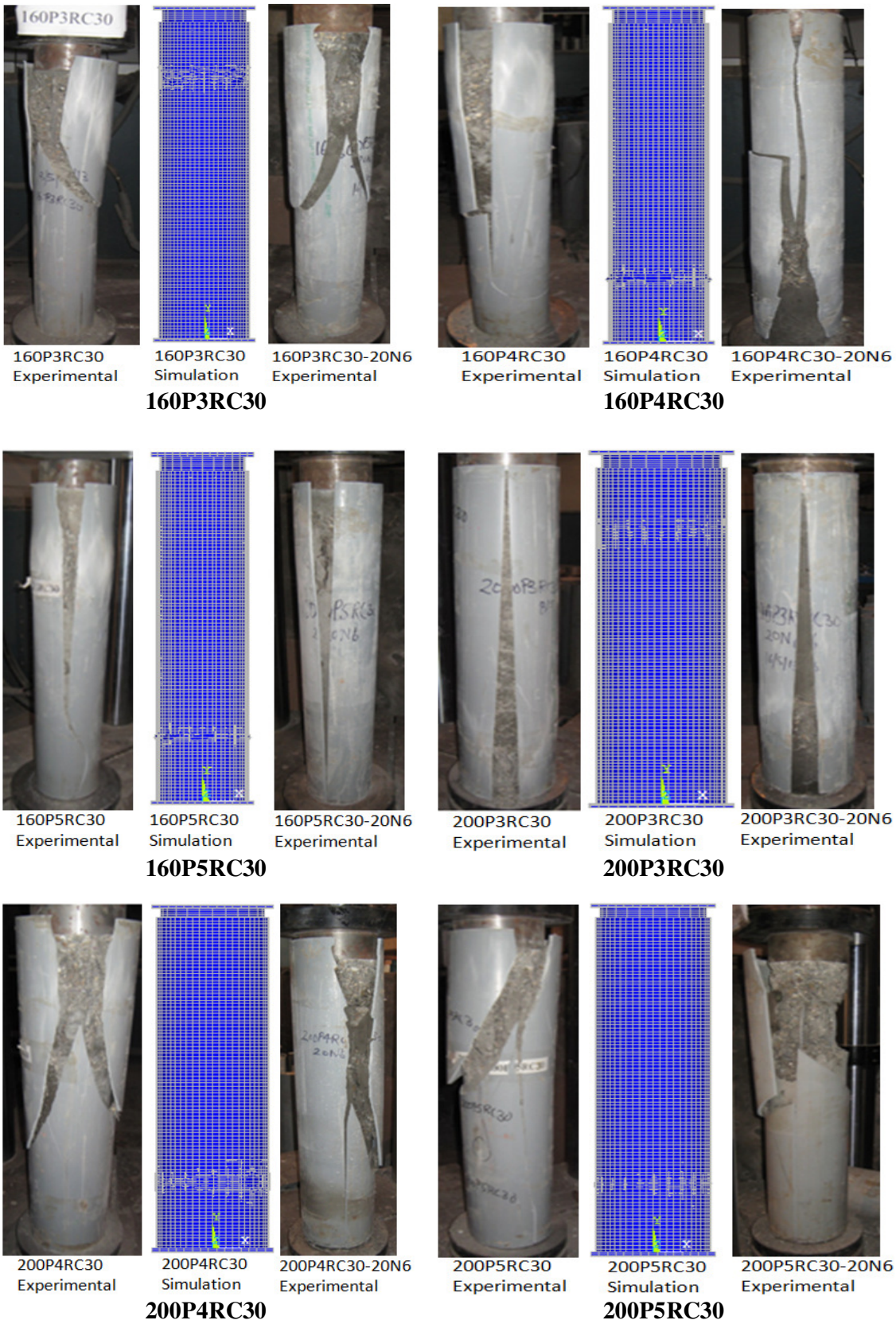

Fig. 7.5 Modes of failure of RCFUT specimens

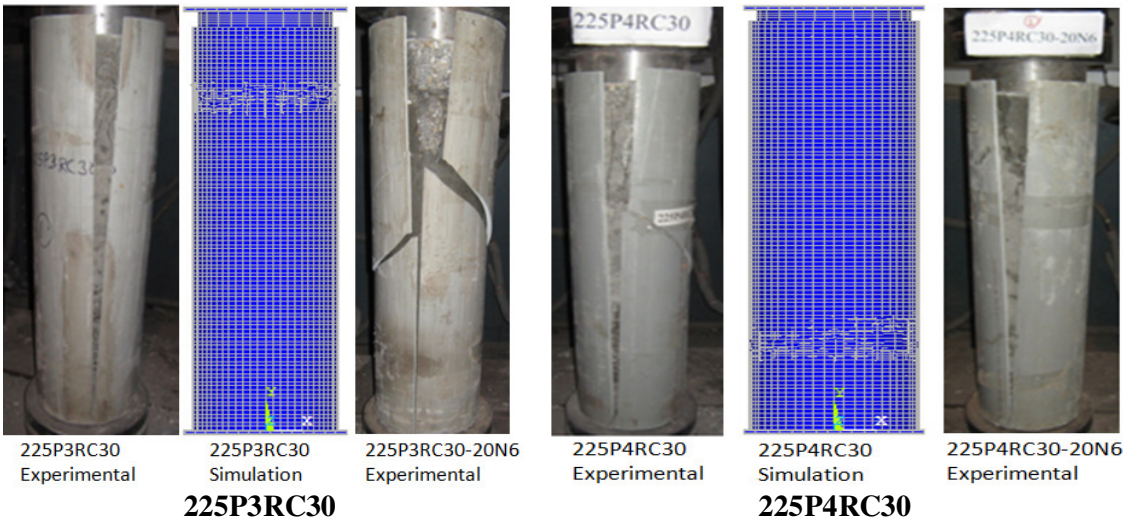

Fig. 7.5 Modes of failure of RCFUT specimens

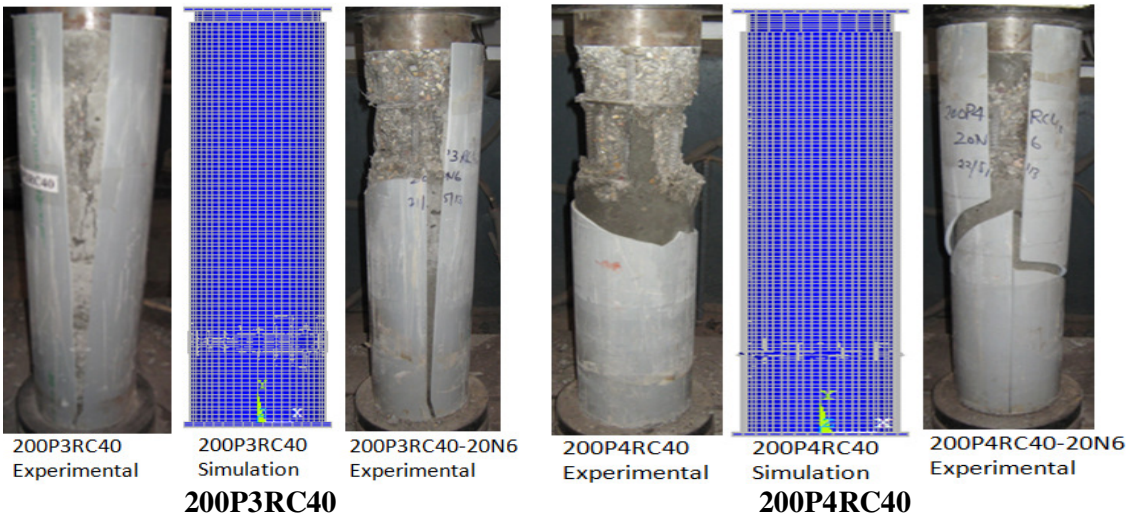

200P3RC40 **200P4RC40**

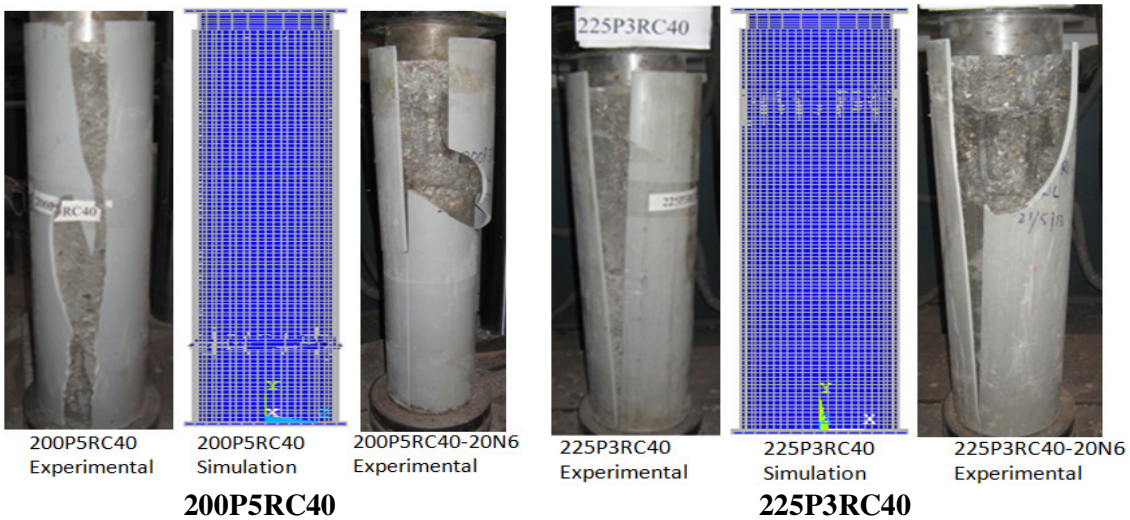

200P5RC40 **225P3RC40**

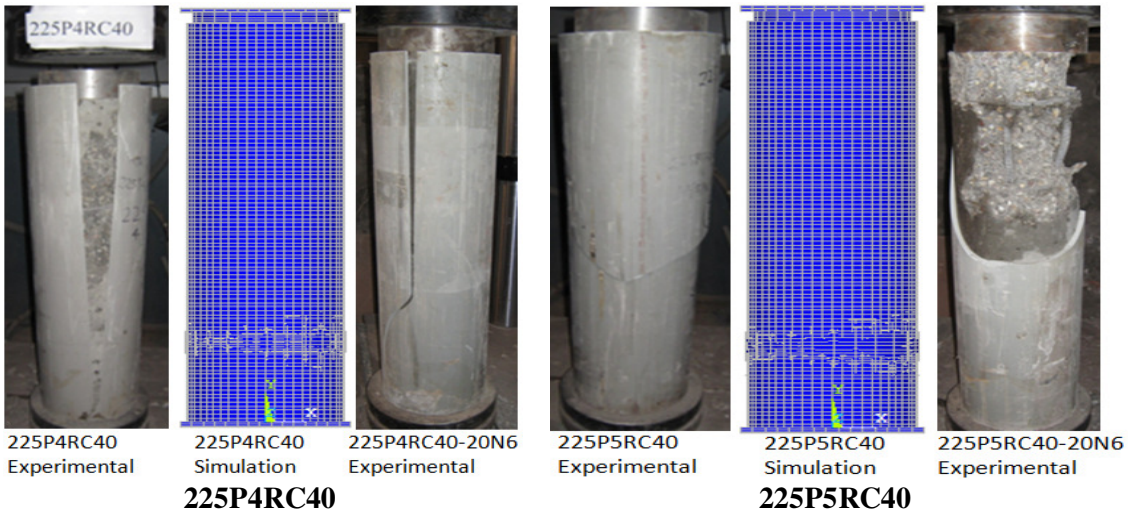

225P4RC40 **225P5RC40**

Fig. 7.5 Modes of failure of RCFUT specimens

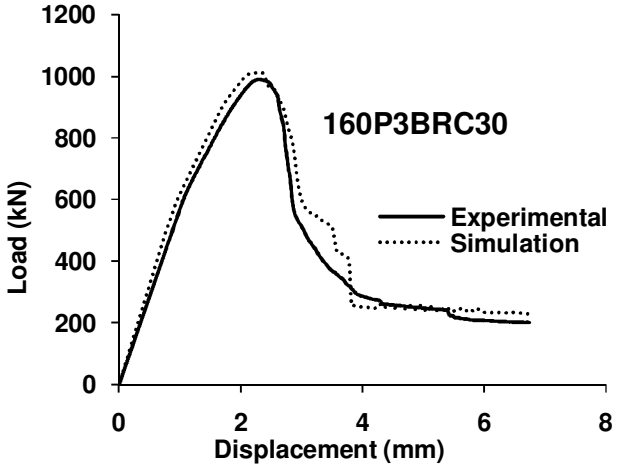

(a)

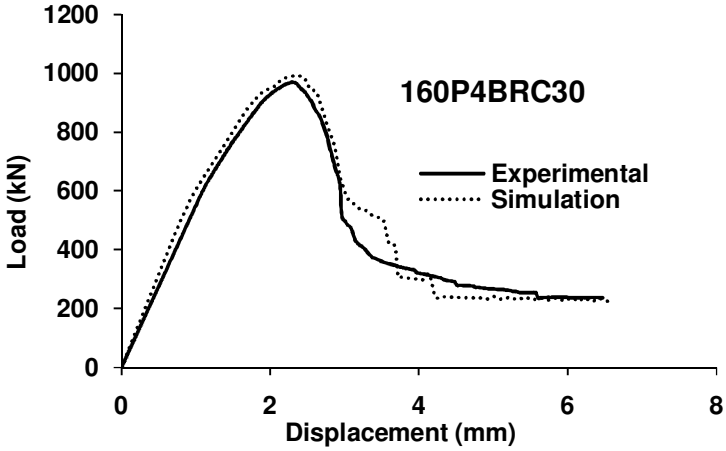

(b)

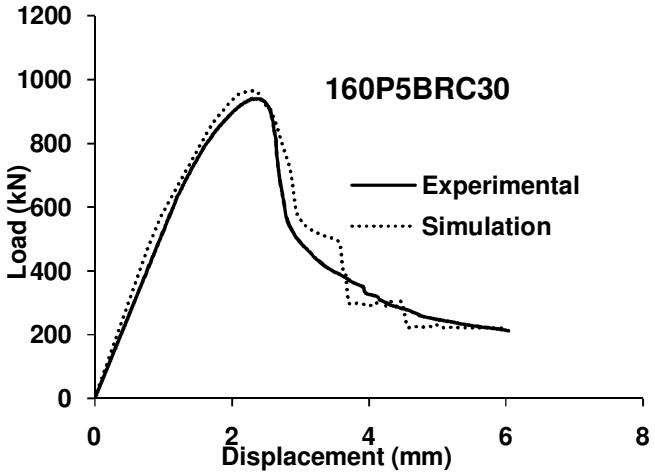

(c)

Fig.7.6(a-r) Load-Displacement curves of bare RCC specimens obtained from experiment and simulation

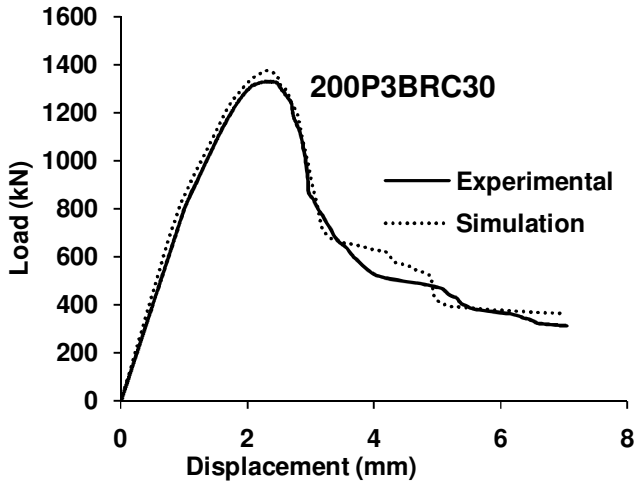

(d)

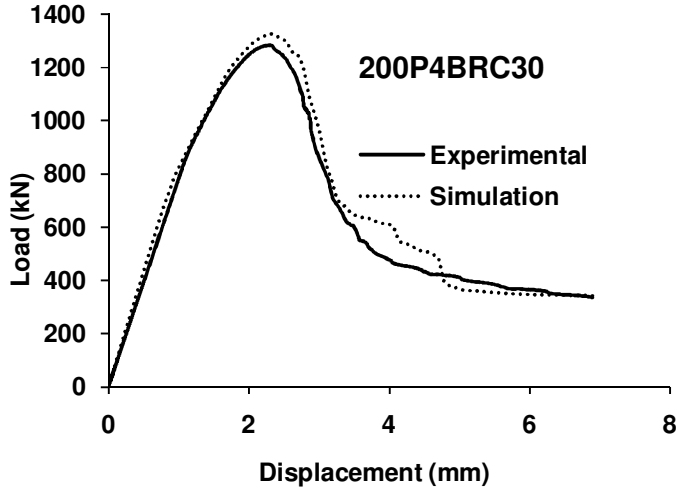

(e)

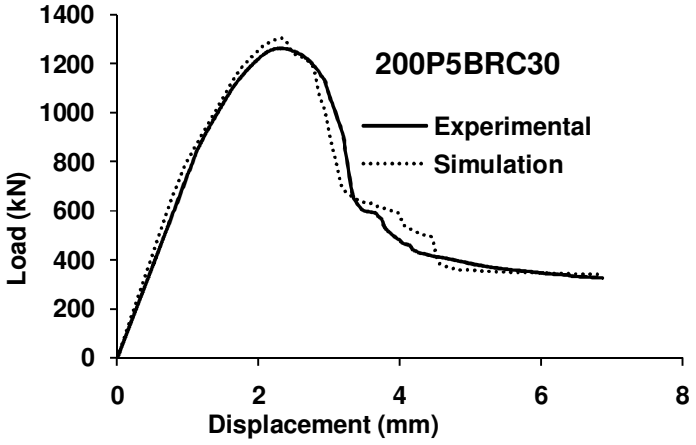

(f)

Fig.7.6(a-r) Load-Displacement curves of bare RCC specimens obtained from experiment and simulation

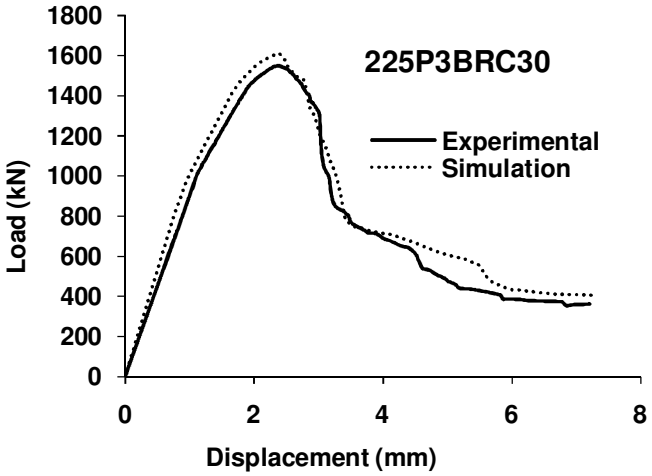

(g)

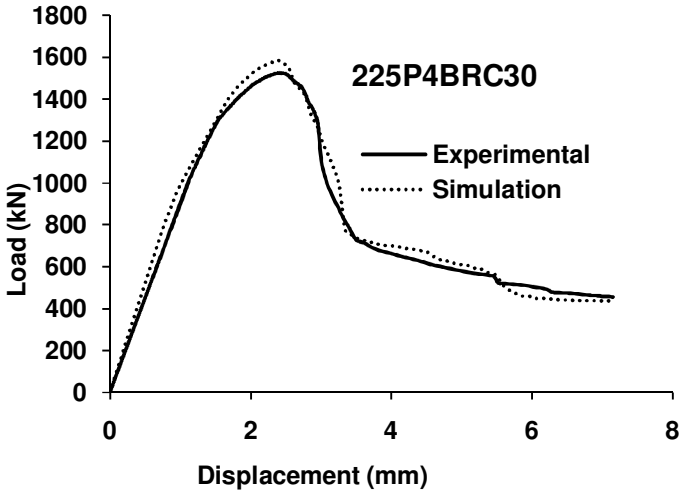

(h)

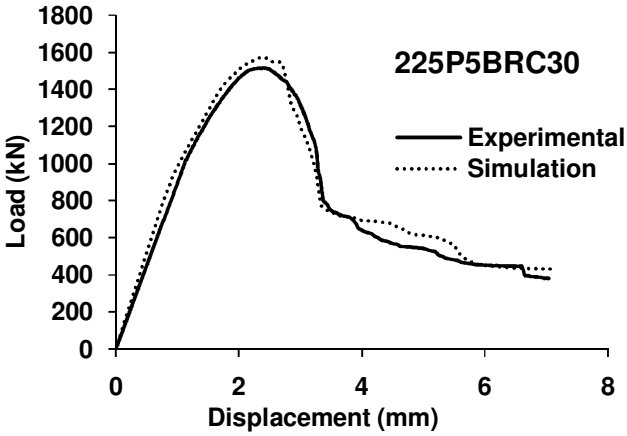

(i)

Fig.7.6(a-r) Load-Displacement curves of bare RCC specimens obtained from experiment and simulation

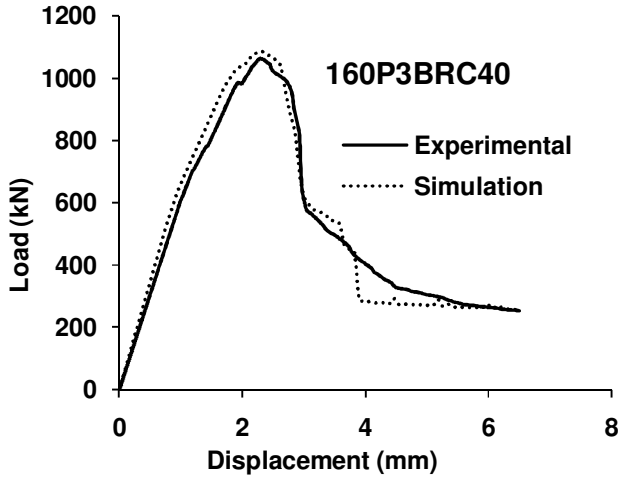

(j)

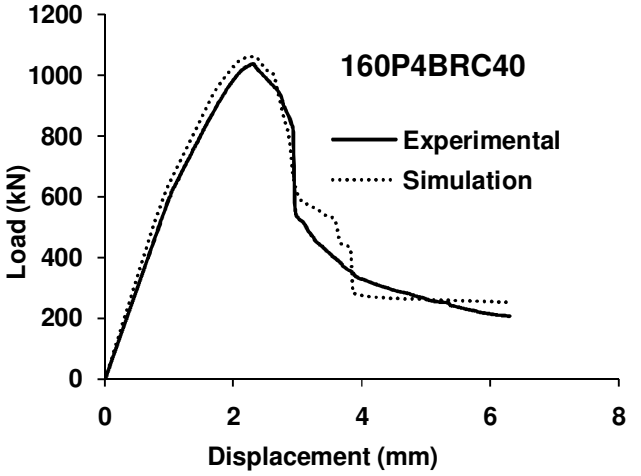

(k)

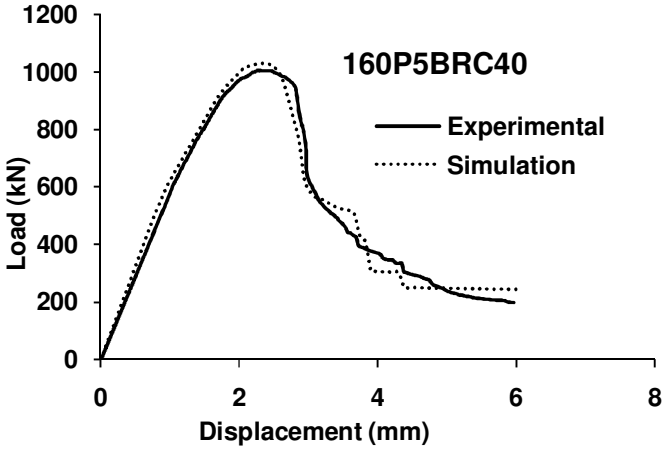

(l)

Fig.7.6(a-r) Load-Displacement curves of bare RCC specimens obtained from experiment and simulation

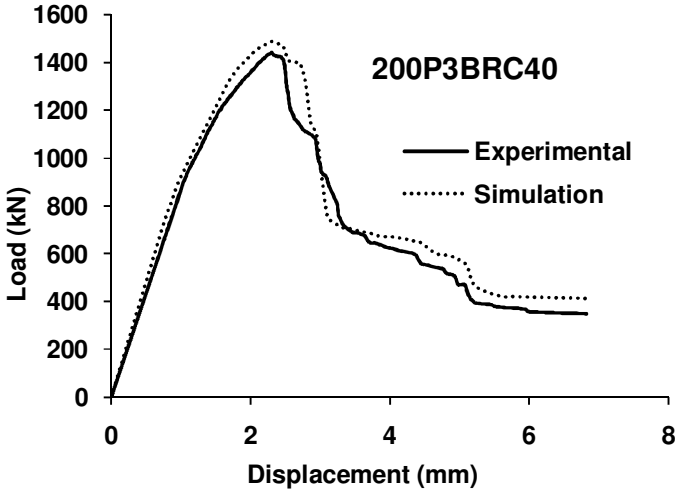

(m)

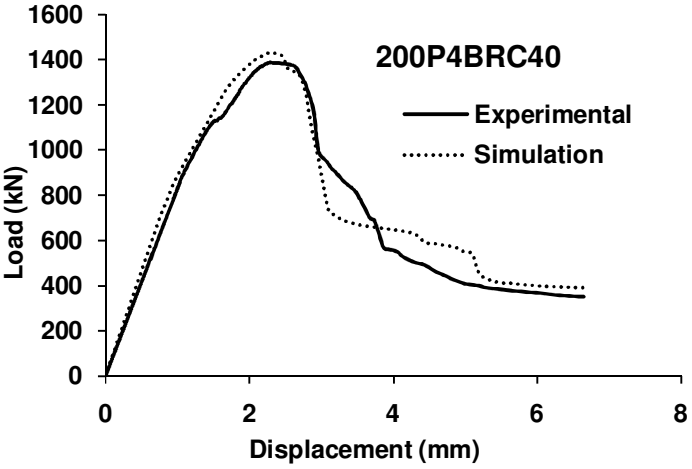

(n)

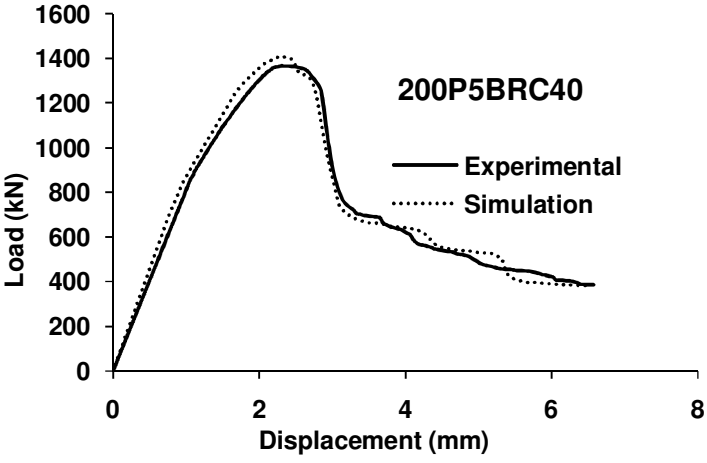

(o)

Fig.7.6(a-r) Load-Displacement curves of bare RCC specimens obtained from experiment and simulation

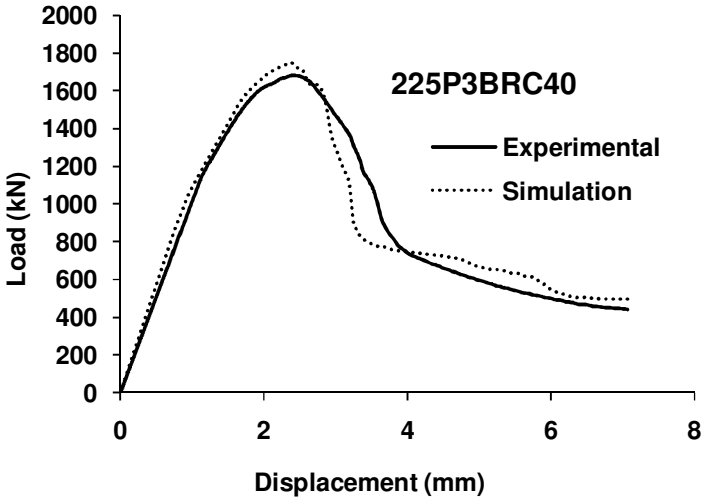

(p)

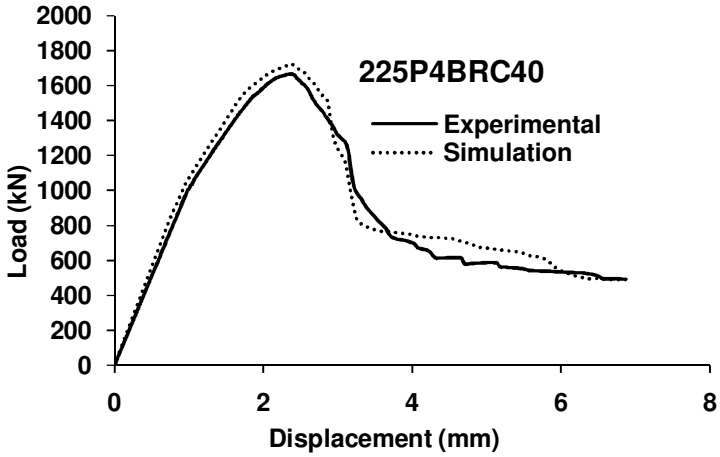

(q)

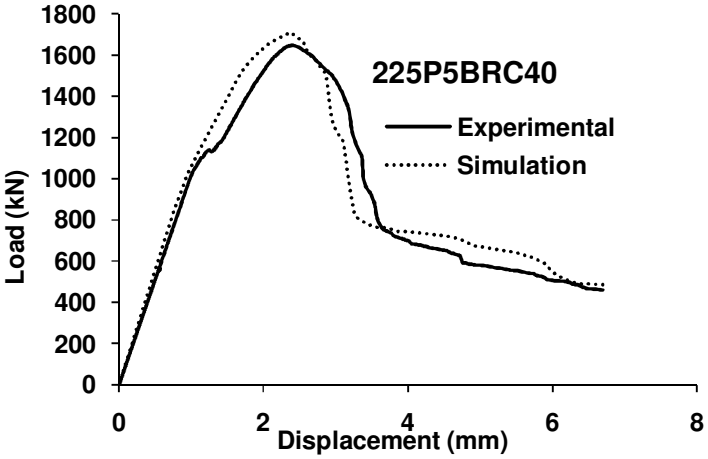

(r)

Fig.7.6(a-r) Load-Displacement curves of bare RCC specimens obtained from experiment and simulation

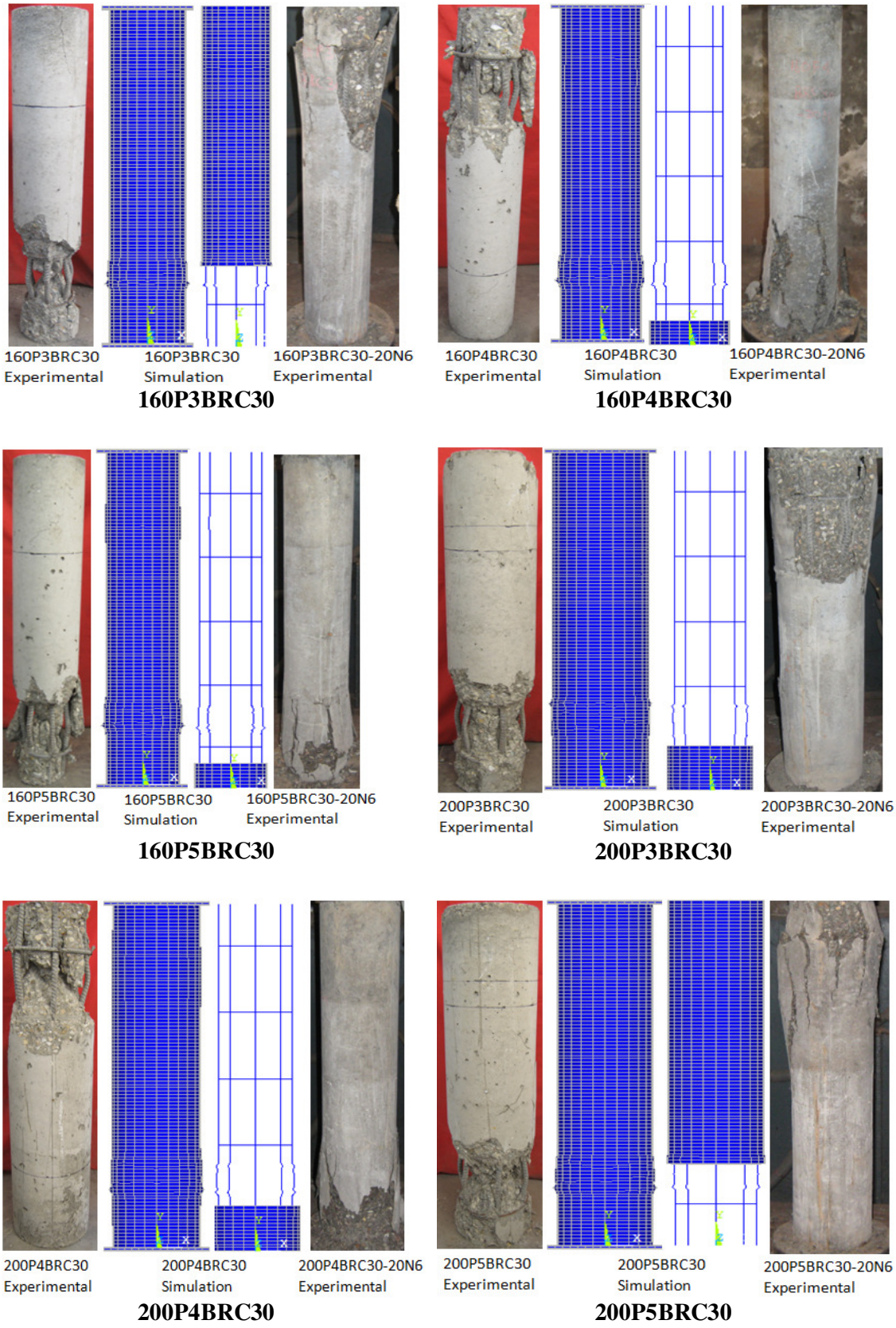

Fig. 7.7 Modes of failure of bare RCC specimens

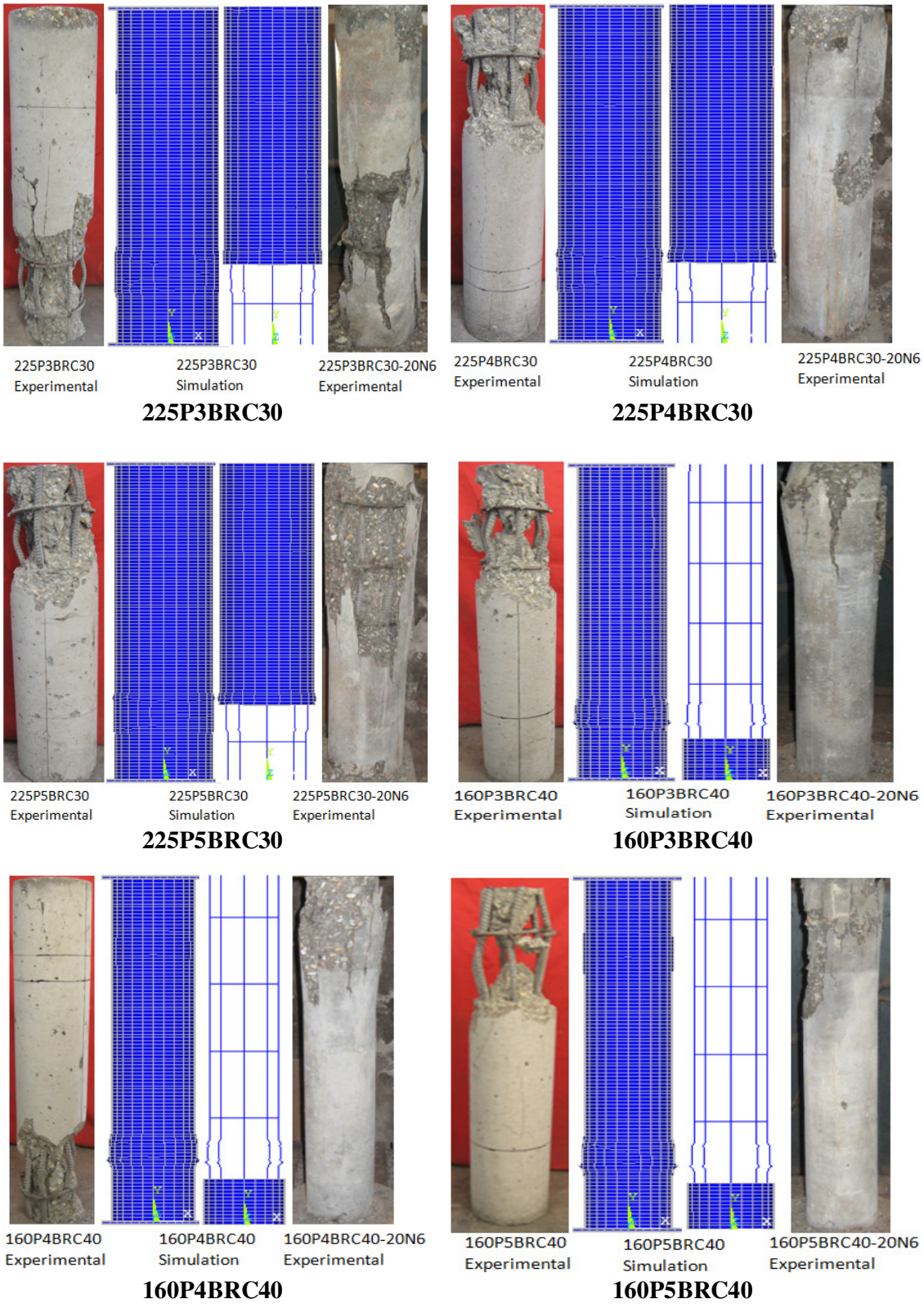

Fig. 7.7 Modes of failure of bare RCC specimens

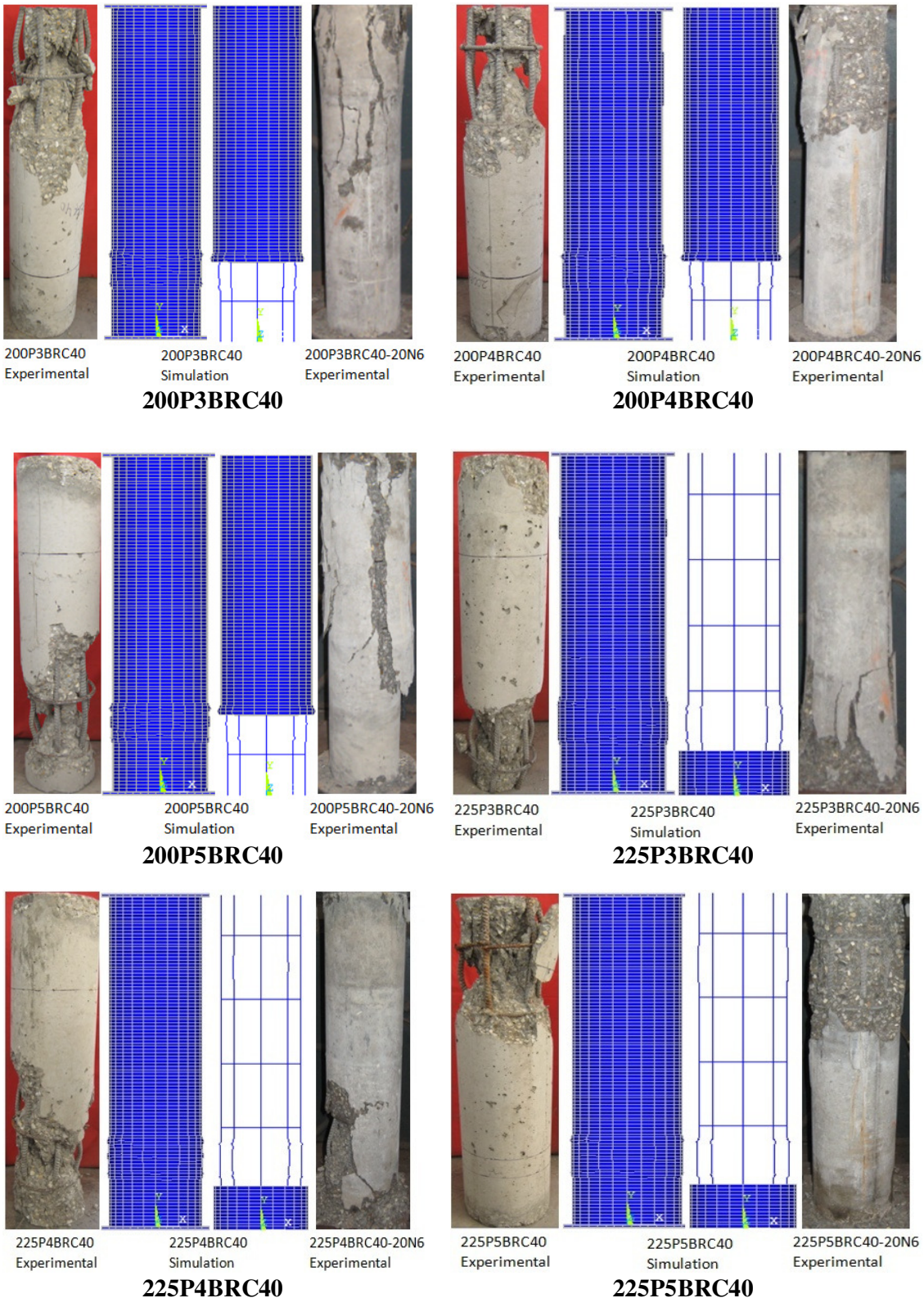

Fig. 7.7 Modes of failure of bare RCC specimens

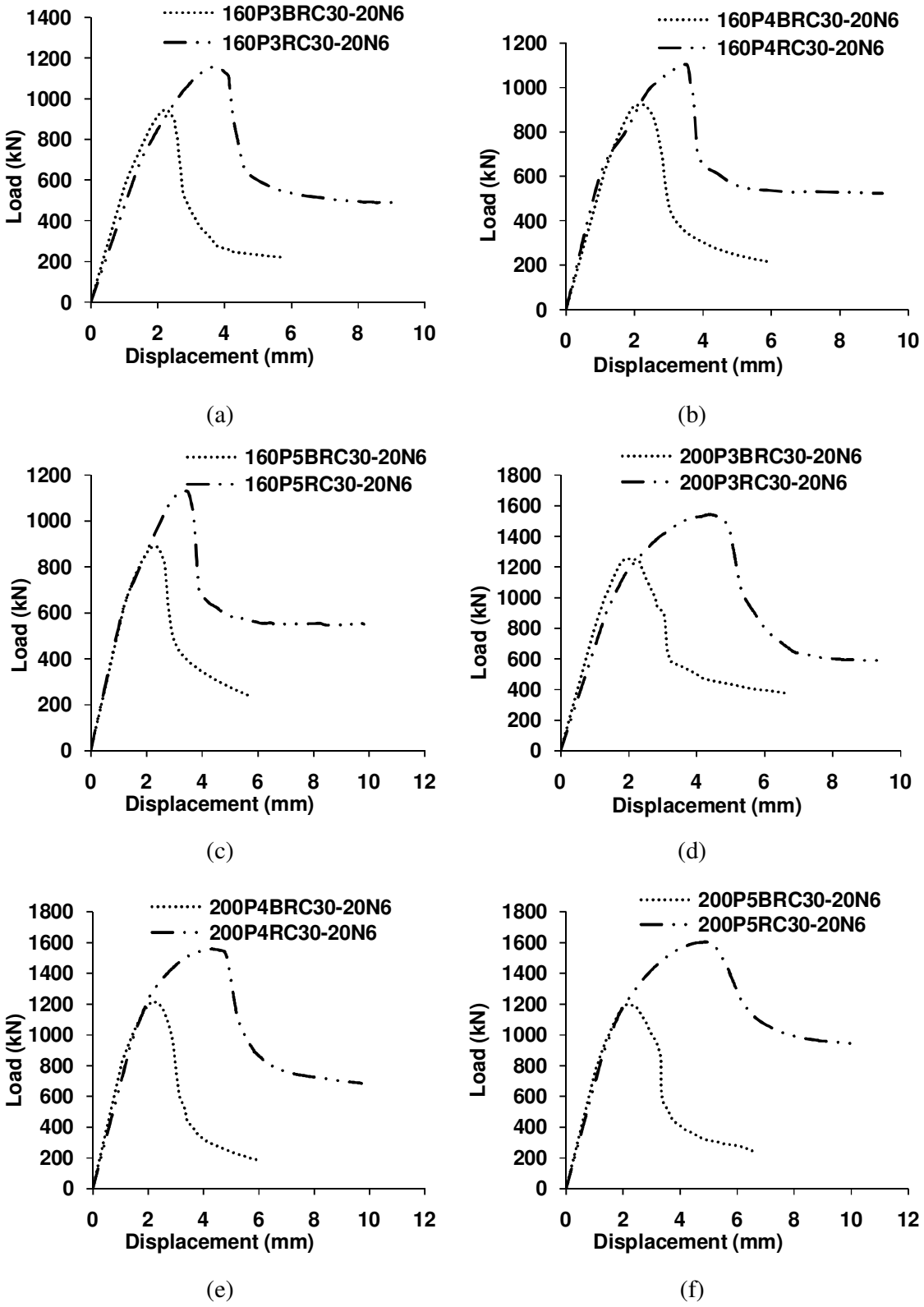

Fig. 7.8 (a-r) Comparison of load-displacement curves of RCFUT and bare RCC specimens submerged in sea water

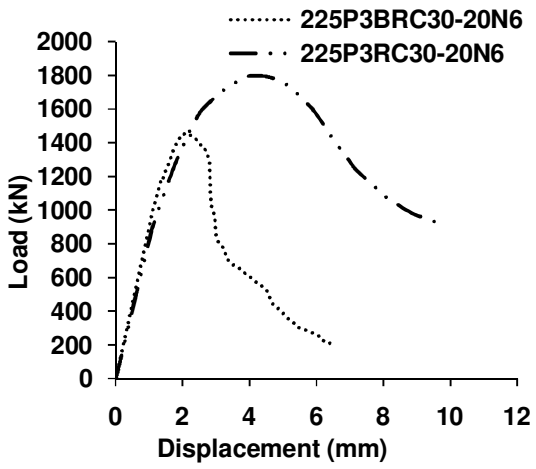

(g)

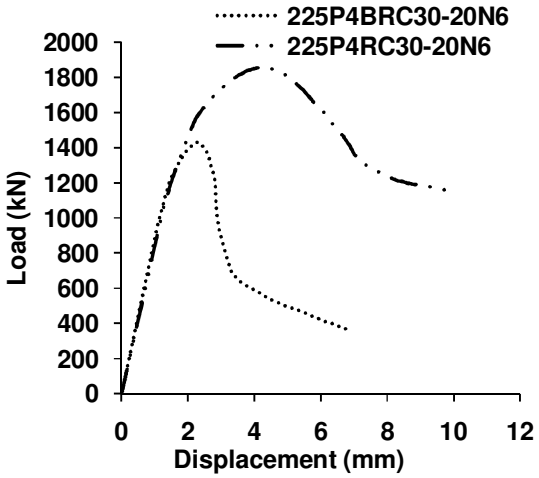

(h)

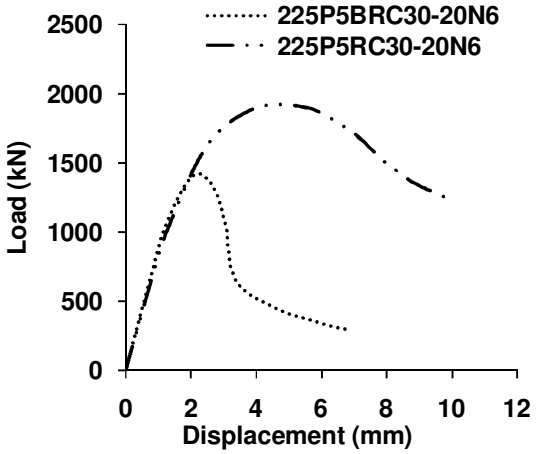

(i)

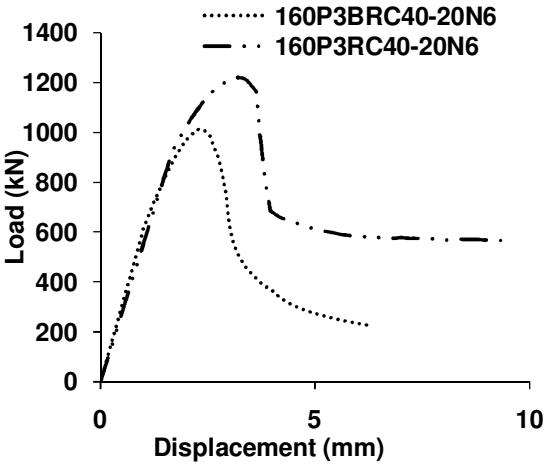

(j)

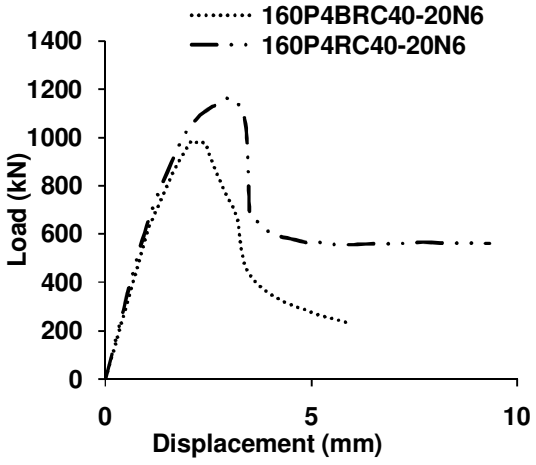

(k)

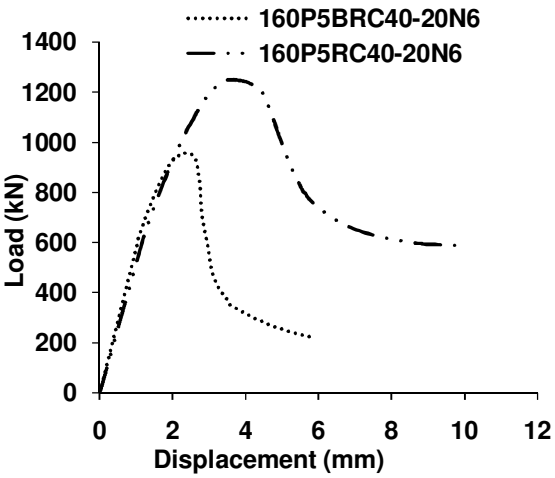

(l)

Fig. 7.8 (a-r) Comparison of load-displacement curves of RCFUT and bare RCC specimens submerged in sea water

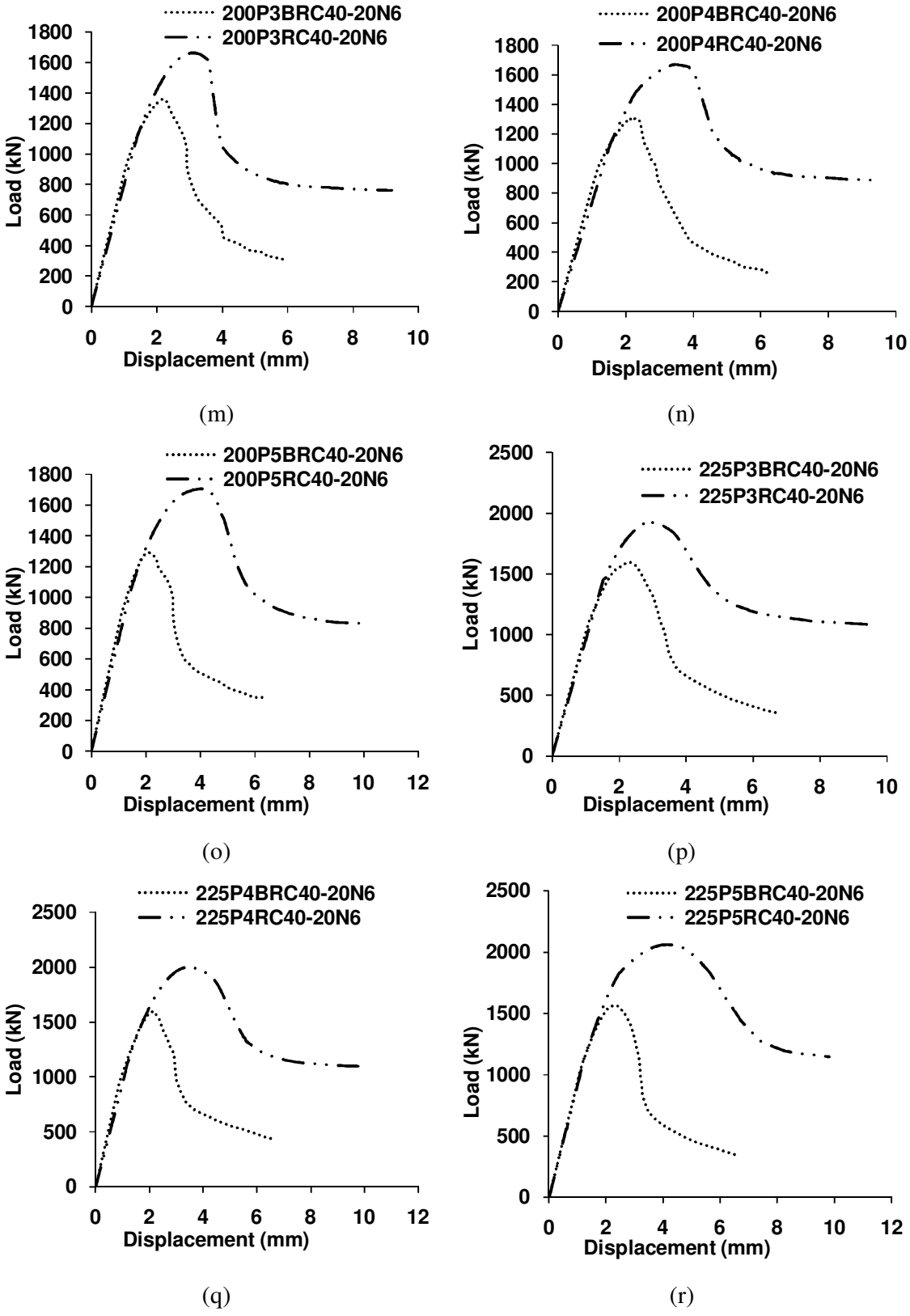

Fig. 7.8 (a-r) Comparison of load-displacement curves of RCFUT and bare RCC specimens submerged in sea water

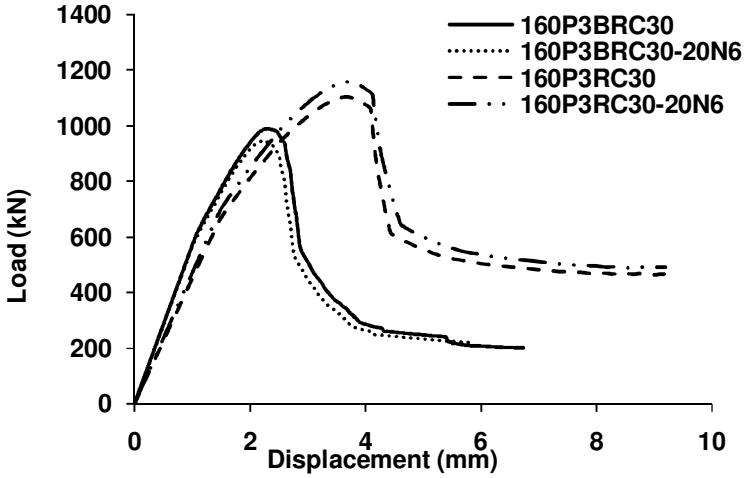

(a)

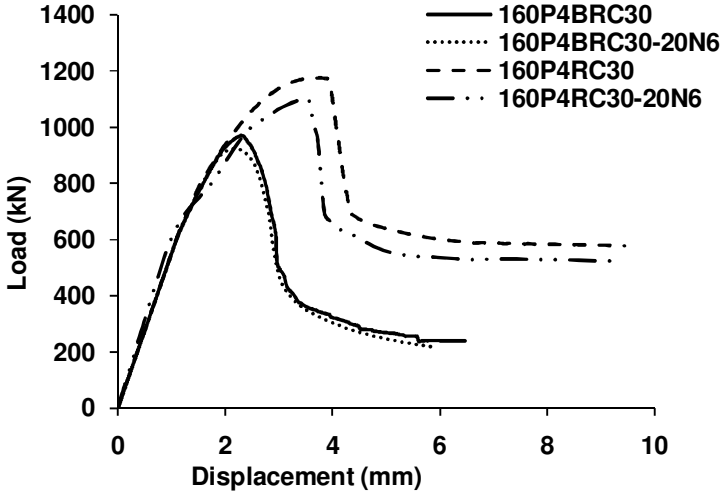

(b)

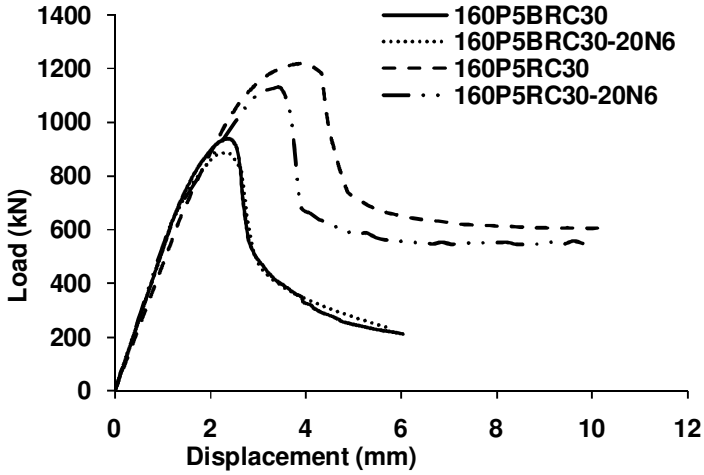

(c)

Fig. 7.9 (a-r) Comparison of load-displacement curves of RCFUT and bare RCC specimens kept in normal and sea water condition

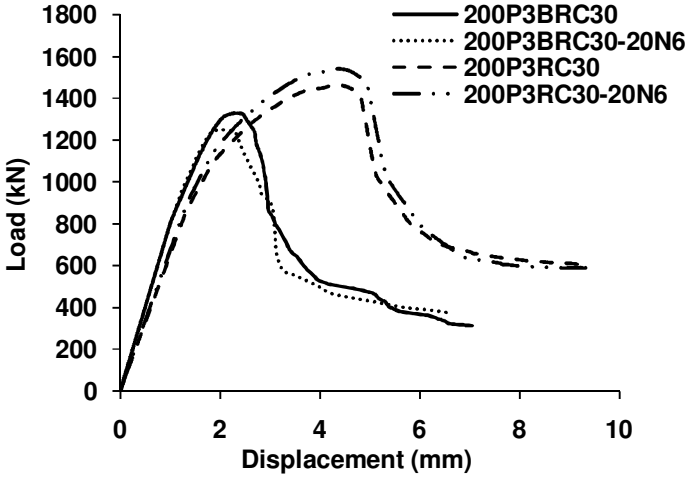

(d)

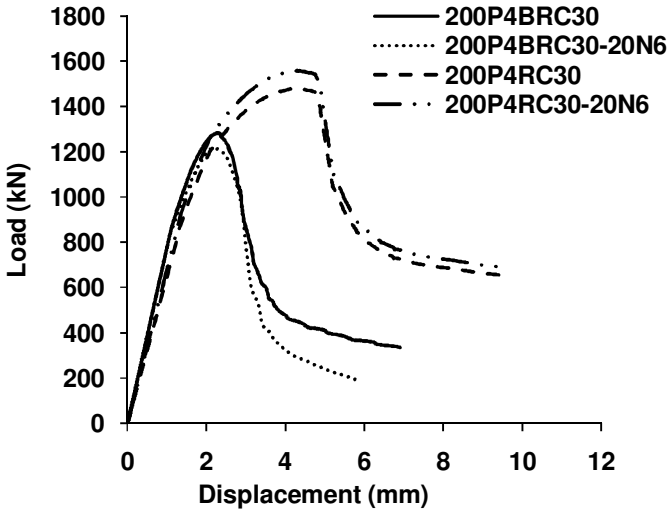

(e)

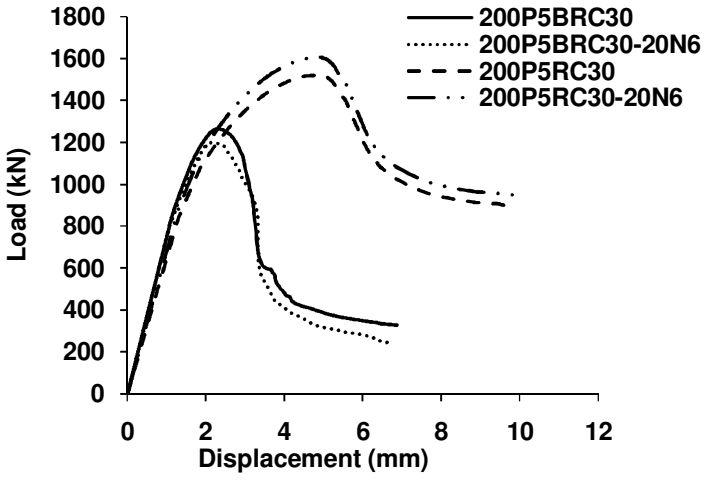

(f)

Fig.7.9 (a-r) Comparison of load-displacement curves of RCFUT and bare RCC specimens kept in normal and sea water condition

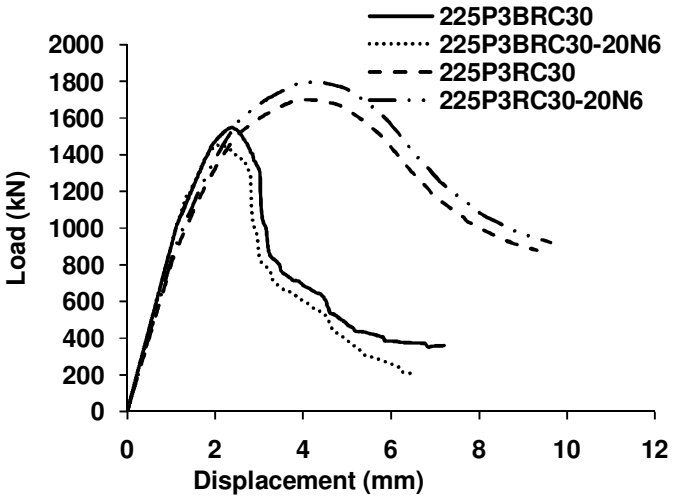

(g)

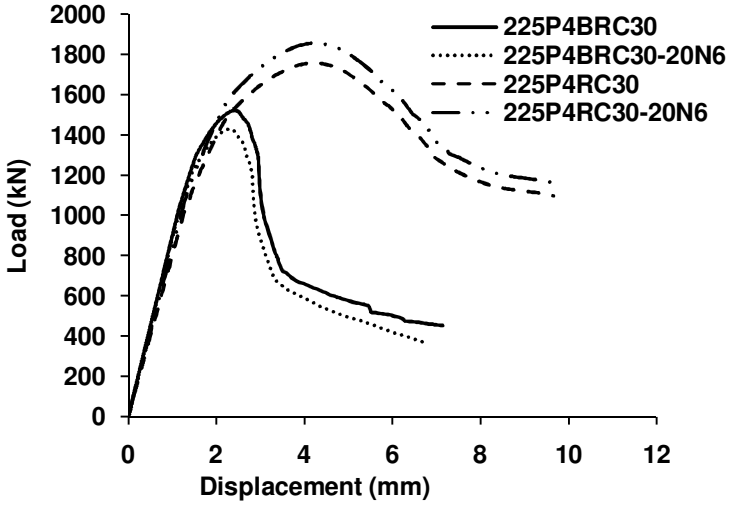

(h)

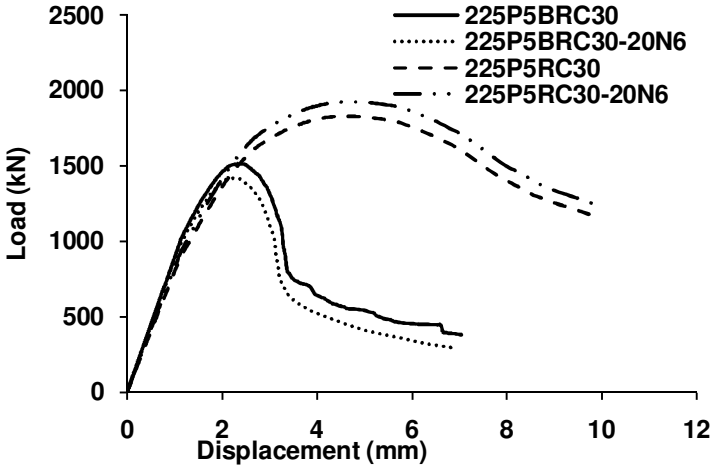

(i)

Fig.7.9 (a-r) Comparison of load-displacement curves of RCFUT and bare RCC specimens kept in normal and sea water condition

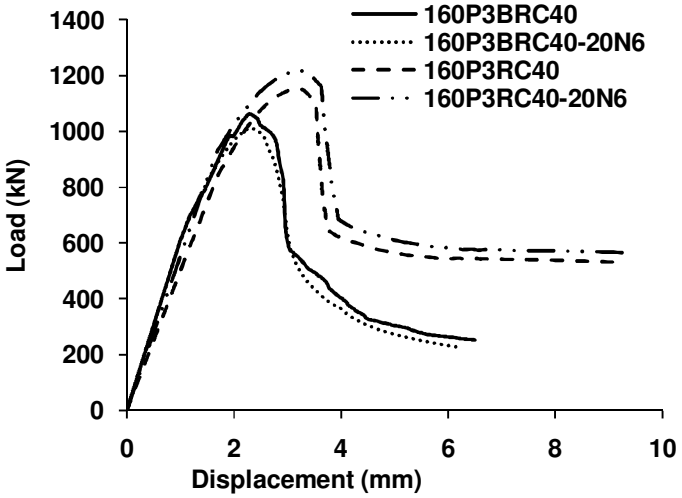

(j)

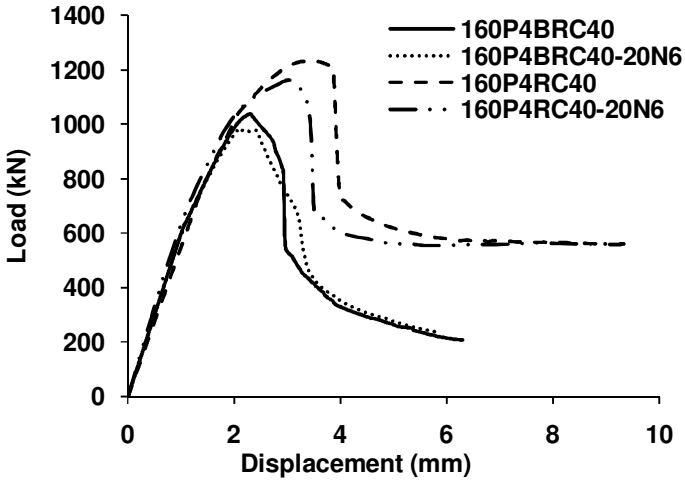

(k)

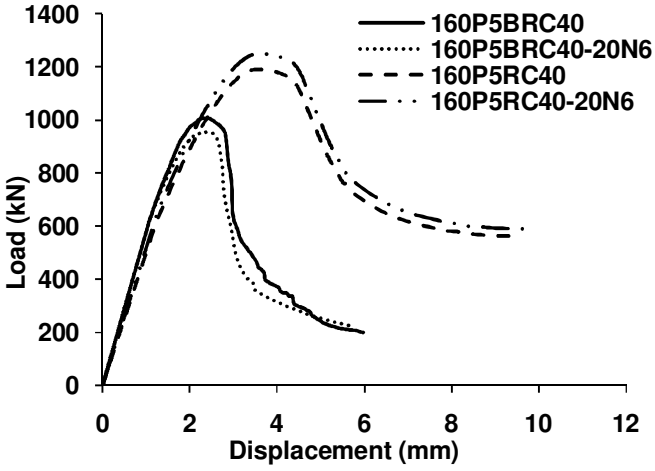

(l)

Fig.7.9 (a-r) Comparison of load-displacement curves of RCFUT and bare RCC specimens kept in normal and sea water condition

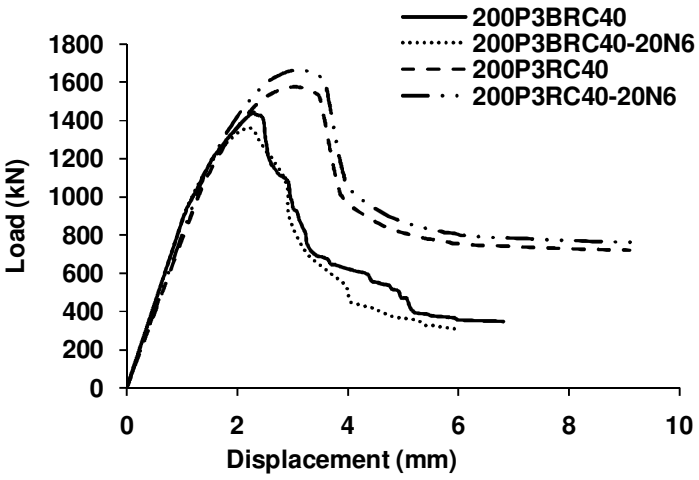

(m)

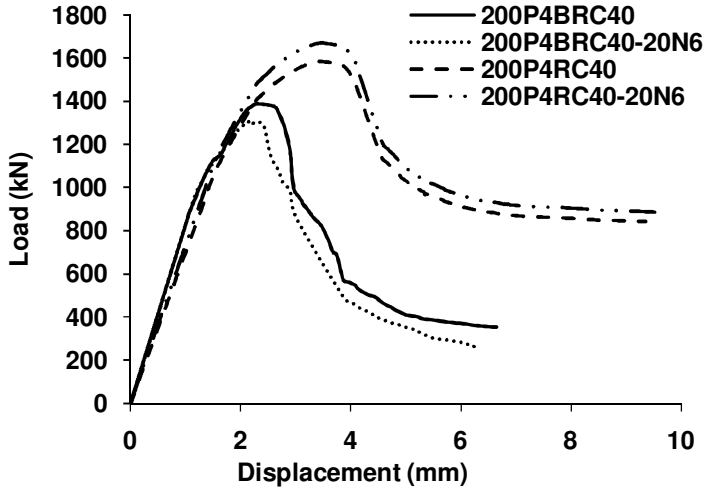

(n)

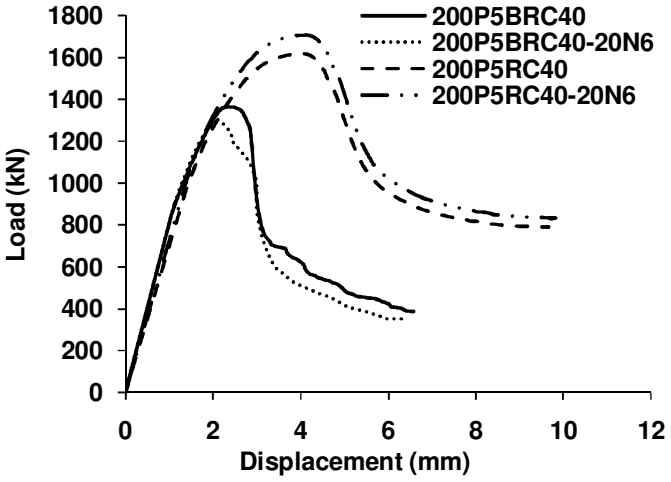

(o)

Fig.7.9(a-r) Comparison of load-displacement curves of RCFUT and bare RCC specimens kept in normal and sea water condition

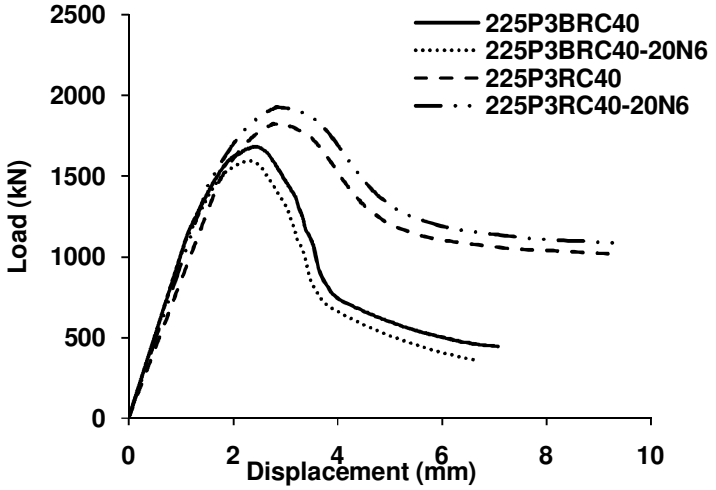

(p)

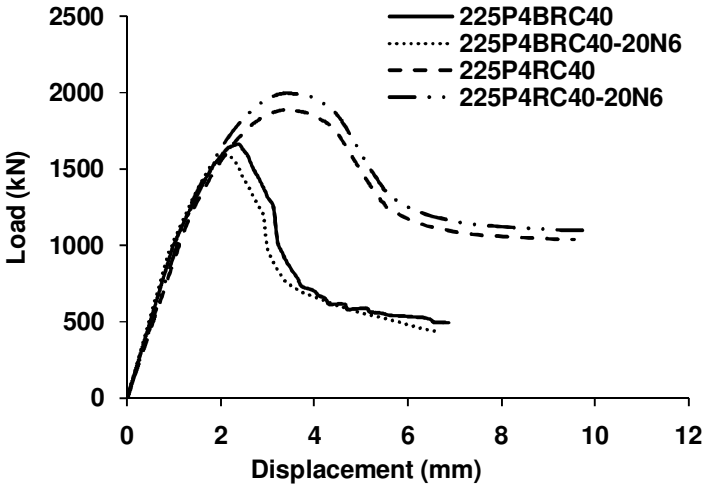

(q)

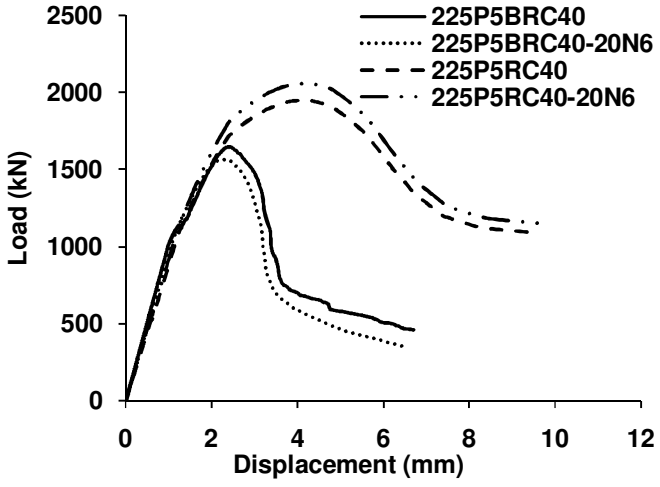

(r)

Fig. 7.9 (a-r) Comparison of load-displacement curves of RCFUT and bare RCC specimens kept in normal and sea water condition

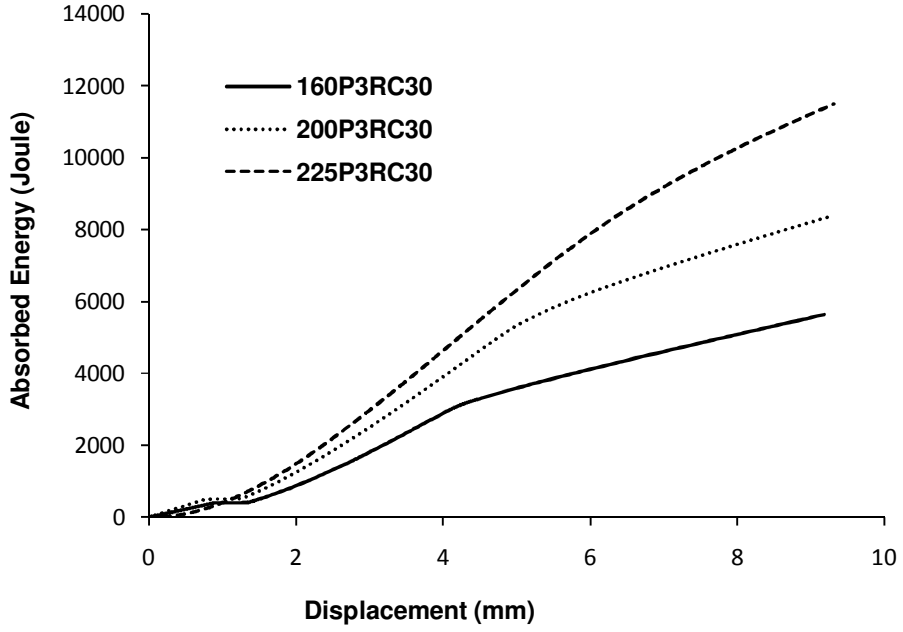

(a)

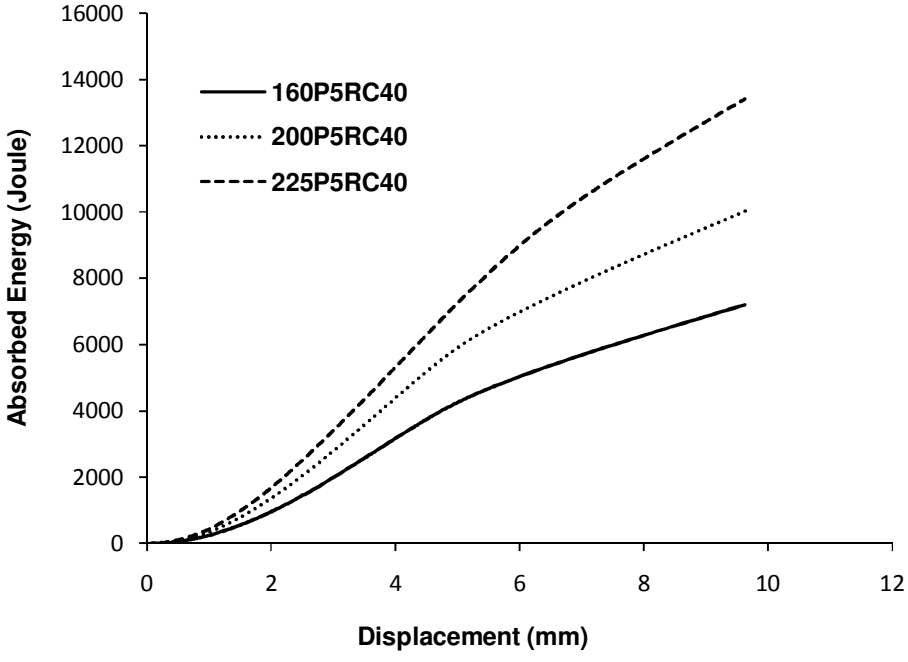

(b)

Fig.7.10 (a-b) Comparison of energy-displacement curves of RCFUT specimens with different diameter of same class of tubes

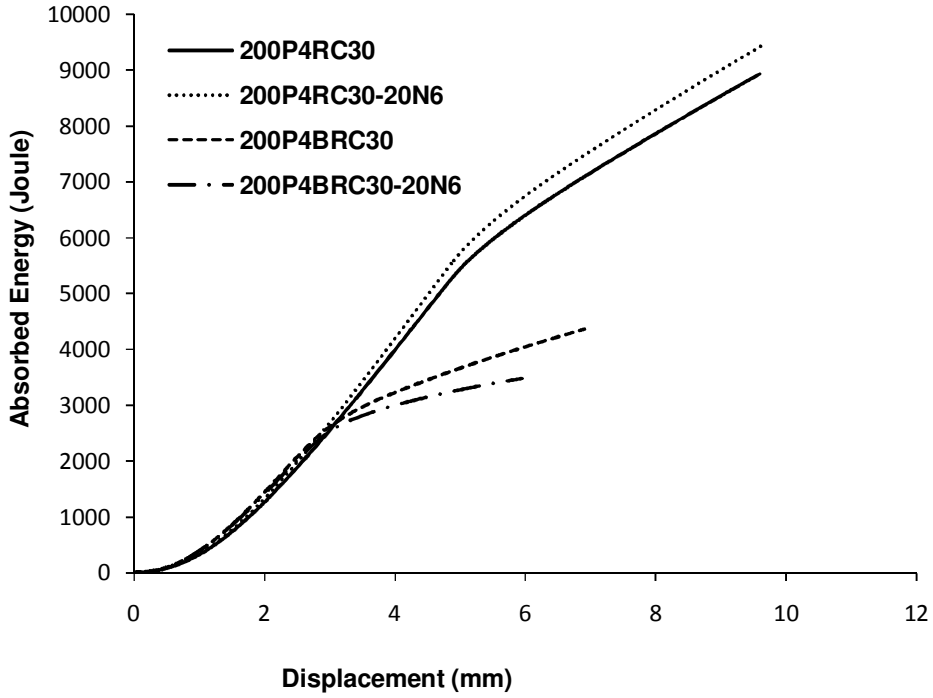

(a)

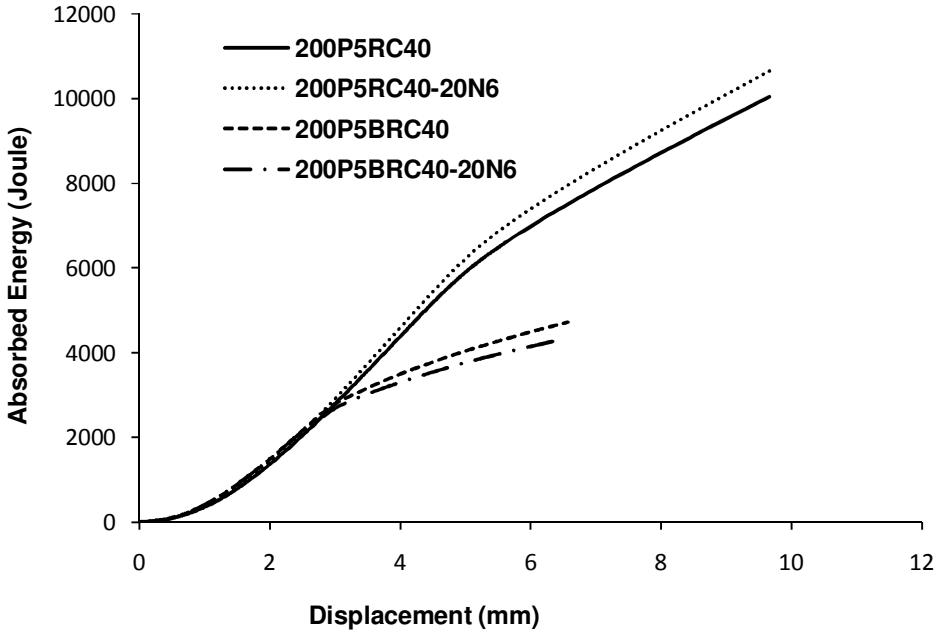

(b)

Fig. 7.11 (a-b) Comparison of energy-displacement curves of RCFUT and bare RCC specimens

Table 7.2 Results showing ultimate load, ductility and energy absorption of bare RCC specimens and RCFUT made with UPVC pipes of class 3, 4 & 5

Specimen	Ultimate load (kN)		Axial Displacement		Ductility ratio $\mu=\Delta_{80}/\Delta_y$	Energy Absorbed (Joule)		Energy ratio $\xi=E_{80}/E_y$
	Exper-iment	Simul-ation	Δ_{80}	Δ_y		E_{80}	E_y	
160P3BRC30	992	1014	2.72	1.88	1.45	1748	949	1.84
160P3BRC30-20N6	944		2.62	1.81	1.45	1597	870	1.84
160P3RC30	1106	1089	4.18	2.76	1.51	3078	1565	1.97
160P3RC30-20N6	1160		4.25	2.77	1.53	3294	1646	2.00
160P4BRC30	970	990	2.77	1.88	1.48	1746	917	1.90
160P4BRC30-20N6	923		2.74	1.76	1.56	1692	818	2.07
160P4RC30	1122	1098	4.20	2.43	1.73	3127	1425	2.19
160P4RC30-20N6	1177		4.27	2.45	1.74	3382	1503	2.25
160P5BRC30	941	964	2.66	1.88	1.41	1610	899	1.79
160P5BRC30-20N6	889		2.73	1.79	1.52	1615	810	1.99
160P5RC30	1162	1126	4.27	2.81	1.52	3326	1678	1.98
160P5RC30-20N6	1220		4.49	2.83	1.59	3727	1776	2.10
200P3BRC30	1331	1376	2.87	1.80	1.60	2588	1214	2.13
200P3BRC30-20N6	1251		2.77	1.63	1.69	2381	1030	2.31
200P3RC30	1462	1428	5.00	2.66	1.88	5333	2061	2.59
200P3RC30-20N6	1545		5.14	2.71	1.90	5805	2221	2.61
200P4BRC30	1284	1326	2.84	1.76	1.61	2476	1150	2.15
200P4BRC30-20N6	1219		2.87	1.69	1.70	2420	1060	2.28
200P4RC30	1480	1443	5.06	2.61	1.94	5521	2036	2.71
200P4RC30-20N6	1560		5.08	2.63	1.93	5840	2154	2.71
200P5BRC30	1262	1306	3.07	1.79	1.71	2727	1159	2.35
200P5BRC30-20N6	1199		3.15	1.71	1.84	2662	1038	2.56
200P5RC30	1522	1489	5.97	2.86	2.09	6792	2318	2.93
200P5RC30-20N6	1605		5.99	2.88	2.08	7192	2455	2.93
225P3BRC30	1549	1610	3.02	1.86	1.62	3190	1464	2.18
225P3BRC30-20N6	1454		2.81	1.70	1.66	2820	1261	2.24
225P3RC30	1701	1679	6.26	2.56	2.45	8246	2269	3.63
225P3RC30-20N6	1796		6.42	2.62	2.45	8928	2457	3.63
225P4BRC30	1526	1585	2.97	1.80	1.65	3113	1419	2.19
225P4BRC30-20N6	1432		2.82	1.71	1.64	2785	1256	2.22

225P4RC30	1759	1757	6.51	2.56	2.54	8905	2371	3.76
225P4RC30-20N6	1858		6.56	2.58	2.54	9473	2522	3.76
225P5BRC30	1516	1576	3.12	1.81	1.72	3293	1407	2.34
225P5BRC30-20N6	1420		2.97	1.73	1.72	2937	1256	2.34
225P5RC30	1830	1831	7.63	2.76	2.76	11091	2671	4.15
225P5RC30-20N6	1924		7.80	2.81	2.78	11859	2832	4.19
160P3BRC40	1064	1088	2.88	1.91	1.50	2016	1037	1.94
160P3BRC40-20N6	1012		2.86	1.81	1.58	1950	931	2.09
160P3RC40	1154	1129	3.59	2.44	1.47	2722	1443	1.89
160P3RC40-20N6	1220		3.73	2.35	1.59	3094	1470	2.10
160P4BRC40	1038	1062	2.9	1.89	1.54	1994	990	2.01
160P4BRC40-20N6	985		2.86	1.77	1.61	1897	876	2.17
160P4RC40	1175	1160	3.75	2.32	1.61	3024	1363	2.22
160P4RC40-20N6	1234		3.9	2.44	1.60	3310	1550	2.14
160P5BRC40	1007	1031	2.92	1.84	1.59	1995	930	2.15
160P5BRC40-20N6	956		2.76	1.77	1.56	1787	873	2.05
160P5RC40	1190	1158	4.91	2.67	1.84	4180	1624	2.57
160P5RC40-20N6	1250		4.97	2.70	1.84	4439	1747	2.54
200P3BRC40	1443	1489	2.66	1.82	1.46	2484	1342	1.85
200P3BRC40-20N6	1361		2.64	1.68	1.57	2418	1170	2.07
200P3RC40	1578	1530	3.66	2.20	1.67	4016	1758	2.28
200P3RC40-20N6	1664		3.76	2.25	1.67	4346	1920	2.26
200P4BRC40	1390	1433	2.91	1.83	1.59	2750	1292	2.13
200P4BRC40-20N6	1306		2.55	1.69	1.51	2218	1137	1.95
200P4RC40	1585	1561	4.37	2.45	1.79	4915	1992	2.47
200P4RC40-20N6	1672		4.39	2.46	1.78	5212	2113	2.47
200P5BRC40	1367	1411	2.91	1.83	1.59	2704	1277	2.12
200P5BRC40-20N6	1294		2.95	1.69	1.75	2632	1120	2.35
200P5RC40	1619	1598	5.00	2.58	1.93	5907	2183	2.71
200P5RC40-20N6	1709		5.08	2.63	1.93	6339	2342	2.71
225P3BRC40	1684	1749	3.21	1.78	1.80	3815	1530	2.49
225P3BRC40-20N6	1599		3.06	1.70	1.80	3451	1401	2.46
225P3RC40	1825	1816	4.13	2.23	1.86	5353	2067	2.59
225P3RC40-20N6	1929		4.33	2.16	2.00	6090	2138	2.85
225P4BRC40	1666	1722	2.97	1.81	1.64	3358	1543	2.18
225P4BRC40-20N6	1596		2.77	1.65	1.68	3015	1345	2.24

225P4RC40	1890	1878	4.94	2.35	2.10	6950	2296	3.03
225P4RC40-20N6	1999		5.00	2.38	2.10	7438	2458	3.03
225P5BRC40	1647	1711	3.18	1.88	1.69	3614	1572	2.30
225P5BRC40-20N6	1565		3.03	1.76	1.72	3304	1412	2.34
225P5RC40	1950	1944	6.05	2.55	2.38	9067	2566	3.53
225P5RC40-20N6	2060		6.1	2.57	2.37	9672	2737	3.53

Note: 160P3RC30 represents the specimen composed of 160 mm dia. UPVC tube of class 3 (nominal pressure of 0.6 MPa) filled with reinforced concrete of grade M30. 160P3BRC30-20N6 represents the bare reinforced concrete specimens obtained by removing the tube from the specimen 160P3RC30.

160P3BRC30-20N6 represents the specimen 160P3RC30 which was submerged in sea water of concentration 20N for 6 months. Similarly other specimens represent the RCFUT and bare reinforced concrete cylinder.

7.5 CONCLUSIONS

The findings of the experimental and numerical study conducted on RCFUT and bare RCC provide an alternate way for the protection of concrete against the attack of salts present in sea water with additional benefit of confinement and ductility. On the basis of results obtained from the testing of RCFUT and bare RCC specimens, following points can be concluded.

1. It was found that concrete showed an increment in strength, ductility and energy absorption capacity when UPVC tube was used to confine reinforced concrete column. The strength RCFUT was recorded 1.08 to 1.23 higher than RCC. The energy absorbed by RCFUT is about 1.91 to 3.37 times that of bare RCC.
2. When the specimens were tested after six months of submergence in sea water, it was found that the strength of RCFUT specimens were 1.2 to 1.37 times that of RCC column specimens. The energy absorbed by RCFUT is about 2.06 to 4.03 times that of bare RCC.
3. The diameter to thickness ratio of tube affects the post peak behavior of curve; Absolute value of the slope of the curve decreases with increases in thickness of pipe with same outer diameter.
4. The failure of RCC specimens occurred due to the crushing of concrete between the stirrups at the top or bottom portion of specimen. The failure of RCFUT specimens

occurred with the crushing of concrete and bulging of tube near the top/bottom portion of specimens showing a ductile-brittle failure.

5. There was an increase (4.88 to 5.76%) in the compressive strength of RCFUT submerged in sea water when tested at six months compared to RCFUT tested at 28 days. This may be due to gain in strength by concrete in six months (Table 2). Reduction in the strength of bare RCC specimens was observed from 4.2 to 6.16 % when submerged in sea water for six months. There was no significant change in the mode of failure and ductility of RCFUT specimens.
6. In composite column like RCFUT, outer tube may work as a wall between concrete and aggressive environment. UPVC tubes used in composite column (RCFUT column) may protect the column from corrosion of steel embedded and degradation of concrete against the attack of salts presents in sea water. Moreover, UPVC tubes may work as a weather proof jacket to the concrete during the whole year.

CHAPTER-8

REINFORCED CONCRETE FILLED UPVC TUBE (RCFUT) OF MINIMUM THICKNESS EXPOSED TO SEA WATER

8.1 GENERAL

In previous chapters, behaviour of plain concrete filled UPVC tubes (PCFUT), reinforced concrete filled UPVC tubes (RCFUT) and bare reinforced concrete columns (RCC) have been discussed. From their results, it is clear that plain concrete filled tubes enhance strength and ductility of concrete core. But to further increase the strength and ductility, it is advisable to provide longitudinal reinforcement. When RCFUT specimens made with UPVC tubes of class 3, 4 and 5 were exposed to sea water of salt concentration 20N for duration of six months, no significant decrease in strength and ductility was observed. It is clear from studies covered in previous chapters that UPVC may protect concrete core from the attack of salts present in sea water. It was realised that UPVC tubes with minimum thickness may also protect reinforced concrete exposed to sea water. Therefore, in this chapter experiments are conducted to see the effect of sea water on reinforced concrete filled UPVC tube (RCFUT) of minimum thickness (i.e. UPVC tube of class-1, nominal pressure 0.25 MPa). The specimens are submerged in sea water of different salt concentration (i.e. 10N, 15N, 20N) for different durations (i.e. 3 months, 6 months and 9 months). Compressive strength, ductility, and modes of failure of reinforced concrete filled in UPVC tubes of class-1 are obtained from experimental data. A line diagram for study program is shown in Fig. 8.1.

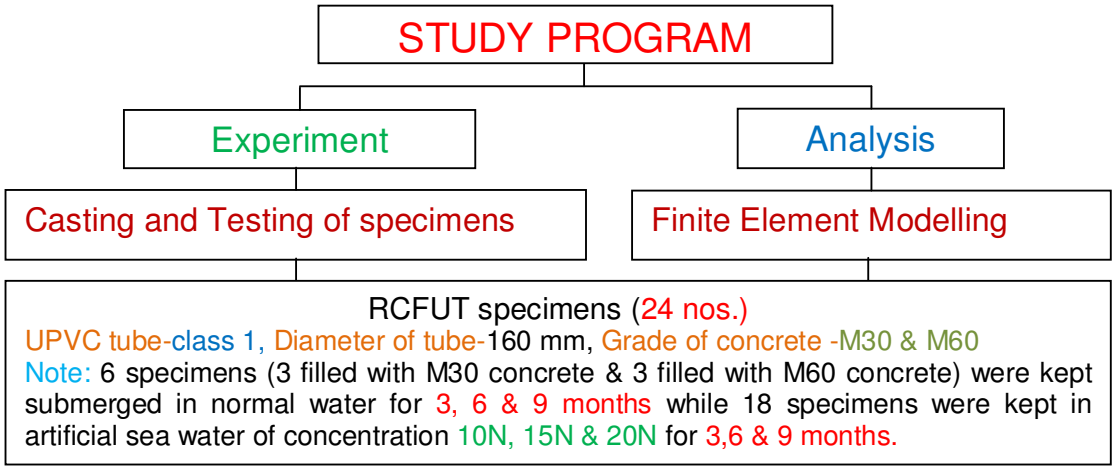

Fig. 8.1 Line diagram for study program of RCFUT made with UPVC pipes of class-1

8.2 CASTING AND TESTING OF SPECIMENS

In second stage of experiments, total twenty four RCFUT column specimens were cast by filling the reinforced concrete in UPVC tube of class-1 (nominal pressure of 0.25 MPa). For casting of specimens, UPVC pipes of diameters of 160 mm and wall thickness 2.3 mm were taken. Length of specimens was kept 800 mm. M30 and M60 grades of concrete were prepared to fill the tubes. 6-12ϕ bars were used as main reinforcement and 8ϕ bars were used for lateral ties spaced @150c/c as transverse reinforcement. Clear cover was taken as 12 mm. Plastic sheets were pasted at top and bottom of specimens and then tightly covered with thick polyethylene before submerging in water. 18 RCFUT specimens were kept completely submerged in artificial sea water of salt concentration 10N, 15N and 20N over the period of 3 months, 6 months and 9 months while 6 specimens were submerged in normal water (0N) for 3, 6 and 9 months. Water tanks of 1000 litre capacity containing sea water of different concentrations were used to keep the specimens for the desired time period. To avoid the evaporation of water from tanks, they were sealed after keeping the specimens inside it. Specimens were tested at 3 months, 6 months and 9 months. Before testing, proper levelling of top and bottom surface of specimen was done with the help of hand grinder. All the specimens were tested by applying axial load on concrete core only. Steel platen of the size of concrete core was used to transfer the load from rigid cross head of machine to the concrete inside the tube. Table 8.1 shows the geometric and material properties of RCFUT made with class 1 UPVC pipes. Typical nomenclatures are used to designate the specimens like 160P1RC30-0N3 represents the specimen made of 160 diameter tube of class 1, filled with reinforced concrete of M30 grade, submerged in normal water for 3 months. Similarly 160P1RC60-10N3 represents the specimen made of 160 diameter tube of class 1, filled with reinforced concrete of M60 grade, submerged in sea water of 10N concentration for 3 months. Other specimens are designated in the same manner.

8.3 NUMERICAL MODELING AND SIMULATION

To simulate the axial compression of reinforced concrete filled in UPVC tube of class-1, Finite element modeling was done in the same manner as RCFUT specimens made with UPVC tubes of class 3, 4 and 5 were modelled (discussed in chapter 7). The specimens exposed to normal environment were modeled with software ANSYS. A three dimensional eight node solid element 'SOLID 65' was used to model the concrete core. Eight node solid element SOLID 45 was used to model UPVC tube. The main reinforcement and lateral ties were modeled by the link element 'LINK8'. Coefficient of friction was taken equal to 0.2. The contact was defined as a surface to surface contact.

Table 8.1 Geometrical and material properties of RCFUT made with class 1 UPVC pipes

Specimen	Dimensions (mm)			Ratios		Unconfined compressive strength of concrete (f_c) (MPa)
	Mean Outer diameter (D)	Thic-kness (t)	Length (L)	D/t	L/D	
160P1RC30-0N3	160	2.3	800	69.45	5	35.08
160P1RC30-10N3	160	2.3	800	69.45	5	35.08
160P1RC30-15N3	160	2.3	800	69.45	5	35.08
160P1RC30-20N3	160	2.3	800	69.45	5	35.08
160P1RC30-0N6	160	2.3	800	69.45	5	35.08
160P1RC30-10N6	160	2.3	800	69.45	5	35.08
160P1RC30-15N6	160	2.3	800	69.45	5	35.08
160P1RC30-20N6	160	2.3	800	69.45	5	35.08
160P1RC30-0N9	160	2.3	800	69.45	5	35.08
160P1RC30-10N9	160	2.3	800	69.45	5	35.08
160P1RC30-15N9	160	2.3	800	69.45	5	35.08
160P1RC30-20N9	160	2.3	800	69.45	5	35.08
160P1RC60-0N3	160	2.3	800	69.45	5	52.38
160P1RC60-10N3	160	2.3	800	69.45	5	52.38
160P1RC60-15N3	160	2.3	800	69.45	5	52.38
160P1RC60-20N3	160	2.3	800	69.45	5	52.38
160P1RC60-0N6	160	2.3	800	69.45	5	52.38
160P1RC60-10N6	160	2.3	800	69.45	5	52.38
160P1RC60-15N6	160	2.3	800	69.45	5	52.38
160P1RC60-20N6	160	2.3	800	69.45	5	52.38
160P1RC60-0N9	160	2.3	800	69.45	5	52.38
160P1RC60-10N9	160	2.3	800	69.45	5	52.38
160P1RC60-15N9	160	2.3	800	69.45	5	52.38
160P1RC60-20N9	160	2.3	800	69.45	5	52.38

8.4 RESULTS AND DISCUSSIONS

Specimens removing out from the sea water tank after 3, 6 and 9 months were tested to investigate the effect of sea water on their load carrying capacity, ductility, and modes of failure. A Finite element model was also developed to simulate the experimental results of specimens kept in normal water. The results of experiments and simulations are presented in Table 8.2. Load-displacement curves obtained from experiments and numerical analysis were plotted in Fig. 8.2. It was found that they were in good match. The obtained load-compression variations are used to calculate the ductility, energy absorption capacity and strength of the specimens. The modes of failure of specimens were also obtained. Fig.8.3 presents the modes of failure of specimens. All the specimens were failed due to the development of the vertical multiple cracks either from bottom or top side with slight bulging of tube. Table 8.2 presents the ultimate load capacity, ductility ratio and energy absorption ratio for different specimens. The ductility ratios μ for the specimens filled with M30 grade of concrete varies between 1.39 and 1.54 and energy ratio ξ varies between 1.7 and 2.0. The value of Δ_{80} decreases with the increase of grade of concrete while value of E_{80} increases with increase of grade of concrete. It is also clear from Table 8.3 that energy absorbed (E_{80}) for the specimens filled with M30 grade of concrete varies from 1952 Joule to 2207 Joule when tested at 3, 6 and 9 months while for the specimens filled with M60 grade of concrete, it varies from 2376 Joule to 2698 Joule when tested at 3, 6 and 9 months. The variation in the load carrying capacity of specimens submerged in sea water and in normal water is within ± 3.5% therefore it may be concluded that there is no significant effect of sea water on the strength of concrete filled in the lowest category of pipe (class 1). For the specimens filled with M60 grade of concrete, there is a sudden drop in the load-displacement curve just after the peak. There is an enhancement in the strength of specimens tested at 6 and 9 months compared to tested at 3 months. This may be due to the increment in concrete strength with time. Some curves are plotted to see the effect of concentration of sea water and duration for which the specimens were submerged in sea water on load capacity of specimens (Fig. 8.4 and Fig 8.5). It was found that there was hardly any significant change in the load capacity for different concentration of sea water and duration for which they were submerged. The energy-displacement curves for different strengths of concrete are shown in Fig. 8.6. The specimen filled with M60 grade of concrete showed higher absorbed energy compared to the specimen filled with M30 grade of concrete, which is obvious. From Fig. 8.6, it can also be seen that the absorbed energy by the specimens submerged in sea water of different concentration is same.

Table 8.2 Results showing ultimate load, ductility and energy absorption of RCFUT specimens made with UPVC pipes of class 1

Specimen	Ultimate load (kN)		Axial Displacement		Ductility ratio $\mu=\Delta_{80}/\Delta_y$	Energy Absorbed (Joule)		Energy ratio $\xi=E_{80}/E_y$
	Experi-mental	Simu-lation	Δ_{80}	Δ_y		E_{80}	E_y	
160P1RC30-0N3	1093	1087	2.98	2.04	1.46	2120	1155	1.84
160P1RC30-10N3	1127		3.14	2.08	1.51	2350	1209	1.94
160P1RC30-15N3	1070		2.85	2.05	1.39	1952	1128	1.73
160P1RC30-20N3	1058		2.95	2.00	1.48	2055	1091	1.88
160P1RC60-0N3	1390	1386	2.88	1.87	1.54	2660	1328	2.00
160P1RC60-10N3	1380		2.91	1.91	1.52	2672	1353	1.97
160P1RC60-15N3	1367		2.78	1.91	1.45	2508	1340	1.87
160P1RC60-20N3	1376		2.67	1.87	1.43	2502	1325	1.89
160P1RC30-0N6	1114	1108	3.09	2.04	1.51	2262	1159	1.95
160P1RC30-10N6	1123		2.96	2.04	1.45	2165	1173	1.85
160P1RC30-15N6	1103		2.93	2.02	1.45	2066	1146	1.80
160P1RC30-20N6	1107		2.88	2.06	1.40	2050	1171	1.75
160P1RC60-0N6	1420	1415	2.84	1.94	1.46	2621	1402	1.87
160P1RC60-10N6	1404		2.82	1.93	1.45	2516	1378	1.83
160P1RC60-15N6	1428		2.82	1.97	1.43	2588	1426	1.81
160P1RC60-20N6	1396		2.97	1.96	1.52	2704	1423	1.90
160P1RC30-0N9	1131	1125	3.12	2.19	1.43	2273	1282	1.77
160P1RC30-10N9	1125		3.08	2.21	1.40	2207	1302	1.70
160P1RC30-15N9	1136		3.17	2.17	1.46	2373	1274	1.86
160P1RC30-20N9	1119		3.18	2.17	1.46	2325	1263	1.84
160P1RC60-0N9	1439	1436	2.89	1.98	1.46	2703	1458	1.85
160P1RC60-10N9	1450		2.91	2.01	1.45	2751	1506	1.83
160P1RC60-15N9	1431		2.98	1.98	1.50	2837	1460	1.94
160P1RC60-20N9	1445		2.86	1.98	1.45	2698	1466	1.84

Note: 160P1RC30-0N3 represents the specimen composed of 160 mm dia. UPVC tube of class 1 (nominal pressure of 0.25 MPa) filled with reinforced concrete of grade M30, submerged in normal water for 3 months similarly 160P1RC60-10N3 represents the specimen composed of 160 mm dia. UPVC tube of class filled with reinforced concrete of grade M60, submerged in sea water of concentration 10N for 3 months. Other specimens are designated in the same manner.

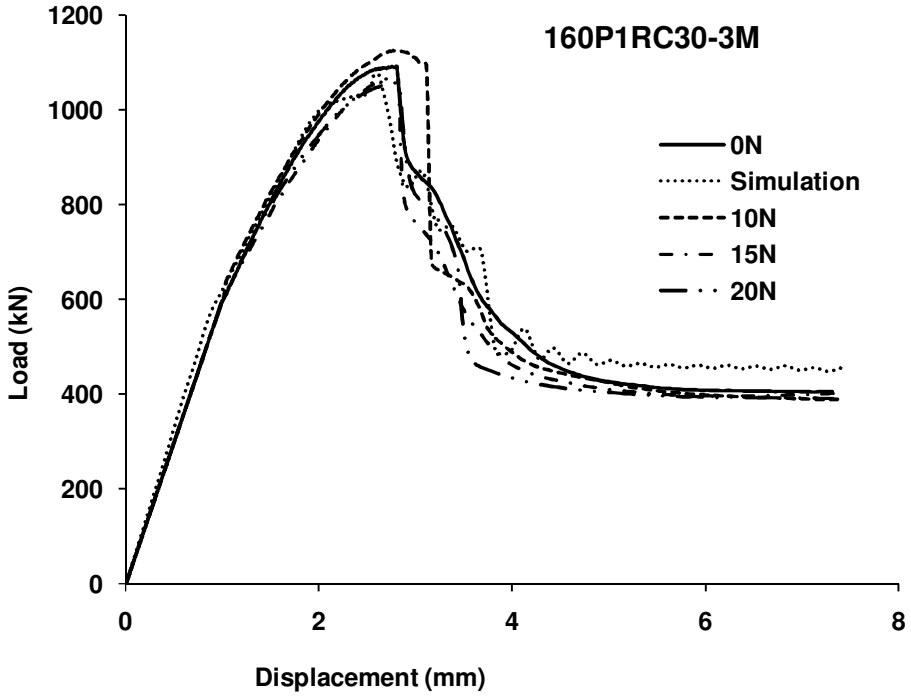

(a)

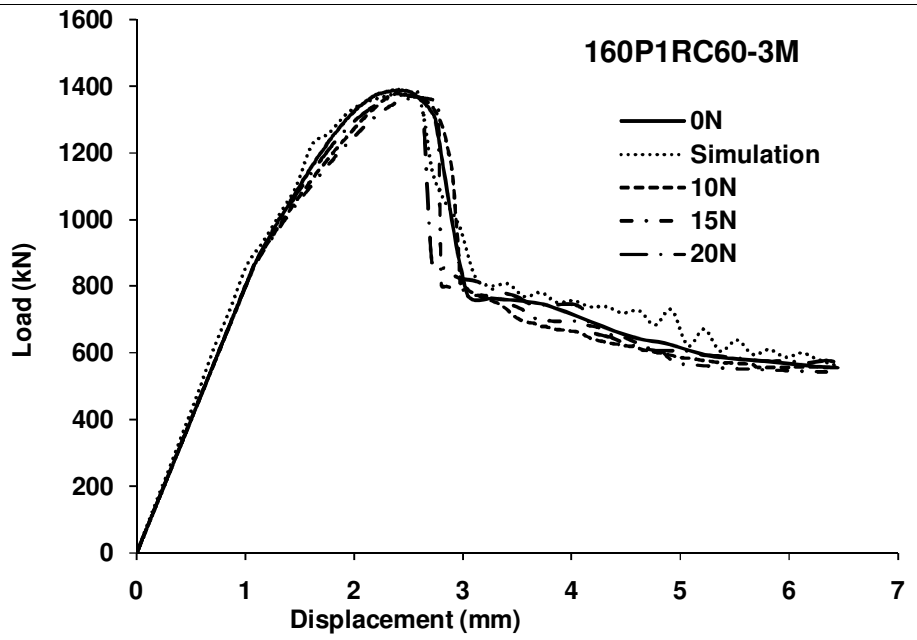

(b)

Fig. 8.2 (a-f) Comparison of load- displacement curves of RCFUT specimens made with UPVC pipes of class-1 submerged in different concentration of sea water

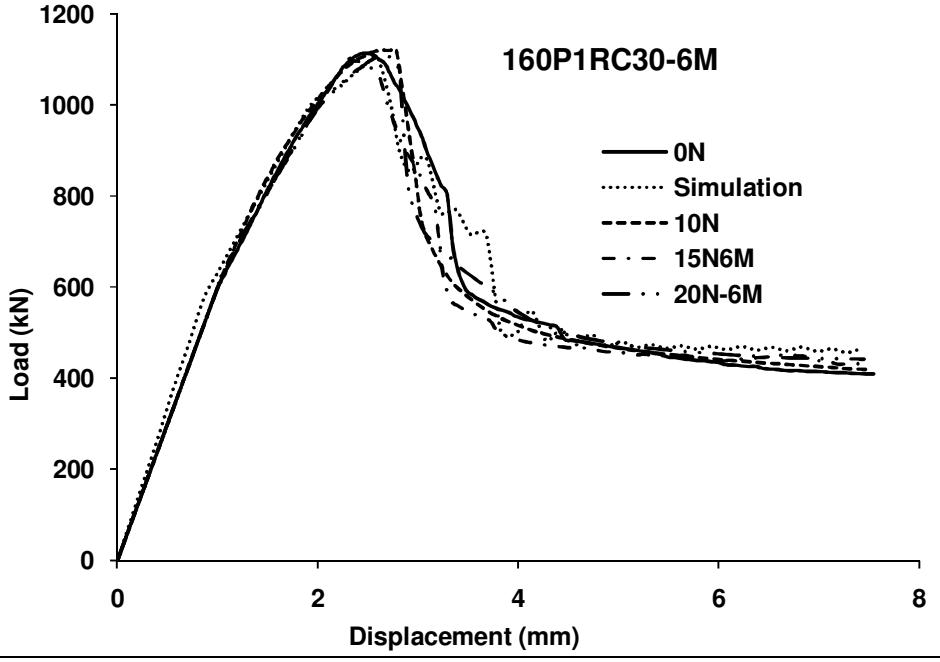

(c)

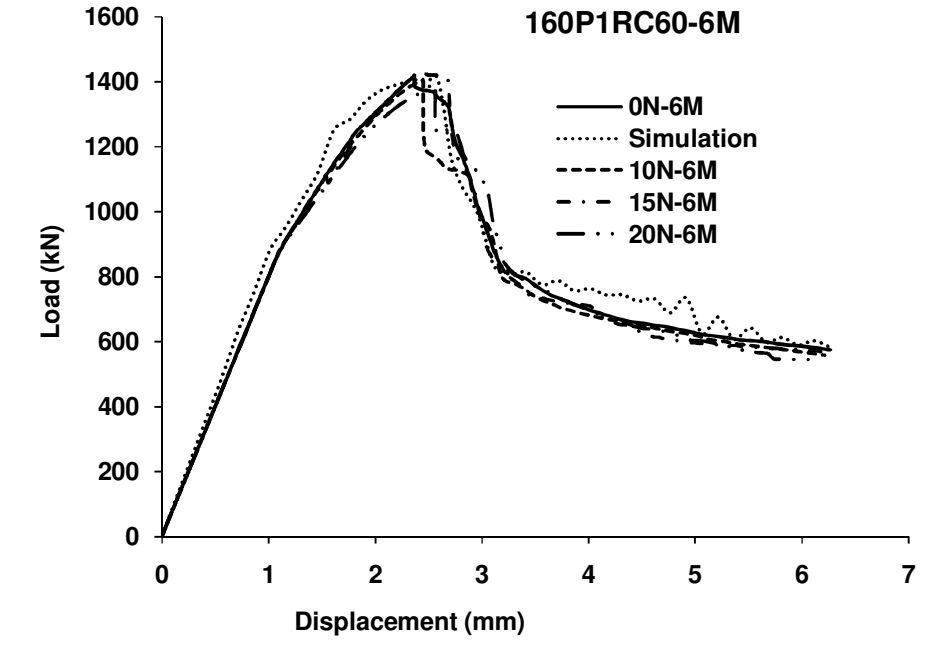

(d)

Fig. 8.2 (a-f) Comparison of load- displacement curves of RCFUT specimens made with UPVC pipes of class-1 submerged in different concentration of sea water

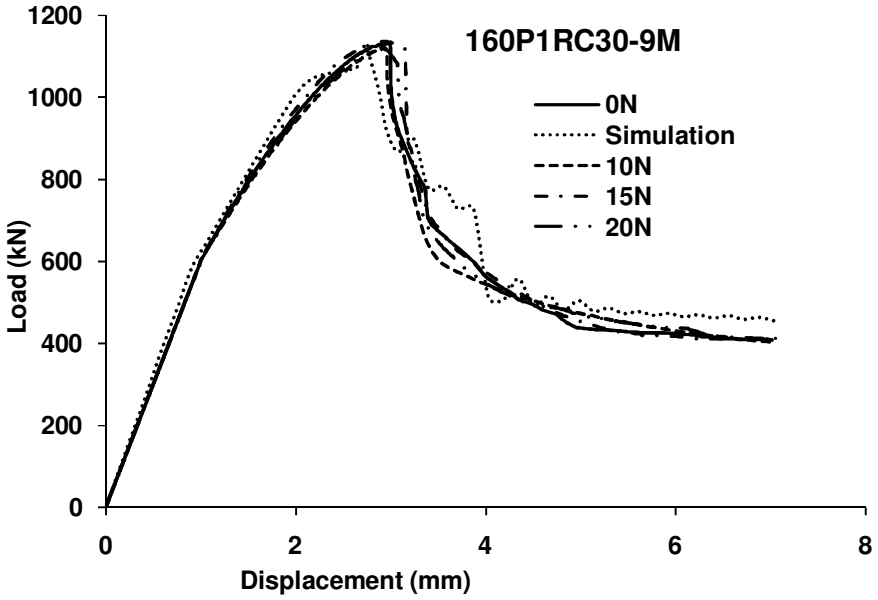

(e)

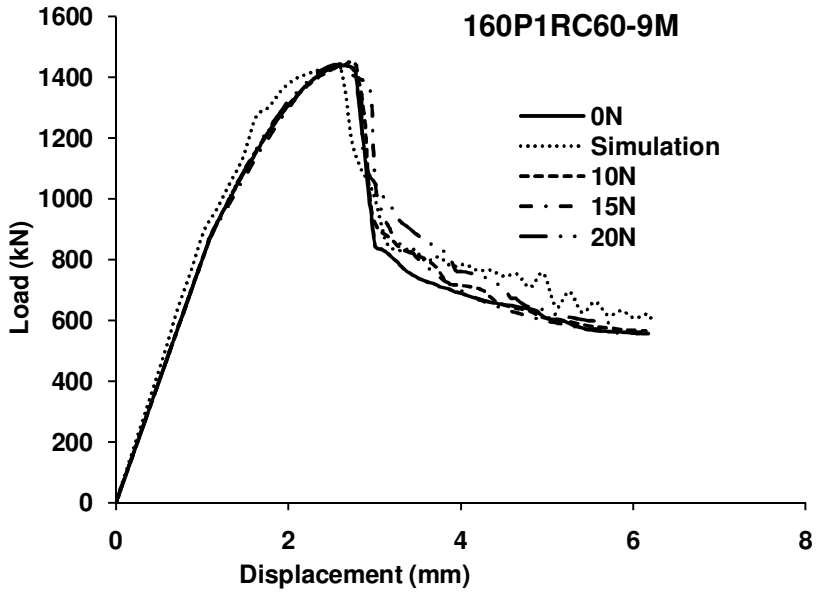

(f)

Fig. 8.2 (a-f) Comparison of load- displacement curves of RCFUT specimens made with UPVC pipes of class-1 submerged in different concentration of sea water

160P1RC30-0N3 160P1RC30-10N3 160P1RC30-15N3 160P1RC30-20N3

160P1RC60-0N3 160P1RC60-10N3 160P1RC60-15N3 160P1RC60-20N3

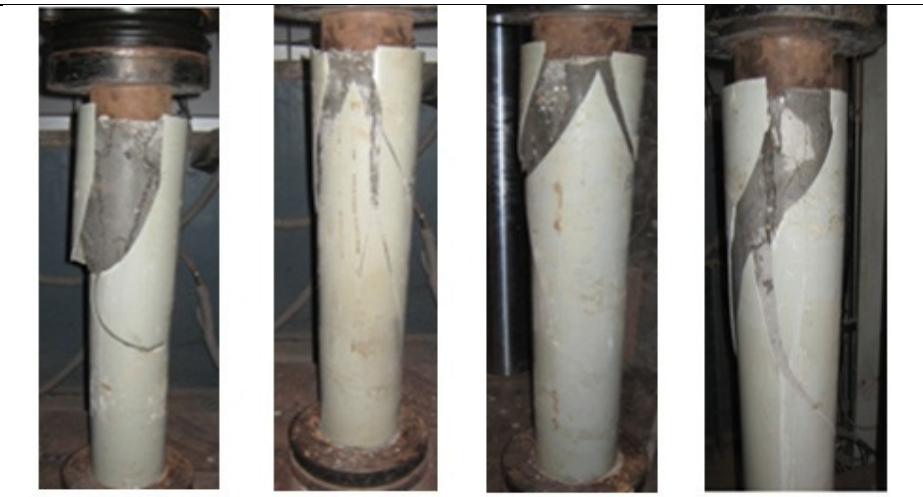

160P1RC30-0N6 160P1RC30-10N6 160P1RC30-15N6 160P1RC30-20N6

Fig. 8.3 Failure modes of RCFUT specimens made with class-1 UPVC pipes

Fig. 8.3 Failure modes of RCFUT specimens made with class-1 UPVC pipes

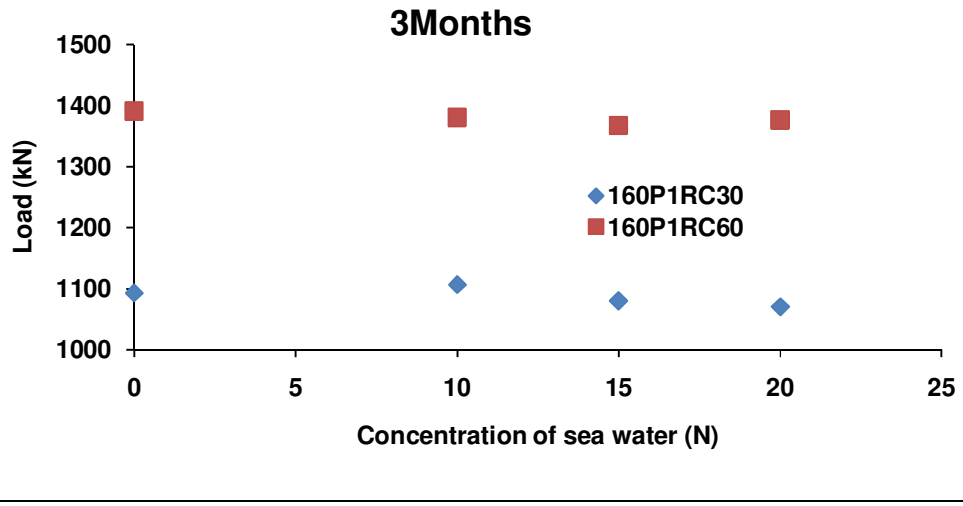

(a)

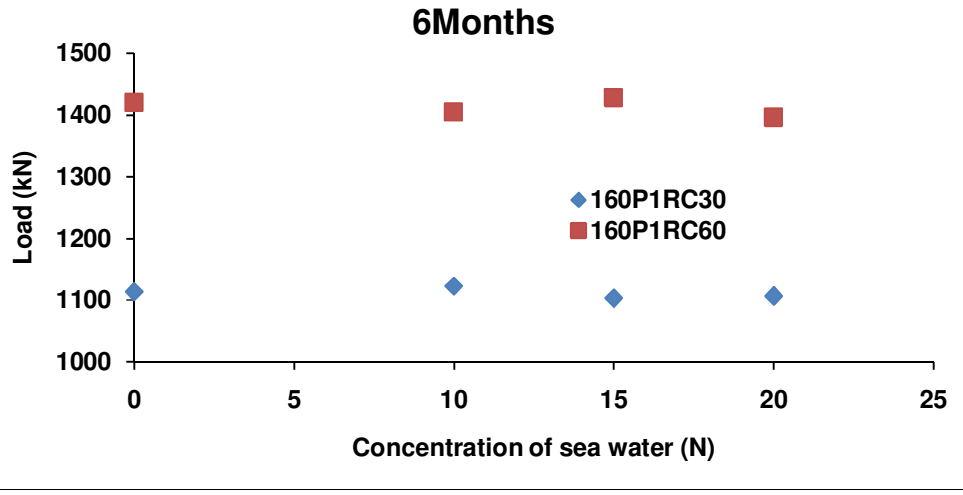

(b)

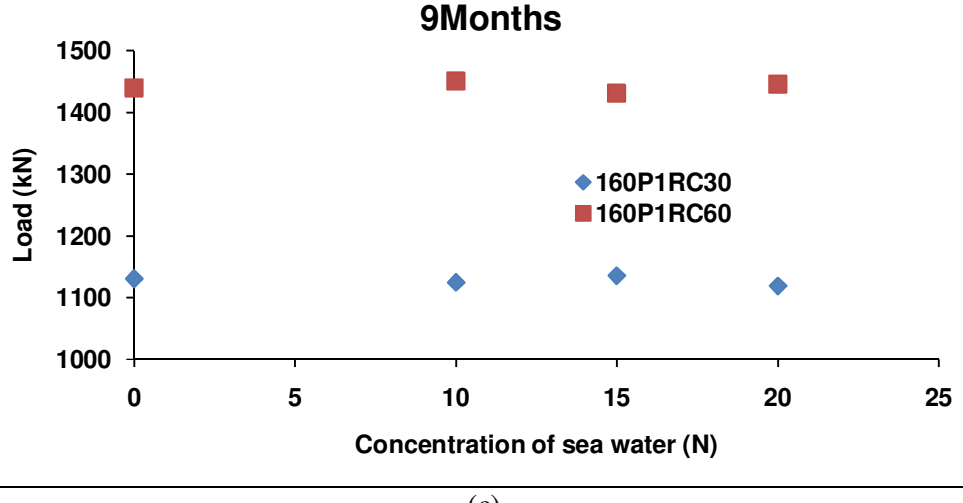

(c)

Fig. 8.4 (a-c) Load capacity of specimens versus concentration of sea water

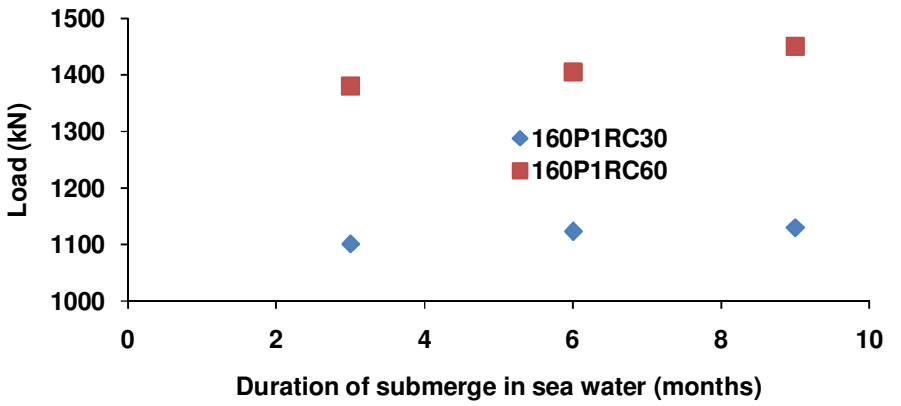

(a)

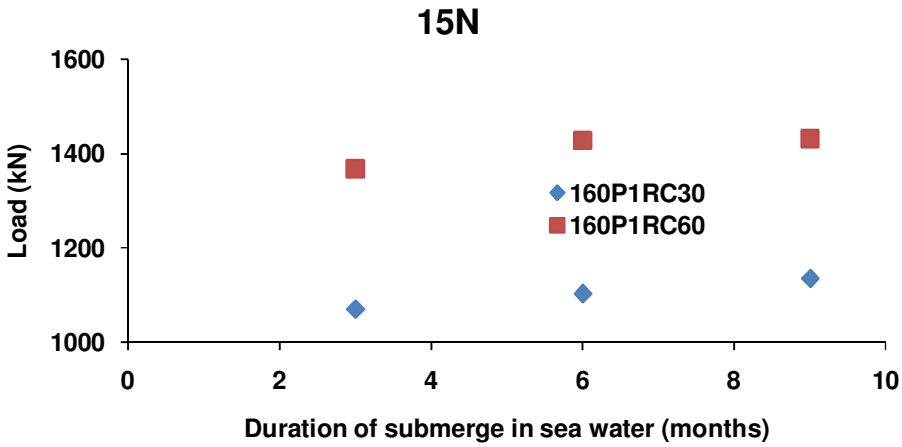

(b)

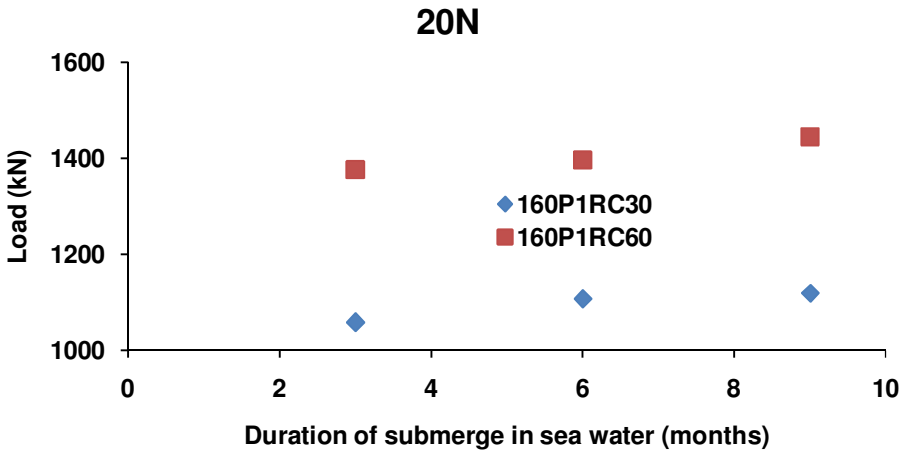

(c)

Fig. 8.5 (a-c) Load capacity of specimens versus duration of submergence in sea water

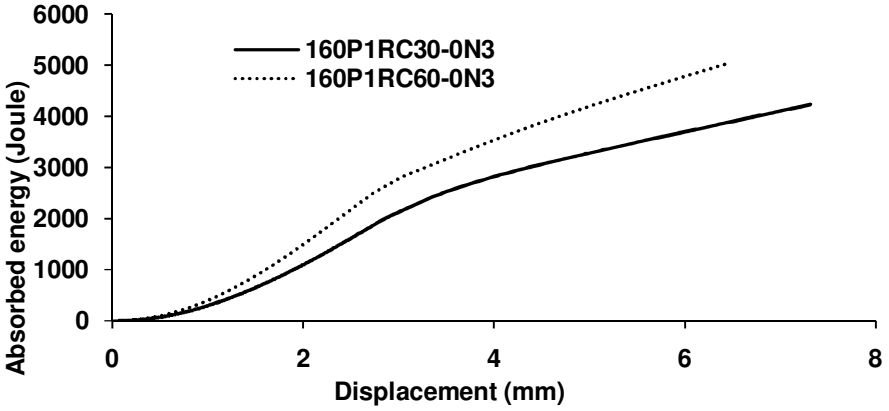

(a)

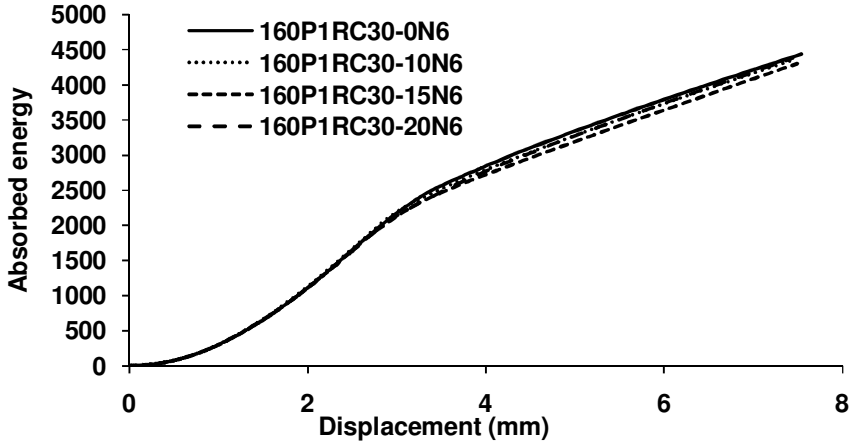

(b)

Fig. 8.6 (a-b) Energy versus displacement curves for RCFUT specimens made with class-1 UPVC pipes

8.5 CONCLUSIONS

In the second stage of experiments, on the basis of results obtained from RCFUT specimens with the use of class 1 UPVC pipes, following points can be concluded.

1. It was found that concrete showed almost equal strengths when the specimens were kept in different concentration of sea water. The maximum percentage variation in the strength was 3.2 %.

2. Slight enhancement in the load carrying capacity of specimens was noticed when tested at 3, 6 and 9 months. It may be due to the increment in the concrete strength with the passage of time.
3. The energy absorbed by the specimens filled with M30 grade of concrete varies from 1952 to 2350 Joule and for the specimens filled with M60 grade of concrete it varies from 2502 to 2837 Joule.
4. The failure of specimens occurred due to the crushing of concrete near the top or bottom portion of specimen.
5. Since there was no significant change observed in the load carrying capacity of RCFUT specimens made with class 1 UPVC pipes. Therefore it may be concluded that the UPVC pipes with minimum nominal pressure capacity can also be used as a protective layer for concrete in sea water.

CHAPTER-9

STRAIN MEASUREMENT WITH DIGITAL IMAGE CORRELATION (DIC) SYSTEM

9.1 GENERAL

Strain gauge or LVDT are used to get the strain at particular location in the test specimen, but for complex investigations, strains are required at number of location on the surface of specimen to study the behaviour of material. To provide a strain map over the entire surface of specimen, a new technology known as Digital Image Correlation (DIC) is developed. The DIC system was first introduced by a group of researchers at the University of South Carolina in 1980s (Salmanpour and Mojsilović, 2013). In this chapter, DIC system is explained and the strains obtained from analysis using DIC are compared with strains obtained from simulations. The work presented in this chapter was done after the proposed work of PhD was almost over. When author came to know about the purchase of DIC system in the Department of Civil Engineering, IIT Roorkee, he planned to cast some token specimens and tested them to get the strain maps at different stage of loading with the use of DIC system.

9.2 DIGITAL IMAGE CORRELATION TECHNIQUES

Digital image correlation (DIC) is an optical technique in which a mathematical correlation analysis is used to examine digital images taken at the time of testing of specimen (Correlated Solutions, Vic-3D v7). In this technique, a number of images are captured with digital camera during the deformation process of specimen to evaluate the change in surface characteristic of material. To apply this technique, a random speckle pattern is required on the surface of specimen. This technique starts with an image taken before loading the specimen (reference image) and then a number of images are captured during the deformation process. All the images show different speckle pattern relative to the reference image. With the help of software, all the images are analysed by correlating all the pixels of reference image and other images, and then a strain distribution map is created.

9.3 DIGITAL IMAGE CORRELATION APPARATUS

This apparatus consists of computer software and two digital cameras mounted on a tripod frame (Fig. 9.1). Two lamps are needed for the proper lighting to specimens to get good images. The digital cameras records the images during the testing of specimen and software analyse the images to calculate axial, transverse and shear strains. All the images are analysed by correlating all the pixels of reference image and other images, and then a strain distribution map is created.

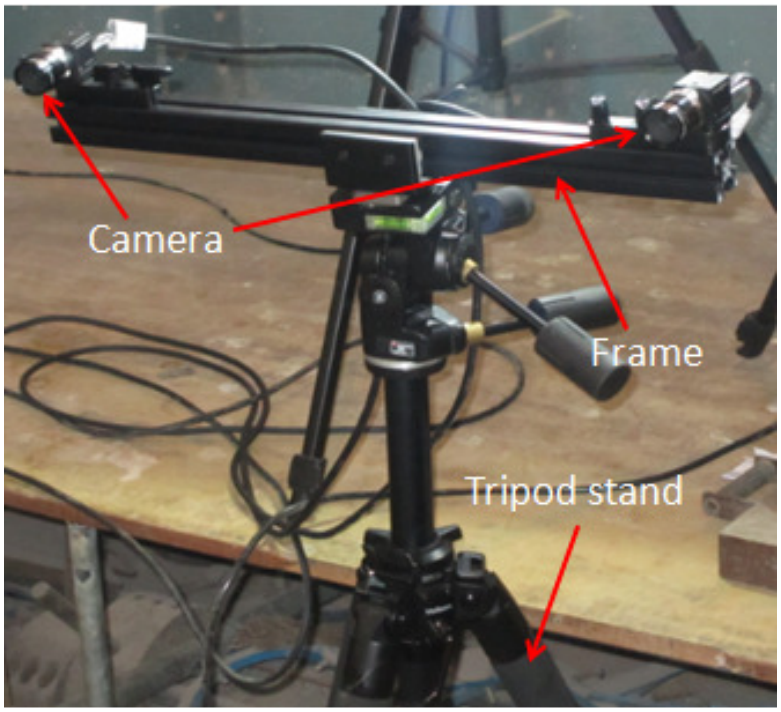

Fig. 9.1 Digital Cameras mounted on a frame with tripod

9.4 PREPARATION OF SPECIMEN AND OPERATION OF EQUIPMENT

For strain measurement using DIC system, tests were performed on some typical specimens like 160P5PC30, 200P5PC30, 225P5PC30, 160P4RC30 and 225P5BRC30 (Table 9.1). These specimens were exclusively cast after completing of proposed PhD work. The surface of specimen is to be prepared before using DIC apparatus. The speckle pattern is applied with white and black paint on the surface of specimen (Fig. 9.2). First a thin layer of white paint is applied on the surface and then black spray paint is used to create dots. There should be approximately two feet distance between specimen and spray. After the speckle pattern is created on surface, the specimen is kept for testing in universal testing machine (UTM). Now

the tripod with digital cameras is fixed in an accessible position. Focal length of lens of cameras is adjusted to acquire clear images. Two eclectic lamps are kept near the machine to provide proper lighting to the specimens. The set-up for Digital Image Correlation is shown in Fig. 9.3. Before using DIC system, stereo system is calibrated with the help of grid (size-28mm) having 14 black dots along length and 10 black dots along width (Fig. 9.4). The process of calibration is shown in Fig. 9.5.

Fig. 9.2 Spackle pattern on specimen

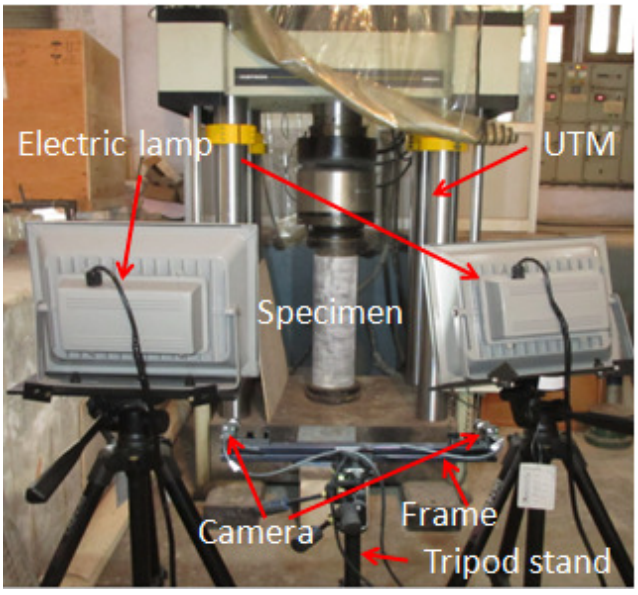

Fig. 9.3 Setup for Digital Image correlation

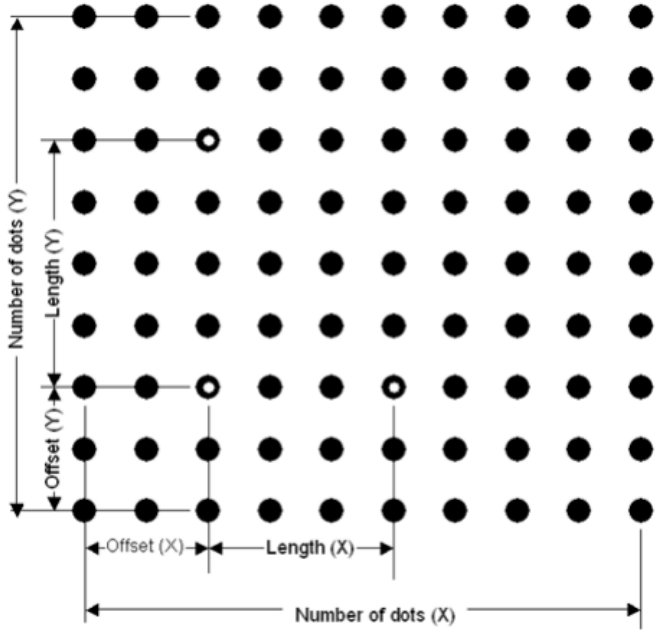

Fig. 9.4 Grid (28 mm) used for calibration

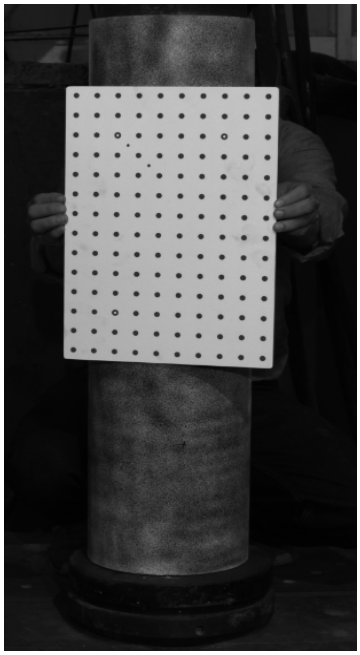

Fig. 9.5 Calibration process

9.5 RESULTS AND DISCUSSIONS

All the specimens are subjected to axial compression in universal testing machine. Table 9.1 shows the results obtained from UTM and DIC system. The load-displacement curves are shown in Fig. 9.6. The deformed shapes of specimens are shown in Fig. 9.7. The images are taken by cameras at every 5 seconds during the deformation process. The recorded digital images are processed using Vic-3D commercial code to obtain strain map. Fig 9.7(e) shows the typical contour map for axial strain. In stain map, different range of strain is shown by different colours. The colour gets disappear in strain map at the surface of specimen where cracks initiate. It can be seen from the strain map obtained from Vic-3D shown in Fig. 9.8. Axial and lateral strains at different applied displacement on specimens are shown in Tables 9.2 to 9.6. The strains obtained from Vic-3D and ANSYS are almost equal at the maximum displacement stage and their values vary at other stages (20 to 80% of maximum applied displacement). Strains measured at different locations are plotted against the applied displacements. Fig 9.9(b) shows the curve between applied displacement and strains at different locations chosen randomly. It can be seen form Fig. 9.9 (b) that the strains are nearly equal from peak load position to failure load position (41.8% to 100% applied displacement). Fig 9.10 (a) shows the curve between applied displacement and strains at different locations chosen along the shear plane. It can be seen form Fig. 9.10 (a) that the strains are increasing from peak load position to failure position (41.8% to 100% applied displacement). It has been observed that the strains at locations along the shear plane are about 10 times higher than the strains at other locations.

Table 9.1 Results obtained from UTM and DIC system

Specimen	Dimensions (mm)			Ultimate Load (kN)	Strains	
	Mean Outer diameter (D)	Thickness (t)	Length (L)		Lateral Strain (e_{xx})	Axial Strain (e_{yy})
160P5PC30	160	7.02	800	784	0.0199	0.014
200P5PC30	200	8.89	800	1173	0.014	0.013
225P5PC30	225	9.97	800	1478	0.0031	0.011
160P4RC30	160	5.22	800	1105	0.041	0.010
225P4BRC30	225	9.58	800	1519	0.0015	0.0063

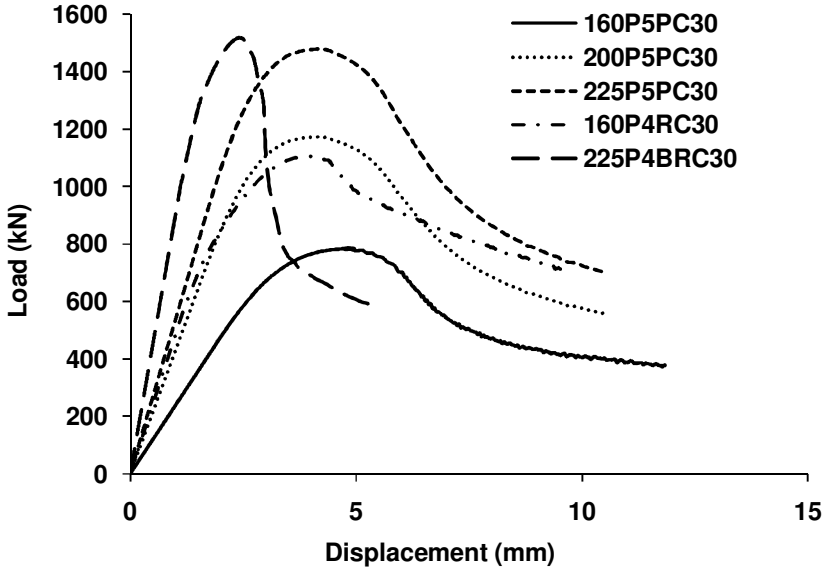

Fig. 9.6 Load-Displacement curves of PCFUT, RCFUT and RCC specimens

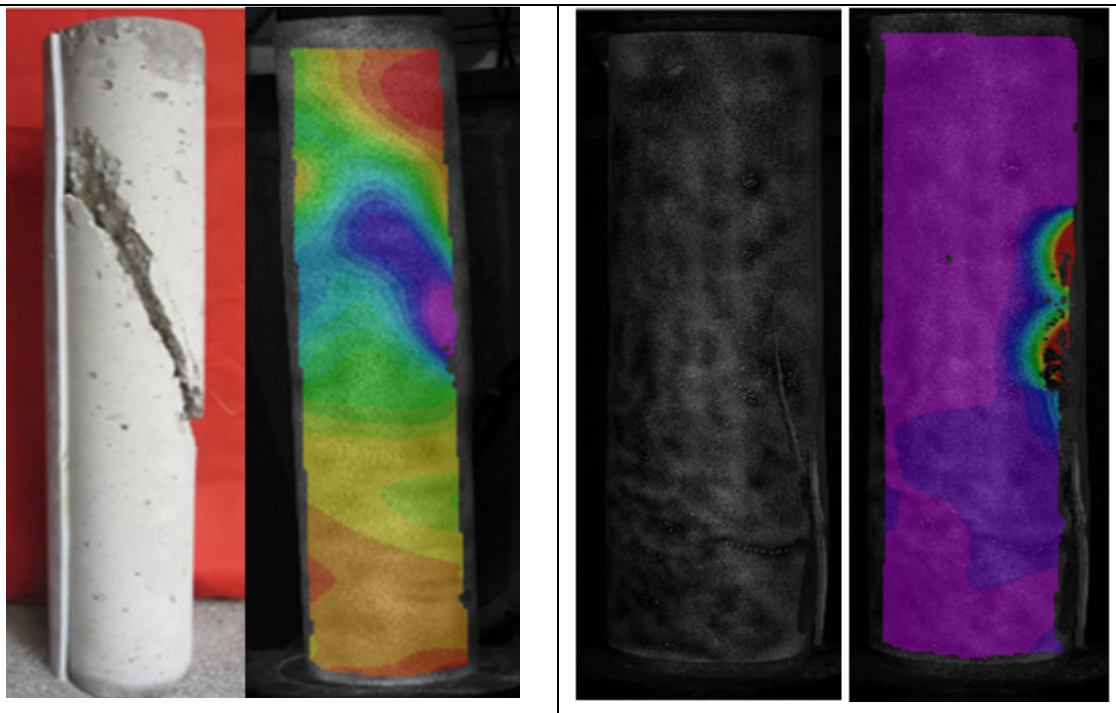

(a) 160P5PC30 (b) 200P5PC30

Fig. 9.7 (a-e) Failure mode of specimens with strain map

(c) 225P5PC30

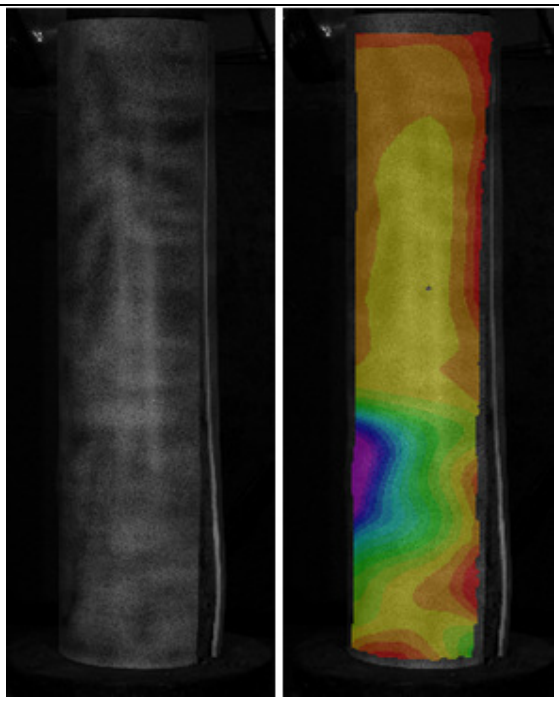

(d) 160P5RC30

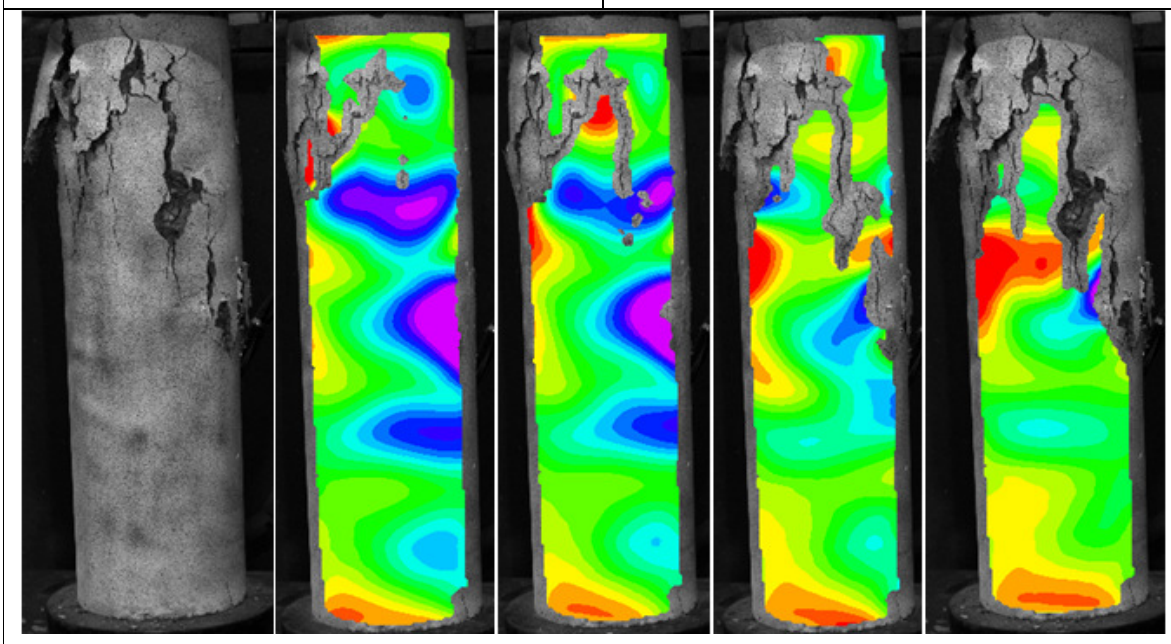

(e) 225P5BRC30

Fig. 9.7 (a-e) Failure mode of specimens with strain map

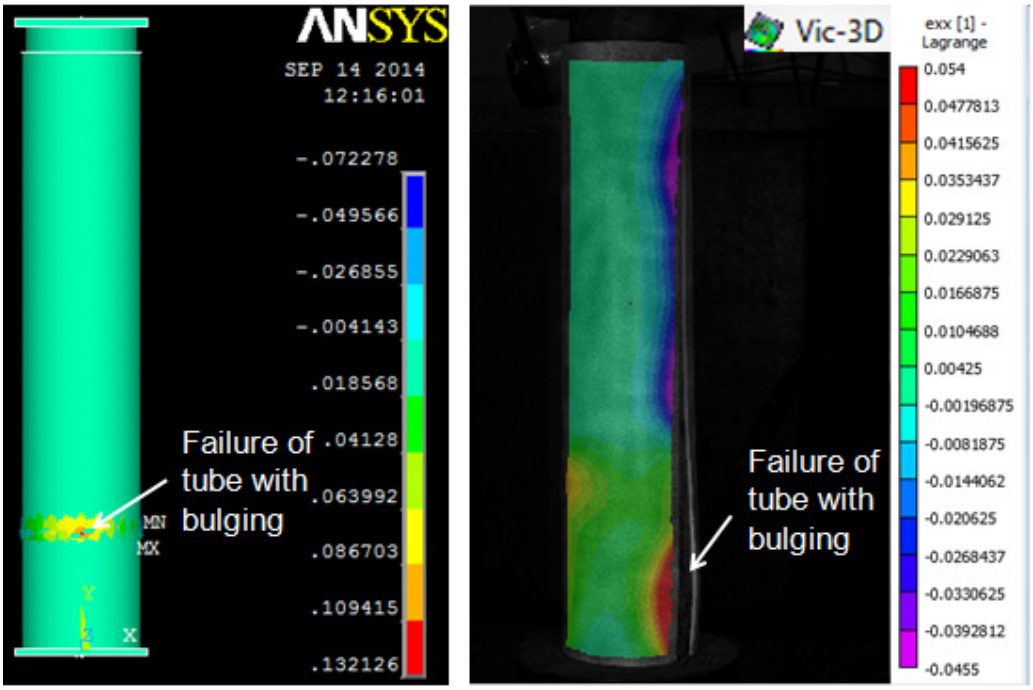

Fig. 9.8 Contour map of axial strain for typical specimen "160P4RC30"

Table 9.2 Strain measurement in the specimen '160P5PC30'

% of Maximum applied displacement	Lateral Strain (e_{xx})		Axial Strain (e_{yy})	
	ANSYS	Vic-3D	ANSYS	Vic-3D
20	0.00136	0.000064	-0.0011	-0.00049
40	0.00245	0.0056	-0.00357	-0.0033
60	0.00643	0.0082	-0.0108	-0.0072
80	0.0125	0.0014	-0.030	-0.0087
100	0.019	0.0199	-0.047	-0.014

Table 9.3 Strain measurement in the specimen '200P5PC30'

% of Maximum applied displacement	Lateral Strain (e_{xx})		Axial Strain (e_{yy})	
	ANSYS	Vic-3D	ANSYS	Vic-3D
20	0.00026	0.00017	-0.0004	-0.003
40	0.0009	0.0037	-0.00189	-0.00678
60	0.002	0.0085	-0.004	-0.0093
80	0.004	0.011	-0.0075	-0.011
100	0.010	0.014	-0.0177	-0.0131

Table 9.4 Strain measurement in the specimen '225P5PC30'

% of Maximum applied displacement	Lateral Strain (e_{xx})		Axial Strain (e_{yy})	
	ANSYS	Vic-3D	ANSYS	Vic-3D
20	0.00022	0.00013	-0.00022	-0.0002
40	0.0007	0.00025	-0.00145	-0.00057
60	0.0015	0.0014	-0.00302	-0.00145
80	0.00293	0.0029	-0.0055	-0.00292
100	0.0070	0.0031	-0.012	-0.0114

Table 9.5 Strain measurement in the specimen '160P4RC30'

% of Maximum applied displacement	Lateral Strain (e_{xx})		Axial Strain (e_{yy})	
	ANSYS	Vic-3D	ANSYS	Vic-3D
20	0.00051	0.00038	-0.001	-0.00031
40	0.00186	0.00327	-0.00352	-0.000727
60	0.0157	0.0166	-0.0212	-0.00188
80	0.0309	0.0316	-0.0374	-0.0051
100	0.044	0.041	-0.052	-0.010

Table 9.6 Strain measurement in the specimen '225P4BRC30'

% of Maximum applied displacement	Lateral Strain (e_{xx})		Axial Strain (e_{yy})	
	ANSYS	Vic-3D	ANSYS	Vic-3D
20	0.0001	0.000022	-0.000179	-0.00017
40	0.0005	0.00007	-0.00115	-0.000515
60	0.0016	0.0006	-0.0056	-0.00125
80	0.0016	0.0014	-0.0097	-0.0033
100	0.00159	0.00153	-0.014	-0.0063

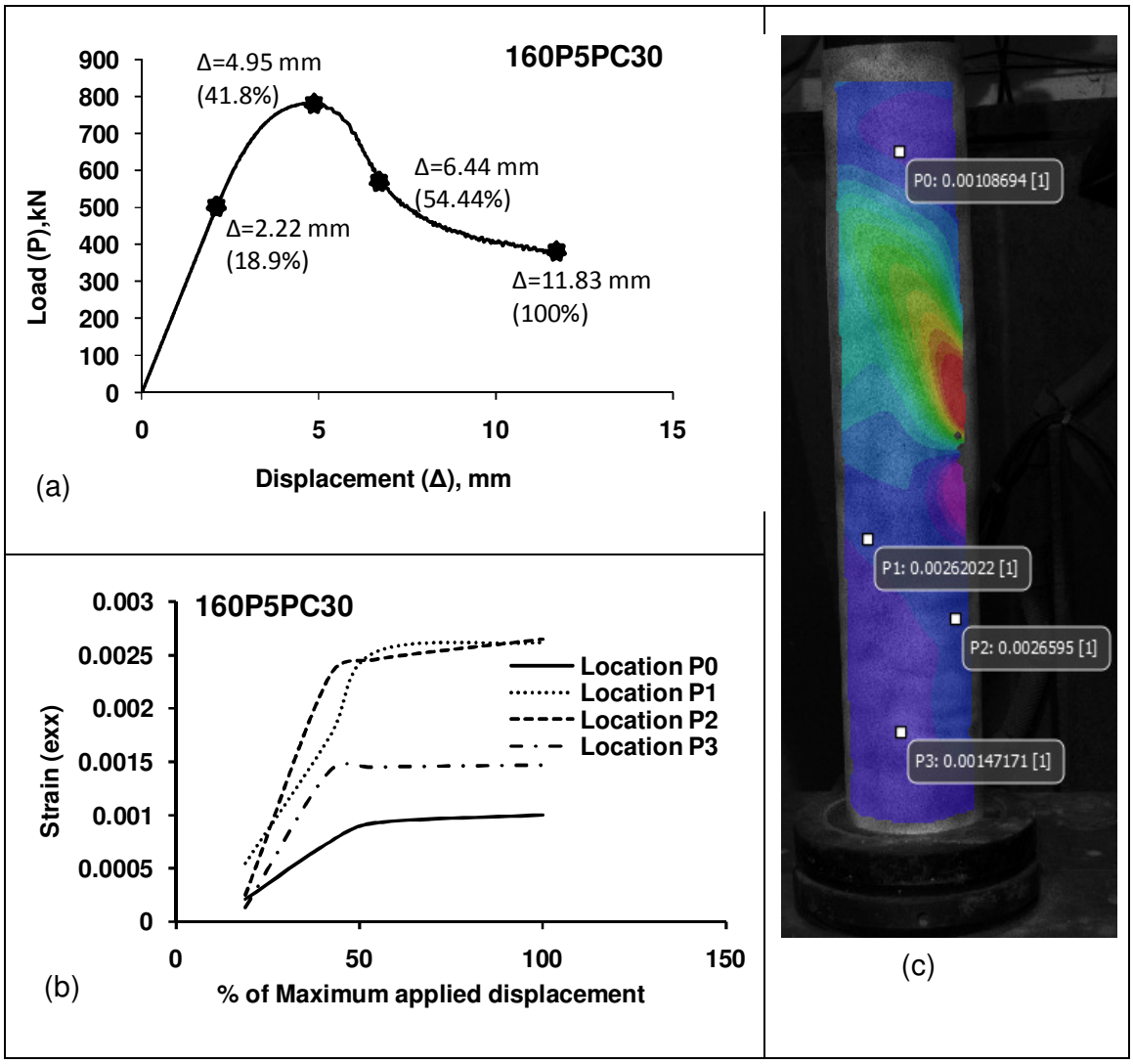

Fig. 9.9 (a) Load-displacement curve showing applied displacement (b) curve between applied displacement and strains at various locations (c) Digital image showing locations

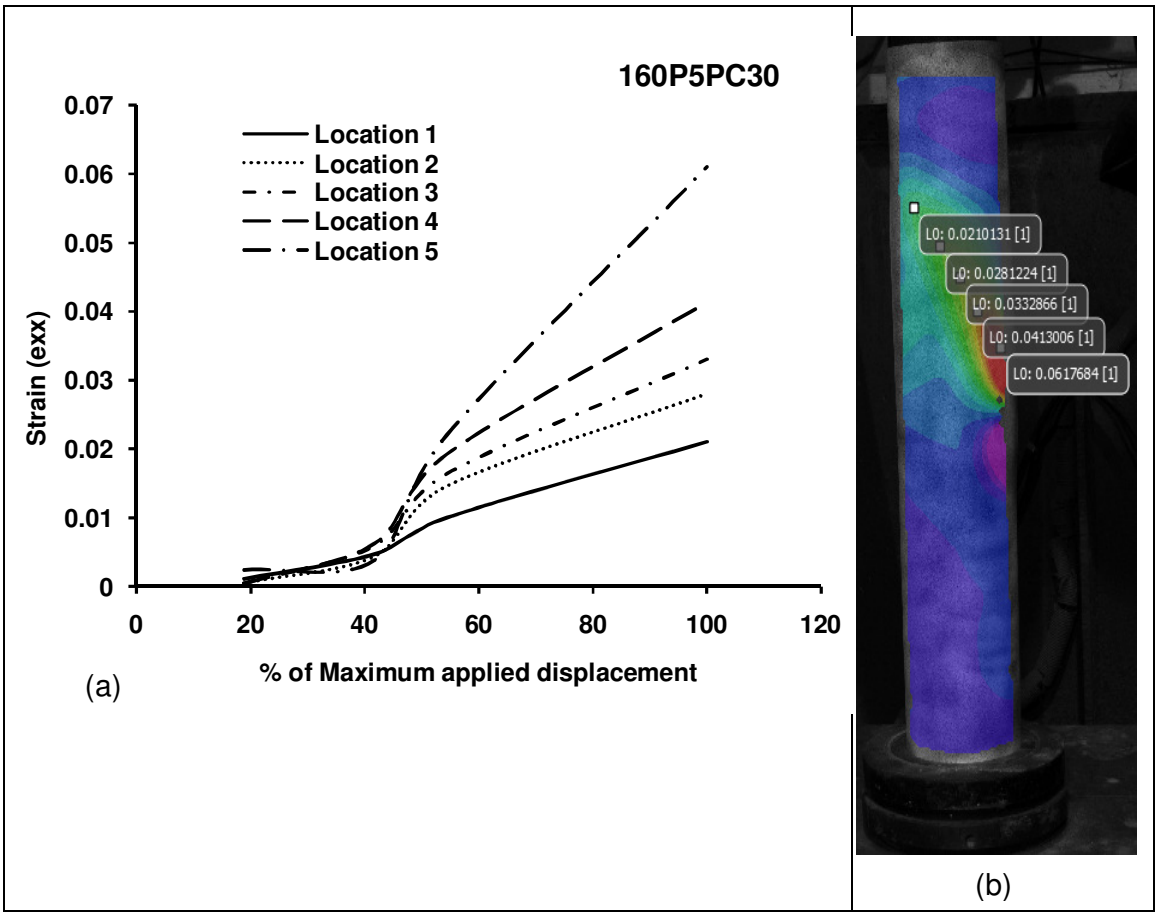

Fig. 9.10 (a) Curve between applied displacement and strains at various locations along shear plane (b) Digital image showing locations along shear plane

9.6 CONCLUSIONS

To get the material behaviour during the deformation process, it is better to use Digital Image Correlation System. From the images which are obtained during the deformation process, the areas where the cracks may develop can be identified. The Vic-3D does not provide strain maps after the cracking of specimen. To obtain better results with DIC system, it is important to have an adequate speckle pattern. More specimens in future may be tested to get the strains with the help of DIC system and it can be compared with the strains measured using other apparatus. It can be seen from the Fig 9.10 (a) that the strains along the shear plane is continuous increasing while strains at other locations increase up to peak load and after that they become nearly equal till failure of specimens (Fig. 9.9 (b)), which is obvious. During deformation process, stressing of specimen can be seen with the help of strain map with different colours on the surface of specimen.

CHAPTER 10

CONCLUSIONS

10.1 GENERAL

Experimental, analytical and numerical studies carried out in the research work have been described in the previous chapters. Further, conclusions drawn in each study have been written in respective chapters. However, following conclusions are included in this chapter in combined form for completeness.

10.2 CONFINEMENT

The confining pressure was obtained with the help of internal hydrostatic pressure test in the laboratory and using the mathematical equation given in literature. The confining pressure varies from 1.15 MPa to 2.25 MPa. A stress-strain model for concrete confined with UPVC tube and subjected to axial compression is proposed. Two parameters k_3 and k_4 are introduced to represent the post peak behaviour of confined concrete. Parameter (k_3) varies from 0.5 to 0.58 and k_4 is taken as $0.8k_3$. On the basis of results obtained, effect of variation of diameter to thickness ratio (D/t) on the failure stress of confined concrete is obtained and discussed with empirical relationship. Failure stress increases as the ratio D/t decreases for the same diameter of CFUT specimens. The strain at failure varies from 1.285 to 1.69. It decreases with the increase of compressive strength of concrete for the same class of pipes.

In case of reinforced concrete column that contains the transverse reinforcement in the form of either spiral or lateral ties; confinement mainly depends upon the vertical spacing between spiral or lateral ties (S) and on the ratio of the volume of transverse steel to the volume of confined concrete core (ρ_s). An effort is made to get an idea about the spacing of lateral ties in reinforced concrete column for the effective confinement. The confinement is governed by the ratio A_{tie}/S^2. The value of A_{tie}/S^2 greater than 0.02 may give the effective confinement.

In the present study, since the ratio A_{tie}/S^2 is 0.0022 which is less than 0.02, the stress-strain model of unconfined concrete was used for the Finite element modeling of concrete in RCC specimens. Even there is no strength gain observed in reinforced concrete column with lateral ties though there is an enhancement in the ductility. The strain at failure was obtained between 0.0075 and 0.009.

10.3 FAILURE PATTERN

The failure pattern of PCFUT specimens depends upon the constraining parameter (α) and confinement ratio (β). Failure of all specimens leads by development of shear crack and macro cracks with slight bulging. Most of the specimens failed quietly but for some specimens, a soft cracking noise was heard when the ultimate load was attained. In the present case the value of α is less than 0.2 and β is less than 0.1 for all specimens. The angle of failure plane in tested specimens measured with horizontal axis was found between 63^0 and 65^0. Angle of failure plane was also calculated from Mohr-Coulomb Theory. The variation in the angle of failure plane calculated from Mohr-Coulomb criterion and experiments is observed from 0 to 2%. It may be seen that the angle of failure plane varies with confining pressure. Its value increases with increase in confinement. It may be concluded that by increasing the confining pressure, angle of failure may be increased to avoid the shear failure.

The failure of RCC specimens occurred due to the crushing of concrete between the stirrups at the top or bottom portion of specimen. At the place of crushed concrete, steel bars were buckled. The failure of RCFUT specimens occurred with the crushing of concrete and bulging of tube near the top/bottom portion of specimens showing a ductile-brittle failure.

10.4 DUCTILITY

Ductility and energy absorption of concrete filled UPVC tubes was studied with the help of load-compression variations. The ductility and energy ratios vary with the class of pipes and diameter of pipes. Ductility and energy ratios both increase with the increase of class of pipes with same diameter and these also increase with the increase of diameter with same class of pipes. In general, ductility ratio decreases with increase in the grade of concrete due to brittleness of concrete. In this study the ductility ratio varies from 1.63 to 2.53 and energy ratio varies from 2.18 to 3.69 for PCFUT specimens. The ductility ratio varies between 1.41 and 1.80 and energy ratio varies between1.79 and 2.49 for bare RCC specimens. On the other hand the ductility ratio for RCFUT specimens varies between 1.51 and 2.76 and corresponding energy absorption ratio varies between 2.0 and 4.19. It is also found that as D/t ratio of the UPVC tube decreases, Δ_{80} and E_{80} increases. The energy absorbed (E_{80}) for bare RCC specimens made with M30 grade of concrete varies from 1610 Joule to 3293 Joule while for bare RCC specimens submerged in sea water varies from 1597 Joule to 2937 Joule. On the other hand, the energy absorbed (E_{80}) for RCFUT specimens filled with M30 grade of concrete varies from 3078 Joule to 11091 Joule while for RCFUT specimens submerged in sea water

varies from 3294 Joule to 11859 Joule. The energy absorbed by RCFUT is about 1.91 to 3.37 times that of bare RCC specimens. Since post peak displacement is important regarding ductile behavior of material, it was found that the displacement after the peak load was about 5 to 10 mm. Load-displacement curves obtained from numerical analysis and experiments were found in good match

10.5 STRENGTH

It was found that concrete showed an increment in load carrying capacity, when UPVC tube was used to confine concrete core. The strength of RCFUT specimens was recorded 1.08 to 1.23 times higher than RCC specimens. The diameter to thickness ratio of tube affects the post peak behavior of load-displacement curve. Absolute value of the slope of the curve decreases with increases in thickness of pipe with same outer diameter. An equation to calculate the load carrying capacity of plain concrete filled UPVC tubular columns is proposed. The ultimate load capacities of all the specimens are calculated using equation no. 5.7. The loads calculated using this equation (no. 5.7) is within 0.35 to 7.5 % of experimental loads. To verify the above proposed equation, the ultimate load capacities of specimens from literature are also calculated using this equation. The calculated load capacities and experimental load capacities (from literature) are plotted graphically. It can be concluded that proposed equation may be used for assessing the load capacity of concrete filled UPVC tubular columns. Load capacity of PCFUT specimens are also obtained from Mohr-Coulomb Theory. Load capacity was calculated by axial stress develop at failure. The load capacities calculated using Mohr-Coulomb theory and experiments vary from 0 to 8 %.

10.6 DURABILITY

There was no significant change in the strength, mode of failure and ductility of RCFUT specimens when submerged in sea water. In composite column like RCFUT, outer tube may work as a wall between concrete and aggressive environment. UPVC tubes used in RCFUT column may protect the column from corrosion of steel embedded and degradation of concrete against the attack of salts presents in sea water. Moreover, UPVC tubes may work as a weather proof jacket to the concrete during the whole year. When RCFUT specimens were made with UPVC tubes of class 1, even then no significant variation was observed in their performance. There was an enhancement in the strength (4.88 – 5.76 %) of RCFUT specimens made by UPVC tube of class 3, 4 and 5 exposed to sea water, tested at six months compared to RCFUT specimens kept in normal condition, tested at 28 days (Fig. 7.9). The maximum variation in

strength of RCFUT specimens made by UPVC tube of class 1 exposed to sea water and normal water was 3.2% (Fig. 8.2). The mode of failure of RCFUT specimens with UPVC tube of class 1 was almost same as failure mode of RCFUT specimens with UPVC tubes of class 3, 4 and 5. Therefore it may be concluded that the UPVC pipes with minimum nominal pressure capacity can also be used as a protective layer for concrete in sea water.

10.7 MAJOR CONTRIBUTIONS

10.7.1 Stress-strain model for concrete confined with UPVC tube

A stress-strain model for concrete confined with UPVC tube is proposed. This model is obtained by modifying the stress-strain model of concrete confined with steel tube. The post peak curve of concrete confined with steel tube is modified by introducing the parameters k_3 and k_4. The Material degradation parameter (k_3) depends on the value of D/t and decreases with the increase of D/t. The parameter k_4 depends upon value of k_3 and equals to 0.8 k_3. An empirical relation is proposed to calculate the value of and k_3. On the basis of obtained results, effect of variation of diameter to thickness ratio (D/t) on the failure stress of confined concrete is obtained.

10.7.2 Effective confinement in reinforced concrete column

Confinement mainly depends upon the spacing between spirals or lateral ties and on the ratio of the volume of transverse steel to the volume of concrete core inside the lateral ties. The confining pressure will be lesser (or not effective) if the spacing of lateral ties is more. There may be a slight increase in ductility with insignificant increase in strength, when lateral ties are at higher spacing. Therefore, to obtain the condition for the effective confinement in R.C. columns, a three dimensional Finite element model was developed to simulate the reinforced concrete columns under axial compression. An unconfined stress-strain model of concrete was tried, which gave good results. With the help of results, a condition for the minimum value of the ratio of cross-sectional area of lateral tie to the square of the spacing between lateral ties (A_{tie}/S^2) was achieved for the effective confinement of concrete core in reinforced concrete column. The value of A_{tie}/S^2 greater than 0.02 and confining pressure greater than 1.0 MPa may give the effective confinement.

10.7.3 Load carrying capacity of CFUT

To design a concrete filled UPVC tubular column (CFUT), an equation is proposed to calculate the load carrying capacity of CFUT. The ultimate load capacities of all the specimens in the present study are calculated using the above equation. The load carrying capacities calculated

using above equation are within ±7.5% of experimental capacities. To verify the above proposed equation, the ultimate load capacities of specimens from literature are calculated using proposed equation. The calculated load capacities are within ±8.5% of experimental capacities. Experimental load capacities (from literature) versus load capacities computed from proposed equation are graphically presented. This equation provides the facility for assessing the load capacity of concrete filled UPVC tubular columns for the design purpose.

10.7.4 RCFUT-a composite column against sea water

The present study provides an alternate way for the protection of concrete against the attack of salts present in sea water with an additional benefit of confinement and ductility by giving a new type of composite column (i.e. RCFUT). On the basis of results obtained, it was found that concrete showed an increment in strength, ductility and energy absorption capacity when UPVC tube was used to confine reinforced concrete column. The strength of RCFUT was recorded 1.08 to 1.23 times higher than reinforced concrete column. The energy absorbed by RCFUT is about 1.91 to 3.37 times that of reinforced concrete column. Enhancement in the strength of RCFUT specimens made by UPVC tube of class 3, 4 and 5 exposed to sea water, tested at six months compared to RCFUT specimens kept in normal condition, tested at 28 days was 4.88 – 5.76 %. The maximum variation in strength of RCFUT specimens made by UPVC tube of class 1 exposed to sea water and normal water was 3.2%. The mode of failure of RCFUT specimens with UPVC tube of class 1 was almost same as failure mode of RCFUT specimens with UPVC tubes of class 3, 4 and 5. In composite column like RCFUT, outer tube may work as a wall between concrete and severe environment. UPVC tubes used in RCFUT column may protect the column from corrosion of steel embedded and degradation of concrete against the attack of salts presents in sea water. Moreover, UPVC tubes may protect concrete from change of weather throughout the year.

10.7.5 Finite element model and numerical simulations

Detailed procedure for 3D Finite element modeling and simulation of concrete filled UPVC tubular column was carried with the help of software ‘ANSYS 12.0’. Material models for concrete core and UPVC tube were obtained and explained. Composite action between concrete core and UPVC tube was modeled. The procedure was presented with recommended properties for modeling such behavior. The proposed model was validated against the experimental results of specimens tested in the present study.

10.7.6 Strain measurement with Digital Image Correlation (DIC) system

Strains on the surface of some typical specimens are obtained using DIC system during the testing of specimens. The digital images, recorded during testing are processed using Vic-3D commercial code to obtain strain map. These strains are compared with the strains obtained from simulations. The strains obtained from Vic-3D and ANSYS are almost equal at the maximum displacement stage and their values vary at other stages (i.e. 20 to 80% of maximum applied displacement). It was observed that the strains on the surface of specimen along the shear plane were increased while at other locations the strains were nearly equal between peak load stage and failure load.

10.8 SCOPE FOR THE FUTURE STUDIES

Based on the present study, following recommendations were suggested for future research work:

1. Experimental study to investigate the effect of high strength concrete on confinement of CFUT column.
2. 3D-Finite element modeling of concrete filled high density polyethylene (HDPE) tubular columns.
3. Experimental study to investigate the behavior of CFUT column subjected to eccentric loading.
4. Experimental study to investigate the behavior of concrete filled double skin composite tubular columns with inner tube as steel and outer tube as UPVC tubes respectively.
5. Refinement of proposed Finite element model for the modeling of eccentric and combined loading.
6. Stress-strain model for concrete confined in double skin tubular column, when steel tube used as inner tube and outer tube as UPVC tube.
7. Experimental study to investigate the behavior of CFUT column with G.I. hollow pipes as reinforcement.
8. Experimental study to investigate the behavior of CFUT column, when recycled aggregate concrete is used for filling UPVC tubes.

REFERENCES

1. ACI-318 (2008). Building code requirements for structural concrete and commentary, Detroit (USA). American Concrete Institute.
2. Agrawal, S.K., and Chourasia, A. (2003). Seismic rehabilitation of RCC structures-How far from reality, International symposium on innovative world of concrete, Pune, India.
3. Agrawal, S.K., and Chourasia, A. (2005). Experimental investigation of seismic strengthening and retrofitting measures of RC multistoried buildings. International conference on advances in concrete composites and structures, Structural Engineering Research Centre, Chennai, India.
4. Ahmad, K., Yadav, R.K., and Chandak, R. (2012). Effect of lateral confinement on strength of concrete, ISCA Journal of Engineering science, Vol.1, no.1, pp.40-44.
5. Ahmad, S.H., and Shah, S.P. (1982). Complete triaxial stress-strain curves for concrete, J. Str. Division, Vol. 108, no. ST4, pp.728-741.
6. Alhozaimy, A., AL-Negheimish, A., Alawad, O.A., Jaafar, M.S., and Noorzaei, J. (2012-a). Binary and ternary effects of ground dune sand and blast furnace slag on the compressive strength of mortar, Cement and Concrete Composites, vol.34, no.6, pp.734–738.
7. Alhozaimy, A., Jaafar, M.S., Al-Negheimish, A., Abdullah, A., Taufiq-Yap, Y.H., and Noorzaei, J. (2012-b). Properties of high strength concrete using white and dune sands under normal and autoclaved curing, Construction and Building Materials, vol.27, no.1, pp.218–222.
8. Anthony, J., Wolanski, B.S. (2004). Flexural behavior of reinforced and prestressed concrete beam using finite element analysis, Master's thesis, Marquette university, Milwaukee, Wisconsin.
9. ANSYS. (2009-a). Contact technology guide, Release 12. ANSYS Incorporation.
10. ANSYS. (2009-b). Element reference, Release 12. ANSYS Incorporation.
11. ANSYS. (2009-c). Structural analysis guide, Release 12. ANSYS Incorporation.
12. ANSYS. (2009-d). Theory reference, Release 12. ANSYS Incorporation.
13. Ansari, F., Li, Q., (1998). High strength concrete subjected to triaxial compression. ACI Mater J, 95(6): 747-755.
14. ASTM-D638-10 Standard test method for tensile properties of plastics. ASTM International, United States
15. ASTM E2015. Standard guide for preparation of plastics and polymeric specimens for microstructural Examination, ASTM International, United States.

16. Attard, M.M., and Setunge, S. (1996). Stress-strain relationship for confined and unconfined concrete, ACI material journal, vol. 93, no.5, pp. 432-442.
17. Baidya, N., Zhang , L., Mendis, P.A., and Fragomeni, S. (2013). Effect of construction sequence in the axial shortening behaviour of composite columns, Materials to Structures: Advancement through innovation, pp.55-59, Sydney, Australia: Taylor and Francis Ltd., London Group.
18. Balendra, T. (1983). A simplified model for lateral load analysis of asymmetrical buildings. Engineering Structures, vol.5, no.3, pp. 154-162.
19. Bangash, M.Y. (2001). Manual of numerical methods in concrete: modeling and applications validated by experimental and site-monitoring data. London: Thomas Telford.
20. Bharatkumar, B.H, Raghu Prasad, B.K., Ramachandramurthy, D.S., Narayanan, R. and Gopalakrishnan, S. (2005). Effect of Fly Ash and Slag on the Fracture Characteristics of High Performance Concrete, Materials and Structures, Vol. 38, no.1, pp. 63-72.
21. Borsaikia, A., Talukdar, S., and Dutta, A. (2006). Study of modal parameters and vibration signatures of notched concrete prisms. Cement and Concrete Research, vol.36, pp 592 – 598.
22. BS EN ISO 527-1 (2012). Plastic- Determination of plastic properties Part-1- general principles. BSI standard publication, U.K.
23. Caddell, R.M., Raghava, R.S., and Atkins, A.G. (1974). Pressure dependent yield criteria for polymers, Material Science and Engineering, vol.13, pp.113-120.
24. Chakrabarti, A., Sheikh, A.H., Griffith, M., and Oehlers, D.J. (2012-a). Analysis of composite beams with longitudinal and transverse partial interactions using higher order beam theory, International Journal of Mechanical Sciences, vol.59, no.1, pp 115-125.
25. Chakrabarti, A., Sheikh, A.H., Griffith, M., and Oehlers, D.J. (2012-b). Analysis of composite beams with partial shear interaction using a higher order beam theory, Engineering Structures, vol.36, no.1, pp 283-291.
26. Chakrabarti, A., Sheikh, A.H., Griffith, M., and Oehlers, D.J. (2012-c). Vibration and Buckling of composite beams with partial shear interactions using a higher order beam theory, International Journal of Structural and Civil Engineering Research, vol.1, no.1, pp 24-42.
27. Chakrabarti, A., Sheikh, A.H., Griffith, M., and Oehlers, D.J. (2013). Dynamic Response of composite beams with partial shear interactions using a higher order beam theory, Journal of Structural Engineering, ASCE, vol.139, no.1, pp 47-56.

28. Choubey, A., Sehgal, D.K., and Tandon, N. (2006). Finite element analysis of vessels to study changes in natural frequencies due to cracks, International Journal of Pressure Vessels and Piping, vol.83, no.3, pp.181-187.
29. Clausen, A. H., Loria, M. P., Berstad, T., and Hopperstad, O.S. (2011). A constitutive model for thermoplastics with some applications, 8th European LS-Dyna Conference, Strasbourg, pp.1-11.
30. Correlated Solutions, Vic-3D v7, Testing Manual and Guide.
31. Desayi, P., Iyengar, K.T.S.A., and Reddy T.S. (1978). Equation for stress-strain curve of concrete confined in circular steel spiral, Materials and Structures, vol.11, no. 65, pp. 339-345.
32. El-Heweity, M.M. (2012). On the performance of circular concrete filled high strength steel columns under axial loading, Alexandria Engg. Journal. pp. 1-12.
33. El-Kareim, A. and Soliman, S. (2011). Behavior of Long Confined Concrete Column, Ain Shams Engineering Journal,; 2, pp. 141-148.
34. Ellobody, E., Young B., Lam, D. (2006). Behaviour of normal and high strength concrete filled compact steel tube circular stub columns, J. Construction Steel Research, Vol. 62, pp. 706-715.
35. Elwi, A.A., Murray, D.W. (1979). A 3D hypoelastic concrete constitutive relationship. J. Engg. Mech., 105(4): pp.623-641.
36. Emmanuel, A. O, Oladipo, F. A., and Olabode, O. E., (2012). Investigation of salinity effect on compressive strength of reinforced concrete. Journal of sustainable development, Vol. 5, no.6, pp. 74-82.
37. Fam, A.Z., and Rizkalla, S.H. (2001). Confinement model for axially loaded concrete confined by circular fiber-reinforced polymer tubes, ACI material journal, Vol. 98, no.4, pp. 451-461.
38. Gao, X.Y., Balendra, T., and Koh, C.G. (2013). Buckling strength of slender circular tubular steel braces strengthened by CFRP, Engineering Structures, vol.46, pp.547–556.
39. Gardner, N. J., and Jacobson, E. R. (1967). Structural behavior of concrete filled steel tubes, ACI material journal, no. 64-38, pp. 404-413.
40. Giakoumelis, G., and Lam, Dennis (2004). Axial capacity of circular concrete-filled tube columns, J. Constructional Steel Research, Vol. 60, pp. 1049-1068.
41. Gupta, K.D., Murty, C.V.R., and Agrawal, S.K. (2003). Seismic shear design of RC structural walls-Part-I, Review of code provisions. Indian Concrete Journal, 77(11), pp. 1423-1430.

42. Gupta, P.K., Sarda, S.M., and Kumar, M.S. (2007). Experimental and computational study of concrete filled steel tubular columns under axial loads, Journal of Constructional Steel Research, Vol. 63, pp. 182-193.
43. Gupta, P.K. (2013). Confinement of concrete columns with unplasticized poly-vinyl chloride tubes, International Journal of Advanced Structural Engineering, Vol.5:9, pp.1-8
44. Hu, H.T, Huang, C. S., Wu, M. H., and Wu, Y.M. (2003). Nonlinear analysis of axially loaded concrete-filled tube columns with confinement effect, J. Str. Engg., Vol. 129, no. 10, pp. 1322-1329.
45. Idorn, G.M. (1967). Durability of concrete structures in Denmark, PhD. Thesis, Technical university of Denmark, Copenhagen.
46. Imran, I. and Pantazopoulou, S.J. (1996). Experimental study of plain concrete under triaxial stress, ACI material journal, vol. 93, no.6, pp. 589-601.
47. IS: 456-2000 (Reaffirmed 2005). Plain and reinforced concrete- code of practice. Bureau of Indian Standard, New Delhi, India.
48. IS: 4985-2000 (Reaffirmed 2005). Unplasticized PVC pipes for potable water supplies-specification. Bureau of Indian Standard, New Delhi, India.
49. IS: 10262-2009. Concrete mix proportioning-guidelines, Bureau of Indian Standard. New Delhi, India.
50. IS: 12235(Part 8)-1986. Methods of test for Unplasticized PVC pipes for potable water supplies. Bureau of Indian Standard, New Delhi, India.
51. Iskander, M.G., P.E., Hassan, M. (1998). State of the practice review in FRP composite piling, Journal of Composites for construction, ASCE, Vol.2, no. 3, pp.116-120.
52. Islam, M.M., Islam, M.S., Al-Amin, M. and Islam, M.M. (2012). Suitability of sea water on curing and compressive strength of structural concrete, Journal of Civil engineering (IEB), Vol.40, no. 1, pp.37-45.
53. Jaafar, M.S., Thanoon, W.A., Khan, S.R., and Trikha, D. (2002). Strength estimation of concrete in different environments using UPV, Pertanika Journal of Science and Technology, vol.10, no.2, pp.179-186.
54. Jain, D.K. (2007). Performance of mineral based concrete in marine environment, PhD. Thesis, Department of Civil engineering, I.I.T. Roorkee, India
55. Kamal, M.M., and Salama, A.E. (1990). Protection of reinforced concrete elements against corrosion by polymer coating, International conference on protection of concrete, University of Dundee, Scotland.

56. Kratky, B.A. and Roan, Y.C. (1986). A steel reinforced concrete filled PVC pipe shelter for vegetable seedlings, Asian Vegetable Research and Development Centre, Taiwan, pp.140-145.
57. Kurt, C.E. (1978). Concrete filled structural plastic columns, J. Str. Division, Vol. 104, no. ST1, pp. 55-63.
58. Laskar, A.I., and Talukdar, S. (2008-a). Rheology of steel fiber reinforced concrete. Asian Journal of Civil Engineering, vol.9, no.2, pp.167-177.
59. Laskar, A.I., and Talukdar, S. (2008-b). A new mix design method for high performance concrete. Asian Journal of Civil Engineering (Building and Housing), vol. 9, no. 1, pp.15-23.
60. Laskar, A.I., and Talukdar, S. (2008-c). Rheological behavior of high performance concrete with mineral admixtures and their blending. Construction and Building Materials, vol.22, no.12, pp.2345–2354.
61. Liang, Q.Q., and Sam, F. (2009). Nonlinear analysis of circular concrete filled steel tubular short columns under axial loading, Journal of Constructional Steel Research, vol. 65, pp. 2186-2196.
62. Liu, J., Sumei Z., Xiaodong, Z., and Lanhui, G. (2009). Behaviour and strength of circular tube confined reinforced concrete columns, J. Construction Steel Research, Vol. 65, pp. 1447-1458.
63. Mander, J. B., Priestley, M. J. N., Park, R. (1988-a). Theoretical stress-strain model for confined concrete, J. Str. Engg., Vol. 114, no. 8, pp. 1804-1830.
64. Mander, J. B., Priestley, M. J. N., Park, R. (1988-b). Observed stress-strain behavior of confined concrete, J. Str. Engg., Vol. 114, no. 8, pp. 1827-1849.
65. Marzouck, M. and Sennah, K. (2002). Concrete filled PVC tubes as compression members, Proc. International congress on challenges of concrete construction at Scotland, U.K.
66. Mather, B. (1964). Effect of sea water on concrete, symposium on effect of aggressive fluids on concrete, Washington D.C., U.S.
67. Menon, D. (2001). Fuzzy logic based estimation of effective lengths of columns in partially braced multi-storey frames. Structural Engineering and Mechanics, vol.11, no.3, pp.287-299.
68. Menon, D., and Reddy, Y.N. (1998). Finite Element modeling of tall slender tubular towers. Journal of Structural Engineering, SERC, vol.24, pp.243–246.
69. Mirmiran, A. and Shahawy, M. (1996). A new concrete filled hollow FRP composite column, Composites: part B; no.27, pp: 263-268.

70. Mohamed, H. and Radhouane, M.M. (2010). Axial Load Capacity of Concrete-Filled FRP tube Columns: Experimental versus theoretical predictions, Journal of Composites for Construction, ASCE, vol.14, no.2, pp. 231-243.
71. Montoya, E., Vecchio F. J. and Sheikh S.A. (2001). Compression field modeling of confined concrete. Structural Engineering and Mechanics, vol. 12, no.3, pp. 231-248.
72. Neelam, M.K. and Kalaga, S. (2002). Elastic properties of PVC pipes, Journal of Structural Engineering, vol.29, pp.91-96.
73. Nielsen, C.V. (1998). Triaxial behavior of high strength concrete mortar, ACI material journal, vol. 95, no.2, pp. 144-150.
74. Oshiro, T., and Tanikawa, S. (1990). A field study of a R.C. building exposed to a marine environment, International conference on protection of concrete, University of Dundee, Scotland.
75. Palaniswamy, R., and Shah, S.P. (1974). Fracture and stress-strain relationship of concrete under triaxial compression, J. Str. Division, Vol. 100, no. ST5, pp. 901-915.
76. Partheepan, G., Sehgal, D.K., and Pandey, R.K. (2008). Finite element application to estimate in-service material properties using miniature specimen. World Academy of Science, Engineering and Technology, vol.2, pp. 472-478.
77. Popovics, S., (1973). A numerical approach to the complete stress-strain curves of concrete, Cement and Concrete Research, Vol. 3, no. 5, pp. 583-599.
78. Ragab, A.R., Mahmoud, M.A., Khorshied, S.A. (2000). Yielding of Commercial Poly (vinyl chloride) pipe material, Journal of applied Polymer Science, vol. 81, pp.991-999.
79. Raghava, R., and Caddell, R.M., (1973). The macroscopic yield behavior of polymers, Journal of material Science, vol.8, pp.225-232.
80. Rai, S.K., and Prasad, J. (2005-a). Non-linear static analysis of shear wall in tall buildings, Proc. of International Structural Engineering Convention. Bangalore, India: Indian Institute of Science Bangalore.
81. Rai, S.K., and Prasad, J. (2005-b). Non-linear static analysis of tall buildings, Proc. of 4th International Conference on Autoclaved Aerated Concrete- Innovation and Development, (pp. 89-100). London, UK.
82. Rai, S.K., Prasad , J., and Ahuja, A.K. (2006). Reducing Drifts and damages in tall buildings by shear wall panels. Proc. of the National Conference on High Rise Buildings: Materials and Construction Practices. New Delhi, India.

83. Raman, S.N., Ngo, T., Mendis, P., and Mahmud, H.B. (2011). High-strength rice husk ash concrete incorporating quarry dust as a partial substitute for sand, Construction and Building Materials, vol.25, no.7, pp.3123–3130.
84. Rao, A.G. and Raghu Prasad, B.K (2011). Influence of interface properties on fracture behavior of concrete, Indian Academy of science, vol.36, part 2, pp. 193-208.
85. Revathi, P., and Menon, D. (2005). Nonlinear finite element analysis of reinforced concrete beams. Journal of Structural Engineering, SERC.
86. Richart, F.E., Brandzaeg, A., Brown, R. L. (1928). A study of the failure of concrete under combined compressive stresses. Bull 185. Champaign (IL, USA); University of Illinios Engineering Experimental station.
87. Roy, H.E.H., and Sozen, M.A. (1964). Ductility of concrete, Proc., Int. Symp. on Flexural Mechanics of Reinforced Concrete, ASCE-ACI, Maimi, pp.213-224.
88. Rutland, C.A., and Wang, M.L. (1997). The effect of confinement on the failure orientation in cementitious materials experimental observations, Cement and Concrete composites, vol.19, pp. 149-160.
89. Saatcioglu, M. and Razvi, S. R. (1992). Strength and ductility of confined concrete, Journal of Structural Eng, vol. 118, no.6, pp. 1590-1607.
90. Saenz, L.P. (1964). Discussion of 'Equation for the stress-strain curve of concrete', ACI journal, vol. 61, no. 9 pp. 1229-1235.
91. Salmanpour, A.H. and Mojsilović, N. (2013). Application of Digital Image correlation for strain measurements of large masonry walls, APCOM & ISCM, Singapore.
92. Samra, R.M. (1990). ductility analysis of confined columns, Journal of Structural Eng., vol. 116, no. 11, pp. 3148-3160.
93. Schneider, S.P. (1998). Axially loaded concrete filled steel tubes, Journal of Structural Eng., vol. 124, no. 10, pp. 1125-1138.
94. Sfer, D., Carol, I., Gettu, R., and Etse, G. (2002). Study of the behavior of concrete under triaxial compression, Journal of Engg. Mech., Vol. 128, no.2, pp. 156-163.
95. Shams, M., and Saadeghvaziri, M.A. (1999). .Nonlinear response of concrete filled steel tubular columns under axial loading, ACI structural journal, vol. 96, no. 6, pp. 1009-1018.
96. Sofi, M., van Deventer, J.S., Mendis, P.A., and Lukey, G.C. (2007). Engineering properties of inorganic polymer concretes (IPCs), Cement and Concrete Research, vol.37, no.2, pp.251–257.

97. Son, Je-Kuk, and Fam Amir, (2008). Finite element modeling of hollow and concrete filled fiber composite tubes in flexure: model development, verification and investigation of tube parameters, Engineering Structures, vol.30, pp.2656–2666.
98. Sridevi, B., and Agrawal, S.K. (1991). 2D Finite element model for planar failure along a Joint, Indian Geotechnical Conference.
99. Subramanian, N., (2011). Design of confinement reinforcement for RC columns, The Indian Concrete journal, Point of View, pp.1-8.
100. Tan, K.T., Bhowmik, T., and Balendra, T. (2013). Confinement model for FRP-bonded capsule-shaped concrete columns, Engineering Structures, vol. 51, pp.51-59.
101. Teng, J.G., Yu T., Wong Y. L., and Dong S.L. (2007). Hybrid FRP-Concrete-Steel tubular columns: concept and behavior, Construction and Building Materials, vol. 21, pp. 846-854
102. Thanoon, W.A., Hamed, A.M., Noorzaei, J., Jaafar, M.S., and Al-Silayvani, B.J. (2004-a). Inelastic analysis of composite sections, Computers and Structures, vol.82, no.20-21, pp.1649–1656.
103. Thanoon, W.A., Paul, D., Jaafar, M.S., and Trikha, D.N. (2004-b). Influence of torsion on the inelastic response of three-dimensional R.C. frames. Finite Element in Analysis and Design, vol.40, no.5-6, pp.611–628.
104. Umar, A., Abbas, H., and Sehgal, D.K. (1994). An extrapolation technique for prediction using coarse mesh. Proc. of 10th Symposium on Earthquake Engineering, Roorkee, India, vol.2, pp. 975-981.
105. Umar, A., Abbas, H., Qadeer, A., and Sehgal, D.K. (1996). Prediction of error in finite element results. Computers and Structures, vol. 60, no.3, pp. 471-480.
106. Wang, J., Yang, Q. (2010). Experimental study on mechanical properties of concrete confined with plastic pipes, ACI material journal, vol. 107, no. 2, pp. 132-137.
107. Ward, M. (1971). Review: The yield behavior of polymers, Journal of material Science, vol.6, pp.1397-1417.
108. Wu, D., Sofi, M., and Mendis, P. (2010). High strength concrete for sustainable construction, International Conference on Sustainable Built Environment (ICSBE-2010), pp. 434-442, Kandy.
109. Wu, Y.F. (2004). Effect of longitudinal reinforcement on the cyclic shear behavior of glass fibre reinforced gypsum wall panels: tests, Engineering Structures, vol. 26, pp. 1633-1646.
110. Xiamuxi, A. and Hasegawa, A. (2012). A study on axial compressive behavior of reinforced concrete filled tubular steel columns, J. Construction Steel Research, vol. 76, pp. 144-154.

LIST OF PUBLICATIONS

Journals

1. Gupta, P.K., Verma, V.K., Devakinandan, M and. (2013), Experimental study on axially loaded concrete filled Unplasticised Poly Vinyl Chloride (UPVC), ICI journal, Vol. 14, no. 2, pp. 45-49, India.
2. Gupta, P.K., Verma, V.K., Singh, H. Khaudhair, Z.A. and Ajay, N. (2013), Ductility and energy absorbing capacity of concrete filled UPVC tubes, International Journals of Construction Materials and Structures, Vol. 1, no. 1, pp. 1-10, India.
3. Gupta, P.K., Verma, V.K., study of concrete filled Unplasticised polyvinyl chloride (UPVC) tubes in marine environment, Journal of Engineering for the maritime Environment, SAGE Publication, U.K., (In press).
4. Gupta, P.K., Verma, V.K., Khaudhair, Z.A. and Singh, H., Effect of tube area on the behavior of concrete filled tubular columns, Computers and Concrete, Techno Press, South Korea, (In press).
5. Gupta, P.K., Verma, V.K., Study of concrete confined by unplasticized polyvinyl chloride tubes , ACI Material Journal, USA, Under Review

Conferences

1. Gupta P.K., Verma, V.K., Ajay Nabam and Ahuja, A.K. (2012), A study on the behaviour of axially loaded Unplasticised Poly Vinyl Chloride (UPVC) concrete filled tubes, The fourth International Conference on Structural Stability and Dynamics at Jaipur, India, pp.662-667
2. Gupta P.K., Verma, V.K. (2014), Numerical study on axial compression of plastic tubes, The fourth International fib Congress on improving performance of concrete structures at Mumbai, India, pp.514-517

3. Gupta P.K., Verma, V.K. (2014), A study on behavior of reinforced concrete columns subjected to axial compression, International Conference on Construction Materials and Structures (ICCMATS) at Johannesburg, South Africa, Accepted.
4. Gupta P.K., Verma, V.K. (2015), Study on confinement in reinforced concrete columns, International Conference on Materials Research and Engineering (ICMRE) at Shanghai, China, Accepted.